Modifications of Highway Air Pollution Models for Complex Site Geometries, Volume I: Data Analysis & Model Development

FHWA-RD-02-036

SEPTEMBER 2002

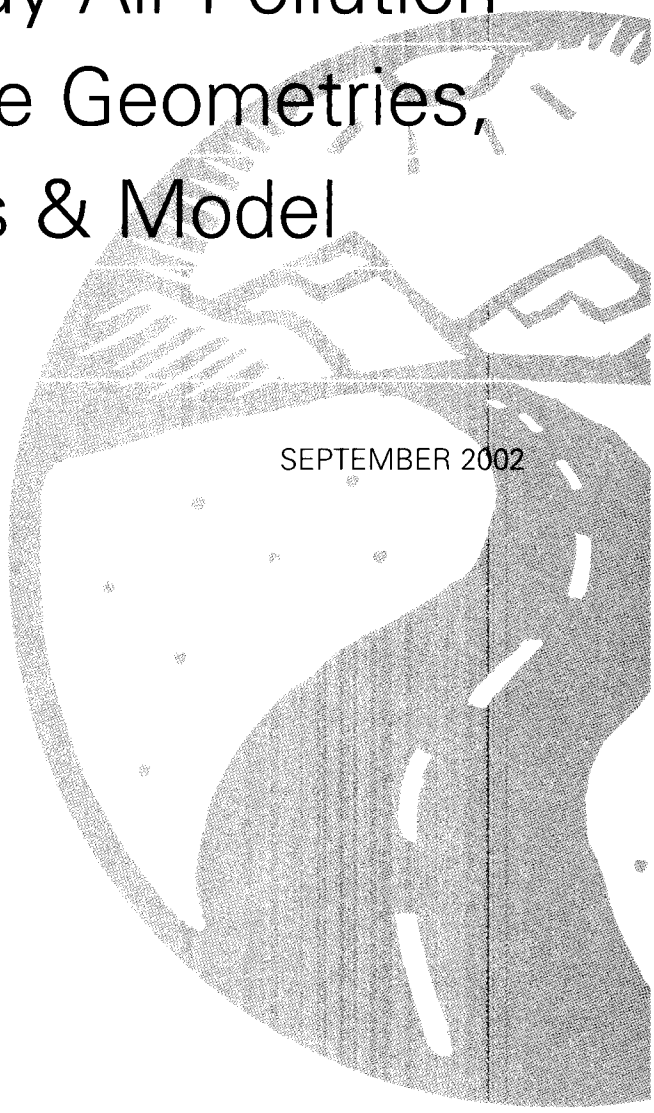

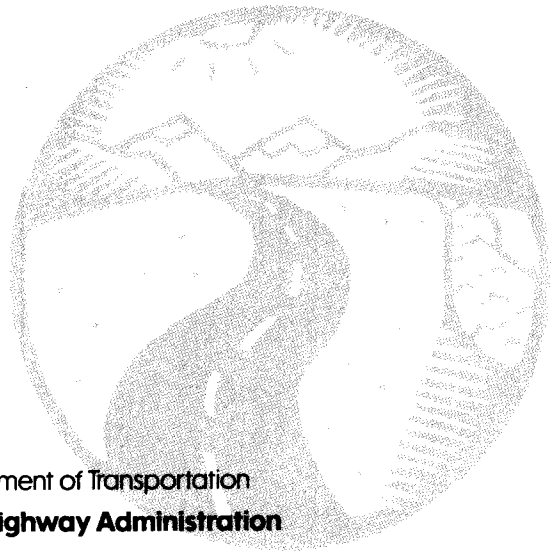

U.S. Department of Transportation
Federal Highway Administration

Research, Development, and Technology
Turner-Fairbank Highway Research Center
6300 Georgetown Pike
McLean, VA 22101-2296

FOREWORD

This study is an evaluation of flow patterns and dispersion of air contaminants for complex site geometries, such as semi-confined, cut-section highways and urban street canyons. Highway vehicle exhaust entrainment, air contaminant dispersion, and impacts from contaminants for such locations are in contrast to those noted from field, wind tunnel, and related models for flat, open sites and can be significantly important in environmental assessments.

This research study was initiated by the Federal Highway Administration (FHWA) to explore the limits of flat, open site dispersion measurements and models, and to develop modified or new dispersion models for complex sites based upon flow, turbulence, and concentration data from full-scale and wind tunnel-scale studies for numerous complex geometries and other variables. After the investigation was underway, the Federal Aviation Administration (FAA) joined in sponsorship of this study because the FAA and the U.S. Air Force have concerns about the wind-perturbing characteristics of buildings at airports and air bases and about air quality and related impacts. Air contaminant problems at complex sites can also result from accidental or deliberate releases of toxic air contaminants. This investigation should also interest others concerned with airflows and dispersion of gases and contaminants. The report includes:

- A review of what is known from flat terrain highway modeling and experimental studies.
- Consideration of the status of street canyon modeling, field studies, and wind tunnel studies.
- Analyses of the experimental flow, turbulence, and concentration data obtained from this program to expand the useful validity range of the original Canyon Plume Box (CPB-1) developed by Dr. Yamartino and European experts for sites in Germany and The Netherlands.
- Creation of a more comprehensive model, CPB-3, that can simulate cut-sections and street canyons having width-to-height ratios (W/H) ranging from ¼ to 6, geometries having unequal height sides, semi-open walls, and roadway curvature, and includes wind direction variability. (A disk with this program, CPB-3-6a [sixth release], is available.)
- Evaluation of the applicability limits of this new model, CPB-3, relative to existing roadway models for open, flat terrain, which are usually satisfactory for most of the areas of cut-sections and downwind of cut-sections with a W/H greater than 6.

This report, which is part of a two-volume series, is Report No. FHWA-RD-02-036, *Modifications of Highway Air Pollution Models for Complex Site Geometries, Volume I: Data Analysis and Model Development.* The other volume in this series is Report No. FHWA-RD-02-037, *Modifications of Highway Air Pollution Models for Complex Site Geometries, Volume II: Wind Tunnel Test Program.*

T. Paul Teng, P.E.
Director, Office of Infrastructure
Research and Development

TABLE OF CONTENTS

Volume I: Data Analyses and Development of CPB-3

APPENDIXES

LIST OF FIGURES

LIST OF FIGURES (continued)

LIST OF FIGURES (continued)

LIST OF TABLES

1. INTRODUCTION AND OVERVIEW

The 1-hour and 8-hour average National Ambient Air Quality Standards (NAAQS) for carbon monoxide (CO) continue to be the most difficult standards to attain for mobile source related projects. As a result, substantial effort in the past decade has gone into developing, refining, and evaluating line source models appropriate for roadways in flat terrain (i.e., rural) environments. These models conform to Environmental Protection Agency (EPA) Guideline specifications and incorporate numerous refinements such as vehicle motion induced initial mixing.

However, efforts to mathematically model the effects of complex site geometry (e.g., street canyons, city intersections, tall buildings) have been generally abandoned in favor of more costly and project-specific wind tunnel or field monitoring evaluations. The absence of detailed simulation models leads one to ponder various mechanisms, including:

- Street canyon vortices (with horizontal rotor axes) creating pollutant recirculation and trapping.

- Building corner vortices (with vertical rotor axes) evacuating the problematic, intersection region.

- Higher levels of ambient, mechanically induced turbulence.

- Lower mean flow velocities.

- Fewer instances of stable temperature stratification due to automotive and other urban heat sources, and whether the net overall tendency is to increase or decrease ambient concentrations.

The objectives of the present study are to:

- Investigate as many of these complex site geometry factors as can conveniently be studied in an unstratified-flow wind tunnel.

- Incorporate these measured effects into a mathematical dispersion model.

- Understand the limits of such a model as well as better understand the range of site geometry conditions under which it is appropriate to apply existing flat terrain models.

Detailed descriptions of the wind tunnel experiments are documented in Report FHWA-RD-02-037 of this study (R. E. Hayden, W.D. Kirk, G.P Succi. T. Witherow, I. Bouderba M. Raad, R. Fuller, and R. Betros, "Modifications of Highway Air Pollution Models for Complex Geometries- Volume II: Wind Tunnel Test Program"), but the overall experimental strategy was developed to:

(i) Consider variations in the basic geometric height (H), width (W), and length (L), of the rectangular-notch street canyon.

(ii) Consider the influence of "real world", two-dimensional phenomena such as unequal upwind/downwind canyon heights, sloping canyon walls, roadway curvature (quasi 2-D), and building porosity (to emulate semi-open garage structures).

(iii) Consider the influence of a few, distinctly three-dimensional phenomena, such as intersections and isolated tall buildings.

(iv) Simulate several specific geometries for which companion full-scale studies exist.

Such a multifaceted strategy was chosen to expand basic understanding of the notch flow problem (via studies i and ii),enable treatment of geometries of practical interest to the Federal Highway Administration (FHWA) (e.g., sloped retaining walls around depressed roadways) and Federal Aviation Administration (FAA) (e.g., the curved airport access road bounded by terminal and garage) via studies ii and iii, and permit connection to full-scale studies (via iv) to facilitate model evaluation. In such an ambitious, broad-spectrum study involving measurements of flow, turbulence, and concentration fields, one risk is that inadequate attention to any single dependence can leave quantitative or even qualitative gaps in understanding some phenomena (e.g., the qualitative nature of the flow changes several times as W/H is increased); however, a multiphased experimental program was chosen to minimize that risk. In addition, a separate 3-day airport pilot study was carried out at the Seattle/Tacoma International Airport (SEATAC) in Washington to establish a full-scale reference point for the complex problem of pollutant sources emitting on a curved roadway bounded by a solid building (i.e., the terminal) and a semi-open structure (i.e., a parking garage) across the street.

In the sections which follow an attempt will be made to:

- Review what is known from flat terrain highway modeling and experimental studies that have relevance to the street canyon environment.

- Consider the status of street canyon modeling, field studies, and wind tunnel studies.

- Analyze the experimental data obtained from this program to expand the useful validity range of the original Canyon-Plume-Box (CPB) model of Yamartino and Wiegand (1986).

- Evaluate applicability limits of this new model, CPB-III, and existing roadway models.

As most of the detailed analyses are described in appendixes A-H, the main report chapters will primarily compile and review the important results.

Section 7 summarizes the major findings of this study.

2. A REVIEW OF FLAT TERRAIN ROADWAY MODELS AND EXPERIMENTAL STUDIES

A. Introduction

Regulatory agency interest in the dispersion of mobile source emissions has generally focused on the localized carbon monoxide (CO)"hotspots"(Midurski, 1978) that can occur in the near vicinity of busy roadways and potentially create violations of the National Ambient Air Quality Standards (NAAQS) for 1-hr and 8-hr exposures to CO. Despite the fact that air pollution potential can be significantly enhanced in confined areas such as depressed roadways or urban street canyons, most of the model development and field evaluation work of the last decade has been concerned with relatively unobstructed, flat terrain environments. Samson (1988) provides a recent review of applicable models and experimental studies.

A major goal of this project is the development (or modification) of highway air pollution models for complex terrain and site geometry environments. Nevertheless, it is useful to review the open highway models and field studies as many of the phenomena important for near-source concentration levels are present in both the open and more complex environments. These common phenomena include:

- Initial dispersion due to vehicle induced mechanical turbulence.
- Enhanced dispersion and/or plume rise associated with vehicle heat emissions.
- Subsequent dilution determined by local wind flow and turbulence levels.

In this section, flat terrain, roadway models and field studies will be reviewed with particular emphasis on the afore-mentioned common phenomena. Section 3 will consider models specifically designed for the urban street canyon environment and full-scale studies used in their evaluation.

B. Flat Terrain Roadway Models

Most of the flat terrain, roadway air pollution assessment models in use today are of the Gaussian plume variety. This is because in this application Gaussian models:

- Are easy to formulate and code.
- Are inexpensive computationally.
- Are moderately flexible in terms of including a wide variety of phenomena.
- Have simple meteorological input requirements.
- Perform as well or better (Martinez et al. 1981) than more sophisticated numerical approaches.

The first two points are obvious given the very simple analytic expression for the coupling coefficient, C/q, whereas the moderate flexibility claim is perhaps a dubious distinction, as it is associated with the absence of any significant physics beyond mass conservation. The fact that mass conservation is maintained for arbitrarily defined plume standard deviations, $\sigma_y(x)$ and $\sigma_z(x)$ is, however, very useful and allowsone to focus efforts on building theoretical behavior or the results of observations into these plume "sigmas."

The Gaussian models, of which there are many, including EPA-HIWAY and HIWAY-2 (Zimmerman and Thomson, 1975 and Petersen, 1980), PAL (Petersen, 1978), CALINE (four different versions, see Benson 1984), and ALSM (Wang and Rote, 1975), generally use the Pasquill dispersion curves (Turner, 1970), approximate initial dispersion via initial sigmas, and are valid only for at-grade or cut section (n.b., some acceptable for elevated) roads in flat terrain. The models differ primarily in the technique used to approximate the line integral and in assumed initial sigmas. The GMG model of Chock (1978a) also falls into this category except that it makes use of further simplifying approximations (e.g., the dependence on wind angle is parameterized rather than obtained from integration of the line) gleaned from the General Motors roadway dispersion experiment (Cadle et al., 1976).

In terms of Gaussian regulatory models, only CALINE-3/4 (Benson, 1979 and 1984) and HIWAY-2 (Petersen, 1980) attempted to incorporate the effects of the early vehicle-induced turbulence into the dispersion algorithms through adjustment of the dispersion coefficients. These vehicle-induced effects were documented in the GM (Cadle et al., 1976 and Chock, 1980), the SRI Highway 101 (Dabberdt, 1977 and Dabberdt et al., 1981) and Long Island Expressway (Rao et al., 1979a) field programs, and their inclusion tended to mitigate model over-prediction problems (Rao et al., 1979b and Sistla et al., 1979) so prevalent (especially in stable cases) in the earlier versions of the regulatory models. The model intercomparison study of Martinez et al. (1981) ranks CALINE-3 as the "best overall" highway model. A subsequent highway model, TEXIN (Messina et al., 1983) developed for the FHWA has essentially incorporated the CALINE-3 algorithm as its dispersion algorithm.

Despite the successes of these open highway Gaussian models, a problem that has recurred is the evaluation of the line integral of the Gaussian plume kernel. Different approximations account for the differences between different models, as well as different versions of the "same" model (e.g., the CALINE series). Many of the approximations in current models are adequate for the far field (i.e., $\sigma(x) >> \sigma(0)$ but nearly all develop inaccuracies in the near field of a finite width line source (FWLS). The correct mathematical treatment of FWLS involves integration over an area source, and line source approximations generally lead to highly empirical formulations of $\sigma(0)$.

Several roadway dispersion models have also been developed utilizing the advection-diffusion equation; among them the models of Danard (1972), Ragland and Pierce (1973), Egan et al. (1973), Kirsch and Mason (1975), Eskridge and Demerjian (1977) Chock (1978b), and Eskridge et al. (1979). In addition to the possibility of treating nonlinear atmospheric chemistry (particularly NO_2 and O_3) in some of the aforementioned, these models appear to offer several fundamental advantages over the Gaussian models, but are often quite costly to run and suffer from K-theory related problems. The principal advantages of a grid model consist of the ability to include wind speed and direction shear and inhomogeneous turbulence through specification of the K-field. However, in addition to the difficulties of determining a K-field that can match regulatory agency dispersion curves, the grid size must be chosen small enough (e.g., 1 to 2m or 3 to 6 ft) so that important, near source impacts can be mathematically modeled. It should be noted that most photochemical grid models (e.g., the SAI model as applied by Weaving and Benjamin, 1980), designed for predicting oxidant formation over large time/distance scales,

generally put roadway emissions into a large grid cell and are thus incapable of predicting the higher "curbside" concentrations. A 2-D Lagrangian model, developed by Lamb et al. (1979), circumvents many of these problems and could be valuable in the assessment of peak NO_2 levels in the near vicinity (i.e., within a few minutes of transport) of roadways; however, the initial version suffered from excessive accumulation of Lagrangian "particles" in zones of low turbulence (Janicke, 1981). Legg and Raupach (1982) discuss the use of corrective drift velocities to compensate for turbulence gradients, but the need to specify σ_u, σ_v, σ_w turbulent velocity fields, as well as the more elusive Lagrangian time scale field, has inhibited widespread use of this technique.

Perhaps the feature of open highway models that is most likely to transfer over to the street canyon or complex terrain settings is the description of the initial, automobile induced dispersion. This phenomenon began to receive intense scrutiny when line source models were found to significantly overpredict in the near field of roadways and when near-roadway, vertical concentration profiles from intensive field studies began to provide the means for analysis. The most detailed of the vehicle-induced turbulence models to describe the observed effects evolved from the Eskridge and Hunt (1979) theory of the turbulent wake behind a single moving vehicle and is now an important component within the ROADWAY (Eskridge and Catalano, 1987) numerical grid model. Unfortunately, this theory is not easily transferred to a Gaussian plume model without further parameterization. A recent attempt at this by Groenskei (1988) suggests that the vehicle wake contribution to $\sigma_z(x)$ continues to grow as $x^{0.25}$ well away from the roadway and is also roughly proportional to $(V/u)^{0.25}$, where V and u are vehicle and wind

peeds respectively. This x dependence due to vehicles is conceptually somewhat more complex than the more usual notion of an initial sigma, $\sigma z(0)$, and yet is not a fundamental problem as the more rapid x growth due to ambient turbulence(e.g., $x^{0.5}$ to $x^{1.0}$) eventually dominates. Nevertheless, most open highway and street canyon models continue to describe the initial mixing by a $\sigma_z(0)$ sub-model. For example, the initial mixing in CALINE-4 is given as $\sigma_z(0) = 1.5 + 0.1*t$ where t is the travel time spent in the turbulent "Mixing Zone" affected by vehicle motions. Similarly, the HIWAY-2 model (Petersen, 1980) takes the greater of $\sigma_z(0) = 3.57 - 0.53u \sin |\Phi|$, where Φ is the angle between the roadway and wind directions, and 1.5m. Both these formulations attempt to capture the observed (e.g., Chock, 1977) effect that vertical dispersion increases as cross-road wind speed decreases. It is clear that both these $\sigma_z(0)$ formulations have also attempted to capture an effect which involves some mixture of vehicle and mean atmospheric dispersion effects.

The situation with respect to initial crosswind dispersion coefficients $\sigma_y(0)$ is less well defined, but this arises because:

- $\sigma_y(x)$ effectively disappears from the problem for most roadway line integrals and disappears completely for the infinite length line under perpendicular flow conditions (i.e., $\Phi = 90°$).

- The relation between $\sigma_y(0)$ and vehicle induced effects changes as a function of Φ (i.e., the perceived mix of along-vehicle and cross-vehicle dispersion changes).

- The line source problem does not allow for $\sigma_x(0)$.

Most conceptual problems disappear when the FWLS problem is considered but the practical difficulty of determining $\sigma_y(0)$ remains and, of course, the full FWLS solution is more computer intensive.

Relatively recent experimental and theoretical studies (e.g., Groenskei, 1988; Petersen et al., 1984; Eskridge and Thompson, 1982; Hunt, 1981; Eskridge and Rao, 1986; Thompson and Eskridge, 1987) suggest that yet more comprehensive formulations for $\sigma_y(0)$ and $\sigma_z(0)$ will be available for future roadway models.

C. Highway Monitoring Experiments

The last decade has seen a number of full-scale highway monitoring experiments. The three largest experiments were the General Motors sulfate experiment (Cadle et al., 1976), the SRI experiments along US-101 and I-280 in California (Dabberdt et al., 1981), and the Long Island Expressway study performed by the New York State Department of Environmental Conservation (Rao et al., 1979a). All of these involved use of SF_6 tracer gas, are described in some detail by Chock (1982), and are archived in a common data base documented by Martinez et al. (1981). This data base also contains the CO measurement data files from a Texas A&M University study by Bullin et al. (1980a) and a California Department of Transportation (CAL-TRANS) study by Bemis et al. (1977).

Several of these experiments measured concentrations directly adjacent to the roadway and were therefore used to determine initial vertical dispersion parameterizations for the CALINE-4 (Benson, 1984) and HIWAY-2 (Petersen, 1980) models.

In addition to pollutant concentration data, the General Motors and Long Island Expressway (LIE) studies involved extensive flow and turbulence data. Sedefian et al. (1981) and Rao et al. (1979 a and b) analyzed the GM and LIE data, respectively, and both observed enhancements in the turbulent energy spectrum in a range corresponding to eddies of order the size of an automobile.

A series of highway monitoring experiments conducted in Texas (Bullin et al., 1980b) included wind, turbulence, traffic and pollutant concentration data and considered "at grade" situations in three cities, an elevated roadway in Dallas, and a cut section in Houston. The cut section, Katy Freeway observations are of particular interest because the 16° pitch of the bordering embankment makes this a borderline case between an open highway and a street canyon situation. Wind tunnel measurements were made for the scale-modeled Katy Freeway site and are reported in volume II.

3. STREET CANYON MODELS AND EXPERIMENTAL STUDIES

A. Introduction

As discussed in the previous chapter, elaborate and well instrumented experiments have led to the development and refinement of a number of models suitable for predicting vehicle generated pollutant concentrations in the near vicinity of relatively open roadways. Comparable progress in the development of models applicable for regulatory use to the urban street canyon has, however, generally not occurred. The empirical STREET sub-model within the larger APRAC model (Johnson et al., 1973), developed and evaluated on the basis of a rather modest, full-scale experiment, contains empirical parameters that are found to vary with street canyon geometry in ways that are not fully understood and, unfortunately, largely ignored in model applications.

Fundamental issues such as the following were never adequately addressed:

- Determination of the street canyon vortex speed as a function of above-roof or other reference wind.

- Characterization of ambient turbulence levels within the canyon.

- Assessment of the relative or absolute efficiencies of turbulent vs. advective ventilation of the canyon.

- Determination of the fraction of pollutant recirculated, or alternatively, the pollutant residence time within the canyon.

Hence, consideration of the often-discussed, yet more subtle, effects include:

- The role of vehicle-induced momentum and thermally-generated turbulence.
- The significance of atmospheric stability,heat island effect, and differential canyon heating.
- The role of along-canyon dispersion.
- Three-dimensional (3-D) effects due to intersections, canyon asymmetries or variations, or nearby large and isolated buildings.

The foregoing effects were rendered moot, except in the purely theoretical and physical (i.e., wind tunnel) modeling arenas.

Despite increasing controls on vehicle emissions, the concern over CO "hot spots" has not gone away, and the 1980's have witnessed a resurgence of interest in the street canyon problem. In this section early as well as recent modeling and field studies will be reviewed to assess the current understanding of the problem.

B. Street Canyon Models

None of the models discussed in the previous section are currently applicable to the case of urban canyons, where separated, helical flow is often the dominant mechanism in determining curbside concentrations. Such vortex circulation was first described by Albrecht (1933), verified by Georgii et al. (1967)

and by Johnson et al. (1971) in urban areas, and simulated in the wind tunnel by numerous groups.

The complexity of the flow within the urban canyon and the paucity of full-scale experimental data has perhaps hindered the development and proliferation of models applicable to the urban canyon environment. The two basic two-dimensional urban canyon models in existence today, the empirically-derived STREET submodel within APRAC (Johnson et al., 1973) and the box model of Nicholson (1975) , are a decade old and have serious limitations.

The APRAC canyon model is given as

$$C_{lee} = C_b + Kq/\{(u + u_o)[(x^2 + z^2)^{1/2} + L_o]\} \qquad (1)$$

$$C_{luv} = C_b + Kq(H - z)/\{(u + u_o)HW\} \qquad (2)$$

where u is the approach wind speed at rooftop level, u_o is a minimal dilution parameter set to 0.5 (m/sec), q is the emission strength (g/m/sec) of the lane of traffic a distance x (horizontally) and z (vertically) from the receptor, and $L_o \cong 2m$ specifies an initial pollutant mixing length scale. The empirically determined constant, $K \cong 7$, is presumably valid for canyons having a height to width ratio comparable to the ratio, $H/W \cong 1$, of the San Jose study (Johnson et al., 1971). The model is recommended for all wind directions; however, for those within 30° of the canyon axis direction the concentration should be computed as the average of equations (1) and (2). The same algorithm appears in the Intersection Midblock Model (IMM) (Benesh, 1978) with the subsidiary condition

$$H > 7\ (DW/U)^{1/2}, \qquad (3)$$

where D is a stability-class-dependent diffusivity, but this criterion greatly limits the meteorological conditions for which (1) and (2) are applicable. Sobottka and Leisen (1980b) have made further modifications to the APRAC street canyon model in order to reproduce the Venloer Strasse (Eng. street) data showing the increase of concentrations as the leeside wall is approached; however, their "MAPS" model is otherwise quite similar in form and performance to APRAC.

The Nicholson (1975) model is a rather simple box model which yields street-canyon-average concentrations. Whereas the crude spatial resolution of this model has probably inhibited its use in regulatory settings, Nicholson's discussion of the basic physics underlying canyon ventilation is significant and fundamental. The extent to which ventilation is dominated by advective or turbulent transfer processes has yet to be decided for full-size canyons, despite recent data of De Paul (1984) (and De Paul and Sheih, 1985) suggesting dominance of turbulent transfer at the top of the canyon. The same controversy, of course, exists with wind tunnel data, yet neither the wake dominated, turbulent transfer dominance advocated by Hoydysh and Chiu (1971) and Hoydysh et al. (1974) or the advection dominance mechanism reported by Wedding et al. (1977) have been adequately evaluated.

The Federal Republic of Germany (FRG) sponsored a project to integrate full-scale and wind tunnel experiments in order to produce an urban canyon model for routine regulatory use, that would explicitly deal with:

- Atmospheric stability, including calm conditions.
- Nonuniformity of emissions in the along-canyon direction.
- Nonvortex and canyon-parallel wind conditions.
- Varying canyon geometry (in the form of varying canyon height-to-width ratios).
- Finite canyon lengths and receptor distance from the nearest upwind intersection.
- Concentrations at the nearest upwind intersection.
- Vehicle-induced turbulence caused by vehicle presence, speed, and thermal emissions.

This model, depicted schematically in figure 1 and documented in appendix H, contains sub models to define flow and turbulence fields within the canyon and then uses a simple Gaussian plume following the flow field and dispersing via time-dependent dispersion coefficients, established by the turbulence sub model, to compute concentrations in the lee of the canyon. The notion of pollutant recirculation then feeds material into a box model that is applied to both lee and windward sides "of the canyon; thus, the name Canyon Plume-8ox (CPB-1) Model. This model, which blends a number of 2-D and 3-D concepts and approximations, has undergone substantial refinement during this FHWA study. Resulting refinements to the flow and turbulence modules are described in section 4, whereas the resultant CPB-3 dispersion module is detailed in section 5.

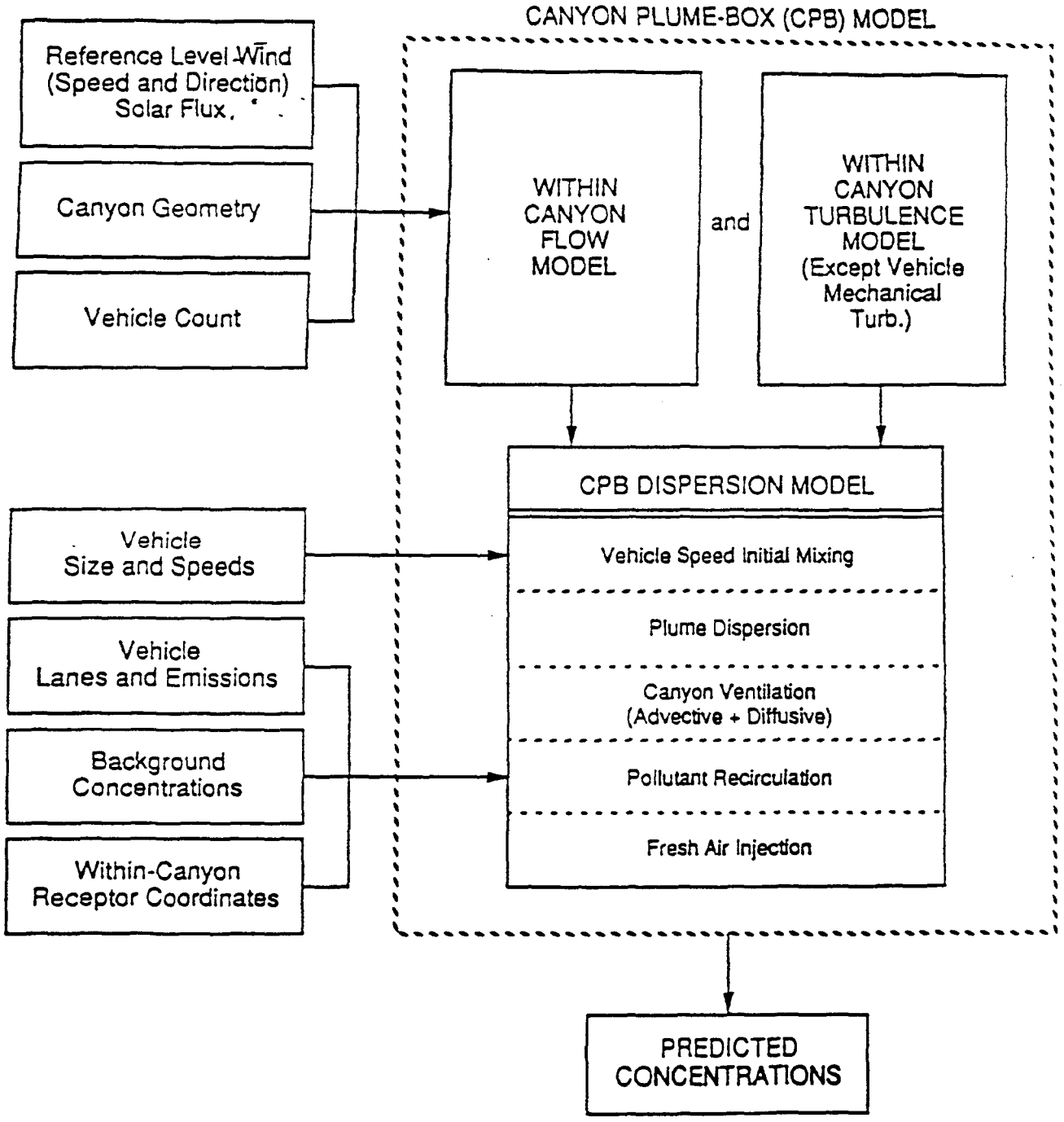

Figure 1. Structure of the Canyon Plume-Box (CPB) Model series showing inputs, outputs, and the three constituent submodels for flow, turbulence, and dispersion.

One component of the CPB-1 model also deals with the case of nonvortex dispersion. Advection directly down the street canyon is the clearest example of such nonvortex dispersion and is a case that can be treated directly with simple, straight-line Gaussian plume techniques. Pollutant reflections from the ground and building walls are included via the method of images, and the efficient summation method of Yamartino (1977) is used to reduce computational effort. Use of the image method to account for the confining effects of the buildings was also employed by Potenta et al. (1982) in their HWY2CAN model and found to yield reasonable results for a deep urban street canyon in New York City.

An alternative, K-theory based, analytic model for the deep street canyon was developed by Sontowski (1978) and later converted into the CANNY model (Spielberg, 1984). This model includes vehicle mixing via an enhanced K_z region near the street. Despite difficulties in specifying the profile $K_z(z)$ within the canyon, this model is used for routine evaluations by the New York City Department of Environmental Protection (DEP).

Finally, we note that a full 3-D numerical grid model which includes complex terrain and buildings has been developed by Kotake and Sano (1981); however, its stream function model for flow, simple diffusivity assumptions, and coarse grid (i.e., Δx = 20m) exclude many phenomena from consideration.

C. Street Canyon Field Studies

The existence of the secondary, vortex flow within the urban canyon was measured by Albrecht (1933); however, Georgii

et al. (1967) conducted the first major field experiment involving both flow field and pollution measurements, and their observation of higher concentrations on the leeward side of the canyon, rather than the windward side, was confirmed by the San Jose street canyon study of Johnson et al. (1973). Their extensive measurements of CO profiles within and above the canyon led to the development of the STREET algorithm within APRAC. Unfortunately, fairly limited measurements of flow and turbulence within the canyon restricted the level of modeling sophistication possible.

The more recent and more extensive TUEV Rheinland field studies in Venloer and Bonner Strasse have already undergone (Sobottka and Leisen, 1980 and Leisen and Sobottka, 1980) substantial analyses and comparison with wind tunnel flow and tracer studies. While this data base undoubtedly represents the most extensive urban canyon study to date, potential limitations arise simply from the multiplexing and data acquisition methods, as documented in Hauschulz et al. (1980). Specifically, measurements are not simple half-hour measures of mean and standard deviation. Instead, there was an underlying 6-minute cycle during which each instrument was interrogated for 1 minute at an instrument dependent sampling frequency (e.g., 2 seconds for u v w sensors and 5 seconds for CO values). Thus, each instrument is monitored for five, 1-minute periods within the half-hour. One can then easily imagine short-term episodes (i.e., of a few minutes duration) of turbulence or pollution that are seen by some but not all instruments; thus, creating some uncertainty in interpretation.

General Motors planned an ambitious street canyon study, analogous to their open highway experiment of Cadle et al.

(1976), but unfortunately, this proposed study fell victim to the recession of 1982. The U.S. Department of Energy (DOE) then sponsored a small but elegant study (DePaul, 1984; DePaul and Sheih, 1983 and 1985) within a Chicago street canyon that has produced some interesting and new types of measurements, including flow and turbulence fields measured with the aid of small neutral-density balloons and SF_6 measurements of the pollutant lifetime within a street canyon. Lamb (1978) also used SF6 to measure residence times within a canyon; however, as meteorological parameters were not measured in any detail,the usefulness of this study lies primarily in:

- Providing a confirmation that the pollutant lifetime concept is reasonable.

- Providing peak concentrations tha t can be used to estimate initial vehicle-induced mixing.

Lamb's average value of τ = 48 sec is consistent with a simple lifetime model, $\tau = \sqrt{2\pi}\ H/\sigma_w$,, for a canyon of order 15 m deep and a weak wind σ_w of 0.1-0.2 m/sec; however, more definitive statements do not appear possible. His measurement of a peak SF_6 concentration of $\cong 10^5$ ppt and the relation, $C = q/(2\pi\sigma_y\sigma_z)$, for the instantaneous concentration, is a bit suspect, as this value is well into the detector saturation region; however, his second highest value of 10,800 ppt suggests a $(\sigma_y\sigma_z)^{1/2}$ of 2.5m and interpretation of his highest value as exceeding 20,000 ppt suggests a value of $\leq$1.85 m.

A number of street canyon studies have also been conducted by State and local agencies involved with transportation related pollution problems. The Minnesota DOT (Mellem and Halvorson, 1985) measured CO at a number of locations around

University and Snelling Avenues in St. Paul and reported reasonable results using a calibrated version of IMM. The New York State DOT (Zamurs, 1984) conducted a 6-month CO monitoring study of several Syracuse streets exhibiting violations of the 8-hr. NAAQS for CO and showed the value of transportation control strategies in reducing violations. Finally, the New York City DEP (H.Nudelman, private communication) is currently (circa July, 1989) carrying out a deep canyon monitoring studies for East 42nd Street and Park Avenue (47-58 th streets) with the objective of testing and improving the predictive power of the CANNY model.

Data from these street canyon studies (and from Houston Texas and SEATAC -Appendix G) has been made available to this project, and comparable BU wind tunnel studies performed to assist in model evaluation and full-scale intercomparison efforts.

D. Wind Tunnel Studies

Roshko (1955) was perhaps the first to explore the situation of skimming primary flow with secondary vortical flow in the 2-D notch by means of a wind tunnel. Hosker (1983, 1987) provides a summary of some early findings with particular attention given to the transition between wake interference and skimming flow regimes. Hoydysh and Chiu (1971) measured tracer concentrations within a relatively complex array of blocks, made a qualitative comparison with the full-scale study of Georgii et al. (1967), and further identified the intermittent existence of corner vortices with vertical axes. Subsequent studies by Hoydysh and Ogawa (1972), Hoydysh et al. (1974), and Hoydysh and Piva (1975) showed the importance of proper conditioning of the approach flow and suggested Reynolds number independence for values above 3400. These studies also suggested that concentrations fall exponentially with increasing

wind speed, u, rather than as u^{-1} and attributed this to making measurements between roughness elements rather than above them; however, their data do not appear inconsistent with a more rapid power law fall of, such as u^{-3}, which has a better theoretical basis. While some of the other features, such as rapid fall of concentration with height in the canyon and increased concentration with increased building density, agree qualitatively with those of full-scale studies, these wind tunnel studies were not done in a systematic way that would enable one to isolate and understand the fundamental phenomena.

Flow in a simple 2-D notch with unit height to width ratio was investigated by Wang et al. (1972) in a water tunnel. Their flow measurements, scaled for a Reynolds number of 2.1×10^{4}, showed a clear vortex completely contained with the notch. Hotchkiss and Harlow (1973) obtained reasonable agreement between these data and their simple flow model based on vorticity conservation.

Cermak et al. (1974) and Wedding et al. (1977) also studied the urban canyon of near unit height to width ratio and found high concentrations near the lower corners of the buildings adjacent to the line source. They also concluded that advection was the dominant mechanism for ventilating the canyon, in direct contrast to Hoydysh et al. (1974) who concluded that turbulent transfer constituted the dominant ventilation mechanism.

Kitabayashi et al. (1976) simulated street canyon flow in a scale model of central Tokyo. Their data further indicated the complexities introduced by vertical-axis, building corner vortices and cross streets, the small effect of ambient stability on dispersion, and the dramatic increase in turbulence and

accompanying decrease in concentrations caused by moving vehicles as compared with static scale model vehicles. This was also a major finding of the CALSPAN study (Skinner and Ludwig, 1976).

Leisen and Sobottka (1980) also included moving vehicles in their scale model companion study to the full-scale study of Venloer and Bonner Strasse, Cologne. They indicate excellent agreement between wind tunnel and full scale dimensionless concentrations $C^* = CuW/Q$ (where W = canyon width) but their analysis of what appears to have been a rather extensive wind tunnel study, offers little additional insight into urban canyon dispersion phenomena.

Builtjes (1983, 1984) has also conducted a wind tunnel study of Bonner Strasse. His 1983 flow measurements also showed reasonable correspondence with the Hotchkiss and Harlow (1973) model. The turbulence field, found to be rather slowly varying throughout the canyon with a maximum near the windward location of the stagnation streamline, was found to be in qualitative agreement with the full-scale study.

Recent studies by Hoydysh and Dabberdt (1986) show the importance of the corner vortices at intersections in advecting material, emitted in upwind canyons, into the street canyon. They also report flow velocities for the step-up and step-down notch and conjecture an exponential, vertical concentration profile for both lee and downwind cavity faces.

4. ANALYSES OF WIND TUNNEL EXPERIMENTS TO IMPROVE STREET CANYON FLOW AND TURBULENCE MODELS

A. Introduction

The original CPB-1 model (Yamartino and Wiegand, 1986 and reprinted as appendix H of this report) contained modules for the flow and turbulence fields based on the analytic flow model of Hotchkiss and Harlow (1973) and a simple, empirical decomposition of the turbulence into mechanical and heat flux components. The main obvious limitations stem from the fact that the appropriate reference height for the above roof wind and all the turbulence model parameters come from the analysis of a single street canyon with peaked roofs and a width-to-height, W/H, ratio of 1.09. The wind tunnel data of Builtjes (1983,1984) suggested that the flow model might be reasonable over the W/H range of 0.5 to 2.0 and that a turbulence correction factor might be appropriate over the same W/H range. However, the need to generalize the CPB-1 model to encompass a wider range of W/H, unequal building heights, curved streets, semi-open or porous buildings, intersections and the addition of a isolated tall building, then required that a systematic wind tunnel experimental program be carried out to explore these phenomena.

In the sections which follow, we first consider the issues surrounding interpretation of the single hot-wire data measured at the BU wind tunnel and then proceed to extract appropriate parameterizations of the effects of various variables on the flow and turbulence fields. Details of the various procedures and analyses are presented in appendixes A-C.

B. Hot-Wire Measurements in Highly Turbulent Environments

A single hot-wire anemometer senses the instantaneous speed of the flow transverse to its axis. Because it is insensitive to the direction (or sign) of the velocity, a turbulent flow having a mean velocity, u, of zero will be measured to have a distinctly positive mean speed, V. While the required correction is most extreme for the zero mean velocity case cited, it can have a serious impact on the characterization of flows having a turbulent intensity, $i_u = \sigma/u$, exceeding 0.3-0.4. As the street canyon flows are almost always more turbulent than this, understanding and being able to model this problem became a prerequisite task of this study. The detailed analyses in appendix A culminate in the development of an iterative solver to go from the V, $i_V (\equiv \sigma_V/V)$ representation of the observations to the needed u, σ representation. This conversion algorithm is primarily based on the assumption that turbulent velocities are exponentially distributed (an assumption which is evaluated to a limited extent). Thus, the distinction between modeling and measurement becomes somewhat blurred in that the use of the data itself requires a model.

C. Modification to the Hotchkiss-Harlow Flow Solution

In appendix B, we begin with the Hotchkiss and Harlow (1973) solution for flow velocity components u (horizontal) and w (vertical) within a 2-D notch canyon of width, W, and height, H.

Their solution is

$$u = u_o(1 - \beta)^{-1}[\alpha(1 + ky) - \beta(1 - ky)/\alpha]\sin(kx) \quad (4)$$

and $$w = -u_o ky(1 - \beta)^{-1}[\alpha - \beta/\alpha]\cos(kx) \quad (5)$$

where $k = \pi/W$, $\beta = \exp(-2kH)$

$\alpha = \exp(ky)$, $y = z - H$,

and u_o is the external, driving wind speed which their solution is designed to match at the point $x = W/2$, $z = H$.

This reference driving wind u_o is not an obviously available quantity but arguments are presented in appendix B for setting $u_o = 0.65\ u_g$, where u_g is the better defined (i.e., at least in the wind tunnel) geostrophic wind.

The influences of various factors on the rotor velocity are then systematically examined and expressed as multiplicative correction factors for equations (4 and 5). These are determined via optimization studies to be reasonably represented as:

$$f_{W/H} = \begin{cases} 1.0 \text{ for } W/H \leq 1.5 \\ 1.0/[1.0 + 0.6 * (W/H - 1.5)^{1.2} \\ \quad \text{for } 1.5 < W/H \leq 6.0 \end{cases} \quad (6)$$

for W/H variation;

$$f_{\Delta H} = 1.0 + 1.08 * \Delta H/H_M \quad (7)$$

for differential building height, ΔH,

where $\Delta H \equiv H_D - H_U$, $H_M \equiv (H_D + H_U)/2$, and

equations (4 and 5) are evaluated using the smaller of downwind building height, H_D, or upwind building height, H_U;

$$f_p^D = 1.0 - 0.86p \text{ for porous downwind buildings and} \qquad (8)$$

$$f_p^U = 1.0 - 0.44p \text{ for porous upwind buildings}$$

and where the porosity is just the degree of openness, such that $0 \leq p \leq 1$; and

$$f_c^+ = 1.0 + 1.15\, d^{0.1}/(W/H)^{0.5} \text{ for } d > 0 \qquad (9)$$

$$f_c^- = 1.0/[1.0 - 2.6d(W/H)] \text{ for } d < 0$$

for positive and negative canyon curvatures, $d \equiv W/D$, and where D is the diameter of the curved canyon roadway center and $d > 0$ for canyons bending "with the flow."

These various individual correction factor formulae, along with the conjectured total, composite correction factor,

$$f_T = f_{W/H} \cdot f_{\Delta H} \cdot f_p \cdot f_c \qquad (10)$$

and its limitations are discussed in appendix B and are implemented into the new street canyon model CPB-3.

D. Modifications to the Empirical Turbulence Model

The empirical turbulence model in CPB-1 was chiefly criticized because (i) it was formulated in terms of the above roof flow velocity, u_o rather than scalar speed, V_o (which can also be a scarce commodity) and (ii) it contained a constant term A_c providing some minimal level of turbulence. The difference between u_o and V_o is generally negligible, except when u_o goes to zero, V_o does not, which also accounts for the need for the constant A_c. The old turbulence model was also heavily tuned to the Bonner Strasse data base and any explanation of spatial variation was completely absorbed into a single multiplicative constant for each u-v-w sensor.

The new turbulence model for the mechanically drive piece can be expressed as

$$\sigma_m/V_o = g(V_o)\,(\cos^2\theta_o + \alpha^2\sin^2\theta_o)^{1/2}\, e^{[-.65(H-Z)/W]} \;/[1 + p'] \qquad (11)$$

where $g(V_o) \equiv (1 + aV_o)/(1 + aV_o/A_m)$, and

$$p' = \begin{cases} 1 \text{ for } W/H \le 3.0 \\ 0.21\,(W/H - 3.0)(H-z)/H \text{ for } W/H > 3.0, \end{cases}$$

$a \cong 0.5 - 0.6$ and $A_m \cong 0.12 - 0.17$.

Specific values for parameters a and A_m depend on the particular turbulence component (i.e., u, v, or w) of interest and are tabulated in appendix B for the peaked roof buildings of Bonner Strasse. Values of A_m for the flat roofs of this wind tunnel study are estimated as being about 31 percent larger.

As the wind tunnel studies shed no light on heat flux terms, the new model retains the original heat flux term, $A_h \cdot h$, where the heat flux, h, involves the sum of solar flux and an automotive flux that is assumed distributed across the full width of the canyon. Whether the exponential term, $\exp[-0.65(H - z)/W]$, should apply to these heat flux terms as well, is a question that cannot presently be fully answered, though the CPB-3 model assumes that it applies to all turbulence terms because of the "filtering" effects of the lower boundary (i.e., the street) on the turbulent energy spectrum.

As with the flow velocity, multiplicative correction factors have been developed for the turbulence field via optimization studies. These correction factors, g, are currently represented as:

$$g_{\Delta H} = 1.0 + 1.08\ \Delta H/Hm \tag{12}$$

for differential building height, ΔH;

$$g_p^D = 1.0 - 0.32p \quad \text{for porous downwind buildings, and}$$

$$g_p^U = 1.0 - 0.10p \quad \text{for porous upwind buildings; and} \tag{13}$$

$$g_c^+ = 1.0/[1.0 + 18d^{1.9}/(W/H)^{1.7}] \text{ for } d > 0$$

$$g_c^- = [1.0 + 1.44(-d)^{0.15}]/[1.0 - 6.4d] \text{ for } d < 0 \tag{14}$$

A correction factor for W/H ratio was not needed as the full W,H dependence is already built into equation (11).

Modeling of the total, composite correction factor,

$$G_T = g_{\Delta H} \cdot g_p \cdot g_c \qquad (15)$$

was also evaluated and found to be more reasonable for turbulence than the corresponding equation (10) for mean flow. It is conjectured that the more incoherent nature of turbulence relative to the more organized nature of the mean flow, make it a better candidate for the independence(or factorization) assumptions implicit in equations (10) and (15).

E. Spectral Characteristics of the Flow

In order to shed further light on the nature of the flow and the production and decay modes of the turbulence, a spectral analysis of the hot-wire data was undertaken. Described in appendix D of this report, a qualitative finding was that turbulence near the bottom-center of the W/H = 1 canyon is similar in character to that observed in the relatively unperturbed flow above the canyon. In addition, turbulence in the lower corners of the canyon showed the effects of the pronounced high-pass filtering due to the presence of the wall boundaries. Finally, the high-shearregion at the top of the canyon is extremely turbulent and showed an anomalous (i.e., not seen at other points) spectral peak at frequencies in the range of f = u/W. No specific mechanism for this effect has been proposed.

5. DEVELOPMENT OF THE CPB-3 DISPERSION MODEL

A. The CPB Modeling Strategy

Assuming a given source strength, two of the most influential factors determining pollutant concentrations are the dilution wind speed and the rate of plume growth in the directions perpendicular to the flow. As depicted previously in figure 1, these two factors have been compartmentalized into the CPB flow and turbulence modules, respectively, and are themselves dependent on meteorological and canyon geometry variables. Generalization of these modules for a variety of canyon geometry variables has been accomplished with the aid of extensive hot-wire measurements of flow and turbulence and is described in section 4 (plus appendices A-C). The output of these modules then serves as input to the CPB dispersion module. The CPB dispersion module itself consists of a number of sub-models which allow computation of the various mechanisms that influence pollutant dispersion. Figure 2 depicts many of the mechanisms, including:

- Initial, vehicle-induced mechanical mixing.
- Subsequent plume dispersion along the rotor path and approximated as plume segments P1, P2, and P3.
- Pollutant exchange at the canyon top via advective and diffusive (i.e., turbulent) flux exchange.
- Pollutant recirculation.
- Fresh air injection near the downwind wall compensating for the advective venting of the canyon.

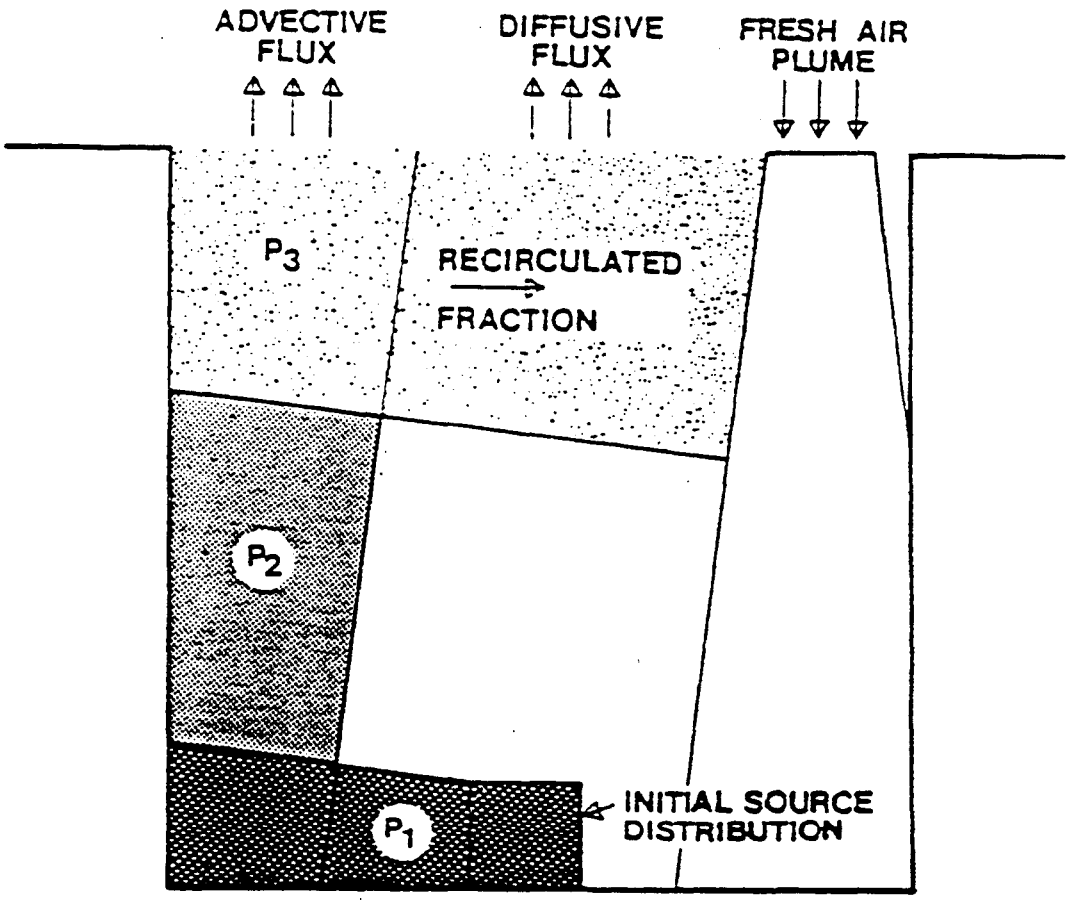

Figure 2. Schematic diagram of the principal mechanisms of the vortex submodel in the canyon plume-box model. Components are described in the text.

Not easily depicted, but also accounted for, are corrections for alongwind diffusion, wall reflections of pollutants, intersections, and wind direction meander. Additional details of the CPB-3 dispersion module will be described in subsequent subsections.

B. Limitations of the CPB-1 and CPB-2 Models

The CPB-1 model was extremely successful in describing the Bonner Strasse observed concentrations of NO_x and CO. The simpler, computationally faster, yet slightly less fundamental CPB-2 (Garben et al., 1987) performed quite well on additional concentration databases from two street canyons in West Berlin and two other canyons in Frankfurt. In several of these "hands-off" model applications, the lack of solar flux data was compensated for by an algorithm to estimate solar flux based on latitude, longitude, day and time.

Nevertheless, both CPB-1 and -2 have a number of limitations that we have attempted to eliminate in this version. For example, for near canyon parallel flows, CPB-1 used a computationally expensive numerical integration scheme to evaluate line source impacts. In CPB-2, this scheme was replaced by an approximation that was valid only for infinite lines so that intersections could no longer be accommodated. During this project we developed a new solution for the finite-length line source at an arbitrary angle to the wind. The theoretical development is detailed in appendix E. This new finite line source equation also includes correction for finite lane or roadway width, a feature formerly only present in the nonvortex portion of CPB-1. Unfortunately, at low canyon-transverse advective velocities, it is necessary to consider the multiple reflections of pollutants from the canyon walls, and the same

approach (i.e., as in appendix E) yields solutions involving differences of the incomplete Gamma function. High accuracy computations of this function can be more computer intensive than the numerical integration used in CPB-1. Thus, while the results of appendix E are directly applicable for open highway modeling, additional effort is needed to make the approach practical for street canyon environments. The CPB-3 model therefore continues to use the numerical integration procedures of CPB-1.

In addition, before considering new, specific 2-D and 3-D generalizations, we note that both CPB-1 and -2 employed a vehicle-wake induced, initial mixing algorithm that involved three fitted parameters, which sensitivity studies (Garben et al., 1987) showed to be very weakly constrained. In appendix F, a comparison of this model (with re-optimized parameters) with the detailed Eskridge and Hunt (1979) vehicle wake theory, that incorporates the results of many block-like and realistic shaped vehicle studies from the wind tunnel and full-scale, shows that the simple model provides an excellent fit to their vehicle velocity dependence predictions computed using the ROADWAY (Eskridge and Catalano, 1987) numerical grid model. This improved version of the vehicle turbulence model is also consistent with the Bonner Strasse data and is incorporated into the CPB-3 model.

Finally, the CPB-1 model, as fully described in appendix H, could not begin to accommodate a situation as complex as the curved SEATAC access roadway and street canyon defined by a curved terminal building and a semi-open parking garage. The new CPB-3 can incorporate the basic geometry of the airport, accommodate the types of meteorological and traffic data acquired during the 3-day pilot study at SEATAC (i.e., as

described in appendix G), and compute realistic estimates of access roadway emissions impacts.

C. Generalizations in 2-Dimensions

As the CPB structure is such that flow and turbulence modules serve as "inputs" which drive rather straightforward dispersion models, the refinements to the flow and turbulence models, described in section 4 and appendices B and C, respectively, basically provide the capability to include the width-to-height ratio, differential building height and building porosity generalizations. Thus, no correction factors to the concentration field within the canyon are envisioned or justified with the exception of sub-grid-scale (SGS) details, such as the presence of small, overhanging canopies, which are not included in, or resolved by, the flow and turbulence models. The clean air jet in CPB-1 is another example of an SGS correction inserted to reproduce vertical concentration profiles at the downwind building. The recent work of Hoydysh and Dabberdt (1986) again confirms the presence of a distinct profile, decreasing with height, which they characterize using an exponential. Rather than adopt such an empirical approach, we have chosen to generalize the sub-model for the clean air jet. At present this simply consists of rescaling the size and position of the jet proportional to canyon width.

D. Generalizations in 3-Dimensions

Inclusion of the curvature correction factors f_c and g_c into the flow and turbulence modules, respectively, permits the CPB model to accommodate roadway/canyon curvature. Such a correction can be thought of as a 3-D, or at least a 2 1/2-D generalization; however, the use of a single hot-wire probe did

not permit determination of an axial flow component in this case, whereas the smoke visualization studies showed clear signs of axial flow divergence for the positive curvature case and convergence for the negative curvature case. Such divergence or convergence can be compensated for by injecting clean air from above the canyon (or exhausting canyon air in the convergence case). This additional advective term, much like the clean air jet, could be developed to satisfy observed trends in the concentration patterns; however, this task is made more difficult because the curved canyon tests involved a point source within the canyon rather than the line source employed in the straight canyon studies. Thus, a special within-canyon point source dispersion model would have to be constructed to bridge the point source - line source "gap." In any case, a more physical model based on measured axial flow speeds would be preferable. At present, no additional corrections for curvature, beyond those for flow and turbulence, have been incorporated into CPB-3.

The existing CPB-1 model is able to account qualitatively for the near-intersection, along-canyon variations in concentrations observed in the BU studies and in earlier studies (e.g., Lombardi, 1978; Wedding et al., 1977; Hoydysh and Dabberdt, 1986); however, more quantitative predictive power (very near to or in the intersections) may require the addition of a vertical exchange flux corresponding to the influence of the vertical-axis, building corner vortices known to be present at intersections. As an existing intersection model already involves a flux conservation assumption, the additional vertical flux term requires some specification of the effective vortex size and its axial pumping velocity. This additional flux term has not yet been added due to a lack of quantitative

understanding of the variables controlling these vertical axis rotors.

One example of an isolated upwind building superimposed on a 2-D street canyon (plus one case of an isolated downwind building) were considered in the BU wind tunnel program and indicates an axial flow convergence (divergence) similar to that seen in the curved canyon studies. Other wind tunnel studies (e.g., Britter and Hunt, 1979; Wise, 1971 a and b) of this phenomenon, that were oriented toward street-level wind speed-up, indicate that the size of the influence is related to all dimensions involved (i.e., building height, length, and width plus canyon height and width). Thus, while qualitative estimates of the size the effect on concentrations can be given, existing data do not provide an adequate basis for inserting an isolated building sub-model into the existing code.

E. The CPB-3 Dispersion Model

The CPB-3 dispersion involves a series of assumptions and sub-models that are now considered in some detail.

Canyon Flow and Turbulence Averaging

As substantiated in appendix H, the above-roof reference wind is first decomposed into cross-canyon and along-canyon components, u_o and v_o, respectively. The Hotchkiss-Harlow flow field equations, (4) and (5), multiplied by the transverse flow correction factor of equation (10), are then used as interpolators to define integral average transport velocities u_b, U_t, w_{lee}, and w_{luv} along the bottom, top, and lee and luv sides, respectively, of the canyon. An average along-canyon velocity,

v, is computed by vertically averaging the simple logarithmic profile,

$$v(z) = v_r \log [(z + z_0)/z_0]/\log [(z_r + z_0)/z_0], \qquad (16)$$

where v_r is the value at reference height z_r and z_0 is surface roughness. In the current model, z_0 is generally fixed at 0.04m to reflect the roughness of the canyon walls. However, for above-roof wind directions within 22.5 degrees of canyon parallel, this roughness is reset to 0.05*H, which is more typical of urban scale roughness lengths and consistent with the BU measured profile in appendix B. However, it should be noted that equation (16) is being used to specify the wind between the roughness elements rather than far above them, as is the common usage of the log profile.

Averaged values of the turbulent velocity standard deviations are then computed by first scaling the mechanical turbulence terms, σ_m, of equation (11) by the turbulence correction factor of equation (15) and then adding in the thermal turbulence terms developed from the full-scale Bonner Strasse study. Turbulence at the top and bottom corners of the canyon is then computed as:

$$\sigma = \sigma_m \cdot g_T \cdot f' + A_h \cdot (S + N_a e_a/W)f, \qquad (17)$$

where A_h is a parameter which describes the increased turbulence driven by the total solar radiation S (in kW/m^2 as measured or as estimated from solar angle and cloud cover) and the equivalent vehicle generated heat flux, computed as the product of the number of vehicles per second, N_a, times the heat loss per vehicle per meter of travel, e_a, divided by the

effective transverse dimension this heat is dissipated over assumed to be the full canyon width, W, in this problem.[1] This addition of automotive and solar-induced heat fluxes was also used successfully by Benson (1984) to compute Pasquill stability class using Smith's (1972) monogram. The factors f and f' are designed to describe the spatial variability of the turbulence field σ_i over the canyon and are known to vary slowly over the W/H = 1 canyon.

The parameters for u and w turbulence components are presented in table 1 and involve an admixture of full-scale and BU wind tunnel results. It should be noted that the bottom f' factors are simply the bottom f factors scaled upward to yield a mean of 1.0. This is appropriate as the explicit z dependence of the within-canyon variation of the mechanical turbulence is now explicitly included in equation (11). Finally, appropriate pairs of turbulence values are chosen to form averages for u and w components along the top, bottom, lee, and luv flow paths.

If the cross-canyon turbulence σ_{ub} divided by the cross-canyon advection speed u_b, both defined at block vehicle half-height above the street, exceeds 4.0, then turbulence is assumed to dominate over advection, and a major algorithmic split occurs.

Nonvortex Dispersion Model

For $\sigma_{ub}/u_b > 4.0$, cross-canyon turbulence dominates advective transport, and no vortex flow is assumed.

---

[1] Bottom is evaluated at $H_V/2$ where H_V is the height of the block-like vehicle.

Table 1. Optimal parameters for the turbulence model given by equations (11), (15), and (17).

Turbulence Component	σ_u	σ_w
e_a(kJ/m)	7.5[1]	7.5[1]
A_m	0.117	0.127
α	0.641	0.805
a(s/m)	0.486	0.586
A_h (m^3/kW/s)	0.287	0.345
f (top, luv)[2]	1.0	1.0
f (bot, luv)	0.647	0.709
f (top, lee)	0.773	0.810
f (bot, lee)	0.618	0.576
f' (top, luv)	1.0	1.0
f' (bot, luv)	1.0226	1.1033
f' (top, lee)	0.773	0.810
f' (bot, lee)	0.9774	0.8967

[1] Assumed auto heat output
[2] f (top, luv) is defined to be 1.0

Concentrations are then computed by assuming a plume diluted with velocity v and traveling parallel to the canyon axis. Plume dispersion parameters are then defined as

$$\sigma_x(t) = B\ell / \sqrt{2\pi} + \sigma_u * t \qquad (18)$$

$$\sigma_z(t) = H\ell / \sqrt{2\pi} + \sigma_w * t \qquad (19)$$

where $B\ell$ is the input lane width in meters, σ_u and σ_w are the four path averaged values previously discussed, and t is travel time along the canyon. The lane height $H\ell$ is given as a function of vehicle speed, V, as

$$H\ell = H_V(0) + H_V(\infty) * [1.0 - \exp(- V/V_C)] \qquad (20)$$

where $H_V(0)$ and $H_V(\infty)$ are length scales determined in appendix F to describe the height of the well-mixed zone behind the vehicle for a range of vehicle speeds and V_C is a vehicle speed representing the transition speed from low speed to high-speed induced wake regions. For a block-like vehicle 1.5m (4.9 ft) high, these parameter values are $H_V(0)$ = 0.26m (0.85 ft), $H_V(\infty)$ = 3.40m (11.15 ft), and V_C = 55 km/h (34 mph). The height scales are then scaled proportionally to actual input vehicle height. The Gaussian plume equation is then numerically integrated along the canyon for each lane of traffic until the upwind intersection is reached or until the advection/diffusion travel time exceeds five lifetimes τ, defined in terms of the e-folding time

$$\tau = (e - 1.0) * H/\sigma_w \qquad (21)$$

Pollutant reflections from the ground and building walls are included via the method of images and the efficient summation method of Yamartino (1977) is used to reduce computational

effort. Use of the image method to account for the confining effects of the buildings was also employed by Potenta et al. (1982) in their HWY2CAN model and found to yield reasonable results for a deep urban street canyon in New York City.

Vortex Dispersion Model

For $\sigma_{ub}/u_b \leq 4.0$ the somewhat more complex, vortex model depicted in figure 2 is used, and it is this model which combines the concept of plume modeling with box modeling of pollution that is recirculated repeatedly by the vortex. In addition, this model considers concentration inhomogeneities on the luv side created by the intrusion and entrainment of clean air, incorporates variations in the along-canyon emission rate, and allows for the presence of intersections. Each of these model features will now be considered in detail.

- Plume model

The largest impacts occur on the lee side where the direct impact of plume P_1 is combined with the recirculated concentration component C_R. As in the case of the non-vortex plume model, the vertical dispersion is given by equations 19 and 20, except that the turbulence, σ_{wb}, near the bottom of the canyon is used in place of the canyon average value σ_w. Along-plume, x, and along-canyon, y, dispersions are ignored as the steady-state, infinite length and perpendicular line source form of the Gaussian plume equation with dilution velocity u_b is assumed.

Rather than deal with a single plume that follows the curved path specified by the wind field module, we assume that the three straight line plumes, P_1 - P_3, provide an adequate

approximation. Initial plume spreads for plumes P_2 and P_3 are computed by taking the sigmas computed using P_1 and P_2 at the canyon lee wall and canyon top, respectively, and pivoting this length clockwise 90 degrees about the lower left and upper left corners of the canyon, respectively. Transport time, t, to a receptor is computed based on the local wind speeds u_b, w_{lee}, and u_t for plumes 1, 2, and 3, respectively, and pseudo-transport times are used to ensure that initial sigmas correspond to the simple geometrical picture described above. Along-plume dilution is nevertheless based on the initial dilution, $1/u_b$, for all three plumes. Since it is not known in advance, for many receptors, which of the three plumes will generate the largest coupling coefficient, all three are computed, and the largest taken as the most direct and hence the most physically reasonable. Plume reflections from the neighboring material surface are also considered. Finally, these direct impact concentrations are added to estimates of the vortex recirculated pollutant concentrations to yield a total (less ambient background) concentration.

- Pollutant Recirculation Model

Estimation of the recirculated concentration, C_R, or the fraction of material, F, that is recirculated requires consideration of the mass budget within the canyon. There are several ways to consider the mass budget within the street canyon. The simplest is to consider the canyon as a first-order linear system of volume (per unit length of canyon) WH, being supplied emissions (per unit length of canyon) at a rate q, and being depleted at a characteristic time scale or lifetime τ. This leads to a uniform canyon concentration of

$$C_R = q\tau/(WH) \qquad (22)$$

that is reasonable only if all time scales associated with pollutant mixing within the canyon are short compared to r. Given the dramatic anisotropy of within canyon concentrations and that SF6 tracer determined lifetimes of 0.5-4 minutes (Drivas and Shair, 1974; Lamb, 1978, De Paul and Sheih, 1983) in street canyons are of the same order as transport times, equation (22) is useful only as a large τ consistency check for a more detailed model.

Considering only the well-mixed component, C_R, and postulating that material depletion occurs by a combination of turbulent transfer at an effective "velocity" $\sigma_{wt}/\sqrt{2\pi}$ at the top of the canyon and advective flushing by a "jet" of clean air of size σ_j and speed w_j, the mass balance equation in the absence of emissions is just

$$(H*W)\ \frac{dC_R}{dt} = -C_R\ \{W'\sigma_{wt}/\sqrt{2\pi} + \sqrt{2\pi}\ \sigma_j w_j\} \qquad (23)$$

where $$W' = W - 2\sqrt{2\pi}\ \sigma_j \qquad (24)$$

is the width of the canyon where turbulent exchange processes are not overpowered by advective inflow and the corresponding out-flow. Equation (23) has the solution $C_R(t) = C_R(0)\ \exp\{-t/\tau\}$ with the lifetime τ expressible in terms of advective and diffusive components τ_A and τ_D, respectively, as

$$\tau^{-1} = \tau_A^{-1} + \tau_D^{-1} \qquad (25)$$

where $$\tau_A^{-1} = \sqrt{2\pi}\ \sigma_j\ w_j/(H*W) \qquad (26)$$

and $$\tau_D^{-1} = W'\sigma_{wt}/(\sqrt{2\pi}\ H*W) \qquad (27)$$

A somewhat more phenomenological way to envision recirculation is to consider the emissions q diluted by the velocity u_b, traveling up the lee half of the canyon, attenuated by the factor F, and traveling down the luv side. This cycling of material repeats itself indefinitely and yields the concentration

$$C_R = q \bullet [F+F^2+F^3+..] / [U_b \ (W/2)]$$
$$= q \bullet F / [U_b \bullet (W/2) \bullet (1-F)] \qquad (28)$$

where F, bounded by 0 and 1, must be expressible in the form

$$F = \exp\{-t_s/\tau\} \qquad (29)$$

with t_s as a yet undetermined time scale. In the very long lifetime limit, $F \cong 1 - t_s/\tau$, and matching between equations (28) and (22) constrains t_s

to be $$t_s \cong 2H/u_b$$

Equations (25-27) and (28-29) now provide a complete model for the recirculated concentration C_R that is intuitively appealing and can be more rigorously justified by including emissions and direct plume losses into equation (23).

- Clean Air Jet

The recirculation model just described leads to a uniform concentration C_R predicted for the luv side of the canyon; however, Johnson et al.(1973) observed a strong luv side vertical dependence that they parameterized as (H-z)/H. While

Bonner Strasse and BU wind tunnel data do not show such a pronounced luv side z dependence, the intrusion and entrainment of the hypothesized clean air jet should give rise to concentration gradients on the luv side.

There are several ways to model a clean air jet, but simplicity and consistency with the other plume elements suggests a form

$$C(x,z)=A_j C_R \left[1-(\sigma_j/\sigma_x(z))\exp\{-1/2(x-x_jj)^2/\sigma_x^2(z)\}\right] \quad (30)$$

where A_j is determined from the normalization condition

$$C_R \equiv (2/W) \int_{W/2}^{W} dx\, C(x,z)$$

to be

$$A_j=\{1-\sqrt{2\pi}\sigma_j/W[\mathrm{erf}\,\frac{W-x_j)}{\sqrt{2}\,\sigma_x(z)}-\mathrm{erf})\frac{(W/2-x_j)}{\sqrt{2}\sigma_x(Z)}]\}^{-1} \quad (31)$$

$$\sigma_x(z)=\sigma_j+\sigma_U, \text{ luv } .(H-z)/w_j \quad (32)$$

and x_j, σ_j (and w_j) are yet to be determined parameters of the clean air jet describing its position, size, and initial strength, respectively. As the presence of three parameters is rather excessive for a "correction term", w_j was constrained to be the vertically averaged value of the flow model w value at the optimal position of the jet $x = x_j$. With the flow jet speed fixed, σ_j now becomes the controlling parameter for the jet's advective flushing strength in equation (23) and its inhomogeneity strength in equation (30). As mentioned previously, both x_j and σ_j are scaled on W in the CPB-3 model with $x_j/W = 0.85$ and

$\sigma_j/W = 0.0125$ to ensure an optimal match with the full-scale study. However, it is also apparent that other variables(e.g.,differential building heights) could influence both x_j and σ_j.

- Variable Along-Canyon Emissions

Unlike the nonvortex model which includes varying along-canyon emission density as part of the numerical integration along the canyon axis, the vortex model implicitly assumes a uniform emission line source. The usual Gaussian type of crosswind integration procedures were rejected because they fail to recognize the recirculating nature of the vortex. This recirculation creates the problem that material from some upwind point, y, could impact the receptor directly with a characteristic σ_y but then impact after one vortex rotation at a later time and with a larger value of σ_y. While a self-consistent formulation can be generated along these traditional lines, the recirculation series, F + F 2 + F 3 + ..., of equation (28) becomes more complex and cannot be rewritten as F/(1-F),and the number of error function terms in the solution becomes unwieldy. A much simpler along-canyon averaging process was instead adopted.

The geometrical travel time between the source and *receptor is first computed based on relative x,z positions, canyon transverse flow speeds, and knowledge of the specific plume (i.e. P3 -P3 , of C_R only) generating the principal source-receptor coupling. The along-canyon upwind source location, $y_o=vt$, is then computed from this transit time and the along-canyon flow speed. An effective emission rate, q_e, is then computed as

$$q_e = \int_{y_o}^{y_I} q(y) \exp[-(y - y_o)/\ell]\, dy/\ell \qquad (33)$$

where $\ell = v\tau$, τ is given by equation (25) and y_I is the distance to the upwind intersection. Such an exponential weighting is consistent with the time constant formulation of concentration decay within a canyon, leads to a simple sum of exponential weights for a q (y) defined "piecewise" along the canyon in a CPB-3 input file, and enables incorporation of concentrations at intersections via a "remainder" term, $C_I \exp[-(y_I - y_o)/\ell]$, that is implied by equation (23).

F. Additional Model Refinements

Wind direction fluctuations and meanderings, as quantified by σ_θ, are known to have a large influence on concentrations and concentration fluctuations from point sources and to affect the averaging time dependence of observations. For line sources, this influence is greatly reduced, especially when the mean flow direction is within about 45° of being perpendicular to the line source. Nevertheless, the theoretical wind direction sensitivity study in appendix E suggests that some inclusion of σ_θ influences is warranted. Thus, a 5-point averaging scheme in θ using uniform weights and θ steps of 0.6928 σ_θ has been incorporated into CPB-3. It should be noted that this step size leads to isotropic wind direction sampling when σ_θ reaches its maximum measurable value of 103.92°. Such a scheme cannot, however, be fully evaluated using existing wind tunnel data where wind direction is held fixed, but must rely on the full-scale measurement data bases. Such a refinement should avoid the criticism that air quality models

are run under constant Θ conditions when, in fact, variation in Θ over an hour can be substantial.

The possibility of having porous canyon walls also requires some correction to the pollutant recirculation model as well as the flow and turbulence fields, as previously discussed in section 4. Such a correction is required because air can now flow into or out of the canyon via the gaps in the walls. For a given downwind wall porosity, P_d, the pollutant first travels across the top of the canyon, yielding a recirculated amount, F, as defined in equation (29). A fraction $(1 - P_d)$ of this pollutant is now assumed siphoned off by the gaps so that the net effect of all recirculations is to yield the infinite series

$$F + F^2(1-P_d) + F^3(1-P_d)^2 + \ldots$$

or simply $$F/[1-F(1-Pd)], \qquad (34)$$

instead of the F/(1-F) of equation (28). For a given upwind wall porosity, P_u, the material is siphoned off even before its first trip across the top of the canyon, so one instead uses the expression

$$F(1-p_u)/[1-F(1-p_u)] \qquad (35)$$

Such an approach is found to give reasonably good results, as discussed in the following section.

6. APPLICATION OF CPB-3 TO WIND TUNNEL EXPERIMENTS

A. Introduction

As discussed in section 5, the extensions to the CPB flow and turbulence modules permit the model to predict resulting concentrations under the same range of extended conditions. Qualitative examination of smoke visualization and concentration data suggest that some configurations, such as the Katy Freeway with its gently sloped sidewalls, may be more appropriately modeled with a conventional regulatory model (e.g., CALINE-3) as the influence of recirculation is greatly, if not completely suppressed, whereas a steeper 45 degree sloping wall canyon showed the need to consider recirculation.

Quantitative evaluations using the recently renormalized, BU concentration data should provide a good characterization of the predictive power and range of applicability of the new CPB-3 model as well as illustrate model usage.

B. Model Application

The CPB-3 model, written in FORTRAN 77, is designed to be run on an IBM XT/AT (or compatible) personal computer without the need of an extensive users guide. This latter aspect is accomplished by driving the model with two, nearly self-explanatory, user input files. These two files, CPBCON.INP and CPBVAR.INP, contain the constant or time-independent information and the variable or time-dependent data, respectively, and are illustrated in figure 3 for the standard W/H = 1 canyon evaluated under very high wind speed conditions (i.e., for a Reynolds number independent limit).

(3a) CPBVAR.INP Structure

```
                    BU: W/H=1
WIND SPEED (m/s):                    65.00
WIND DIR. & STD. DEV. (deg.):        270.000 0.0
GLOBAL RADIATION (kW/m2):            0.0
TRAFFIC VOLUME FOR EACH LANE (SAME ORDER) IN veh/s
TRAFFIC (veh./lane/second):          0.001
TRAFFIC SPEEDS FOR EACH LANE (SAME ORDER) IN km/hr
TRAFFIC SPEEDS (km/hr):              0.0
EMISSION DENSITY FOR EACH LANE (SAME ORDER) IN mg/m/veh
EMISSION DENSITIES (mg/m/veh):       4000000.
CONCENTRATIONS AT EACH RECEPTOR (SAME ORDER AS COORDS.) IN ppm
CO CONCS AT THE RECEPTOR:            102.6289.0775.6643.1539.9433.38
BACKGROUND-CONCENTRATIONS IN ppm
BACKGROUND CONCENTRATIONS:           0.00000
BACKGROUND-SUBTRACTED INTERSECTION-CONCENTRATIONS IN ppm
+Y INTERSECTION CONCS:               0.0
-Y INTERSECTION CONCS:               0.0
```

(3b) CPBCON.INP Structure

```
BU WIND TUNNEL W/H=1 USING CPB-3 MODEL

POLLUTANT:                          CO

DIMENSIONS OF THE STREET CANYON AND THE LANES
CANYON WIDTH(m) & CURVATURE:         35.000 0.0
LEFT WALL HGT.(m) & POROSITY:        35.000 0.0
RIGHT WALL HGT.(m) & POROSITY:       35.000 0.0
HEADING(deg.) OF +Y OF STREET:       0.00
+Y END OF STREET CANYON(m):          1000.
-Y END OF STREET CANYON(m):          -1000.
NUMBER OF LANES:                          1
+X POSITION OF LANES(m):             17.50
HEIGHT OF VEHICLES(m):               0.000
WIDTH OF LANES(m):                   0.000
NUMBER OF RECEPTORS:                      6
X,Y,Z RECEPTOR COORDINATES(m):       0.0000.0 5.000
X,Y,Z RECEPTOR COORDINATES(m):       0.0000.017.500
X,Y,Z RECEPTOR COORDINATES(m):       0.0000.030.000
X,Y,Z RECEPTOR COORDINATES(m):       35.0000.0 5.000
X,Y,Z RECEPTOR COORDINATES(m):       35.0000.0 17.500
X,Y,Z RECEPTOR COORDINATES(m):       35.0000.030.000
```

Figure 3. CPB-3 input files for the standard canyon (W/H = 1).

The coordinate system axes and sense of left and right become clear if one imagines an observer standing with the canyon wall to the observer's left (x = 0) while facing toward the intersection which is in the +y direction. Thus, the direction the observer faces defines the +y direction, the +x direction is to the observer's right and +z is up, with z = 0 being street level. Roadway curvature, d (i.e., the ratio of canyon width to roadway center diameter), is positive (negative) if the road curves of to the observer's right (left). The wall heights, HL and HR, refer to the walls at the observer's left and right, respectively.

Any user who is supplied the model will also have sample input files. The user is encouraged to simply modify these files as the variable descriptions must appear exactly as shown in figure 3. Table 2 presents those input variables which have numerical limits or constraints. Input file line lengths may not exceed 256 columns.

The standard canyon in the BU wind tunnel consisted of 3.5-in (0.0889m)-high blocks with a narrow line source (i.e., effectively a simple slit in the floor) located midway between two blocks also separated by 3.5 in (0.0889m). Given the BU evidence that they are above the Reynolds number dependent region, we scale the canyon dimensions to 35m (114.8 ft). All other dimensions are scaled proportionally.

BU concentration studies were carried out at a geostrophic wind speed of 10m/s (32.8 ft/s), thereby suggesting a reference height wind of 65 percent of this, or 6.5 m/s (21.32 ft/s), as discussed in appendix B. this speed is not quite high enough for the modeled CPB-3 turbulent intensities to become speed independent, so we scale the speed upward by a factor of 10.

Table 2. CPB-3 input variable constraints.

VARIABLE (UNITS)	LOWER LIMIT	UPPER LIMIT	BOUND CHECK OR PROTECTION
a) CPBCON.INP			
STREET HEADING (DEGREES)	0	360	F
NUMBER OF LANES	1	9	F
+X POSITION OF LANES (m)	0	W	N, L
HEIGHT OF VEHICLES (m)	0.0	H	N, L
WIDTH OF LANES (m)	0.0	W	N, L
NUMBER OF RECEPTORS	1	20	F
X, Y, Z RECEPTOR COORDINATES (m)	REASONABLE PREDICTIONS ONLY WITHIN CANYON		R
b) CPBVAR.INP			
WIND SPEED (m/s)	> 0.0	--	--
WIND DIRECTION (DEGREES)	0.0	360.	F
WIND DIR. STD. DEV. (DEGREES)	0.0	103.923	U
GLOBAL RADIATION (kW/m^2)	0.0	0.6	E, N
TRAFFIC VOLUMES (Veh./lane/s)	0.0	--	N, L
TRAFFIC SPEEDS (km/h)	0.0	--	N, L
EMISSION DENSITIES (mg/m/veh.)	0.0	--	N, L
OBSERVED CONCENTRATIONS (ppm)	--	--	N, R
BACKGROUND CONCENTRATION (ppm)	0.0	--	N

Symbols and codes:

E = Estimated upper limit of 0.6 kw/m^2 with sun directly overhead in a cloudless sky

F = Fatal Error, Message printed and CPB-3 stops

H = Height of canyon

≡ MAX((HL + HR)/3, MIN(HL,HR)) with HL, HR as height of left and right canyon walls

L = Number of values must equal number of lanes

N = No check for upper or lower bounds

R = Number of entries must equal number of receptors

U = Value exceeding upper bound is reset to upper bound

W = Width of canyon

Such scaling factors should leave invariant the BU-defined quantity C*, given as

$$C^* \equiv \chi \; u_g \; H/q \qquad (36)$$

where χ is observed concentration,
and u_g is geostrophic wind speed,

provided that q is defined appropriately. As the CPB-3 model predicts CO concentrations in parts-per-million (ppm), it becomes necessary for intercomparison with wind tunnel C* to define the emission rate as

$$q = u_g \cdot H \cdot (40/35), \qquad (37)$$

where the factor of 40/35 is needed to compensate for the fact that

$$\chi(mg/m^3)/\chi(ppm) \simeq 40/35 \text{ for CO.}$$

The resulting value of 4000 mg/m/sec is then increased 1000-fold for a per vehicle emission density so that a very low traffic volume, and hence negligible automotive heat output, can be used. Figure 3 shows the completed input files.

C. CPB-3 Modeling of Idealized Canyons

Figure 4 displays the CPB-3 model output, contained in CPBWRIT.DAT, for the input files in figure 3. The scatter plot and model performance estimators indicate nearly perfect CPB-3 predictive power, but this occurred only after one critical renormalization. All turbulent velocity standard deviation estimates were multiplied by one-half. This drastic action was

```
 ESTIMATED VERSUS OBSERVED CONCENTRATIONS USING CPB-MODEL (DIMENSIONLESS)
-I.....I.....I.....I.....I.....I.....I.....I.....I.....I.....II
-I                                                              I-Y WORD     0.000
 I                                                              I FROM       0.000
-I                                                              I-TO       200.000
 I                                                              I X WORD     0.000
-I                                                              I-FROM       0.000
 I                                                              I TO       200.000
-I                                                              I-             -
 I                                                              I
-I                                                              I-
 I                                                              I
-I                                *                             I-
 I                              *                               I YMAX      98.886
-I                           *                                  I-YMIN      30.577
 I                                                              I XMAX     102.620
-I                                                              I-XMIN      33.380
 I              *                                               I NTOT       2.000
-I            **                                                I-NBAD       1.000
 I                                                              I NGOOD      1.000
-I                                                              I-NOVFL      0.000
 I                                                              I NINC       1.000
-I.....I.....I.....I.....I.....I.....I.....I.....I.....I.....II
CALL TO SUBROUTINE  SCTCOR:LIN-FIT.          6  ENTRIES
AVE(X), SIG(X) =  63.9700       29.0074
AVE(Y), SIG(Y) =  60.1916       27.2568
2-PAR. FIT:Y=AX+C; A= 0.937E+00 C= 0.244E+00
           X=MY+B; M= 0.106E+01 B= 0.850E-01
           R,(95% C.L.)= 0.997  ( 0.97, 1.00)
           ERR=0.223E+01 EA=0.345E-01 EC=0.239E+01
           ERR=0.238E+01 EM=0.390E-01 EB=0.254E+01
1-PAR. FIT:Y=AX        0.940E+00
           X=MY        0.106E+01
MSE-DECOMPOSITION OF H.THEIL (MSE=     20.38)
==========================================
FRACTION BIAS                        :0.7006
FRACTION DYNAMIC VARIABILITY         :0.1253
FRACTION STOCHASTIC                  :0.1741
```

Figure 4. CPB-3 model output for the standard canyon (W/H = 1).

one of several alternatives possible to correct a seemingly internal inconsistency between the BU flow, turbulence and concentration estimates. In fact, the problem is somewhat worse than a factor of two, but a portion of this is accounted for by using the overall σ_u, σ_w mechanical turbulence estimates (i.e., A_m in table 1) from the less turbulent, Bonner Strasse study and as discussed in appendix C. The problem could be as easily explained by a systematic underestimate of the line source's mass flow rate, but checks of the experimental logs show this not to be the case.

Despite the need for this correction, the CPB-3 model is quite successful in describing interreceptor differences, with low mean square error and high correlation coefficient (i.e., 0.997) performance factors which are not so completely controllable by a single renormalization factor.

Given this adjustment, required by the W/H = 1 canyon, we now consider the deep canyon with W/H = 1/4. This canyon environment produced the highest concentration and C^* values of the experimental program and is characteristic of situations found in large metropolitan cities (e.g., New York City).[2]

Figure 5 shows the CPB-3 output scatter plot and statistical measures for this case. Despite the average overprediction by 27 percent, estimation of interstation variation is not unreasonable. Figure 6 shows the greatly improved results of the nearly identical calculation except for the addition of a small amount (σ_θ = 10°) of horizontal wind meander. Such an amount of directional meander could either come from genuine

[2]Note that H in equation (36) was held fixed at 0.0889m (3.5 in), despite the actual H, to facilitate intercomparisons.

```
 ESTIMATED VERSUS OBSERVED CONCENTRATIONS USING CPB-MODEL (DIMENSIONLESS)
-I.....I.....I.....I.....I.....I.....I.....I.....I.....I.....II
-I                                          *                    I-Y WORD   0.000
 I                                                  *            I FROM     0.000
-I                                                               I-TO     200.000
 I                                                               I X WORD   0.000
-I                                    *     *                    I-FROM     0.000
 I                                                               I TO     200.000
-I                                                               I-
 I                                  *       *                    I
-I                                                               I-
 I                                                               I
-I                                                               I-
 I                                                               I YMAX   192.404
-I                                                               I-YMIN    68.259
 I       *         *                                             I XMAX   166.180
-I                                                               I-XMIN    25.800
 I                                                               I NTOT     2.000
-I                                                               I-NBAD     1.000
 I                                                               I NGOOD    1.000
-I                                                               I-NOVFL    0.000
 I                                                               I NINC     1.000
-I.....I.....I.....I.....I.....I.....I.....I.....I.....I.....II
CALL TO SUBROUTINE  SCTCOR:LIN-FIT.          8  ENTRIES
AVE(X), SIG(X) =  105.956       45.6556
AVE(Y), SIG(Y) =  134.545       47.4711
2-PAR. FIT:Y=AX+C; A= 0.954E+00 C= 0.334E+02
           X=MY+B; M= 0.883E+00 B=-0.128E+02
           R,(95% C.L.)= 0.918  ( 0.60, 0.99)
           ERR=0.204E+02 EA=0.169E+00 EC=0.193E+02
           ERR=0.196E+02 EM=0.156E+00 EB=0.221E+02
1-PAR. FIT:Y=AX        0.123E+01
           X=MY        0.797E+00
MSE-DECOMPOSITION OF H.THEIL (MSE=   1132.55)
==========================================
FRACTION BIAS                        :0.7216
FRACTION DYNAMIC VARIABILITY         :0.2547E-02
FRACTION STOCHASTIC                  :0.2758
```

Figure 5. CPB-3 model output for the deep canyon (W/H) = 0.25), assuming a σ_θ = 0. The model is seen to significantly overpredict the wind tunnel observations.

```
 ESTIMATED VERSUS OBSERVED CONCENTRATIONS USING CPB-MODEL (DIMENSIONLESS)
-I.....I.....I.....I.....I.....I.....I.....I.....I.....I.....II
-I                                                              I-Y WORD   0.000
 I                                                              I FROM     0.000
-I                                                              I-TO     200.000
 I                                                              I X WORD   0.000
-I                                        *         *           I-FROM     0.000
 I                                                              I TO     200.000
-I                                                              I-
 I                                                              I
-I                                   *         *                I-
 I                                                              I
-I                                 *         *                  I-
 I                                                              I YMAX   151.815
-I                                                              I-YMIN    90.309
 I                                                              I XMAX   166.180
-I                                                              I-XMIN    95.480
 I                                                              I NTOT     2.000
-I                                                              I-NBAD     1.000
 I                                                              I NGOOD    1.000
-I                                                              I-NOVFL    0.000
 I                                                              I NINC     1.000
-I.....I.....I.....I.....I.....I.....I.....I.....I.....I.....II
CALL TO SUBROUTINE  SCTCOR:LIN-FIT.          6  ENTRIES
AVE(X), SIG(X) =  127.645      23.8577
AVE(Y), SIG(Y) =  119.937      27.0565
2-PAR. FIT:Y=AX+C; A= 0.848E+00 C= 0.116E+02
           X=MY+B; M= 0.660E+00 B= 0.485E+02
           R,(95% C.L.)= 0.748  (-0.16, 0.97)
           ERR=0.201E+02 EA=0.376E+00 EC=0.487E+02
           ERR=0.177E+02 EM=0.293E+00 EB=0.358E+02
1-PAR. FIT:Y=AX       0.937E+00
           X=MY       0.105E+01
MSE-DECOMPOSITION OF H.THEIL (MSE=    338.98)
==========================================
FRACTION BIAS                          :0.1753
FRACTION DYNAMIC VARIABILITY           :0.2516E-01
FRACTION STOCHASTIC                    :0.7996
```

Figure 6. CPB-3 model output for the deep canyon (W/H) = 0.25, assuming a σ_θ = 10°. The model is seen to be in reasonable agreement with wind tunnel observations.

meander or small and unstable along-canyon flows which might exist for a variety of reasons.

Next, we consider the interesting case of a standard (i.e., W/H = 1) canyon but with a porous downstream wall having a fractional openness or porosity, p = 0.41, typical of a parking garage. If one considers only the changes to the flow and turbulence modules, the predicted CPB-3 concentration would rise 16 percent to a value of 114.8. However, the effect of the gaps in the wall on the recirculated pollutant fraction via equation (34) lowers the peak concentration about 9 percent below the standard canyon peak value to 92.9. An alternative expression to equation (34),

$$F(1-p_d)/(1-F) + p_dF, \qquad (38)$$

gives a better intercomparison value of 101.4 but is somewhat more difficult to justify theoretically.

Use of the downwind porosity variable also permits an alternative method for evaluating the downwind facing step problem. Setting p_d = 1.0 is equivalent to having the downwind wall disappear. Despite the fact that appendixes B and C do not recommend using p > 0.5, the resulting concentration of 131.0 is in better agreement with observations than the much higher value of 159.8 that results from setting the upwind building height to zero. Unfortunately, the upwind facing step problem is complicated by the very different approach flow z profile such that neither the porosity approach nor the approach of setting the upwind building height to zero produces reasonable flow, turbulence, or concentration fields.

The dimensionless, peak concentration predictions, C*, for a number of BU measured geometries are displayed along with measured values in figure 7. Intercomparisons with canyon average observations (i.e., dark shading) are not presented.

Most of the predictions are reasonably close to observed values, as is the rank ordering of C* values. However, the wide canyon (i.e., W/H = 2) comparison is rather poor. Tracer concentration studies involving larger W/H ratios were not undertaken, so it is difficult to know whether this point represents an anomaly or the beginning of a systematic trend.

It should be noted, however, that these wide canyon data come from some of the earliest experiments involving the moving vehicles mounted on a belt. Thus, it is not obvious that these data are directly comparable in all other respects.

It should be also noted that the CPB-3 model does not explicitly account for canyons with sloping or nonperpendicular walls. The value computed assumes a mean W/H = 2, that the vertical walls are bent over, and that the flow is in a terrain-following coordinate system. While the CPB-3 model appears appropriate for this steep walled canyon because recirculation clearly plays a role, it is not appropriate for shallow walled canyons (e.g., Katy Freeway) where there is no recirculation.

Finally, we consider the predictive power of the CPB-3 model in the near vicinity of an intersection. Figure 8 (adapted from volume II, figure 59) shows the observed C* in a W/H = 1 canyon at various distances from the intersection. The superimposed CPB-3 curve, normalized to the 2-D result at

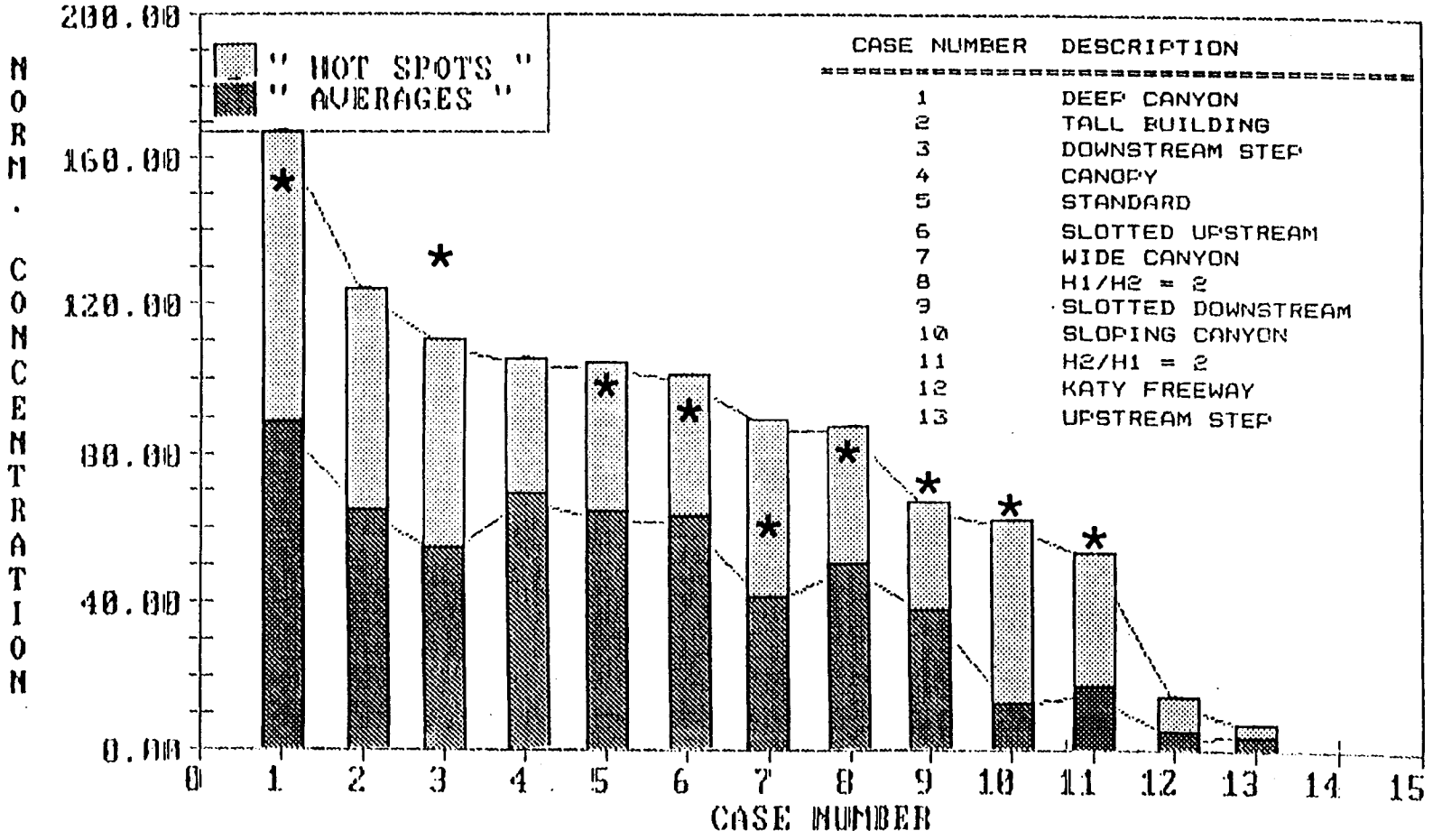

Figure 7. Comparison of observed and CPB-3 predicted "Hot Spot" concentrations for various canyon configurations. Observed average values are also indicated. Predictions are displayed as "*".

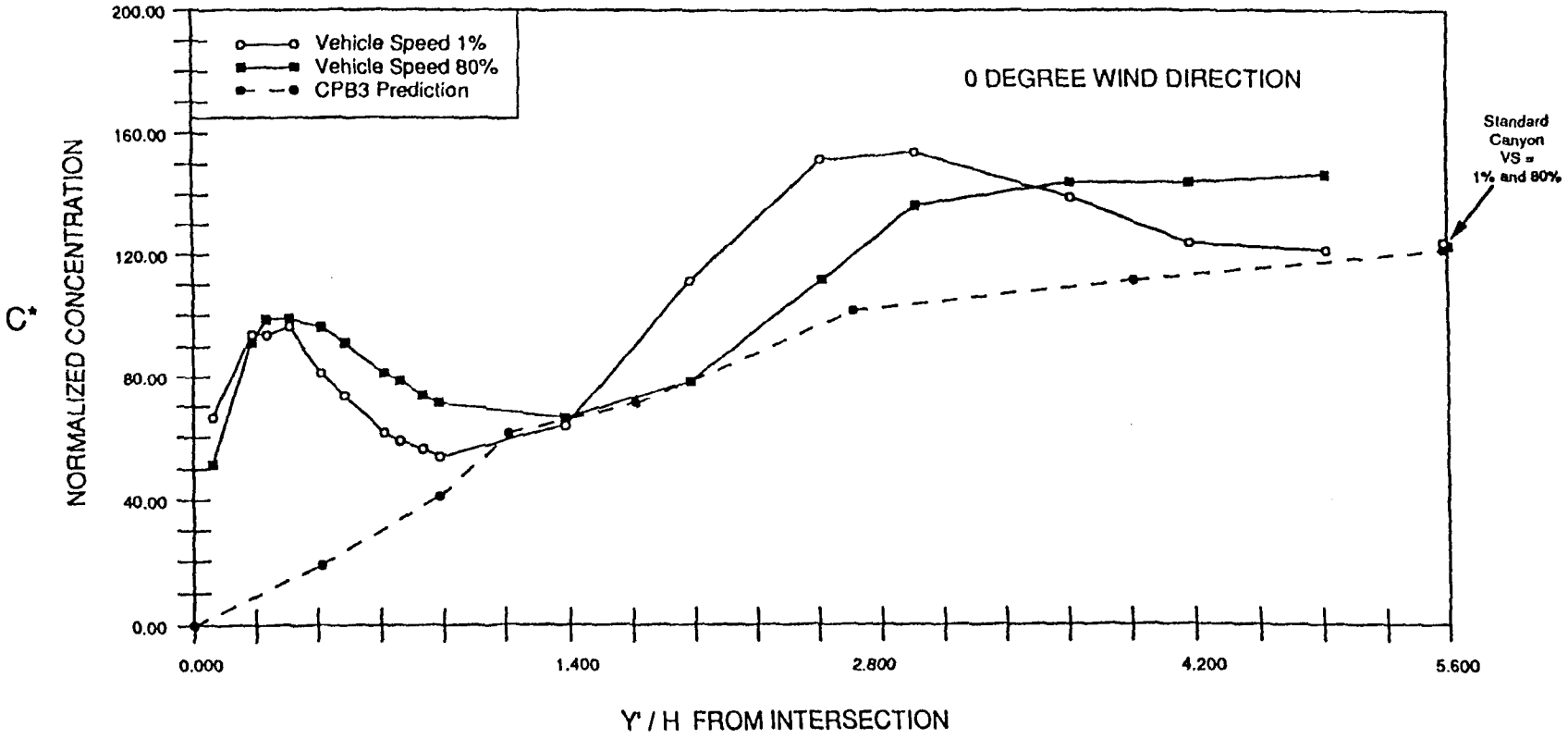

Figure 8. Observed and predicted concentration profiles in the vicinity of an intersection.

Y/H = 5, exhibits qualitatively reasonable behavior but clearly misses the pronounced peak at Y/H ≅ 0.5, probably due to the vertical axis rotor, and also the broad enhancement near Y/H ≅ 3 of unknown origin.

D. CPB-3 Intercomparisons with Scale-Model Urban Settings

Wind tunnel simulations of full-scale experiments conducted in St. Paul (MN), Syracuse (NY), Manhattan (NYC) yielded peak C* values in the relatively narrow ange of 80 to 100. These values are generally c onsistent with the CPB-3 predictions for the standard, W/H = 1 canyon and minor variations of that canyon as discussed in the preceding subsection. Beyond this general observation of "consistency," more detailed simulation of these full 3-D scale model environments requires additional 3-D flexibility beyond the current capabilities of the CPB-3 model.

A simulation has also been run for the SEATAC International Airport canyon environment that was considered in the field study reported in appendix G. Values of C* exceeding 180 have been obtained for the case of the above roof wind coming from the terminal. This incoming flow direction is also likely to transport background contributions from aircraft emissions on the "airside" of the terminal to the street canyon. Thus, there is significant potential for creating hot-spots at the terminal entrance. Given the complexity of the actual geometry, additional study and simulations are warranted.

E. CPB-3 and Open Highway Models: Domains of Applicability

The rather general case of the cut-section highway of arbitrary width and sloping sidewalls is depicted in figure 9 and provides a basis for discussing the domains of applicability of CPB-3 versus those of an open highway dispersion model such as CALINE 3/4. Figure 9 indicates that it is convenient to separate the modeling domain into five separate domains or

zones: the approach flow zone where an equilibrium wind profile u(z) is established; the lee wall recirculation region which exists for walls steeper than some critical angle < (of order 45 degrees); a flow reattachment region where the wind is once again in the direction of the approach flow but can have quite different vertical profiles of speed and turbulence; the downwind wall recirculation region dominated by a smaller, but more rapidly rotating, vortex than the lee wall rotor; and finally a post-canyon region where flow speeds and dispersion rate slowly relax toward their approach flow values.

The CPB-3 model is capable of dealing with cut-sections narrow enough that the flow reattachment region (zone 2) has been unable to form and the two rotors have coalesced to form a single rotor filling the entire cut-section. Thus, CPB-3 is likely to be applicable for cut-sections having width-to-height ratios less than about six, and is only capable of yielding concentration predictions within the section. Table 3 shows the various spatial domains of applicability for the CPB-3 model along with those of CALINE-3 (or 4). It is interesting to note that the two models complement each other in terms of where they are applicable. Basically, CPB-3 deals with recirculating flow and CALINE-3 deals with normal (i.e., nonrecirculating) flow dispersion problems. In principle, it should be possible to build a composite model involving elements of the two existing models, but this has not yet been attempted.

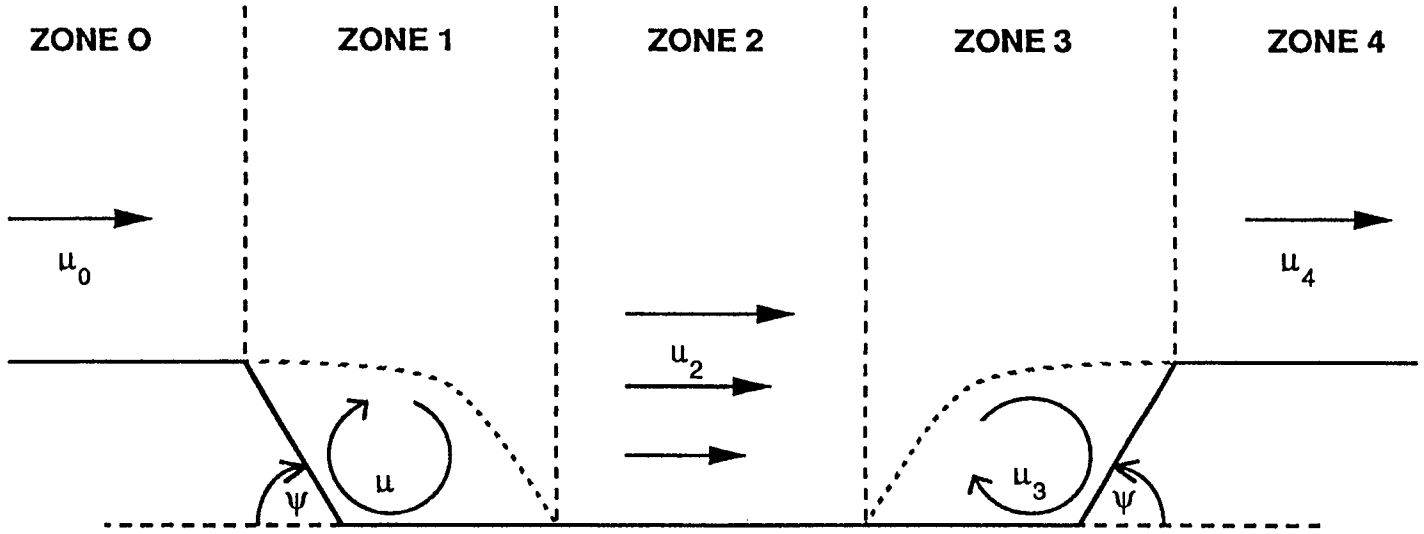

Figure 9. The basic zones involved in street-canyon and open highway modeling. In open highway models the wall angle Ψ goes to zero, recirculation zones 1 and 3 vanish and all zones exhibit the same $u(z)$ profile (ignoring vehicle induced effects). In the CPB-3 model, zone 2 is assumed to be vanishingly small for $W/H \leq 6$, so that zones 1 and 3 combine to form a single vortex zone 1/3.

Table 3. Regimes (zones) of applicability for open highway (e.g. CALINE-3) and CPB-3 models.

	Approach Flow Zone 0	Lee Rotor Zone 1	Flow Reattachment Zone 2	Upwind Rotor Zone 3	Post-Canyon Zone 4
CALINE-3	User selected z_0 specifies approach flow $u(z)$	not applicable	Region above vehicles treated as a mixing	not applicable	Dispersion modeled using $\sigma_z(x)$ which match regulatory values at 10km Depressed roadways accounted for with initial $\sigma_z(0)$
CPB-3	Above-roof wind assumed displaced logarithmic with $d = 0.96\ H$ and $z_0 = 0.05\ H$ Along-canyon component has $z_0 = 0.05\ H$ for near-parallel flows and $z_0 = 0.04m$ for rotor flows	Single rotor for zone 1, 3, or 1/3 combined Full flow, turb., and concentration predictions within canyon for $\psi \geq 45°$	not applicable	Single rotor for zone 1, 3, or 1/3 combined Full flow, turb., and concentration predictions within canyon for $\psi \geq 45°$	not applicable

F. Dispersion Downwind of a Cut-section Roadway

The extensive BU data base offers fertile ground for many additional studies. One example of this involves the use of concentrations observed at receptors outside of, and downwind of, the standard W/H = 1 canyon to extract the effect of a canyon or cut-section roadway as an "initial mixer" of automotive emissions. This "far field" view back towards the canyon is summarized in figure 10. As $\sigma_z(x)$ and C* from an infinite line source are closely coupled by the relation, $\sigma_z(x)/H = \sqrt{2/\pi}\,[u(H)/u_g]/C^*$, one is able to infer by backward extrapolation an initial mixing of $\sigma_z(0) \leq 0.1H$ for the expression such as $\sigma_z(0) \leq 0.1 * MIN(H,W)$ may be more appropriate.

Also, shown in figure 10 is the Briggs (1973) parameterization, $\sigma_z = 0.2x$, for the neutral stability (C), McElroy-Pooler (1968) urban dispersion coefficients. The close correspondence between this EPA regulatory model curve and the wind tunnel data estimates (i.e., except for the last data point at x/H =3.5), indicates an appropriate dispersion rate within the wind tunnel, but also suggests that the observations may be consistent with $\sigma_z(0) = 0$, which accounts for our previous use of the inequality symbol in $\sigma_z(0) \leq 0.1*H$. The occurrence of an effective $\sigma_z(0) = 0$ for material downwind of a notch wherein the material is already well mixed does not create any conceptual problems in separated flow cases, provided there is no significant momentum exchange across the z = H interface. However, in the terrain following flow assumed in CALINE-3 and appropriate for gently-sloped, cut-section highways, a zero initial σ_z subsequent to vehicle induced initial mixing would be causally impossible. The σ_z in this case may "shrink,"

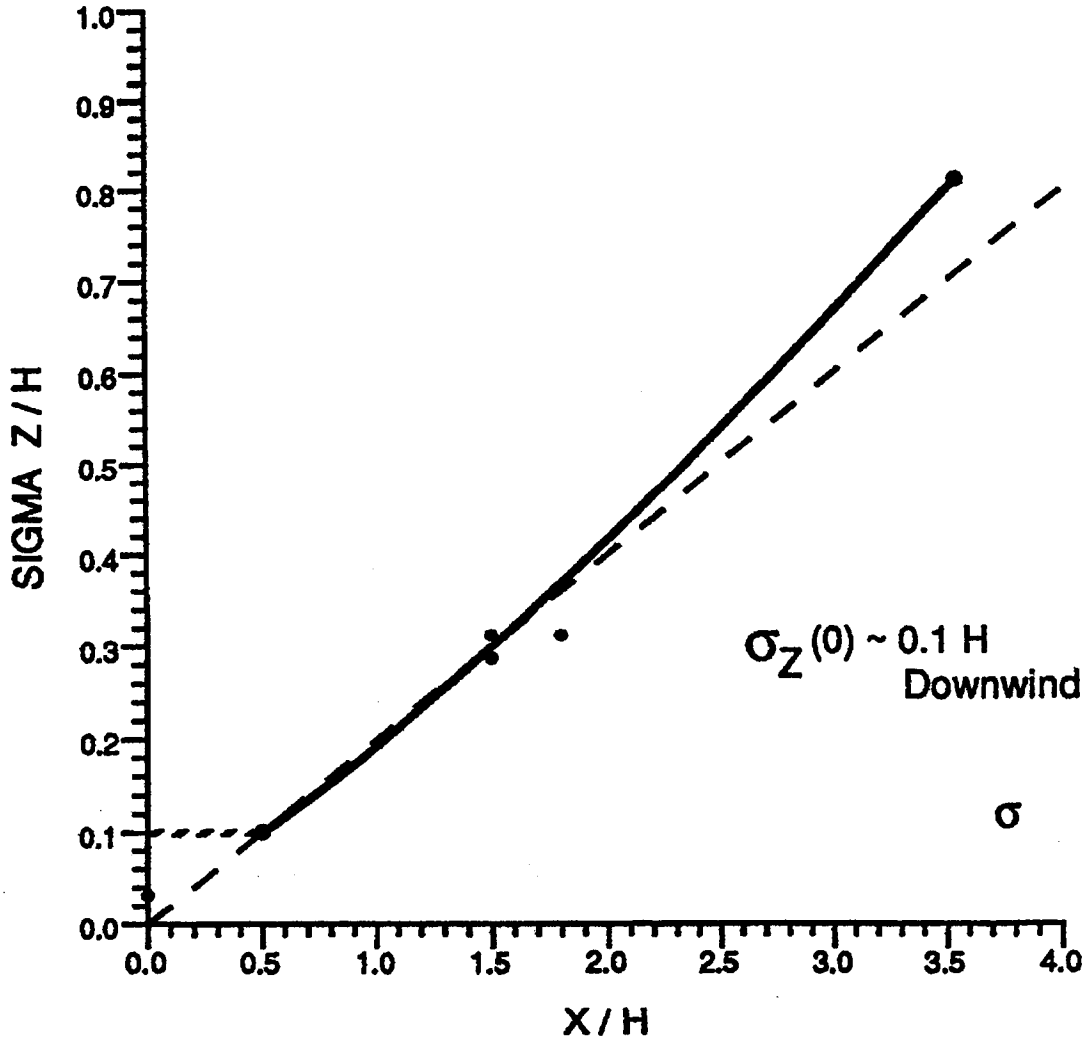

Figure 10. Dispersion Downwind of W/H = 1 Canyon.
The solid line is a freely drawn curve through the wind tunnel data values (shown as dots).
The dotted line is simply a horizontal line connecting X=0 with the data point at X/H=0.5 and establishes the upper limit of $\sigma_z/H=0.1$.
The dotted line, $\sigma_z=0.2.X$, corresponds to Briggs' formula for the McElroy-Pooler urban dispersion coefficients for C stability.

however, as the streamlines compress in z to compensate (i.e.,to ensure $\nabla \cdot \underline{u}=0$) for the flow's x acceleration as it leaves the cut-section. Thus, it is possible that gently-sloped cut-sections are more effective than steep or vertical walled notches at dispersing vehicle emissions and reducing concentrations at downwind receptors.

The CALINE-3 model accounts for the higher concentrations within a cut-section by reducing the wind speed (and consequently raising the time spent) in the "mixing zone" by the factor 0.72H 0.83 for H > 1.5m; however, the resulting larger σ z at the exit to the cut-section is not allowed to"shrink" as the wind speed is allowed to return linearly to its original value over the downwind distance interval 3H.

In their highway model intercomparison study, Wackter and Bodner (1986) analyzed the 25 events yielding the highest concentrations at the six receptors outside of the cut-section of the Santa Monica Freeway study (Bemis et al., 1977). This cut-section had moderately steep walls of 30°and the experimental data, including the within-and above-cut-section CO data, had already been used in the development of CALINE-3's cut-section correction methodology. Nevertheless,the observed CO average of 10.8 ppm was predicted by CALINE-3 to be 3.3 ppm.[3] This more than three-fold underprediction(i.e.,3.27) should be compared with the velocity reduction factor of 3.75 which CALINE-3 would compute for this 7.3m (24ft)deep

[3] Underpredictions were even more severe for HIWAY-2 (C = 2.9 ppm) and GMLINE (C = 1.5 ppm). PAL showed slight overprediction (C = 12.5 ppm) but was unable to reproduce the observed variability in the data.

cut-section. Had the subsequent flow speedup been compensated for with an appropriately shrinking σ_z, such underprediction may have been eliminated.

7. CONCLUSIONS

This study has led to a number of theoretical improvements and empirical generalizations and extensions to the CPB-1 model and resulted in the creation of the CPB-3 model. These improvements include:

- Extension of the flow and turbulence modules within CPB-1 to include differential building heights, semi-open or porous structures, curved canyons and various combinations of these effects. These extensions were based on empirical modeling of the BU hot-wire data base.

  Refinement of the vehicle-wake induced initial mixing algorithm based on intercomparisons with predictions of the ROADWAY numerical grid model.

- Development of a new integral solution for the finite length and width line source.

- Modification of the pollutant recirculation model to include the effects of porous (i.e., partially open upwind and downwind canyon walls.

- Inclusion of the wind direction variability, σ_θ, during the hour via θ averaging in order to escape the constant θ limitation of many regulatory models.

CPB-3 peak concentration predictions for various 2-D and 3-D idealized canyons are found to be generally in good quantitative agreement with BU wind tunnel simulations.

Predictions are also in qualitative agreement with the three scale-model urban studies, which all produced peak C* in the 80 to 100 range characteristic of the standard, W/H = 1 canyon and its minor variations. Comparisons with the two sloped canyon studies show that the CPB-3 model is appropriate for steep-walled canyons (e.g., 45 °) but is not appropriate for the gently-sloped sidewall Katy Freeway situation. In the Katy Freeway situation, the flow is capable of following the canyon profile so that no major flow separation occurs. Existing open-highway dispersion models (e.g., CALINE-3/4) would likely be more appropriate for this situation.

The new CPB-3 model now also has the capability to simulate the curved terminal/roadway/garage configuration found at a number of large commercial airports. Analyses of the 3-daypilot study carried out at SEATAC International Airport has shown that the present flow and turbulence correction factors are not inconsistent with what is observed in the full-scale\setting. CPB-3 modeled concentrations suggest that a substantial hot-spot potential exists with such configurations.

APPENDIX A

INTERPRETATION OF HOT-WIRE ANEMOMETER SIGNALS IN HIGH-TURBULENCE ENVIRONMENTS

Introduction

Use of a single hot-wire anemometer in wind tunnel investigations is generally considered reasonable when the flow is (i) primarily perpendicular to the wire and (ii) turbulent intensities are less than about 35 percent. The first of these limitations arises because of the hot wire's demonstrated 10-20 percent sensitivity to axial flows (Champagne and Sleicher, 1967) and the sensitivity of this axial flow coefficient on such factors as the length-to-thickness ratio of the wire and the turbulent intensity itself (Champagne et al., 1967). The restriction to low turbulent intensities is generally imposed because of the rectification issue. That is, the wire's sensitivity to speed (or the absolute magnitude of velocity) causes negative velocity components to be interpreted as though they were positive. The net effects of this are that estimates of the mean velocity are overestimated, the shape of the velocity probability distribution function (pdf) is distorted, and estimators of higher pdf moments (e.g., the standard deviation) are biased.

Tutu and Chevray (1975) have investigated the sensitivity of cross-wire probes to rectification and turbulent velocity correlations in moderately turbulent flows (<35 percent), whereas Checkel (1985) considers signal processing of a fully turbulent flow (i.e., no mean velocity) in the absence of velocity correlations (i.e., $\overline{u'w'} = 0$ assumed for a wire aligned along the y or v axis). Both of these papers assume

that the underlying pdf of turbulent velocities is Gaussian; however, this assumption is widely accepted (E. Plate, 1982) only for fully developed turbulence (i.e., homogeneous and stationary) and not for the highly intermittent and turbulent flows within the urban street canyon environment.

In this appendix, we consider the basic pdf observed above and within the wind tunnel modeled street canyon having a height-to-width ratio of unity. Establishing the double-exponential as a reasonable pdf hypothesis, we then develop a formalism for converting hot-wire measurements of mean speed and speed turbulent intensity to the more conventional mean velocity and standard deviation of velocity.

Wind Tunnel Observed PDF

Figure 11 indicates the 2-D street canyon geometry and hot-wire locations considered. In each case, the hot-wire, oriented parallel to the canyon axis (+y), primarily experiences a mean flow, u, and along-flow turbulent fluctuation, u', plus an orthogonal component w'. After transformation of the voltage signal via the nonlinear voltage-speed calibration relation, an instantaneous speed, V, is recorded at a rate of about 300 Hz. Figures 12 through 17 show the observed pdfs, P(V), for each of the measurement locations. Each plot contains the 2048 samples collected over a time span of about 6.7 seconds. Also shown are the curves representing the maximum likelihood fits to the data for assumed Gaussian and double-double-exponential pdfs for the underlying turbulence. Visual intercomparison of these curves with the data distributions indicates that the exponential pdf is more reasonable for locations A,B,C at the bottom of the canyon and point 1 just at the top of the canyon, whereas the Gaussian pdf is more reasonable for points 2 and 3

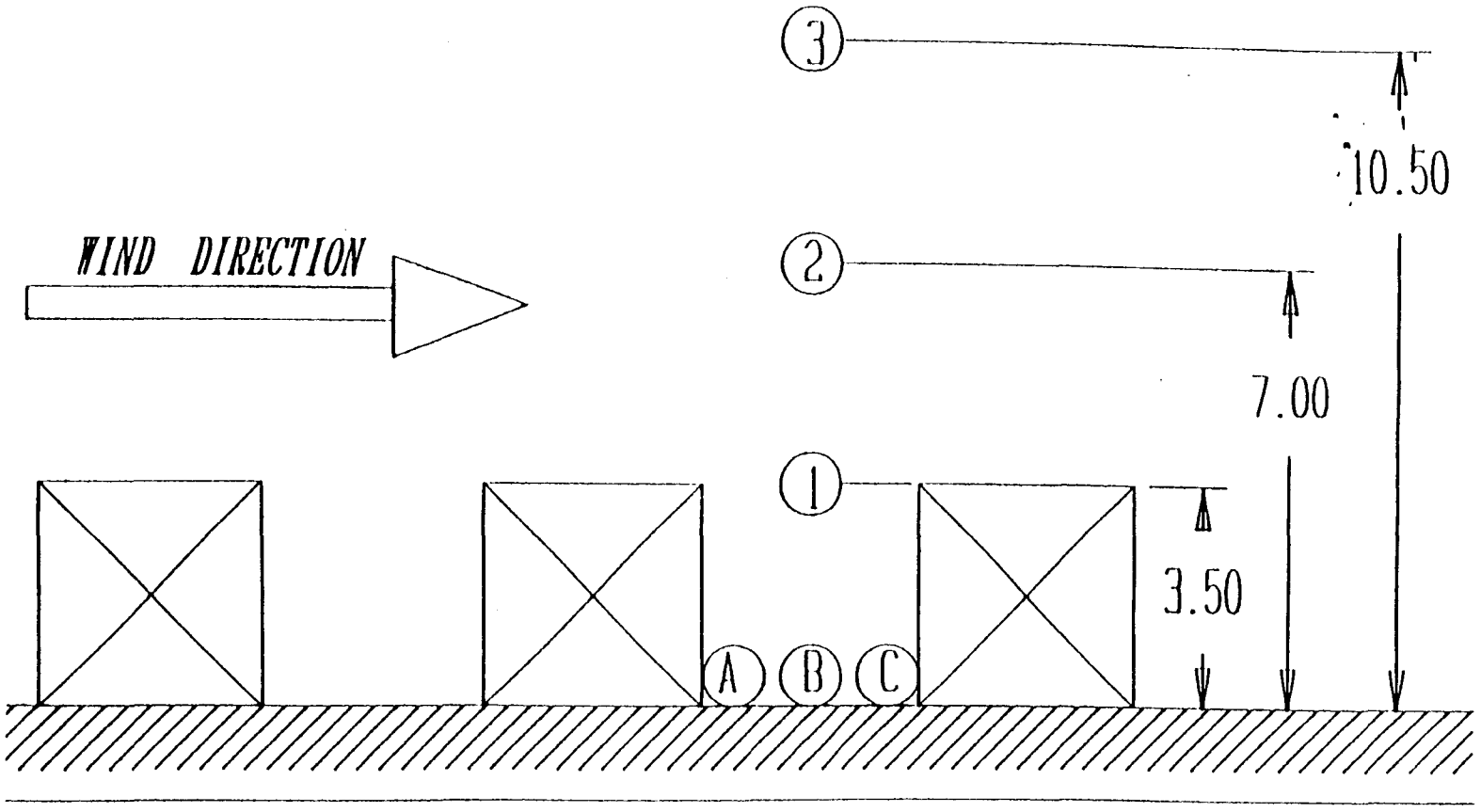

Figure 11. Hot wire measurement locations for the W/H = 1 canyon.

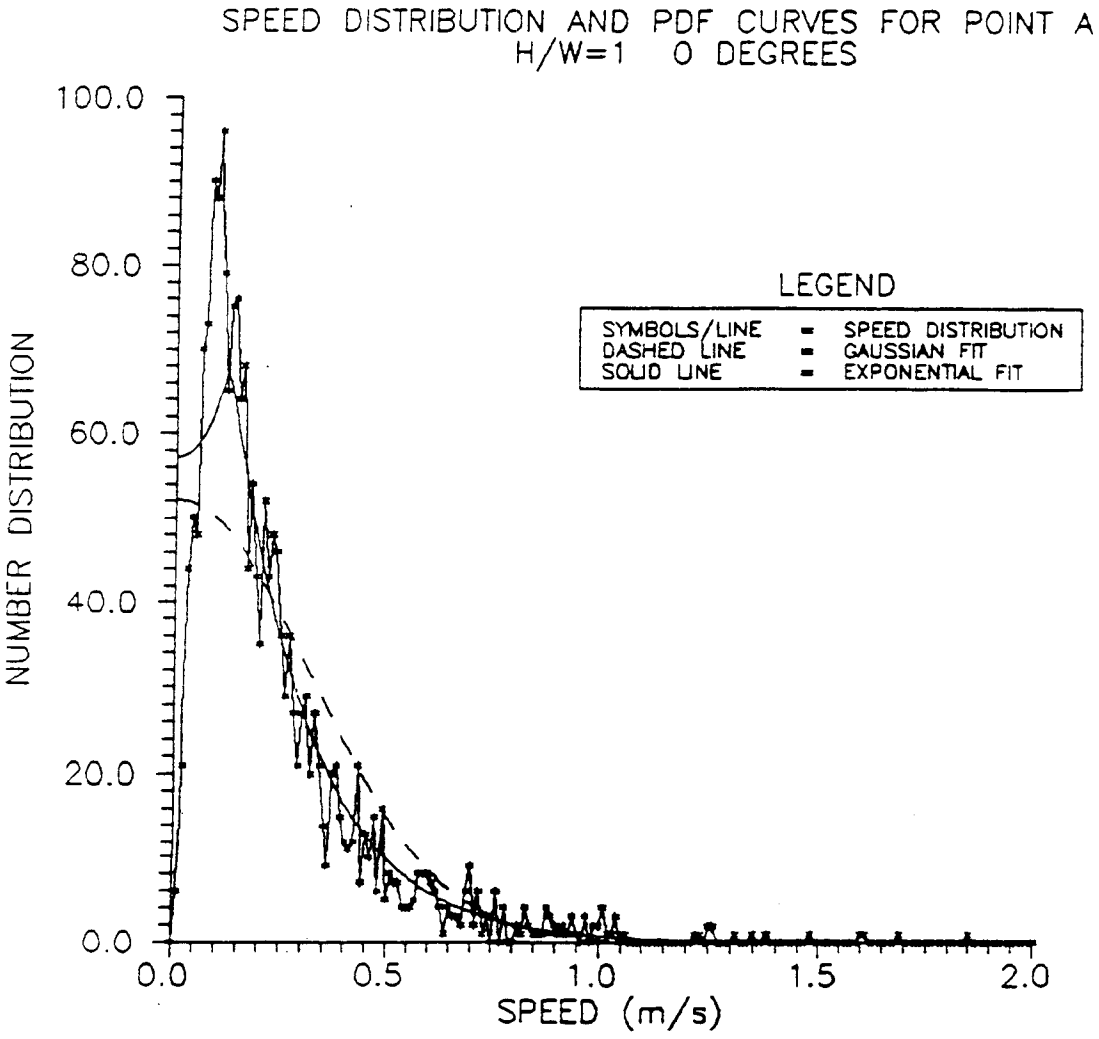

Figure 12. Hot wire speed probability distribution function (PDF) for the W/H = 1 canyon at location A.

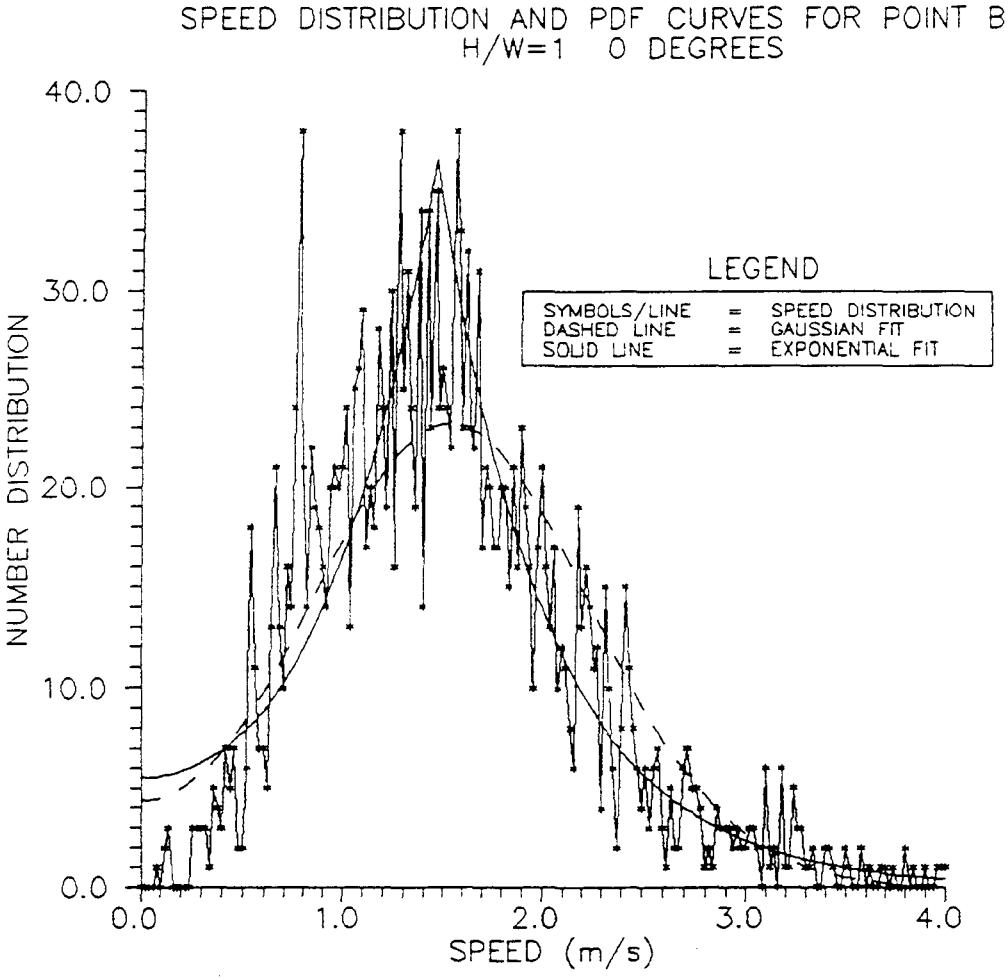

Figure 13. Hot wire speed PDF at location B.

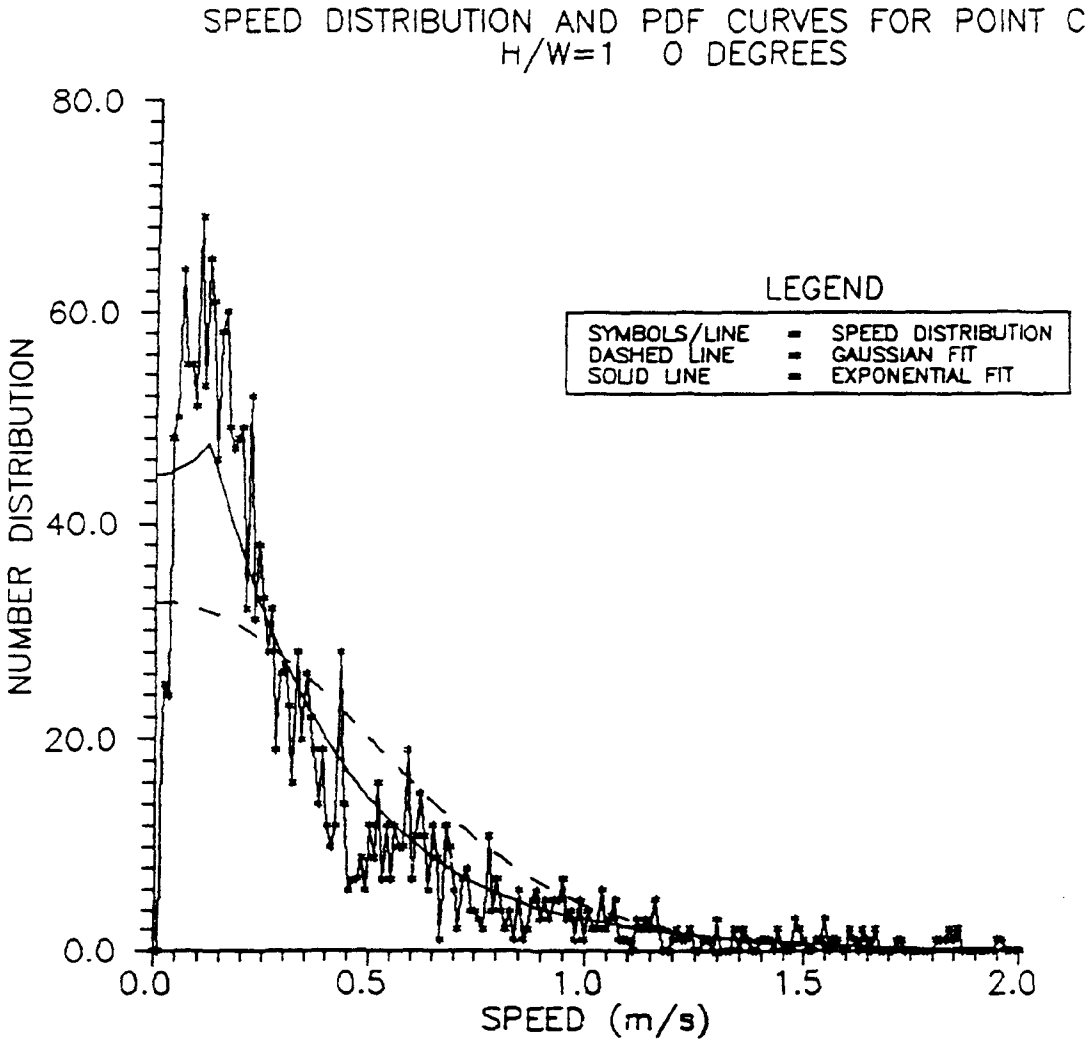

Figure 14. Hot wire speed PDF at location C.

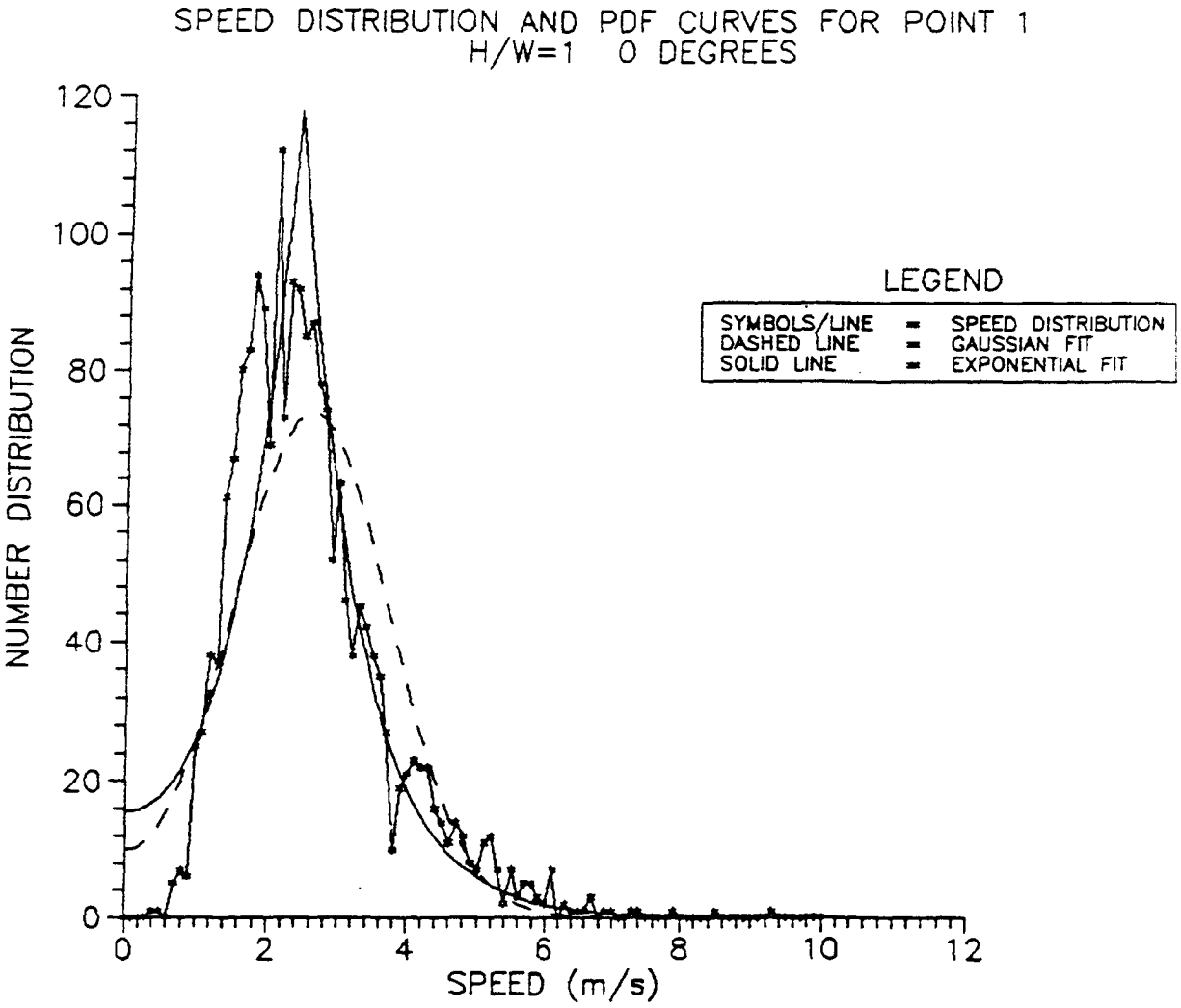

Figure 15. Hot wire speed PDF at location 1.

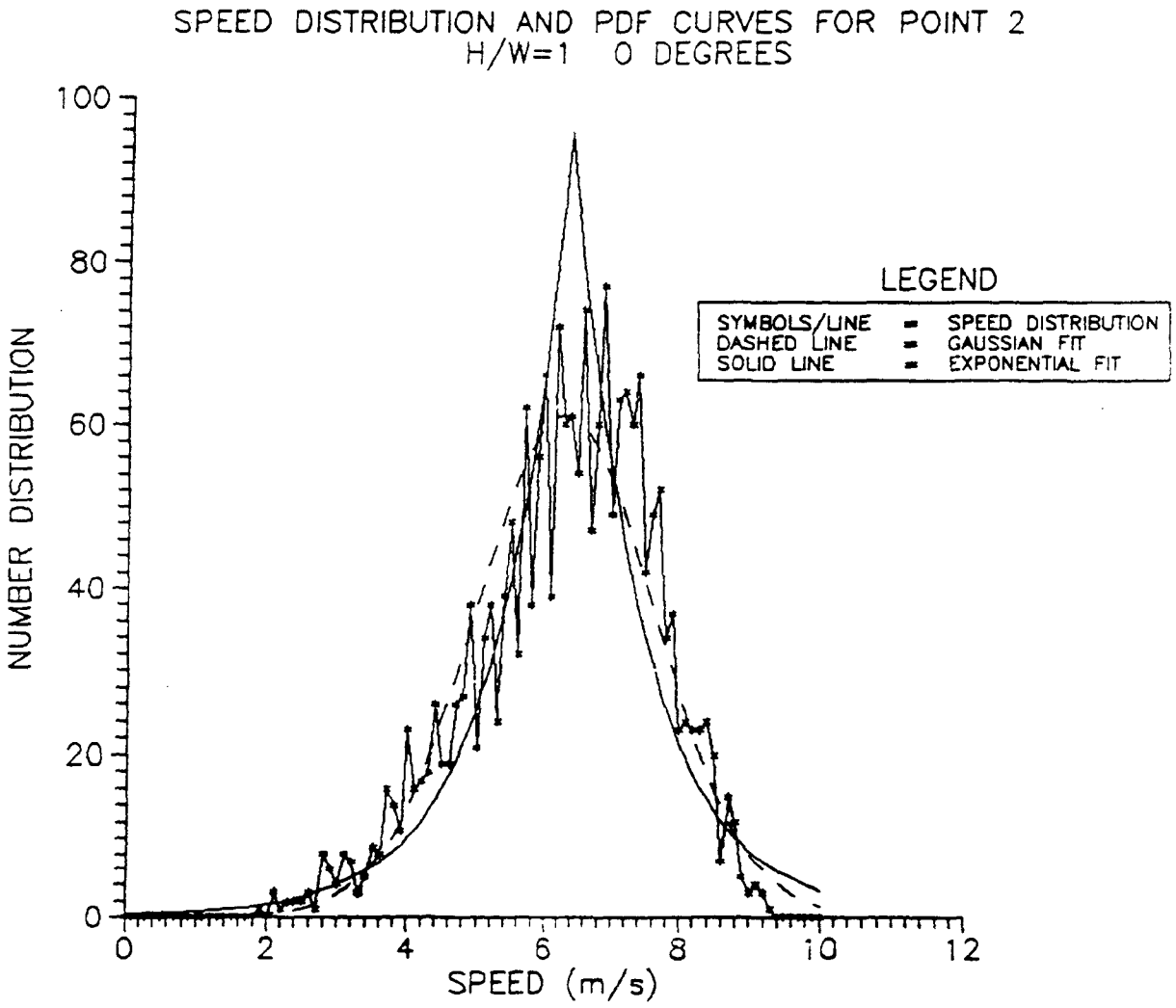

Figure 16. Hot wire speed PDF at location 2.

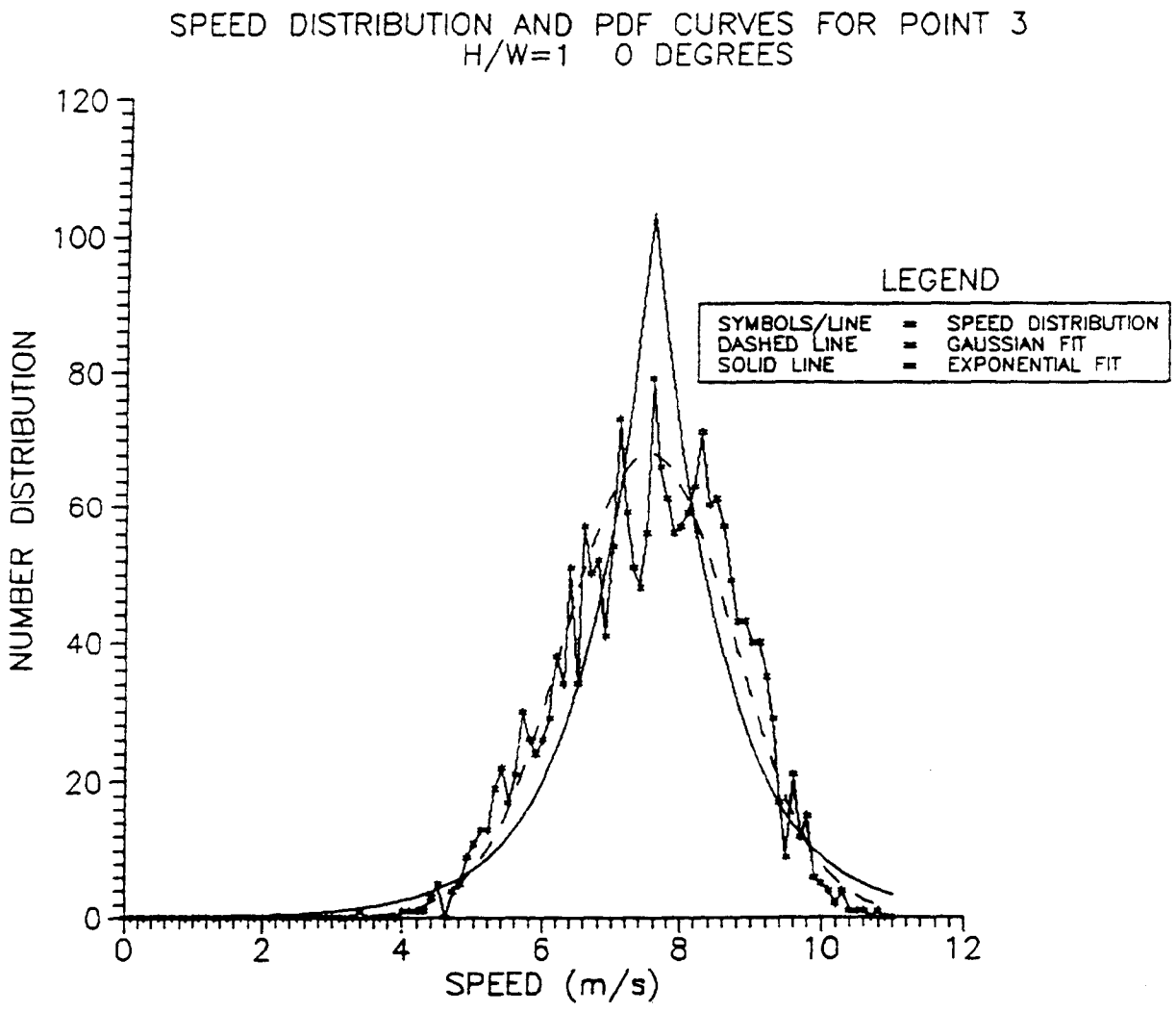

Figure 17. Hot wire speed PDF at location 3.

above the canyon. This general statement is consistent with earlier comments about the Gaussian nature of turbulence in an environment of fully developed turbulence and the more intermittent, non-Gaussian turbulent flow within the canyon. The theoretical basis of these pdfs and comparison of the relative "goodness-of-fit" will be considered in the following section.

Theoretical PDF Models and their Application

The quantity measured by the hot-wire, after voltage-speed conversion, is most generally,

$$V = +[(u+u')^2 + (w+w')^2 + k^2(v+v')^2]^{1/2} \qquad (39)$$

where k = 0.1 to 0.2 is the wire's sensitivity to axial flow,

u, w are the mean, wire-transverse flow velocities, and

u', w' are the corresponding turbulent velocity components.

In the street canyon with canyon axis and wire oriented perpendicular to the above canyon flow, v = 0 can be assumed. Individual v' are generally nonzero, even for these canyon perpendicular flows; however, the k^2 weighting of less than about 5 percent makes the contribution of this component negligible. If we now rotate our coordinate system about the wire's axis until w = 0, one may redefine V as

$$V = + [(u+u')^2 + w'^2]^{1/2} \qquad (40)$$

where any notation regarding the needed rotation has been suppressed. Finally, for simplicity and conservatism (as will

be shown later), we neglect the effect of w'^2, inclusion of which would greatly complicate the mathematics.

A Lagrangian-based theory (i.e., as seen in the reference frame moving with the mean flow u) would represent the pdf of turbuxent velocities as

$$P(u') = \exp[-1/2u'^2/\sigma^2]/[\sqrt{2\pi}\,\sigma] \qquad (41)$$

for Gaussian turbulence or as

$$P(u') = \exp[-\sqrt{2}\,|u'|/\sigma]/[\sqrt{2}\,\sigma] \qquad (42)$$

for the Laplace or double-exponential pdf. Both of these pdfs consider $-\infty \leq u' \leq \infty$, which is reasonable but neither pdf corresponds to the observed form of the pdf, P(V). In order to derive this pdf, we note that

$$V = u + u' \quad \text{for } u' \geq -u$$

and

$$V = -(u + u') \quad \text{for } u' \leq -u$$

Alternatively, we may express these two regimes as

$$|u'| = V - u \quad \text{for } u' \geq -u$$

$$|u'| = V + u \quad \text{for } u' \leq -u$$

Thus, one may transform the pdfs of equation (40) to yield

$$P(V) = \{\exp[-1/2(V-u)^2/\sigma^2] + \exp[-1/2(V+u)^2/\sigma^2]\}/[\sqrt{2\pi}\,\sigma] \qquad (43)$$

and

$$P(V) = \{\exp[-\sqrt{2}|V-u|/\sigma] + \exp[-\sqrt{2}|V+u|/\sigma]\}/[\sqrt{2}\,\sigma] \qquad (44)$$

for the Gaussian and exponential pdfs, respectively. Cast in the form of a pdf in V, P(V), one could easily conjecture P(V) that are lognormal or Maxwellian to correspond to other relevant Eulerian frame theories, but it is difficult to then project these distributions back into a Lagrangian P(u') basis that has reasonable intuitive appeal.

It is seen that the pdfs in equations (43) and (44) are completely and conveniently characterized by two parameters corresponding to the mean velocity, u, and the standard deviation of turbulent velocity, σ. Evaluation of the best or optimal values for u and σ is accomplished by noting that the likelihood function, $\mathcal{L}(u,\sigma) \equiv \Pi_i\, P(v_i,u,\sigma)$, takes on a maximum value when parameters u and σ are optimal (e.g., see Ross, 1972). Computationally, this is accomplished by minimizing the value of $F = -\ln \mathcal{L}$, as minimization software abounds, and the log transformation avoids the often astronomically small or large values of $\mathcal{L}$ resulting from the product of the many P values.

Table 4 presents the results of these optimization studies for each of the six sampling locations. As seen by the optimal values of F, the exponential pdf provides a superior fit for sampling points within the canyon, whereas the Gaussian pdf is better for points 2 and 3 above the canyon. Thus, the results of the optimization study confirm what is visually apparent from figures 12-17.

Table 4. Optimal parameters for the Gaussian and double-exponential probability density functions of equations (43) and (44).

SAMPLING POINT	GAUSSIAN			DOUBLE-EXPONENTIAL		
	μ	σ	F	μ	σ	F
A	0.019	0.313	-888.708	0.119	0.275	-1043.89[1]
B	1.530	0.704	2141.28	1.455	0.796	2094.51[1]
C	0.007	0.501	70.0772	0.117	0.450	-186.801[1]
1	2.562	1.107	3097.35	2.357	1.223	3028.71[1]
2	6.255	1.337	3500.14[1]	6.396	1.511	3596.16
3	7.478	1.197	3274.96[1]	7.564	1.381	3421.72

[1] Indicates the better of the fit results. Note that no interpretation can be given to the absolute value of F. Only the relative size of $F = -\ln L$ for various conjectures and the same data sample can be interpreted.

Efforts to include the effect of the perpendicular turbulence component, w', have met with mixed success. First, we note that as the hot-wire data are generally reported via the two quantities of mean speed, $\overline{V}$, and speed turbulent intensity $i_V = \sigma_V/\overline{V}$, it is impossible to extract more than two alternative measures from these data. Thus, the two new parameters, $\overline{u'w'}$ and σ_w, must be eliminated. If one assumes uncorrelated, isotropic turbulence, then $\overline{u'w'} = 0$ and $\sigma_w = \sigma_u = \sigma$, and the necessary integration can be accomplished to yield

$$P(V) = V\Phi(1/2,1; -2uV/\sigma^2)\exp[-1/2(V-u)^2/\sigma^2]\sigma^2 \qquad (45)$$

where Φ is the confluent hypergeometric (or Kummer) function. In at least one case (e.g., sampling point B) this pdf provides a superior fit to the data; however, the range of i_V that such a hypothesis can accommodate is $0 \leq i_V \leq 0.523$. As many of the observed i_V values exceed this cutoff of 0.523 and approach 1.0 (a few cases exceed 1.0), one begins to doubt that this more complicated, 2-D turbulence model is appropriate.

A Hot-wire Measurement Conversion Algorithm

Having selected the appropriate pdf in V, P(V), one is then able to compute the required quantities $\overline{V}$ and $\sigma_V = [\overline{V^2} - \overline{V}^2]^{1/2}$ by solving the integrals

$$\overline{V^n} = \int_0^\infty dV\ V^n\ P(V) \qquad (46)$$

for $n = 1,2$. The details of this integration process are quite straightforward for the three pdfs given by equations (43-45). The results are

$$\overline{V} = u\ \mathrm{erf}(p/\sqrt{2}) + \sigma\sqrt{2/\pi}\ \exp(-p^2/2) \qquad (47)$$

for the 1-d Gaussian turbulence assumption,

$$V = u + \sigma \exp(-\sqrt{2}p)/\sqrt{2} \qquad (48)$$

for the 1-d Double-Exponential hypothesis,

where $V^2 = u^2 + \sigma^2$ for both 1-d hypotheses

and where $p = u/\sigma$, and

$$V^n = \Gamma(1 + n/2)(\sqrt{2}\sigma)^n \Phi(-n/2, 1; -p^2/2) \qquad (49)$$

for the 2-D, isotropic, uncorrelated Gaussian turbulence conjecture. Equations (47 through 49) enable one to go from the two parameters u and σ to the hot-wire measured quantities V and $i_V = \sigma_V/V$, but, unfortunately, these equations cannot be inverted analytically and so must be solved iteratively to obtain u and σ from the measured quantities. Fortunately, the turbulent intensity $i_u \equiv \sigma/u$ can be written as a function of the single quantity p so that the iterative search need be conducted only on a single variable rather than two.

As previously mentioned, the 2-D isotropic, uncorrelated Gaussian turbulence model only allows values of i_V less than 0.523. That is, $i_V = 0.523$ corresponds to $i_u = \infty$; thus, leaving a significant fraction of the measured data uninterpretable. Figure 18 shows the relationship between i_V and i_u for the 1-d Gaussian and double-exponential distributions. In these cases, the maximum values of i_V are 0.755 and 1.0, respectively. Because the double exponential conjecture allowed the maximum amount of data to be interpreted and correspondingly caused the smallest corrections at low turbulent intensities, it was selected as the conversion hypotheses for the BU wind tunnel data.

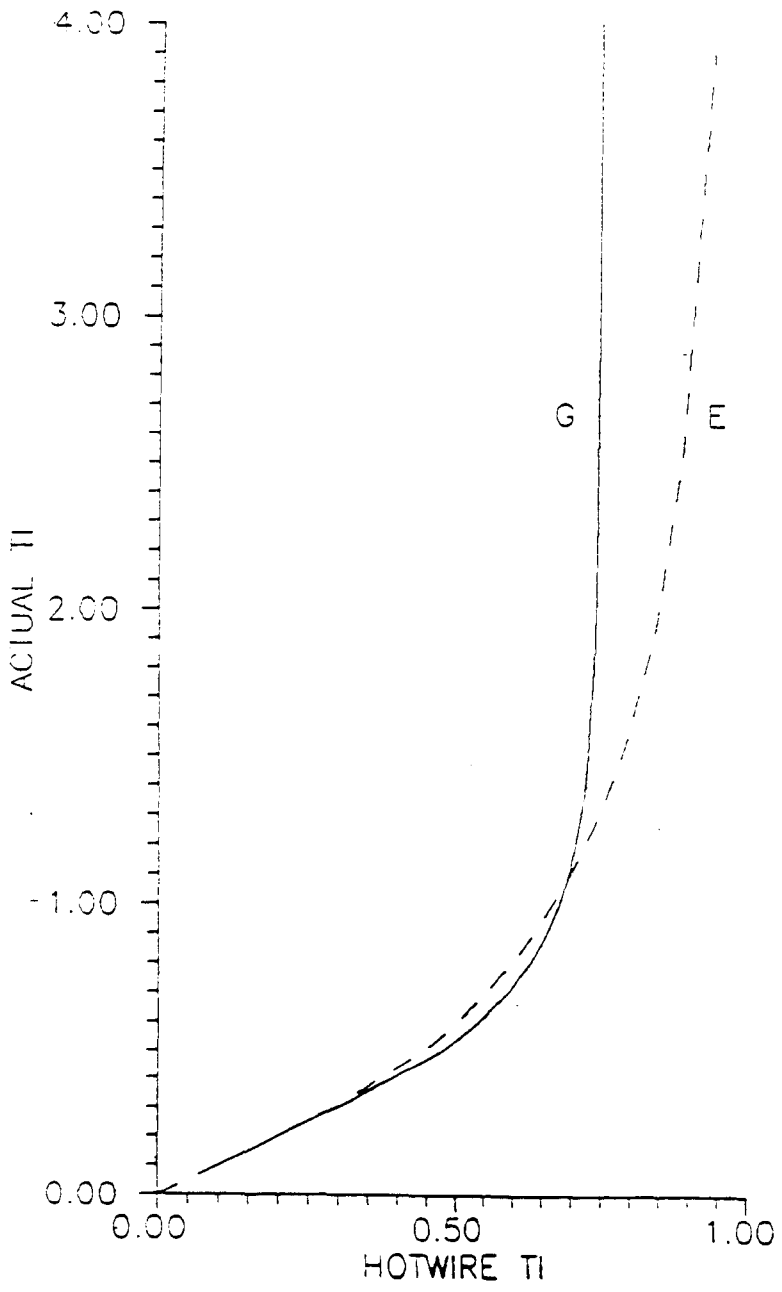

Figure 18. Velocity turbulent intensity, i_u, vs. hot-wire speed turbulent intensity, i_v, conversion curves for the 1-D Gaussian and double exponential turbulence distribution assumptions.

Table 5 shows the effect of converting from the V, i_v representation to the u, i_u representation for the W/H = 1 street canyon. Values of u and V correspond closely in the relatively low turbulence zone above the canyon, but differ so markedly within the canyon as to suggest a completely different physical picture of the flow. For example, in the downwind, lower corner of the canyon (i.e., point C) the mean V of 0.341 is due purely to turbulence, such that the mean advective velocity, u, is zero.

Table 5. Effect of conversion of hot-wire measurements to mean transport velocity and turbulence for the W/H = 1 canyon.

Sampling Point	Hot-Wire Measured		Computed Values		
	V(m/s)	i_v	u(m/s)	σ(m/s)	i_u
A	0.231	0.922	0.100	0.298	2.98
B	1.535	0.451	1.502	0.761	0.507
C	0.341	1.075	0.0	0.482	∞
1	2.565	0.429	2.522	1.195	0.474
2	6.255	0.214	6.254	1.345	0.215
3	7.478	0.160	7.478	1.197	0.160

The geotrophic or maximum wind speed was 9.72 m/s.

APPENDIX B

ANALYSIS OF HOT-WIRE DATA FOR WITHIN-CANYON MEAN FLOW: COMPARISON WITH THE HOTCHKISS-HARLOW MODEL

Introduction

The presence of a relatively weak vortex in the lee, and a smaller, stronger vortex upwind of an isolated building has been confirmed in numerous full-scale and wind tunnel studies. In the case of the rectangular notch of $W/H \cong 1$, these upwind and lee rotors merge to form a single, strong, stable, rotor. It was for this rotor, driven by a skimming flow above the notch, that Hotchkiss and Harlow (1973) developed an approximate solution to the linearized Navier-Stokes equation. Their solution for the mean velocity components within the canyon is

$$u = u_o(1-\beta)^{-1}[\alpha(1 + ky) - \beta(1-ky)/\alpha] \sin(kx) \qquad (50)$$

and

$$w = -u_o ky(1 - \beta)^{-1}[\alpha - \beta/\alpha] \cos(kx) \qquad (51)$$

where

$$k = \pi/W, \quad \beta = \exp(-2kH),$$

$$\alpha = \exp(ky), \quad y = z-H,$$

and u_o is the external, driving wind speed which the solution is designed to match at the point $x = W/2$, $z = H$. Their solution is divergence free, but is approximate, because it does not give back the same vorticity expression which they used as a starting point. In addition, their linearization approximation is equivalent to assuming a very low Reynolds number flow, as is seen from the mathematical development of Shen and Floryan (1985). However, our purpose here is not

to critique their mathematics but to further examine the regime of validity of this quite useful expression for the velocity field.

The Reference Wind

The primary need is for an expression to predict the canyon transverse, advective wind at the bottom of the canyon where the automotive sources are present. Correct predictive behavior along the sides or near the top of the canyon is of secondary importance. In Yamartino and Wiegand (1986), the full-scale, Bonner Strasse flow data were reasonably modeled using a reference or driving wind, u_o. Measured at a height of $z \cong 1.5H$ rather than at the appropriate theoretical height of $z = H$. Knowing the height at which it is reasonable to measure the wind and what value of wind speed is appropriate to use in equations 50 and 51 constitutes a first critical problem.

In his wind tunnel study of the Bonner Strasse, with peaked roof buildings on both sides defining a canyon of aspect ratio (W/H) = 1.09, Builtjes (1984) showed that at $z \cong 1.5H$ the wind speed shear is quite large and that measurements taken at this height are also a function of canyon width. His suggestion to measure at higher elevations (Builtjes and Vermeulen, 1980) is, however, difficult and expensive to accomplish in full-scale studies, and such data are, of course, unavailable for routine modeling studies.

The geostrophic wind speed is a much more logical and readily obtainable "reference" quantity, and examination of the TNO and BU wind tunnel data show:

- TNO measurements at $z \approx 1.5H$ for the Bonner Strasse case gave a wind speed of 61 percent of the geostrophic wind.

- BU measurements of the W/H = 1 canyon, corrected for turbulence, indicate that use of a reference wind equal to 65 percent of the geostrophic wind, u_g leads to perfect agreement with equation (50) near the bottom center of the canyon.[4]

Thus, it becomes convenient, and consistent with previous work, to define the reference wind u_o in terms of the geostrophic wind as

$$u_o / u_g = 0.65 \pm 0.05 \qquad (52)$$

where the $\pm$ 0.05 is based on variability between the BU and TNO data and between different BU runs.

Such a scaling in terms of the geostrophic flow only has some universality if the canyons themselves are the main roughness elements giving rise to the wind profile. This notion can be supported by fitting the turbulence corrected profile above the blocks with the log profile

$$u(z) = u^* \ln[(z-d)/z_o]/k \qquad (53)$$

[4]This value of about 65 percent u_g is also measured at $z \approx 2H$ for these flat roof blocks: not markedly different from the $z \approx 1.5H$ for the peaked roofs.

where k is the von Karman constant and optimal values of the parameters are

$$u_* = 0.795 \text{ m/sec}$$
$$z_o = 0.166 \text{ in, and}$$
$$d = 3.37 \text{ in.}$$

Results of this wind profile fit are displayed in figure 19. While the roughness length, z_o, and displacement height, d, may be functions of canyon width, they are primarily functions of canyon height H. Scaled by this height of 3.5 in (0.0889m) one obtains $\alpha = z_o/H = 0.0474$ and $\beta = d/H = 0.963$.

Now presuming that the reference height is taken as a multiple, r, of building height and that geostrophic speeds are achieved at about 10H, use of the profile equation enables us to express u_o/u_g as

$$u_o/u_g = \ln[(r-\beta)/\alpha]/\ln[(10-\beta)/\alpha] \quad (54)$$

which is now fully independent of H. Inserting the values of a and β, choosing r = 2 as discussed earlier, and correcting for the approximate 5 percent overshoot in the prediction of the geostrophic speed at z = 10H, one obtains

$$u_o/u_g = 0.62, \quad (55)$$

in good agreement with the constant value of 0.65 from equation (52).

Width-to-height Ratio Variation

Based on equation (52), the BU-measured canyon bottom-center velocities, corrected for turbulence according to the procedure

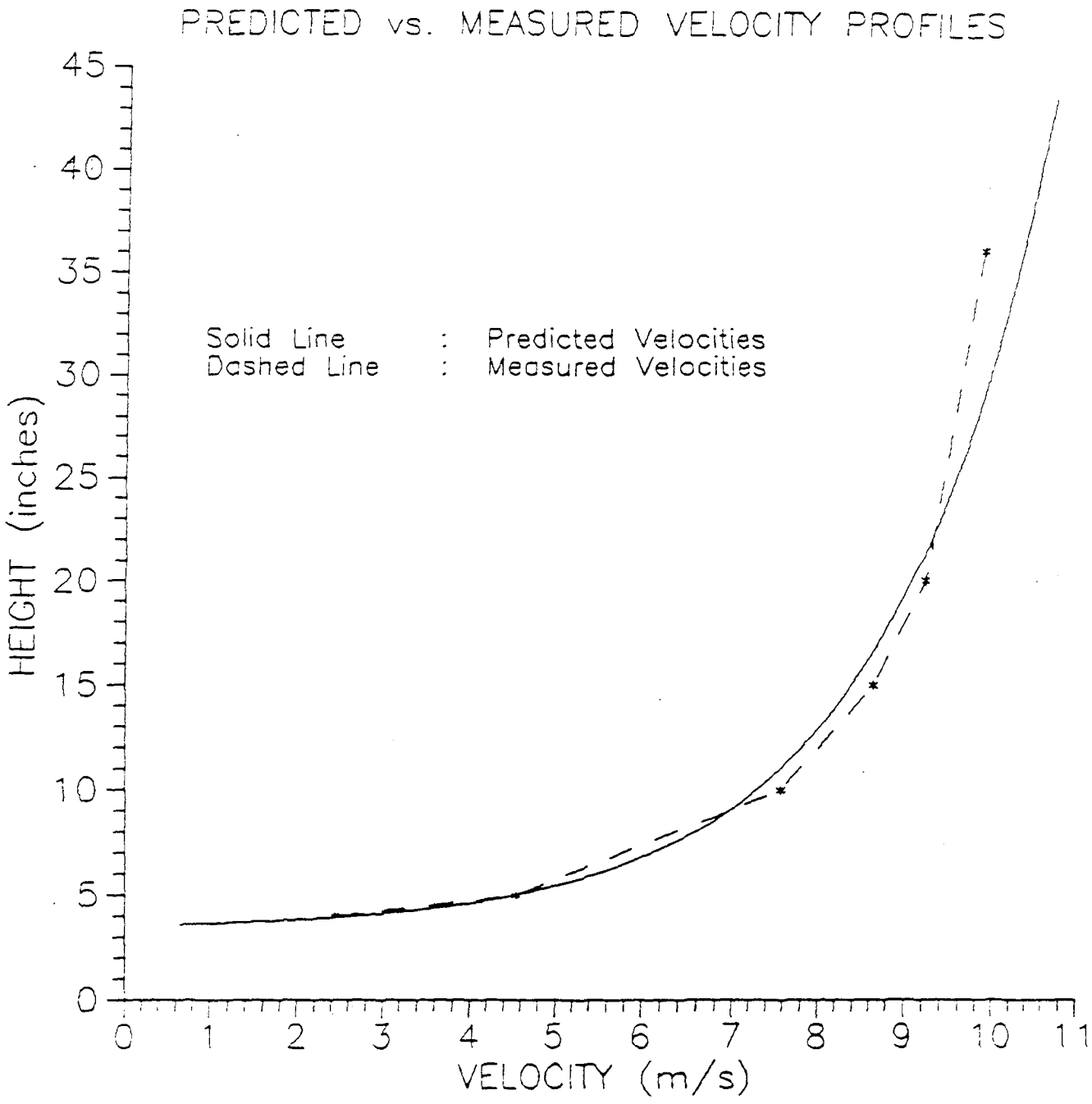

Figure 19. Predicted vs measured velocity profiles above a series of W/H=1 street canyons of height 3.5 in (0.0889m). The prediction incorporates optimal values of friction velocity, roughness, length and displacement height into a logarithmic profile as discussed in the text.

described in appendix A and normalized by u_o, are plotted in figure 20 along with the corresponding value of equation (50) also normed by u_o. The agreement between predicted and observed is, as predetermined by equation (52), perfect at W/H = 1, but is also very reasonable at W/H = 1.5. The rapid drop for narrower canyons is also correctly predicted qualitatively, and the quantitative agreement at W/H = 0.5 (i.e., 0.04 observed vs 0.02 predicted) is acceptable given that both numbers are small, and thus represent an almost complete suppression of canyon transverse flow, and because the V to u conversion uncertainty is quite high in this highly turbulent situation (i.e., i_V = 0.96). This suppression of canyon transverse flow for W/H $\leq$ 0.5 is consistent with the assumption of canyon parallel flow in Sontowski's (1978) CANNY model designed for the deep street canyons of New York City.

Predictions for canyons wider than W/H = 1.5 consistently exceed the observations in a pattern that becomes worse as the canyon widens. This degeneration of performance at larger W/H is expected because the concept of a single vortex filling the canyon, that is implicit in the Hotchkiss-Harlow solution, is not confirmed by observations. Hosker (1987), in his review of various wind tunnel experiments, indicates that the skimming flow, single vortex situation exists only for W/H $\leq$ 1.55. For wider canyons, one is dealing with the combined effect of a lee recirculation zone plus the frontal separation zone/vortex of the downwind obstacle. The combined effect of these two rotors is also to pump material upwind across the bottom of the canyon so some aspects of the Hotchkiss-Harlow (H-H) model may be useful though the details (e.g., vortex center location) are incorrect. Thus it is useful to tabulate the observations and H-H predictions with the objective of extracting a H-H renor-

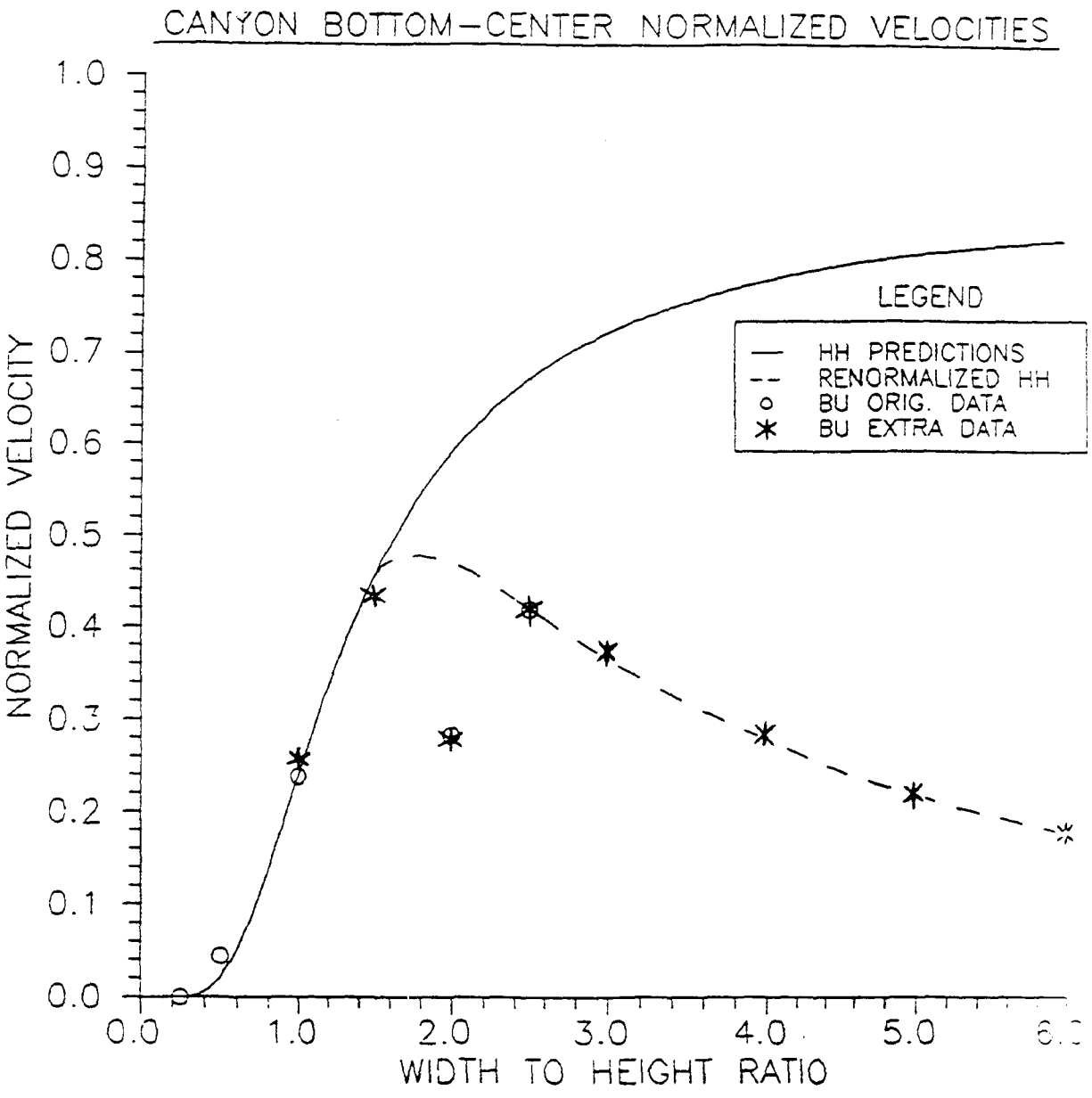

Figure 20. Street canyon bottom-center normalized velocities as a function of canyon width-to-height ratio, W/H. The Hotchkiss-Harlow (H-H) predictions (solid line) are from equations (50-51) whereas the renormalized H-H predictions (dashed line) include multiplication by the correction factor, $f_{W/H}$, given by equation (56).

malization factor, $f_{W/H}$ ≡ observed/HH predicted, computed at the bottom-center of the canyon. Table 6 presents these results for $W/H \geq 1$.

Table 6. Comparison of observed velocities and Hotchkiss-Harlow predictions at the bottom-center of rectangular street canyons.

W/H	Measured u/u_o	H-H Prediction	Renormalization Factor $f_{W/H}$	Modelled $f_{W/H}$
1	0.238	0.24	1[1]	1.0
1.5	0.432	0.454	0.95	1.0
2.0	0.282	0.589	0.48	0.79
2.5	0.418	0.670	0.62	0.63
3.0	0.372	0.721	0.52	0.51
4.0	0.283	0.776	0.36	0.36
5.0	0.217[2]	0.804	0.27	0.27
6.0	0.176[3]	0.820	0.21	0.22

All velocities are corrected for turbulence.

[1] Determined by equation (52)
[2] Somewhat less than the maximum value of u measured along the bottom
[3] Only point available: not clear if u is a maximum.

Examination of these tabulated values of $f_{W/H}$ over the limited range of W/H exceeding 1.5, suggests the empirical relation

$$f_{W/H} = \begin{cases} 1.0 \text{ for } W/H \leq 1.5 \\ 1.0/[1.0 + 0.6*(W/H - 1.5)^{1.2}] \\ \qquad \text{for } 1.5 < W/H \leq 6.0 \end{cases} \qquad (56)$$

As seen in figure 20, the HH equation renormalized by multiplying by $f_{W/H}$ of equation (56) provides a good fit to all the data points except for W/H = 2.0. It is at this W/H ratio that one is tempted to conjecture a destructive interference between lee and building upwind rotors, in much the same fashion as two gears of diameter H and in contact would find it difficult to both turn clockwise simultaneously. Such a very large wind shear near the canyon center would create strong dissipation and slow the rotors. While beyond the scope of this study, investigation of various properties of this "anti-resonance" (i.e., should it exist), such as its width $\delta(W/H)$, would provide insight into how strong the tendency is to form a single elliptical rotor vs a pair of circular rotors.

Use of the empirical equation (56) to provide within-canyon speeds clearly extends the usefulness of the H-H equation uations; however, at a large enough W/H, the notion of a single vortex is less useful than that of separate recirculation and frontal separation vortices. This transition can be studied by considering hot-wire measurements within a distance H of the upwind and downwind walls (i.e., but away from the highly turbulent corner or Moffatt vortex zones) as W/H increases toward the backward and forward step limits. Table 7 shows a uniform convergence toward the rear step, "weak vortex"

strength of $u/u_o \simeq 0.035$, whereas the forward step "strong vortex" appears to converge toward $u/u_o \simeq 0.29$ before jumping down to the forward step value of 0.18.

Table 7. Observed velocities near the rearward and forward canyon walls as a function of W/H. Canyon center speeds are also presented.

W/H	x(Hot-Wire)/H (from wall)	u/u_o Rearward Facing	u/u_o Canyon Center	u/u_o Forward Facing
2.5	0.39	0.103	0.418	0.357
3.0	0.50	0.069	0.372	0.320
4.0	0.71	0.039	0.283	0.285
5.0	0.79	0.038	0.217	0.295
∞	0.50	0.035	-	0.183

However, the forward step study was performed using literally no upwind canyons to roughen the flow and create an appropriate urban approach flow. Thus, the large W/H (≥ 4) result of $u/u_o \simeq 0.29$ is considered the appropriate strength for the one-sided urban canyon. The fact that the vortex in front of the forward facing step is about eight times stronger than the recirculation zone behind the rearward facing step is in marked contrast to the HH model or numerical calculations using a stream function (e.g., Shen and Floryan, 1985) which predict equal strength rotors adjacent to the lee and downwind walls.

Some insight into this leading/trailing rotor asymmetry is obtained by examining a numerical simulation (Bernier, 1985) of

a trailing rotor. As seen in figure 21, the rotor center is located at about $z \approx 0.73H$ with the peak counterflow speed of $u/u_o \approx 1/4$ occurring at $z = H/2$ rather than near $z = 0$ as predicted by the H-H model. Counterflow speeds near $z \approx 0$ are seen to be very small (i.e., $u/u_o \approx 0.05$) as measured in the wind tunnel. Thus, the trailing face rotor may not be so much weaker than the leading face rotor, but simply confined to the upper half (i.e., $0.5 \leq z/H \leq 1$) of the region. A downwind wall may well be needed to cause this rotor to fill the region and generate peak counterflow speeds near $z \approx 0$.

Further examination of table 7 and other hot-wire sampling locations indicate that whereas $W/H = 4$ represents rather complete decoupling of the lee and forward step rotors from one another, the intervening x regime (near $z \approx 0$) has monotonically varying counterflow velocities intermediate in strength between those of the two rotors. For $W/H > 4$, the variation in counterflow speed with x shows a relative minimum near the canyon center and one begins to suspect development of a new flow regime near the center of the canyon. Of course, for large enough W/H this central region will no longer involve counterflow velocities but will contain an evolving boundary layer of positive velocities. Thus, beyond $W/H = 4$, one loses confidence in equations (50-51) to provide even a qualitatively reasonable description of the flow. Unfortunately, the scarcity of data for $W/H > 4$ and the inability of the single hot-wire to detect the sign of the flow make one reluctant to conjecture a reasonable flow model for these wider canyons. It should also be noted that the flow visualization studies suggest that the existence of a single rotor for $W/H > 2$ is quite sporadic.

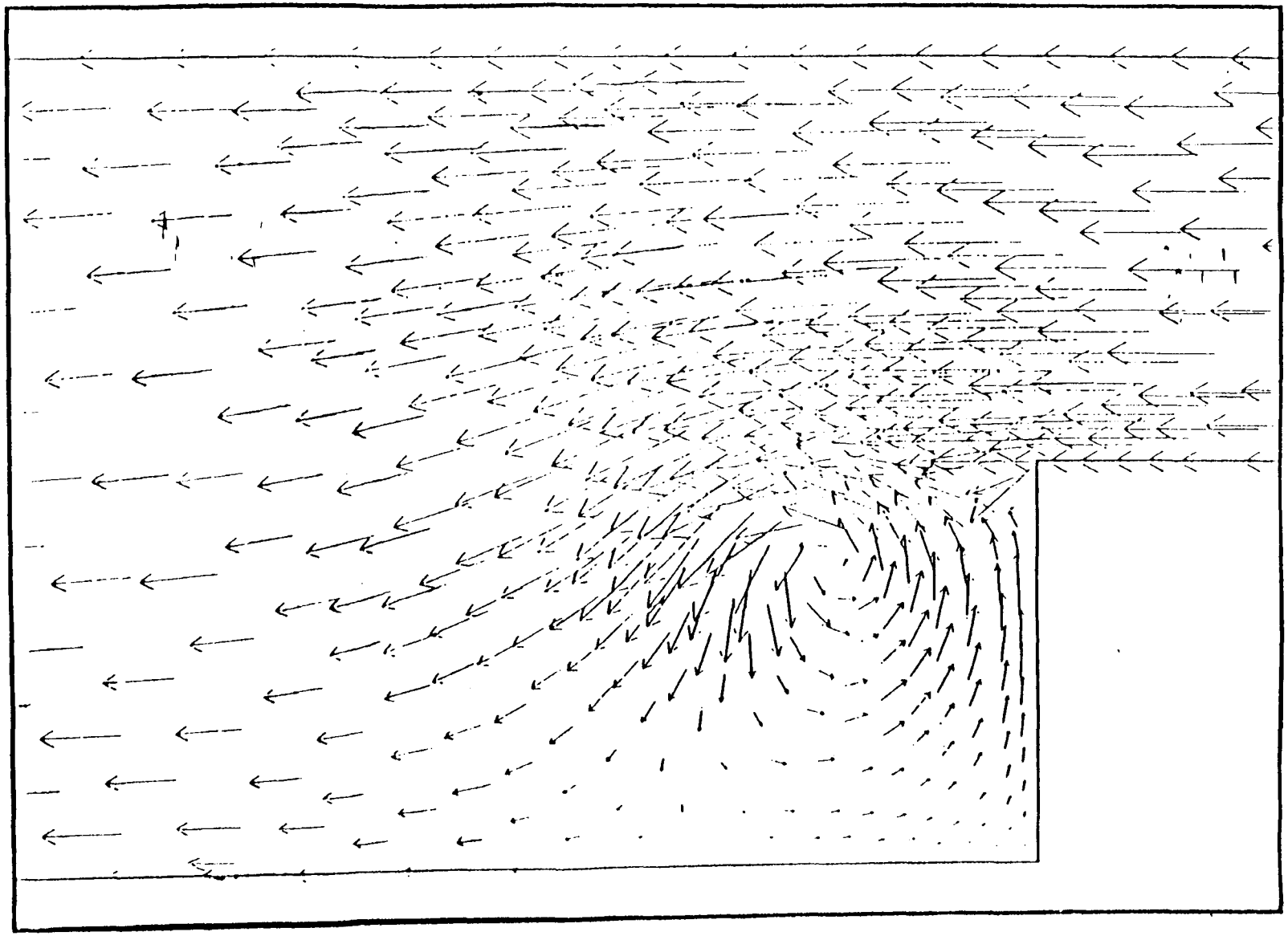

Figure 21. Numerical grid model simulation of flow over a rearward facing step (Bernier, 1985).

Building Height Variation

The preceding analyses are all for the case where lee and luv side buildings have the same height, H. One BU measurement involved an upwind canyon of height $H_U = W$ and a downwind canyon of height $H_D = 2W$. This resulted in a bottom center vortex speed of $u/u_o = 0.412$ or 72 percent higher than for the simple W/H = 1 canyon.

In a full-scale study of an asymmetric street canyon, (i.e., H_G = 24m, H_S = 20m, W = 24m in Lyon, Joumard and Vidon's (1980) data suggest that the transverse counterflow speed at street level increases about 58 percent when the flow is toward the greater building, H_G, rather than toward the smaller building H_S.

Assuming that the basic quantitative features of the rotor (i.e., shape and vertical extent) are determined by the smaller building H_S and the ratio W/H_S, a simple linear perturbation expression for the maximum, canyon-transverse, recirculation velocity is:

$$u/u(W/H_S) = 1.0 + a \cdot \Delta H / H_M \equiv f_{\Delta H} \qquad (57)$$

where $\Delta H = H_D - H_U$ can be positive or negative,

$H_M = (H_D + H_U)/2 = (H_G + H_S)/2$, and

$$a = \begin{cases} 1.08 \text{ based on the BU data and} \\ 1.25 \text{ based on Joumard and Vidon.} \end{cases}$$

Choosing the more conservative a = 1.08, one now has the additional multiplicative correction factor, $f_{\Delta H}$, for the basic HH

equations (50 and 51). Given the very limited data from which equation (57) has been developed, we further constrain $f_{\Delta H}$, to be in the range 0.5 to 2.0.

Building Porosity Variation

In several of the wind tunnel experiments, the fixed 3.5 in (0.0889m) high block was replaced with a stack of seven, 0.5 in (0.00127m) slabs or their spacer equivalent. Thus, a situation was created involving a solid face on one side of the canyon and a semi-open structure on the other side of a canyon of unit width-to-height ratio. As the semi-open structure consisted of 4 solid slabs and 3 open spaces, we define its porosity, p, as p = 3/7 = 0.43.[5]

Given the fact that the downwind building produces a stronger vortex than an upwind building, one expects a porous downwind wall to show the most dramatic effect on slowing the rotor. Experiments showed that the vortex strength at the bottom center of the canyon dropped to 64.8 percent of the solid wall result when the porous wall was the downwind structure and 81.9% when it was the upwind structure. Thus, we are led to the following correction factors for porosity:

$$f_p^D = 1.0 - 0.86p \text{ for porous downwind buildings, and} \qquad (58)$$

$$f_p^U = 1.0 - 0.44p \text{ for porous upwind buildings.}$$

[5]Due to the slabs being slightly less than 1/2 in (0.00127m), an 1/8 in (3.18×10^{-3}m) shim was used, leading to a corrected porosity of p = 0.41.

Such a porosity variable should enable one to deal with situations where one side of the canyon is defined by a parking garage of semi-open construction. Measurements were also made for the narrower W/H = 0.5 situation, but the lower speeds and higher turbulent intensities render these data less definitive.

Street Canyon Curvature Variation

Up to this point the canyons considered have all been 2-D in nature, but the curved street canyon situation is not only possible, but is often found at modern commercial airports. Such a design with the parking garage at the hub and jetways emanating radially from a concentrically curved terminal leads to minimal passenger walking and maximal parking room for the aircraft.

Considering the diameter of curvature, D, as defined at the middle of the street canyon, one is led to propose the variable $d \equiv W/D$ as the principal variable defining departure from two-dimensionality. As the radius of curvature typically carries a sign we define d positive when the canyon bends with the flow and d negative when the canyon bends into the flow. Thus, if the wind is coming across the terminal from the jetways, d will be positive. Figure 22 shows the turbulence compensated, canyon-bottom, advective velocities, normalized by the zero-curvature counterpart, for d in the range - 0.31 to + 0.31. Clearly, the behavior is not simply a function of curvature, so studies were carried out using the other available variable (W/H) as well. Dimensionless correction factors f_C^+ and f_C^-, expressed as,

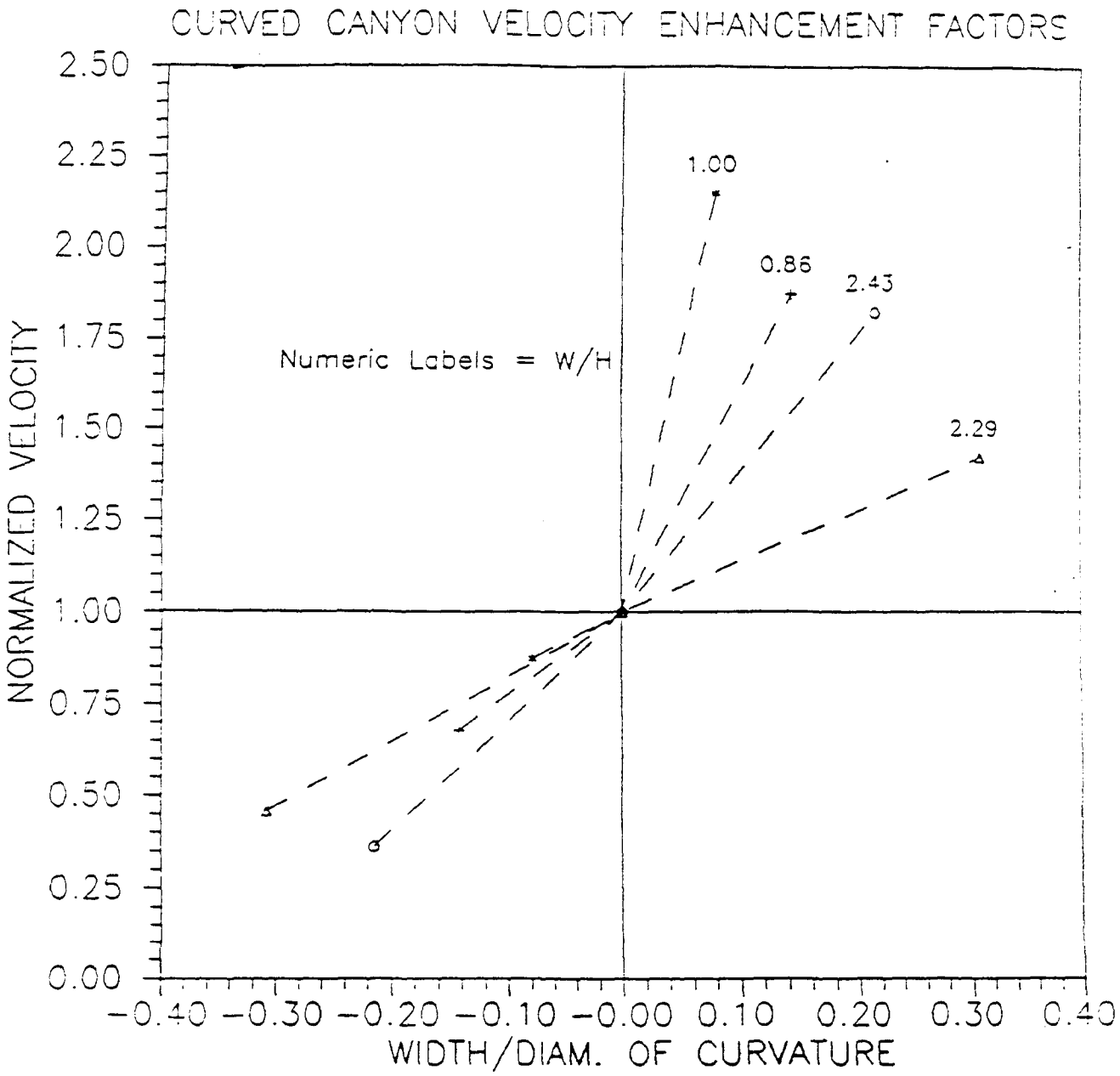

Figure 22. Street canyon bottom-center velocities for curved street canyons normalized by straight canyon velocities for several curvatures and W/H values. The curvature parameter, d, is defined in the text as d = W/D.

$$f_C^+ = 1.0 + 1.15\ d^{0.1}/(W/H)^{0.5} \text{ for } d > o$$

and (59)

$$f_C^- = 1.0/[1.0 - 2.6\ d(W/H)] \text{ for } d < o,$$

with $d \equiv W/D$, were then developed for positive and negative curvature, respectively. One notes that because of the $d^{0.1}$, only a small amount of convex (or positive) curvature with respect to the flow is needed to achieve a large fraction of the maximum effect. For example, d = 0.001 will yield 50 percent of the maximum positive curvature, flow speedup influence. Table 8 shows the comparison of observed and equation 59 predicted, vortex speed correction factors.

The agreement is hardly perfect, but more complex formulations did not appear warranted, given the range of d and (W/H) considered.

Combined Effects

Thus far, we have considered correction factors to the H-H equations 50 and 51 for:

- Width-to-height ratio via equation 56 for $f_{W/H}$.
- Unequal building heights via equation 57 for $f_{W/H}$.
- Building porosity via equation 58 for f_p.
- Canyon curvature via equation 59 for f_c.

Table 8. Curved canyon speed correction factors.

Expt	W/H	d	u(d)/u(d=0)	Predicted f_c
77	1	+0.0787	2.15	1.89
85	1	-0.0787	0.88	0.83
81	2.429	+0.215	1.82[1]	1.63
83	2.429	-0.215	0.36[1]	0.42
87	2.286	+0.308	1.42[1]	1.68
89	2.286	-0.308	0.46[1]	0.35
97	0.857	+0.143	1.87[2]	2.02
99	0.857	-0.143	0.68[2]	0.76

[1] Linear interpolation of W/H = 2.-0 and 2.5 straight canyon, bottom-center velocities was required. These interpolated, normalized speeds were 0.40 and 0.36 for W/H ratios of 2.429 and 2.286, respectively.

[2] The H-H predicted normalized speed of u/u_o = 0.168 for W/H = 0.857 was assumed as no straight canyon counterpart was measured.

In situations where multiple factors are present, the correction factors, all unity for the W/H = 1 symmetric, nonporous, uncurved canyon, might be expected to combine multiplicatively to form a total H-H correction factor, f_t, where:

$$f_t = f_{W/H} \cdot f_{\Delta H} \cdot f_p \cdot f_c \qquad (60)$$

One test of this relation involves consideration of the combined curved canyon and porous building tests performed to simulate a realistic airport situation.

The results presented in table 9 do not provide strong support for the concept of factorization or multiplicativity of the separate correction factors. Instead, we see that:

- The presence of a slotted building downwind has less of a slowing effect on the flow when the canyon has positive curvature.

- The presence of a slotted building upwind has negligible effect (or even a slight enhancing effect) on the flow speeds when the canyon has negative curvature.

- The slight height difference in buildings has a nearly negligible influence.

The weakened effect of porosity may be substantially due to the along-wind size of the slotted building. In the slotted block tests used to develop the porosity factor f_p, the alongwind block dimension was 3.5 in (0.0889m), or the same as the block height. The slotted parking garage, however, was about 18 in (0.457m) deep and was even blocked upwind in the case of test

Table 9. Curve-slotted canyon speed correction factors.

Test	W/H_s[1]	d	Observed u/u_0	Observed[2] Speed Multi-plier	$f_{\Delta H}$	f_p[3]	f_c	Predicted Speed Multi-plier
95	2.37	0.308	0.467	1.22	0.96	0.63	1.66	1.01
93	2.37	-0.308	0.211	0.55	1.04	0.81	0.35	0.29

[1] As no shim was used, the garage had a smaller height of H_s = 3.375 in (0.0857 m).

[2] Observed speed multiplier involved use of interpolated normalized speed of 0.383 for W/H = 2.37.

[3] A porosity of 3/7 was used.

93 (volume II test numbering scheme). Thus, with pressure gradients reduced by a factor of about five (= 18/3.5), and possibly much weaker for the blocked garage case, the actual f_p would be expected to be much closer to unity. Nevertheless, test 93 remains difficult to explain without conjecturing an additional mechanism to inhibit the dramatic slowdown predicted on curvature alone.

Finally, the more reasonable behavior of test 95 is most welcome as this corresponds to the potentially more serious pollution case of flow from the "terminal airside" where aircraft and automotive emission effects combine.

APPENDIX C

ANALYSIS OF HOT-WIRE DATA FOR WITHIN-CANYON TURBULENCE: EXTENSION OF AN EMPIRICAL MODEL

Introduction

The intent of this appendix is to follow a path similar to that followed in appendix B for the within-canyon flow. However, in the case of flow, we began with an approximate solution for the Navier-Stokes equation and evaluated empirical correction factors for departure from the symmetric, 2-D canyon. In the case of within-canyon turbulence, we begin with an empirical model (Yamartino and Wiegand, 1986: henceforth YW) that was tuned to match four, u-v-w measurement locations within the full-scale Bonner Strasse study. This canyon, with its peaked-roof, European style houses, has been modeled in the TNO wind tunnel by Builtjes (1983,1984) and exhibits somewhat different flow and turbulence characteristics than its rectangular notch counterpart measured in this study at the BU facility. In the sections which follow, these differences will sometimes be invoked and at other times, ignored, depending on the issue and data available.

As mentioned, this appendix will parallel the previous one in its search for empirical canyon-perturbation correction factors, but will first focus on an attempt to improve and generalize the original turbulence submodel.

Bonner Strasse Revisited

The original CPB-1 turbulence model of YW (reprinted in appendix H) received some criticism on the grounds that:

- It was formulated in terms of the vector mean wind speed (VMWS) quantities, (u,v,w), which are seldom measured.

- It contained a constant term A_c representing a minimal level of turbulence.

- The additivity of mechanical and thermal terms did not precisely agree with current formulations (e.g., Hicks, 1985) involving the friction velocity, u*, and the convective scaling velocity, w*.

The last of these issues was addressed in YW. The simple linear combination used proved somewhat superior (i.e., lower mean square error (MSE)) to addition rules involving u* and w* squared or cubed; however, it was indicated that the sensitivity to heat flux terms was only about one-third that of the mechanical terms, so that the superiority of a particular addition rule may not be highly significant statistically.

The first two issues are coupled in the sense that a zero VMWS does not imply a zero scalar wind speed, V, or the absence of turbulence σ, so that some minimal turbulence was needed under these conditions. However, both objections can be removed simultaneously by replacing the mechanical term,

$$A_m(s_o^2 + \alpha^2 v_o^2)^{1/2} + A_c, \quad (61)$$

where $s_o^2 = u_o^2 + w_o^2$ and the
subscript o denotes reference height values,

with a formulation based on the reference height, scalar average speed, V_o, such as:

$$V_o(\cos^2 \theta_o + \alpha^2 \sin^2 \theta_o)^{1/2} g(V_o), \quad (62)$$

$$\text{where } g(V_o) \equiv (1 + aV_o)/(1 + aV_o/A_m) \quad (63)$$

and θ_o is the azimuth of the reference wind.[6]

This rational polynomial form for $g(V_o)$ is designed to incorporate the properties that at large V_o, the scalar and vector speeds are nearly identical and $g(V_o) \rightarrow A_m$; whereas at zero vector wind the observed V_o represents 100 percent turbulence.

Although equation (62) is somewhat more complex in appearance than equation (61), it has the same number of adjustable parameters and is more practical for an applied model. Further, the parameter optimization study results, presented in table 10, show that the equation substitution was not only reasonable but led to superior results. One notes that the parameter, a, generally fell in the range 0.5 - 0.6 s/m, whereas the new A_m values were slightly smaller than the old values, which is expected because V_o is larger than the vector wind. It should be noted that in the BU wind tunnel studies, the geostrophic and

---

[6] This redefinition ignores the effect of the vertical component, w_o. The w_o were generally small and have a negligible impact on the azimuthal angle.

Table 10. Comparison of optimal parameters and fitting results for turbulence models based on vector (orig.) and scalar (new) wind speeds and given by equations (61) and (62), respectively.[1]

Turbulence Component	σ_u orig.	σ_u new	σ_v orig.	σ_v new	σ_w orig.	σ_w new	σ_T orig.	σ_T new
Λ_m	0.124	0.117	0.180	0.172	0.133	0.127	0.129	0.120
Λ_c(m/s)	0.161	---	0.212	---	0.163	---	0.161	---
a(s/m)	---	0.486	---	0.549	---	0.586	---	0.535
Correlation coefficient, r	0.879	0.876	0.769	0.790	0.901	0.912	0.908	0.912
Average percent deviation	16.2	16.8	24.8	23.9	15.3	14.5	14.3	13.9
r.m.s. percent deviation	21.1	21.7	32.6	31.0	19.6	18.5	18.3	17.9

[1]All runs assume a vehicle heat output of 7.5 kJ/m. All model parameters not listed were held fixed at original values.

reference height winds (as discussed in appendix B) were high enough and had low enough turbulent intensities that V_o and u_o do not differ by more than 1 to 2 percent and henceforth are considered interchangeable.

Width-to-height Ratio Variation

The typical hot-wire measurement locations sampled in the BU study are show in figure 23. As W/H was varied, location B was kept at the canyon center and at a height of 1/4 in (6.35 by 10^{-3}m), location 1 was kept at canyon top-center, and locations A and C were put in the lower corners, 1/4 in (6.35 x 10^{-3}m), from the canyon walls and floor. Ideally one would like to begin with consideration of the turbulent components σ_u, σ_v, and σ_w everywhere within the canyon, but these data are neither available nor could they be usefully input to the CPB series of models. The most critical turbulence measures needed by the CPB model are:

- The mean σ_w across the bottom of the canyon at source height. (Denoted σ_{wb}, this quantity determines the rate of spread of the plume as it is advected from the vehicles to the lee wall and, along with advection velocities and initial dilution, determines the peak concentrations at curbside.)

- The mean σ_w across the top of the canyon. (Denoted σ_{wt}, this quantity determines the exchange rate with cleaner air about the canyon and thus strongly influences the fraction of pollution which is recirculated within the canyon and, consequently, pollutant concentrations throughout the street canyon.)

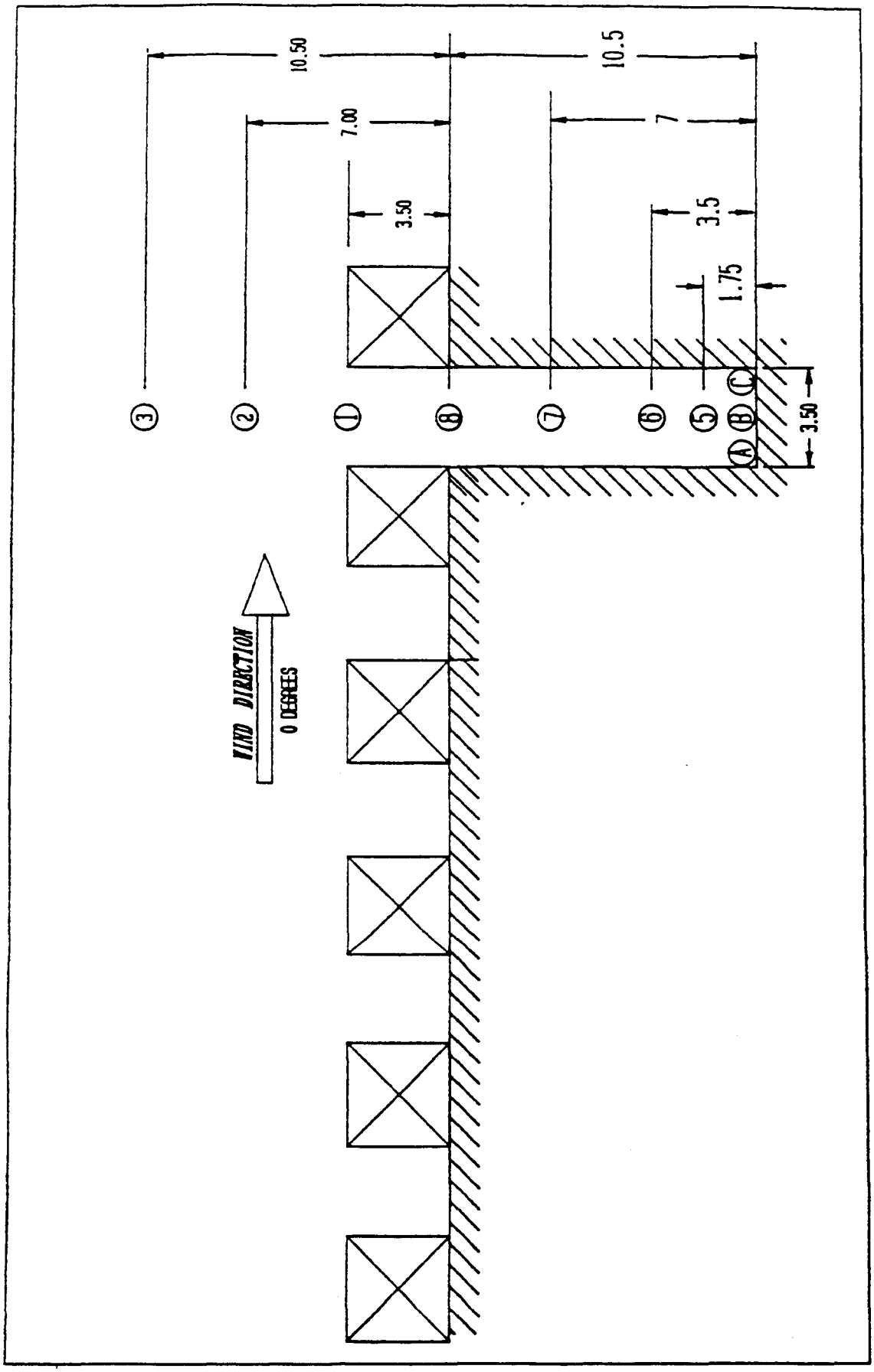

Figure 23. Hot wire measurement locations for the W/H = ½ canyon.

- The mean σ_u up the lee and luv canyon walls. (Denoted $\sigma_{u,\ lee}$ and $\sigma_{u,\ luv}$, these quantities are needed for the plume, P2, moving up the lee wall and the "fresh air" plume moving down the luv wall, respectively. While of interest for the sake of model completeness, these plume components do not influence peak, within-canyon concentration and thus are of secondary importance from a regulatory viewpoint.)

As discussed in appendix A, the single hot-wire used in these studies cannot resolve σ_u and σ_w separately but sees a combined, and not necessarily simple, influence of the two dimensions. Noting from table 10 that σ_u and σ_w were comparable in the Bonner Strasse, we make the simplifying assumption that

$$\sigma_u \equiv \sigma_w = \sigma_t = \sigma/\sqrt{2}, \tag{64}$$

where $\sigma_t \equiv (\sigma_u\ \sigma_w)^{1/2}$ is proportional to the area of the turbulence ellipse and σ is the hot-wire measured turbulence corrected for rectification bias.[7]

The turbulence levels observed at canyon top-center and bottom-center and normalized by the reference wind u_o are shown in figure 24 as a function of width-to-height ratio, W/H. The larger values of σ/u_o seen at the canyon top show substantial scatter but no systematic behavior in W/H. The smaller σ/u_o values at canyon bottom-center show a nearly systematic increase with W/H for low/moderate values of W/H followed by

[7]The YW paper erroneously defined σ_t as $(\sigma_u^2 + \sigma_w^2)^{1/2}$.

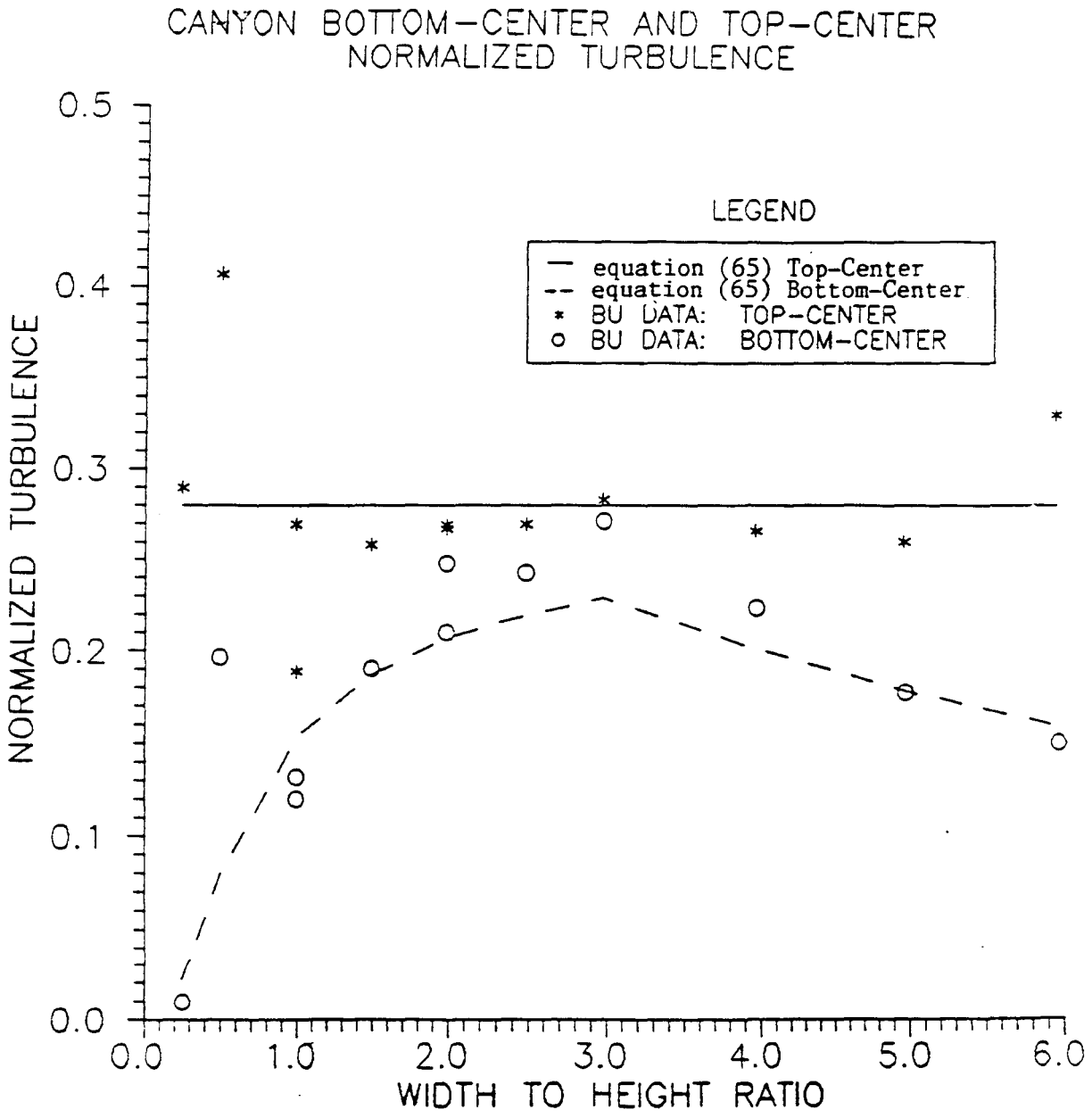

Figure 24. Street canyon top-center and bottom-center normalized turbulence as a function of canyon width-to-height ratio, W/H. Predictions are given by the empirical turbulence model of equation (65).

a gradual falloff for W/H exceeding 3.0. Also shown in figure 24 are predictions of the new empirical equation

$$\sigma/u_o = a \exp[-b(H-z)/W]/[1.0 + p'] \qquad (65)$$

where $p' = 0$ for $W/H \leq 3.0$,

$p' = c[W/H - 3.0](H-z)/H$ for $W/H > 3.0$,

and $a = 0.28$, $b = 0.65$, and $c = 0.221$ are the three, non-dimensional, fitted constants of the model. This model, the best of many different conjectures, basically says that the constant and peak turbulence, $\sigma/u_o = a = 0.28$, at the canyon top is exponentially damped as it moves down the canyon and with the canyon width, W, providing the relevant length scale. The factor $[1 + p']$ accounts for the observed falloff above $W/H = 3$ and is pure empiricism.

Not shown in figure 24, but used in the parameter fitting, are an additional five hot-wire measurements from the central interior of the narrow canyons (i.e., $z/H = 1/2$ for $W/H = 1/2$ and $z/H = 1/8$, $1/4$, $1/2$, and $3/4$ for $W/H = 1/4$). These points were added because of the anomalously high turbulence for $W/H = 1/2$ and the dramatic drop in turbulence between $W/H = 1/2$ and $W/H = 1/4$. It is interesting that $W/H = 2$ showed a dramatic suppression of flow speed whereas $W/H = 1/2$ shows a dramatic increase in turbulence. The two effects may be related by special instabilities resulting from a conjectured switching between single rotor and double rotor modes.

Absent from equation (65) is any reference to the cross-canyon distance, x, as is observed in the Hotchkiss-Harlow equations for the flows; yet, there are substantial x variations, with

turbulence levels in the downwind corner (location C) typically 2-3 times the lee corner values (location B). Unfortunately, these corner values do not have a fixed relationship with respect to the bottom-center value (location B). That is, for some W/H the turbulence at B shows a relative maximum, whereas at other W/H the turbulence increases monotonically between lee and luv. In addition, the later supplementary experiments at W/H = 2.5,3,4, and 5 used seven sampling points across the bottom of the canyon and showed that turbulence can peak somewhere between center and luv receptors with corner locations suffering an added suppression, possibly due to wall proximity effects (i.e., the wall and floor were 1/4 in (6.35 x 10^{-3}m) away). Triple-wire measurements of Builtjes (1984) show that boundaries do suppress the component of turbulence perpendicular to them so that σ_u varies substantially across the bottom of a canyon whereas σ_w is relatively constant. Because our interest is primarily in the more constant of these two quantities (i.e., σ_w along the canyon bottom and top and σ_u along the sides), the development of a more complete turbulence model including x dependence or where turbulence decays (and is produced) along the mean flow trajectory, has been deferred.

These supplementary data also provide some insight into what happens as W becomes large and the decoupled rearward/forward step situation is encountered. Table 11 presents the turbulence levels near the lee and downwind faces but away from the corner measurement sites. As mentioned previously, the x dependence pattern of σ/u_o changes as a function of W/H, making development of a full x,z dependent model difficult. One also notes that the forward facing step value converges with increasing W/H toward a value of about 0.25 whereas the rearward step value undergoes a dramatic drop from the 0.13-0.17

Table 11. Observed canyon-bottom turbulence near the rearward and forward canyon walls as a function of W/H. Canyon center turbulence values are also presented.

W/H	x(Hot-Wire)/H (From wall)	σ/u_o Rearward Facing	σ/u_o Canyon Center	σ/u_o Forward Facing
2.5	0.39	0.145	0.243	0.187
3.0	0.50	0.125	0.271	0.277
4.0	0.71	0.167	0.224	0.234
5.0	0.79	0.125	0.178	0.260
∞	0.50	0.034	--	0.234

range to a value (i.e., 0.034) four to five times smaller. This convergence/nonconvergence behavior is exactly opposite that seen for the mean flow (i.e., appendix B, table 7), where the rearward step showed a converging tendency and the forward step showed the dramatic jump. Somehow the presence of the downwind wall is effective at keeping near lee wall turbulence high at W/H values far beyond its ability to influence near lee wall mean flow.

Before moving on to consider other variations measured in the wind tunnel, it is useful to compare equation (65) with the full-scale Bonner Strasse values reported in table 10. Note that at speeds equivalent to the wind tunnel speeds, one anticipates $g(V_o) = 0.15$ (i.e., about 25 percent higher than the infinite V_o limit of $A_m = 0.12$) for σ_t/u_o at 15m (49 ft) luv and a canyon center value, involving equal weighting of f_{luv} and f_{lee}, of $\sigma_t/u_o = 0.135$. Now the comparable wind tunnel measured value is $a/\sqrt{2}$ or 0.198 which must be corrected further downward by the exponential factor of 0.895, to account for the fact that the u-v-w is located 3.4m (11 ft) below the 18.4m

(60 ft) roofline in a 20m (66 ft) wide street, to yield σ_t/u_o = 0.177, a full 31 percent higher than the equivalent Bonner Strasse value. Whether such a difference is due to the peaked roofs of Bonner Strasse or to the oversimplistic notion that the canyon top-center value can be interpolated by computing $(f_{luv} + f_{lee})/2$, or to a more fundamental difference between full-scale and wind tunnel scale studies, remains partially unresolved. However, BU measurements at z = H/2 for W/H of 2.5,3.0,4.0, and 5.0 indicate that $\sigma_{center}/(\sigma_{lee} + \sigma_{luv})$ = 0.51, in very good agreement with the $(f_{luv} + f_{lee})/2$ interpolation hypothesis.

Finally, we note that the Bonner Strasse observed ratio of 0.72, for average turbulence at z = 4m (13 ft) divided by that at z = 15m (49 ft), compares well with the equation (65) predicted value of 0.70; thus, providing additional assurance that equation (65) is not unreasonable for full-scale applications.

Building Height Variation

The preceding analyses are all for the case where lee and luv side buildings have the same height, H. In the one BU measurement involving an upwind canyon of height H_U = W and a downwind building of height H_D = 2W, a bottom-center turbulence of σ/u_o = 0.226 was observed. This is 79 percent higher than the average value observed for the W/H = 1 canyon.[8] The fact that the flow speed increases a comparable 72 percent indicates

[8] Correction factors for the empirical turbulence model are based on ratios with observed data rather than on ratios with equation (65), should this equation change at a later date.

local turbulent intensity has increased by a factor of only 1.04. Given that no additional data are available, we assume the local turbulent intensity is constant and we define the multiplicative turbulence correction factor, $g_{\Delta H}$, to be the same as the velocity correction factor given by equation (57).

That is,

$$g_{\Delta H} = \sigma/\sigma(W/H_S) = 1.0 + a \cdot \Delta H/H_M \qquad (66)$$

where $\Delta H = H_D - H_U$ can be positive or negative,

$H_M = (H_D + H_U)/2 = (H_G + H_S)/2$,

H_S and H_G is the smaller and greater building height, respectively, and

$a = 1.08$ is taken from appendix B.

As in the case of the velocity correction factor, we further constrain $g_{\Delta H}$ to lie in the range 0.5 to 2.0.

Building Porosity Variation

In several of the wind tunnel experiments, the fixed 3.5 in (0.0889m) block was replaced by a series of slabs separated by spacers, leading to an "openness" or porosity factor of p = 0.41. In these tests the velocity at the canyon bottom-center dropped to 64.8 percent and 81.9 percent of the solid building (i.e., p = 0) value for the slotted building being the downwind and upwind structure, respectively. The effect of the porosity on turbulence was far less pronounced, with σ/u_o values dropping to 86.7 percent and 95.9 percent of the solid building value for the slotted building being the downwind and upwind

structure, respectively. This suggests the following linear correction factors for porosity:

$$g_p^D = 1.0 - 0.32p \text{ for porous downwind buildings, and} \qquad (67)$$

$$g_p^U = 1.0 - 0.10p \text{ for porous upwind buildings.}$$

Such a porosity variable should enable one to deal with situations where a semi-open, multi-level parking garage defines one side of the street; however, use of p values greater than 0.5 is discouraged as the p = 1 (i.e., no building) limit corresponds to the one-sided canyon and the results of using equation (67) for p = 1 are clearly incorrect.

Street Canyon Curvature Variation

The need to model curved street canyons and the curved airport terminal/roadway/garage complex necessitated extending the turbulence model via curvature correction factors, as was done for vortex flow velocity (see appendix B). Defining the diameter of curvature, D, for the midpoint of the roadway and the dimensionless, signed curvature, d (i.e., d > 0 when the canyon "bends" with the flow, d < 0 when against the flow, and d = 0 is a straight canyon), empirical correction factors were sought through optimization. To some extent these dimensionless correction factors g_c^+ and g_c^- acted contrary to their flow velocity counterparts. This is intuitively reasonable as slowdown of a flow might be expected to increase turbulence and vice-versa. The negative curvature data, however, showed turbulence enhancement at low d and suppression at high d, whereas, the flow velocity always showed a suppression for negative curvature. The final curvature correction factors are

$$g_c^+ = 1.0/[1.0 + 18d^{1.9}/(w/H)1.7] \text{ for } d > 0$$

(68)

and $$g_c^- = [1.0 + 1.44(-d)^{0.15}]/[1.0 - 6.4d] \text{ for } d < 0$$

and both are designed to yield unity at d = 0.

Table 12 shows the comparison between observed and equation (68) predicted canyon, bottom-center turbulence correction factors. The agreement is superior to that found with their velocity correction counterparts but then the size of the perturbation corrections was much smaller for turbulence than for speed.

Combined Effects

Empirical correction factors for observed turbulence levels (i.e., rather than corrections to the predictive equation (65) which includes basic W/H variability) have been developed for:

- Unequal building heights via equation (66) for $g_{\Delta H}$.
- Building porosity via equation (67) for g_p.
- In curvature via equation (68) for g_c.

In situations where multiple factors are present, the correction factors, all unity for the W/H = 1 symmetric, nonporous, uncurved canyon, might be expected to combine multiplicatively to form a total correction factor, g_t, for the equation (65) predicted normalized turbulence, where

$$g_t = g_{\Delta H} \cdot g_p \cdot g_c \qquad (69)$$

Table 12. Curved canyon turbulence correction factors.

Expt	W/H	d	$\sigma(d)/\sigma(d=0)$	Predicted g_c
77	1	+0.0787	0.926	0.874
85	1	-0.0787	1.346	1.319
81	2.429	+0.215	0.785[1]	0.823
83	2.429	-0.215	0.859[1]	0.902
87	2.286	+0.308	0.705[1]	0.680
89	2.286	-0.308	0.811[1]	0.743
97	0.857	+0.143	0.610[2]	0.632
99	0.857	-0.143	1.040[2]	1.084

[1]Linear interpolation of W/H = 2.0 and 2.5 straight canyon, bottom-center turbulence was required. These interpolated, normalized turbulence values were 0.241 and 0.237 for W/H ratios of 2.429 and 2.286, respectively.

[2]Linear interpolation of W/H = 0.5 and 1.0 straight canyon bottom-center turbulence yielded a normalized value of 0.146 for W/H = 0.857.

One test of this multiplicativity hypothesis involves the combined curved canyon/porous building tests performed to simulate a realistic airport situation.[9]

The predicted turbulence multiplier factors, g_t, presented in table 13 are within 15 percent of those based on W/H_S interpolated observed value of σ/u_o of 0.24. Fortunately, in this W/H region, the predicted σ/u_o of 0.22 from equation (65) is in reasonably good agreement with this W/H interpolated value; thus, eliminating this source of uncertainty. In addition, the potentially more serious pollution case of flow from the "terminal airside" (i.e., Test 95), where aircraft and access vehicle emission effects combine, shows agreement with the equation (69) hypothesis within 6 percent. Why such a factorization or multiplicativity hypothesis works reasonably well for turbulence levels but not very well for flow velocity deserves theoretical as well as experimental attention. Perhaps the incoherent nature of turbulence relative to the more organized nature of mean flow make it more amenable to the factorization hypothesis.

---

[9]With a small amount of asymmetry, ΔH, as well.

Table 13. Curved-slotted canyon turbulence correction factors.

Test	W/H_s [1]	d	Observed σ/u_o	Observed [2] Turbulence Multiplier	g_H	g_p [3]	g_c	Predicted Turbulence Multiplier
95	2.37	0.308	0.130	0.542	0.96	0.863	0.693	0.574
93	2.37	-0.308	0.202	0.843	1.04	0.957	0.743	0.739

[1] As no shim was used, the garage had a smaller height of H_s = 3.375 in (0.0857m).
[2] Observed turbulence multiplier involved use of interpolated normalized turbulence of 0.239 for W/H_s = 2.37. This value is also in good agreement with the equation (65) predicted value of 0.230.
[3] A porosity of 3/7 = 0.429 was used.

APPENDIX D

SPECTRAL CHARACTERISTICS OF THE HOT-WIRE ANEMOMETER DATA

Introduction

In developing theories and empirical relations for how the turbulence field varies within and above the urban canyon, it is useful to consider the time series and spectral characteristics of the data, in addition to the probability density function (pdf) properties analyzed in appendix A. The motivation for this method of analysis stems from the fact that during the analyses of the Bonner Strasse, full-scale study (Yamartino and Wiegand, 1986), the standard deviations of the velocity components within the canyon (i.e., σ_u, σ_v, and σ_w) were comparable to those in the above roof flow. This led to the conjecture that the turbulence was primarily advected into the canyon rather than produced within it. As only first and second moments of the velocities were retained during the TUEV Bonner Strasse study, this conjecture could not be further evaluated.

In this appendix, we consider first the time series of hot wire measured velocities. Consideration of the autocorrelation and power spectra then provides additional insight into the character of the turbulence.

Time Series

A series of 2048 instantaneous speeds were recorded for the W/H = 1 canyon geometry at each of the six hot-wire locations shown in figure 11. These raw time series, an example of

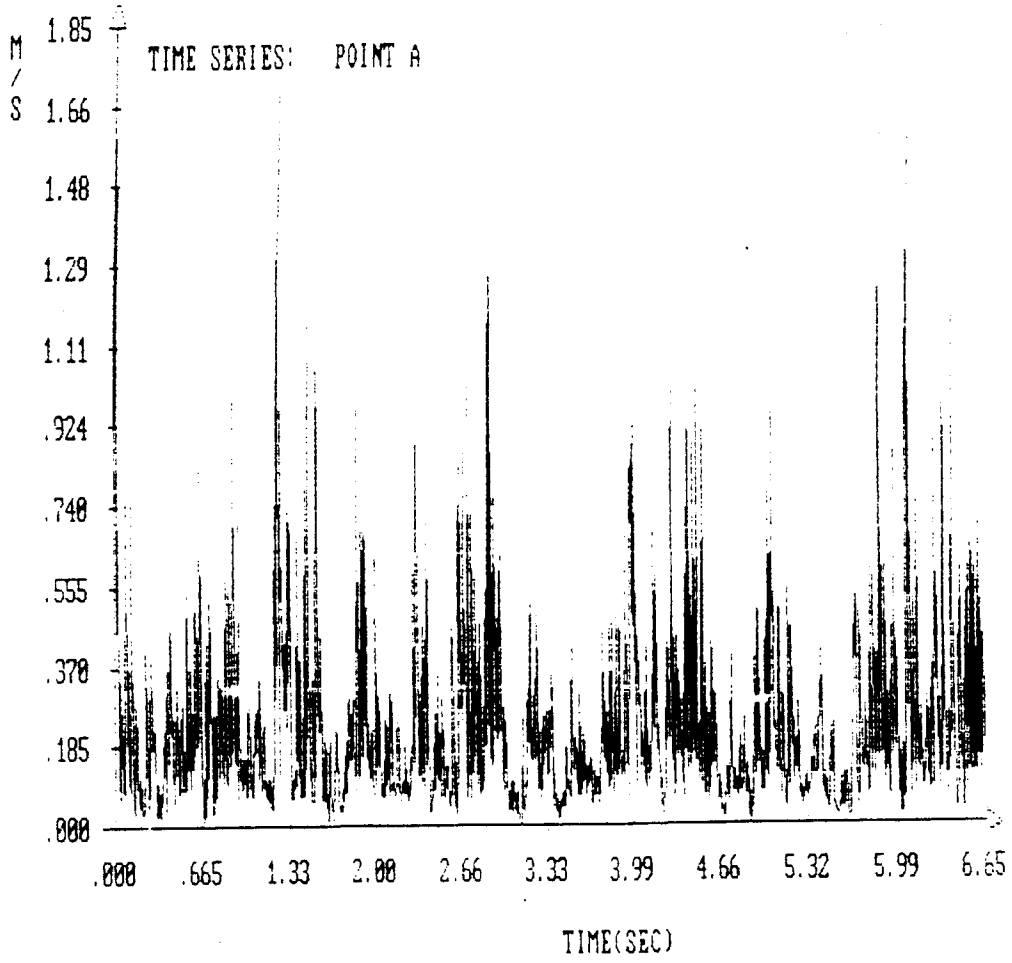

Figure 25. Raw time series of hot wire speeds at location A.

which is shown in figure 25 and which cover measurement periods of 6.65 seconds, were then:

- Filtered with a 3-point Blackman moving averager to remove frequencies beyond the Nyquist folding frequency.

- Demeaned to eliminate the average speed or d.c. component.

- Tapered down to zero at the initial and final 10 percent portions of the series by using a cosine form factor.

This final tapering step is designed to avoid "shocks" to the spectra and is clearly evident in the processed time series of figures 26 through 31. Also apparent in these series for sampling points A and C is the asymmetry of the signals above and below zero. This situation is directly attributable to the hot-wire rectification limitation (i.e., the hot-wire senses only speed and not the sign of the velocity component). This effect is most pronounced at the higher turbulent intensity locations, A and C, and is of some concern in these analyses as the non-linear rectification process causes frequency harmonics (i.e., particularly the 2nd harmonic) to be generated; thus, obscuring the underlying physics.

Consideration of the series for points 3, 2, and 1 shows that maximum turbulent velocities increase by about 50 percent as one moves from the relatively unperturbed flow (point 3) down to the point (i.e., 1) just at the top of the canyon. Also evident at point 1 is the loss of lower frequency components, clearly present at points 2 and 3. Some local, high frequency turbulent production is probably destroying the integrity of these lower frequency components.

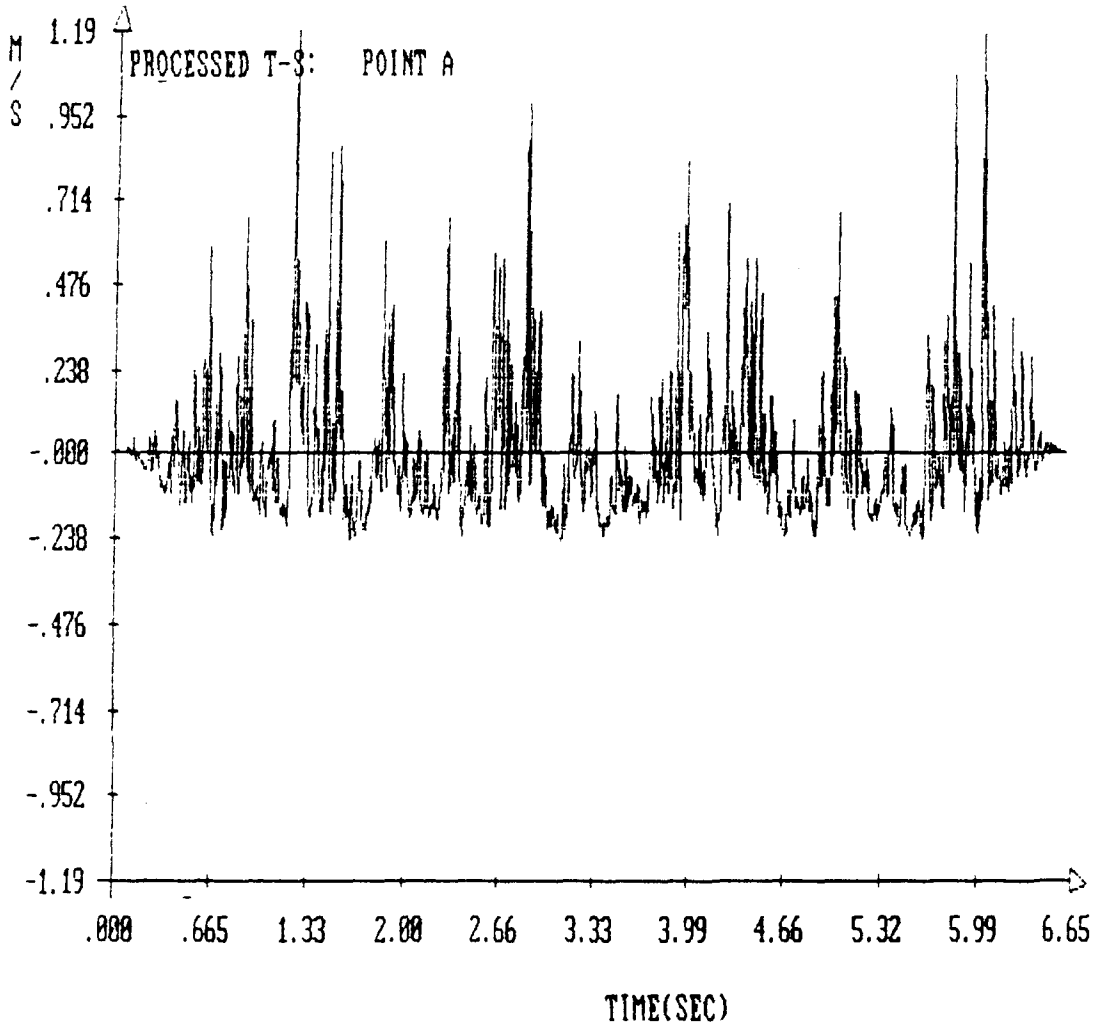

Figure 26. Processed time series of hot wire speeds at location A.

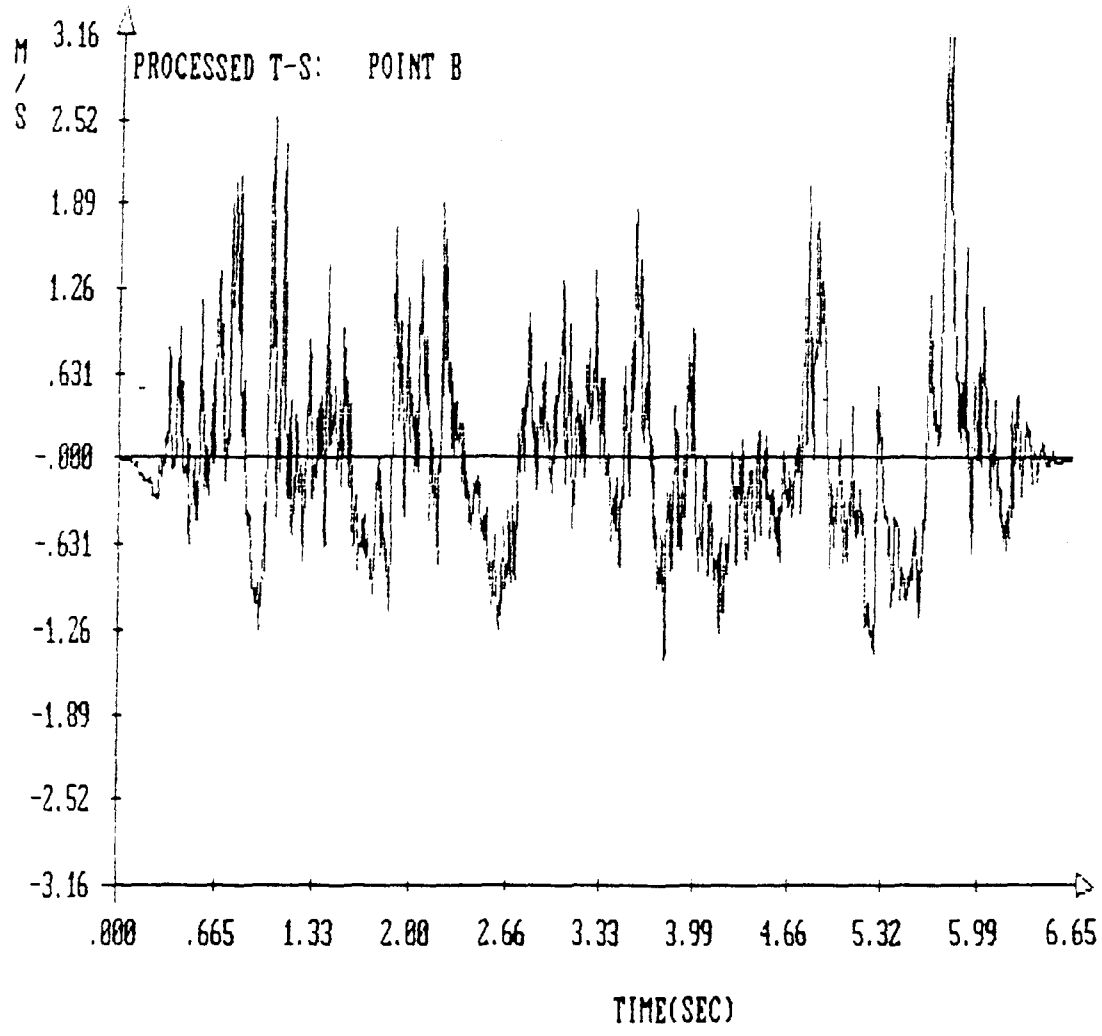

Figure 27. Processed time series of hot wire speeds at location B.

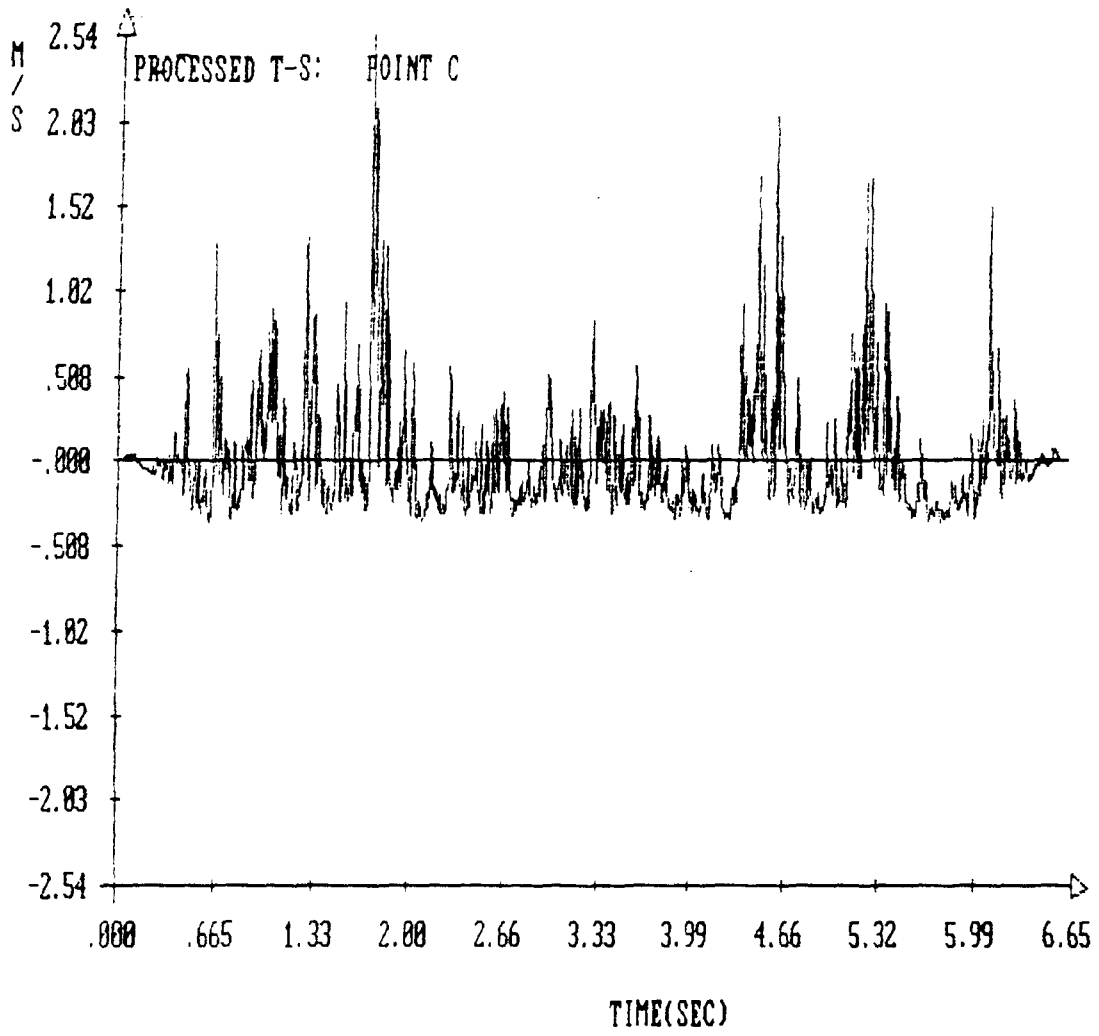

Figure 28. Processed time series of hot wire speeds at location C.

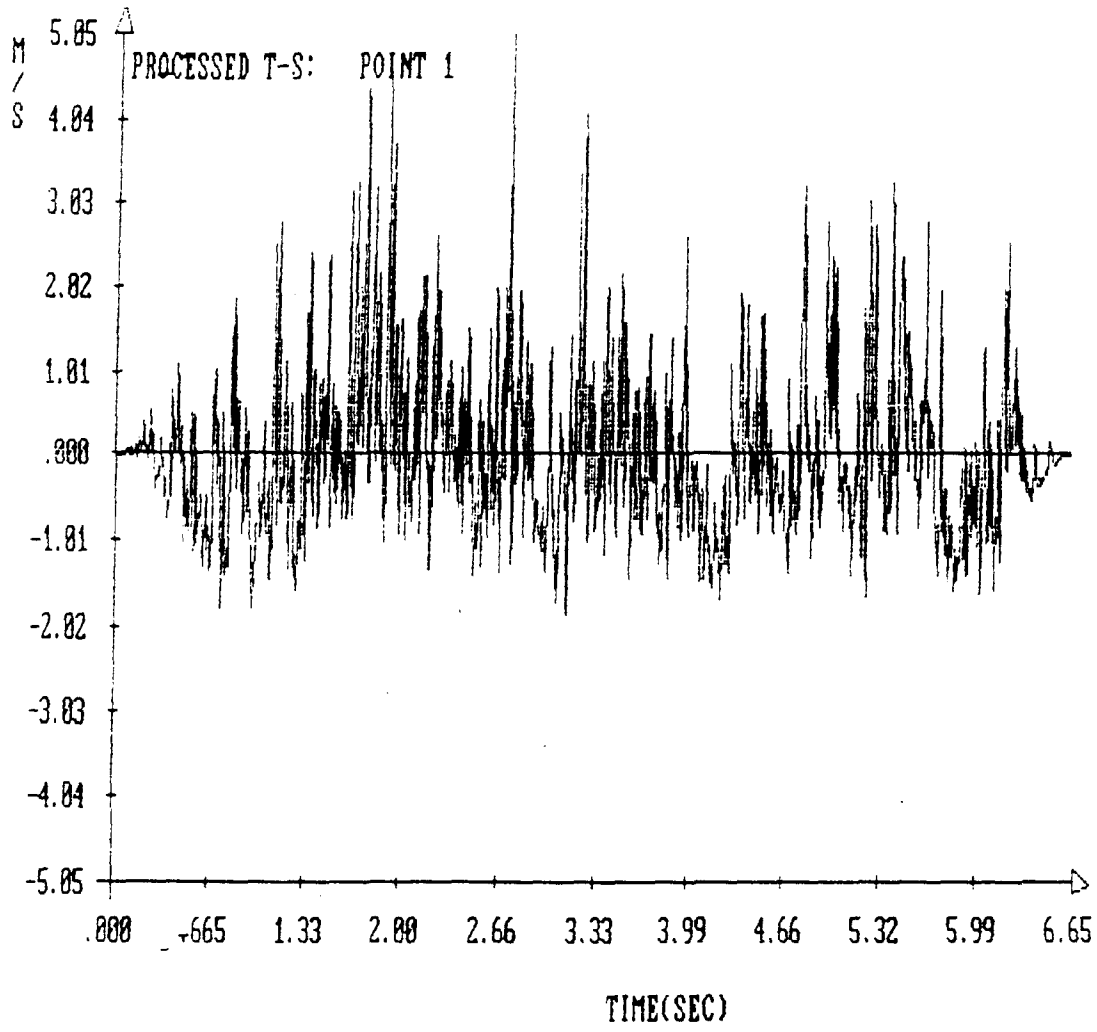

Figure 29.- Processed time series of hot wire speeds at location 1.

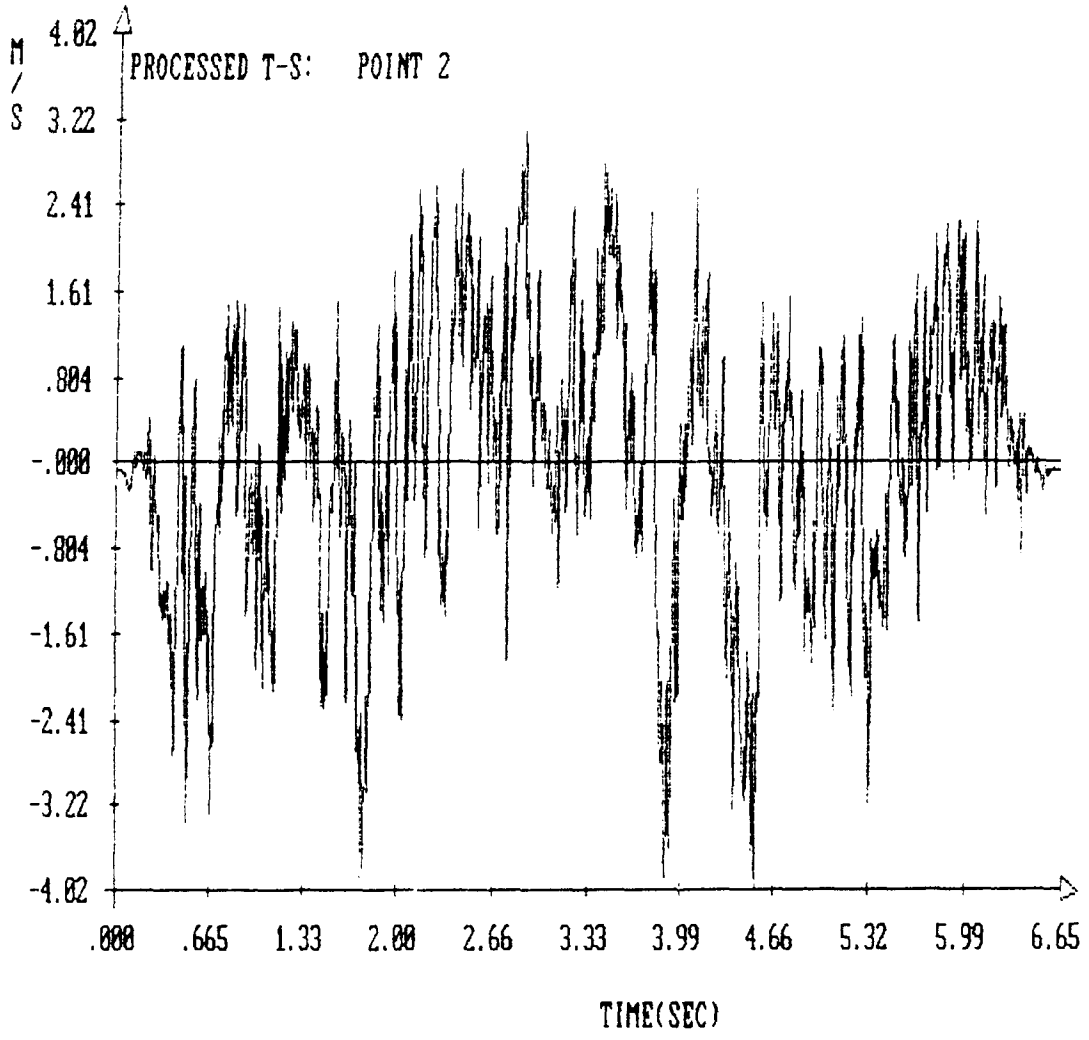

Figure 30. Processed time series of hot wire speeds at location 2.

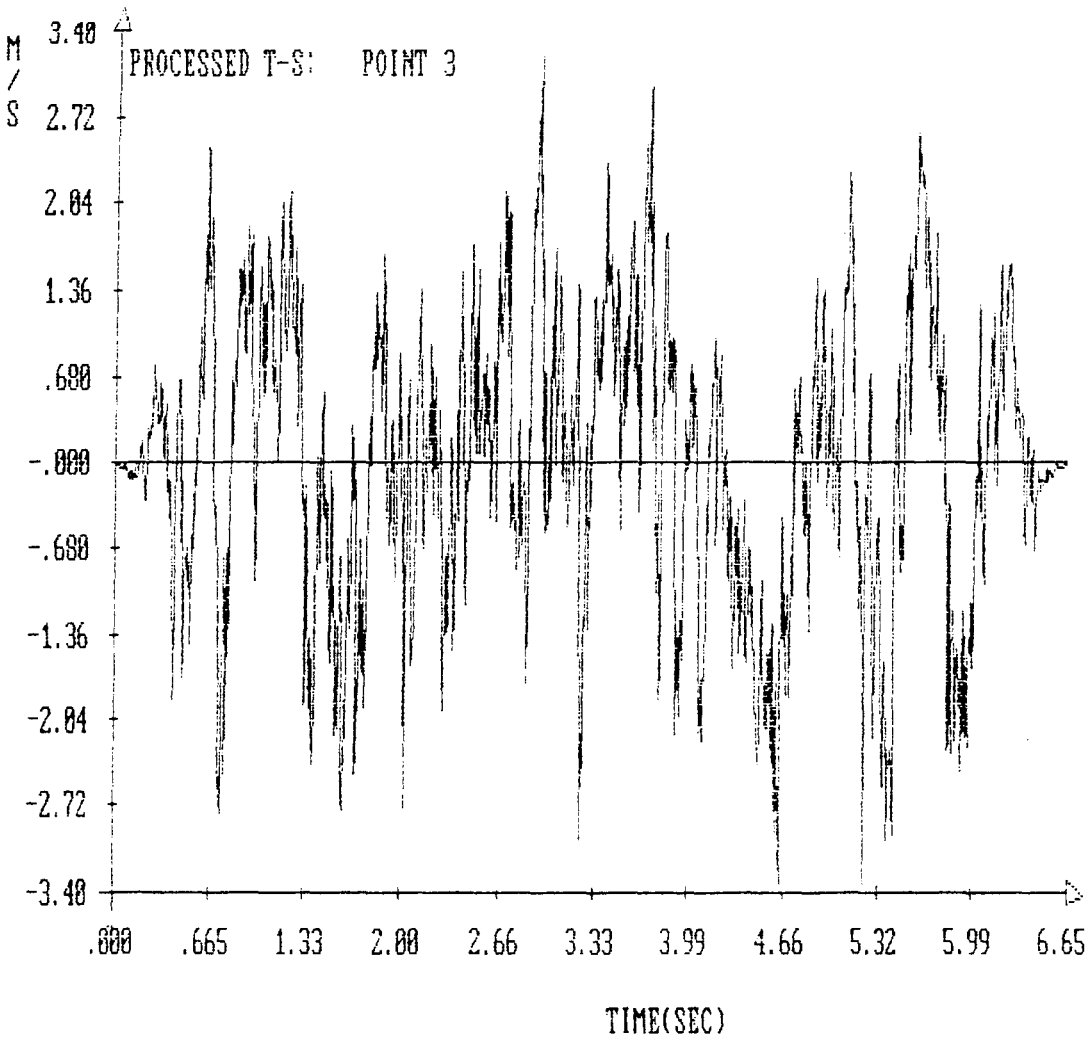

Figure 31. Processed time series of hot wire speeds at location 3.

Autocorrelations

The Eulerian autocorrelation, r, is defined as

$$r(t) = \langle V'(t+t')V'(t')\rangle / \langle V'^2(t')\rangle \qquad (70)$$

where V' is the speed fluctuation and $\langle\ \rangle$ denotes averaging over time t'.

Normalized such that r(0) = 1, the rate at which r drops reveals how quickly "memory" fades within a turbulent flow. In fact, the Eulerian time scale, τ_e, the usual measure of the time scale of this memory, is operationally defined as the first value of t for which r falls to 1/e = 0.368.

The correlograms for the first 0.3 seconds of lag time, t, are presented in figures 32 through 37, and visual examination of these indicates the approximate Eulerian time scales given in table 14.

Table 14. Approximate Eulerian time scales.

Sampling Point	τ_e(sec)	$\tau_e/\Delta t$
A	0.015	4.6
B	0.06	18
C	0.03	9.2
1	0.012	3.7
2	0.07	22
3	0.065	20

These time scales are all very short compared to the full sample period of 6.65 sec; thus, indicating that the sampling

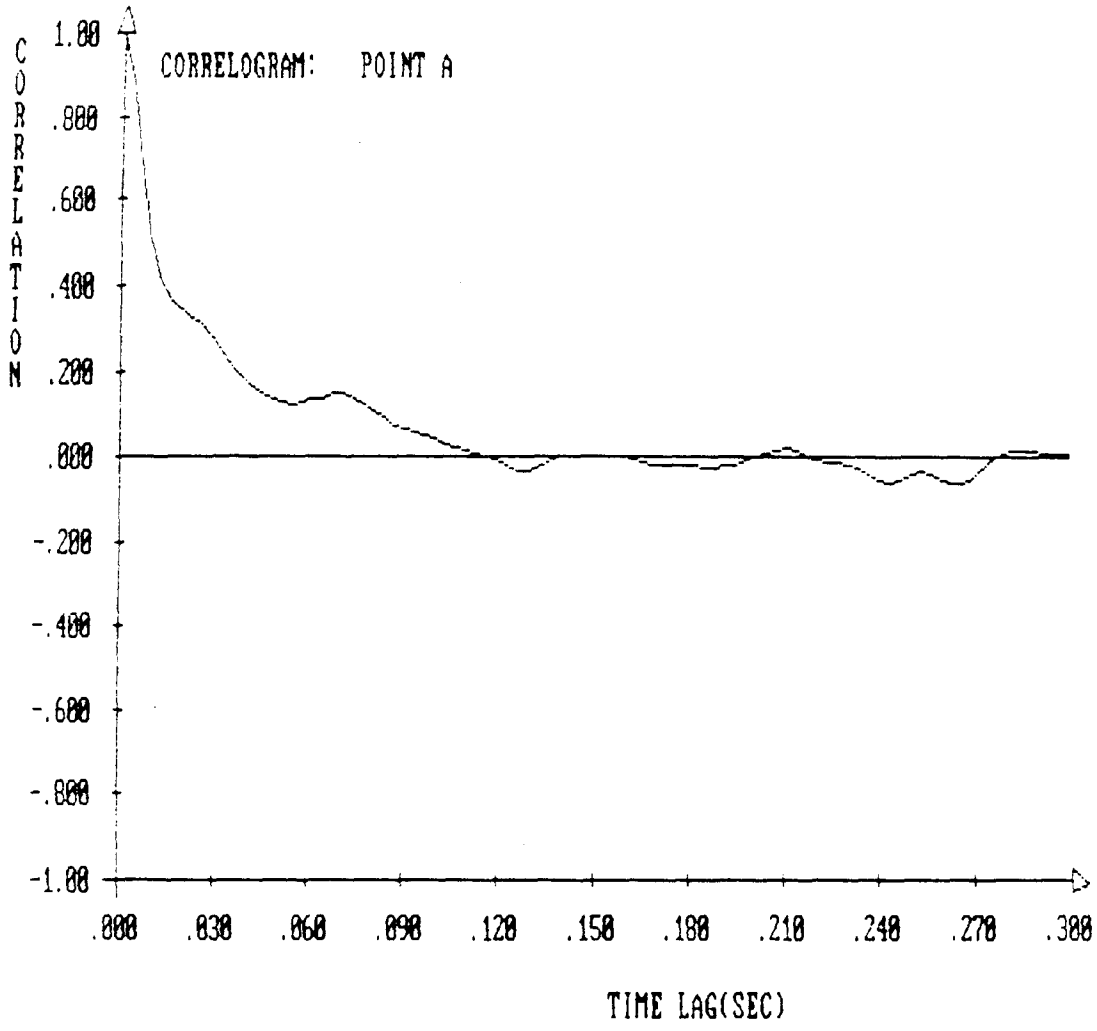

Figure 32. Correlogram of hot wire speeds at location A.

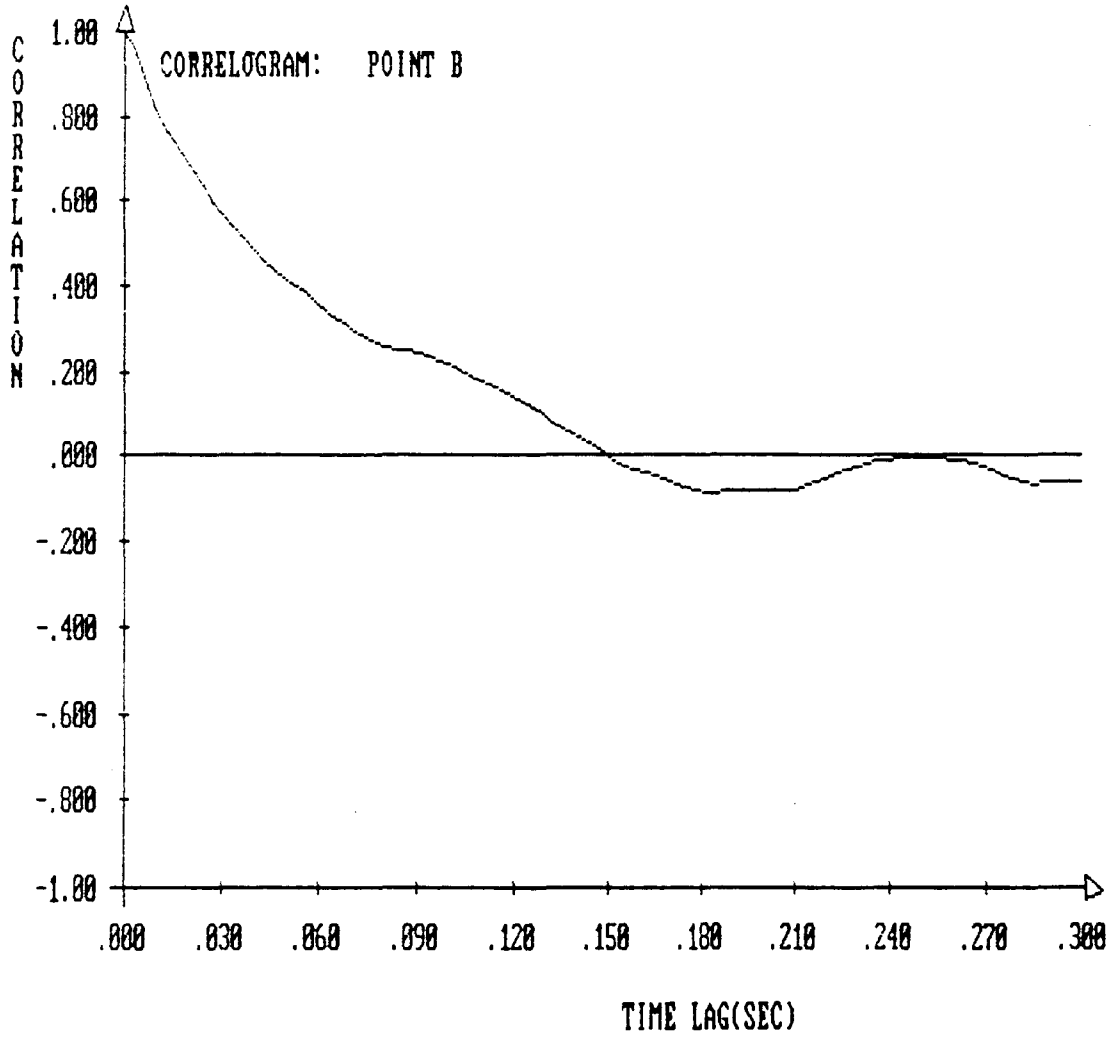

Figure 33. Correlogram of hot wire speeds at location B.

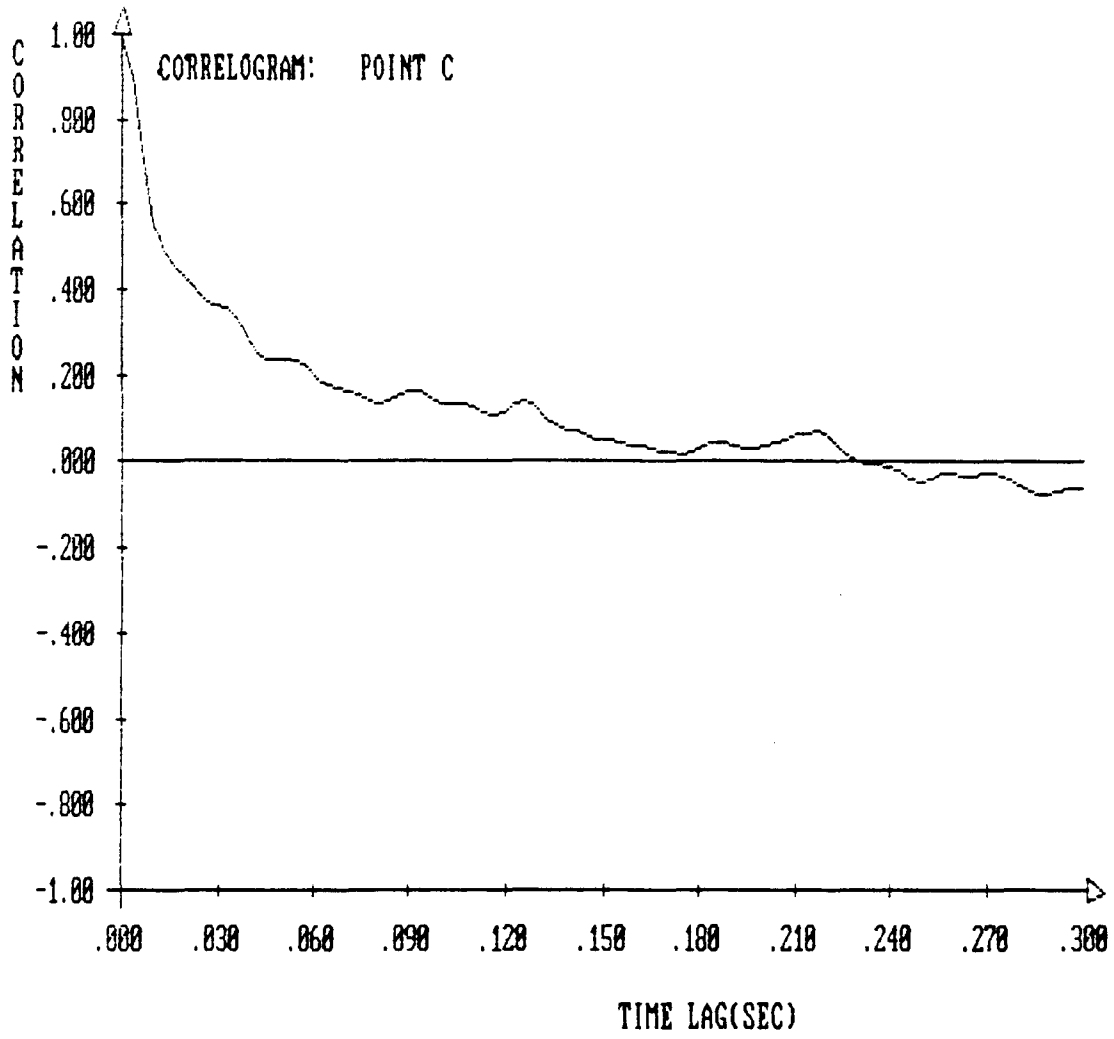

Figure 34. Correlogram of hot wire speeds at location C.

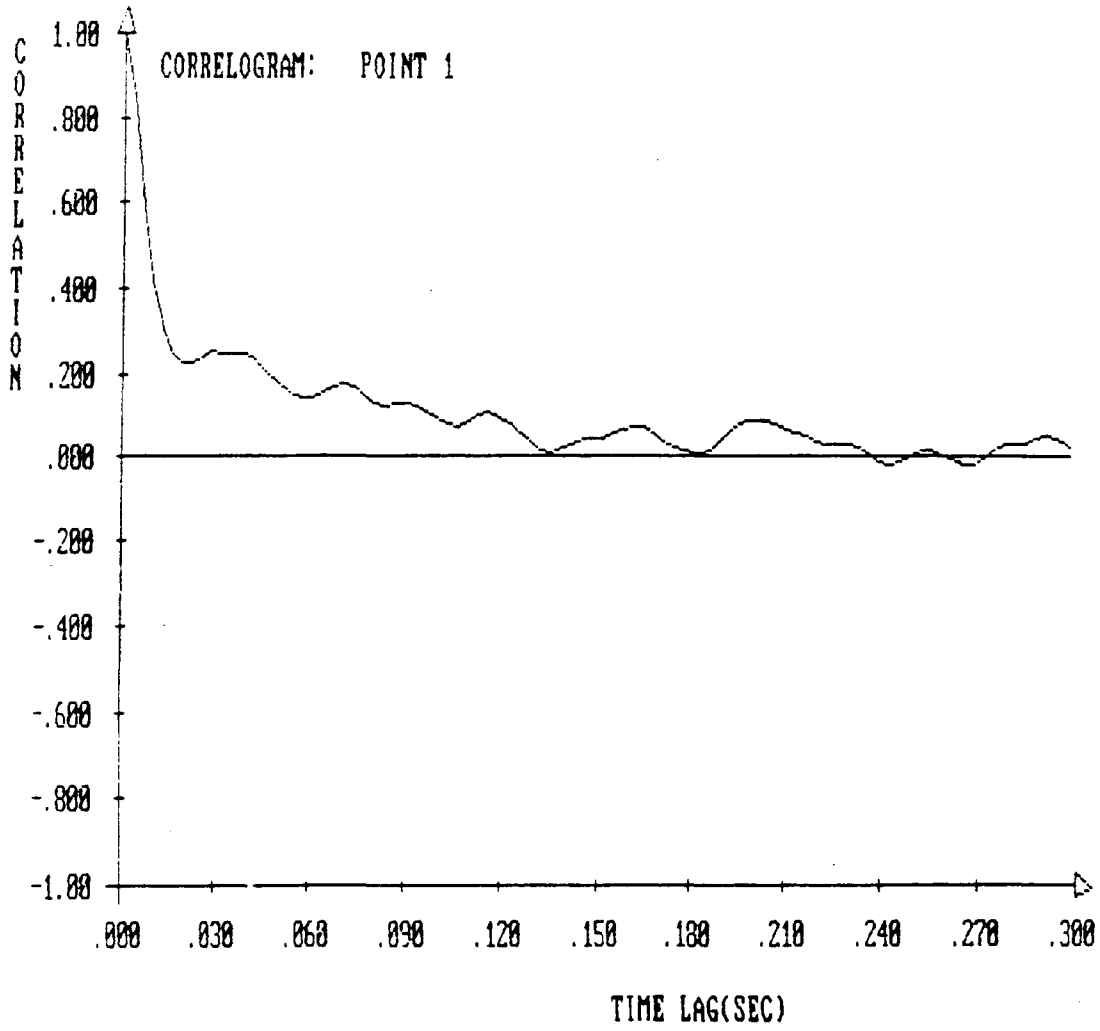

Figure 35. Correlogram of hot wire speeds at location 1.

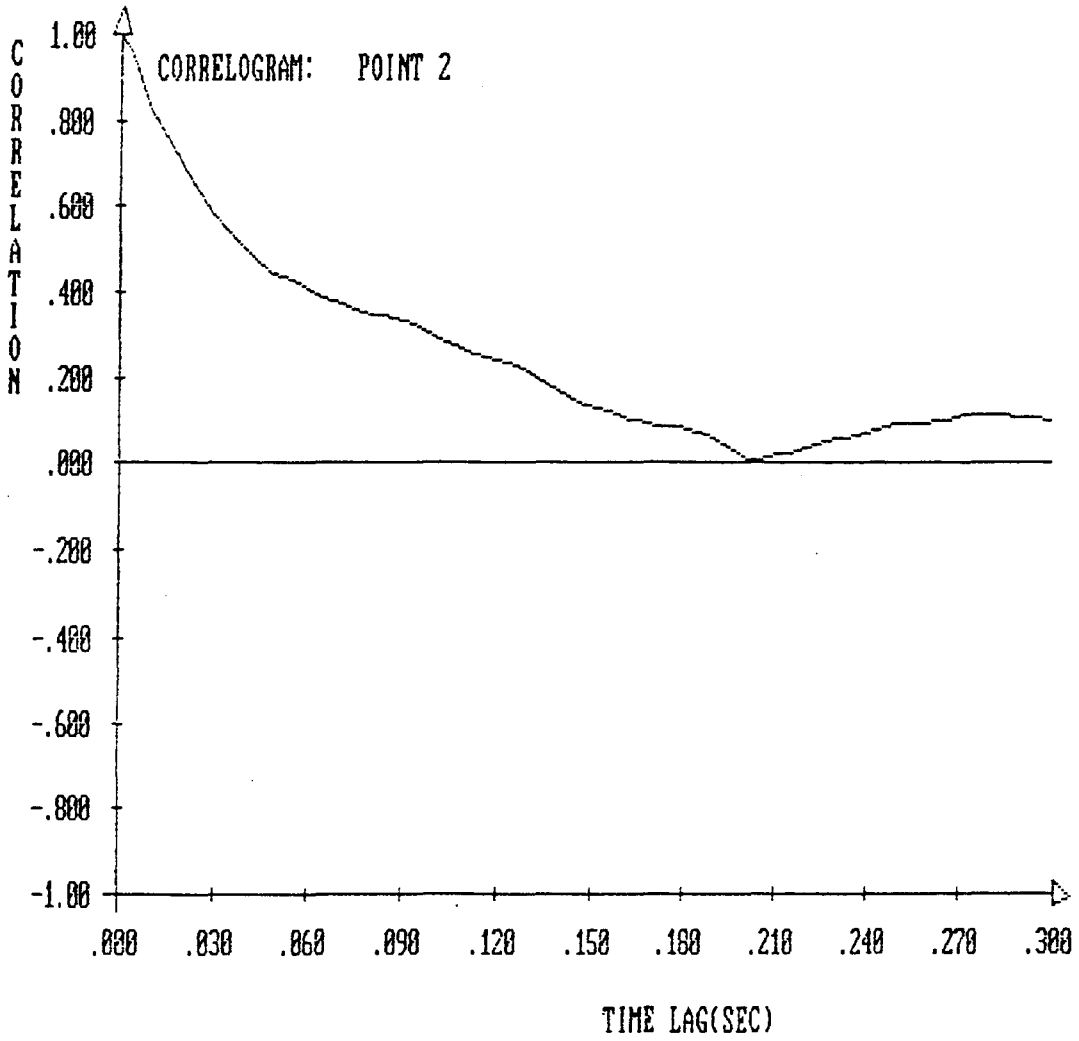

Figure 36. Correlogram of hot wire speeds at location 2.

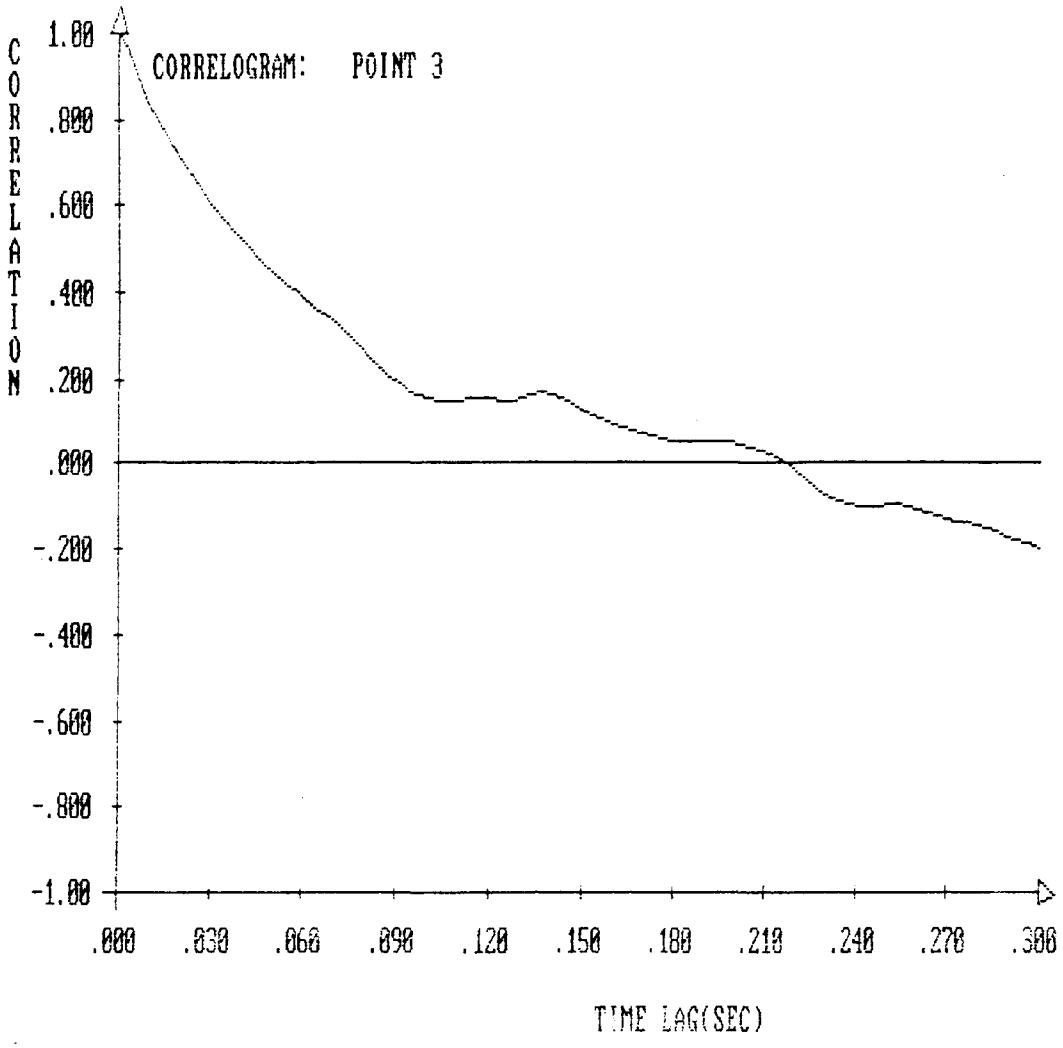

Figure 37. Correlogram of hot wire speeds at location 3.

period was adequately long. However, the Te values scaled by the sampling-time step, Δt, of 3.247×10^{-3} sec indicate that the sampling frequency may not have been high enough to capture all the higher frequencies contributing to the turbulent energy.

Examination of figures 32 through 27 and table 14 also reveals:

- The largest ^{T}e are at point 2 and 3 in the relatively unperturbed flow regime.

- The ^{T}e in the corners (i.e., A and C) are substantially suppressed, probably due to the inability of the larger, low-frequency eddies to enter these corner regions.

- The ^{T}e at point B is nearly as large as at points 2 and 3, suggesting that the turbulence at the bottom center of the canyon is not unlike that well above the canyon.

- The smallest ^{T}e is surprisingly found at point 1. Only the local production and decay of a relatively high-frequency, incoherent turbulent component could explain this low ^{T}e relative to points 2 and 3 and point B.

Power Spectra

Fourier amplitudes of the time series shown in figures 26 through 31 were computed using an efficient FFT algorithm. The spectral density, S(n), was then computed as the product of this amplitude and its complex conjugate as a function of frequency, n. Actually presented in figures 38 through 43 are the frequency-weighted spectral energy densities, nS(n), so as to emphasize the higher frequency regime. The very rapid

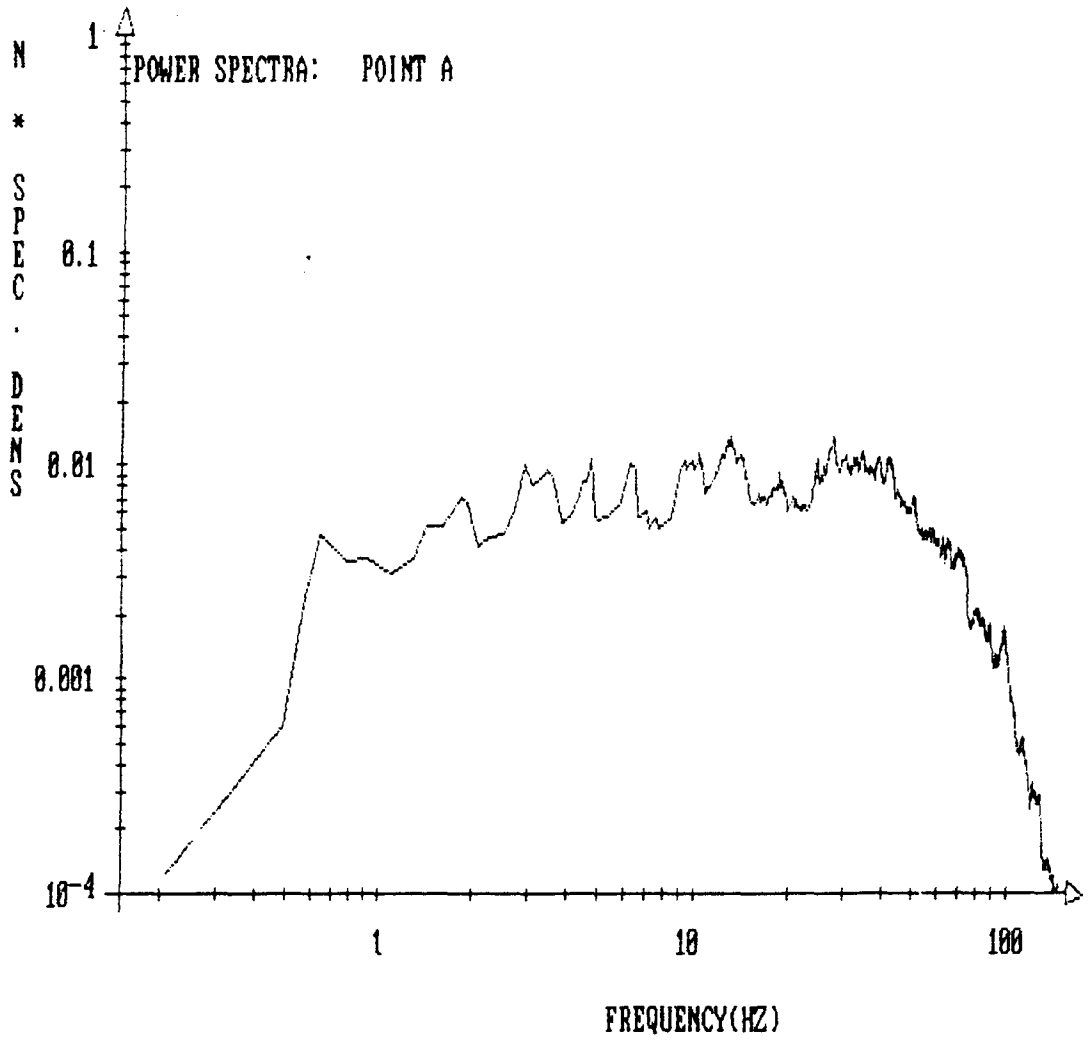

Figure 38. Spectral energy density of hot wire speeds at location A.

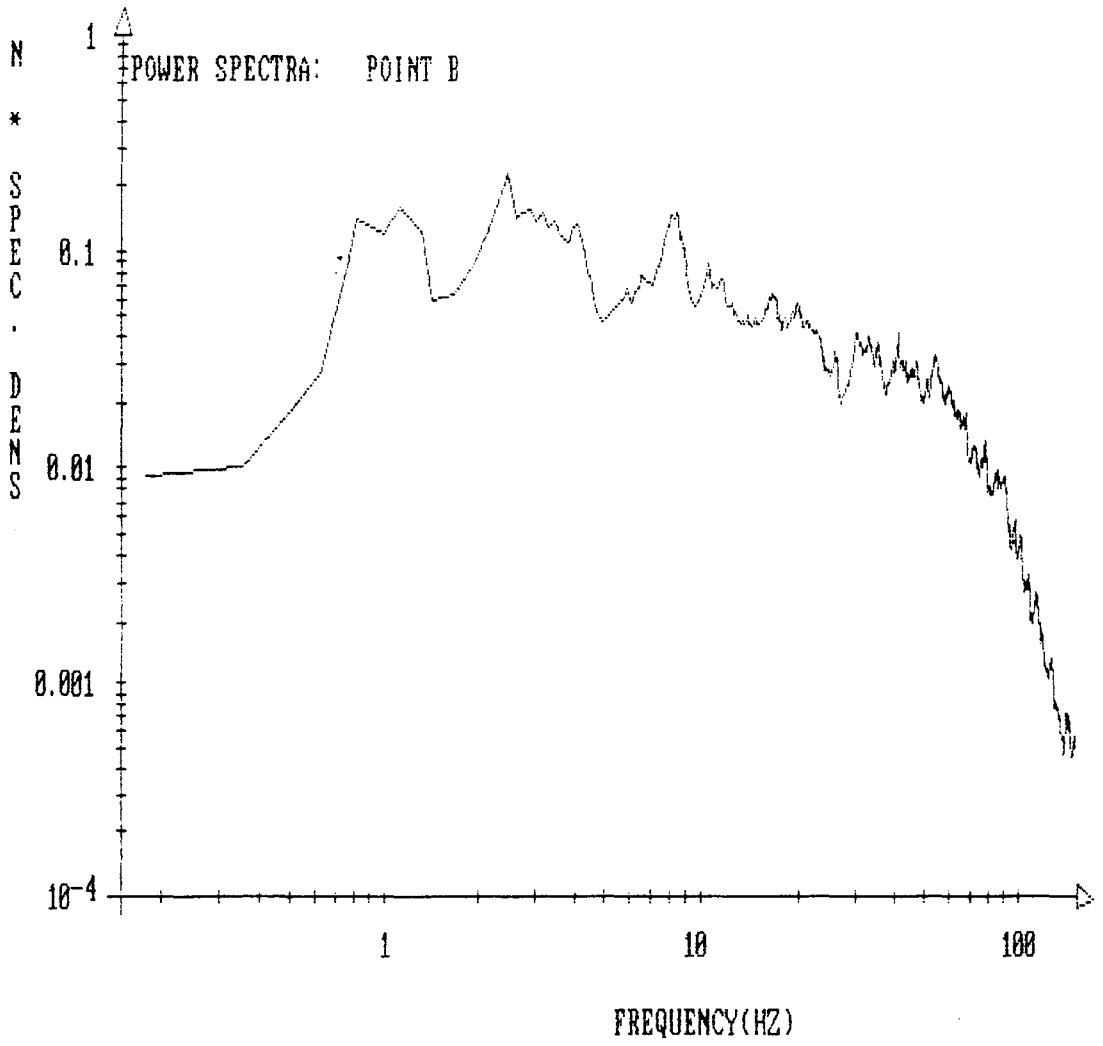

Figure 39. Spectral energy density of hot wire speeds at location B.

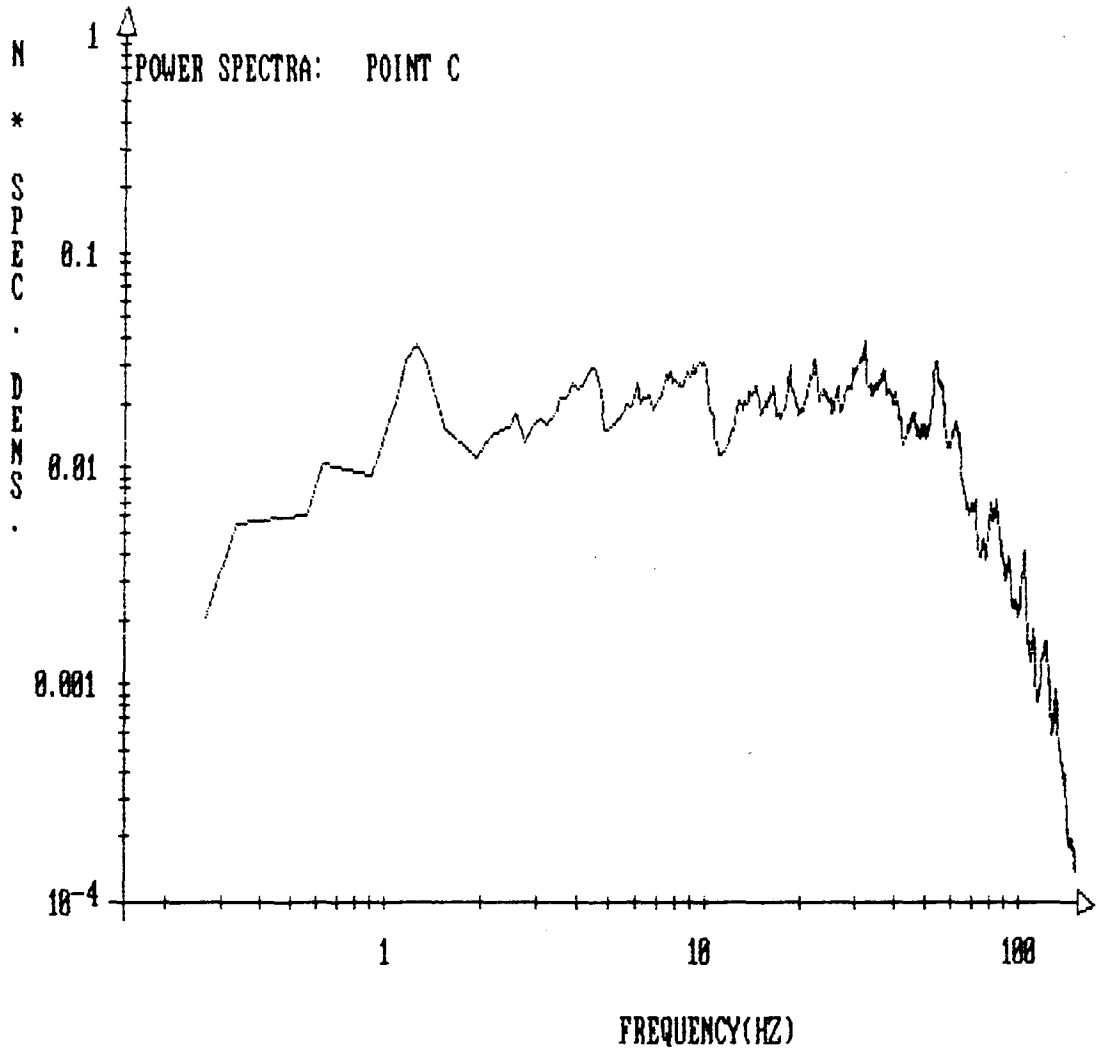

Figure 40. Spectral energy density of hot wire speeds at location C.

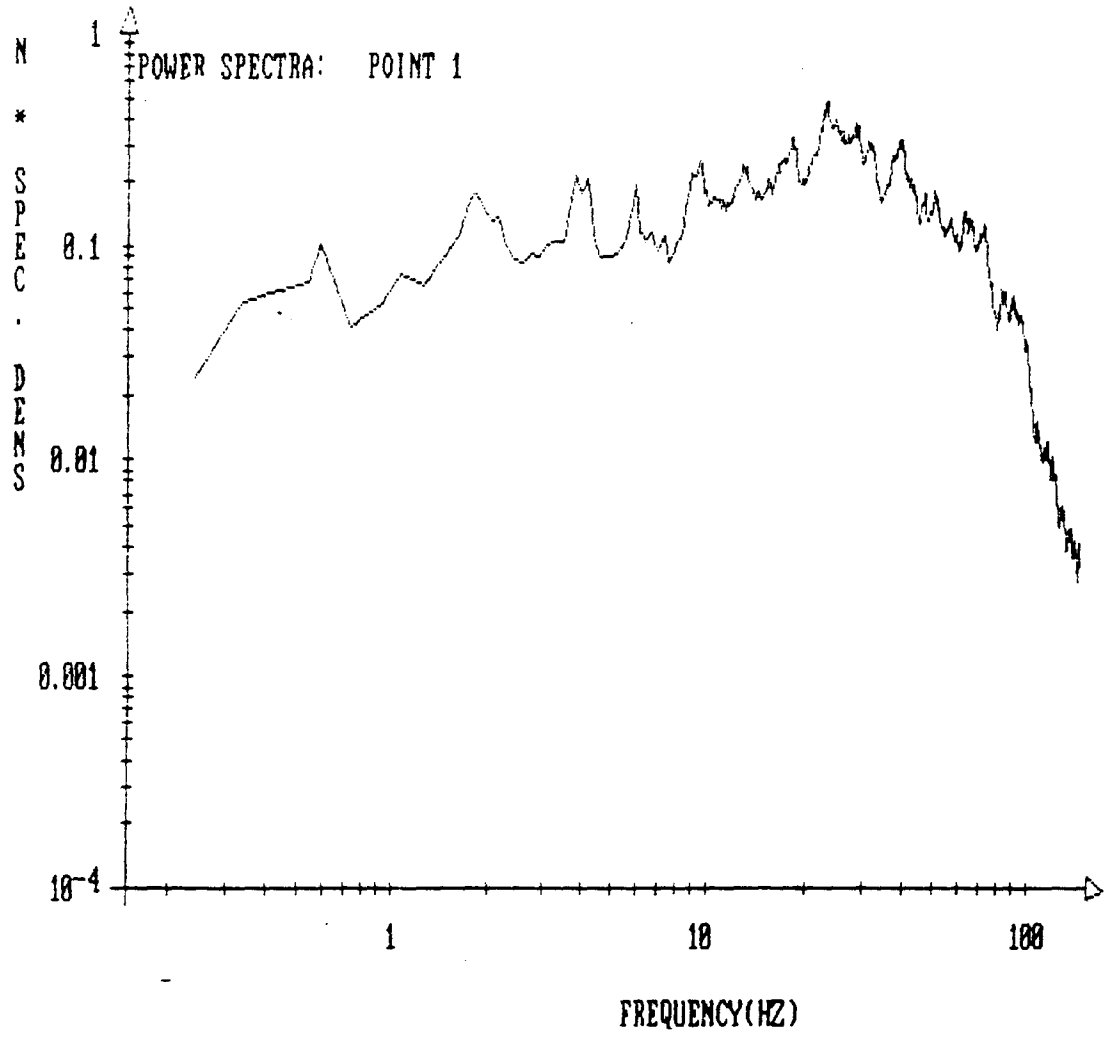

Figure-41 Spectral energy density of hot wire speeds at location 1.

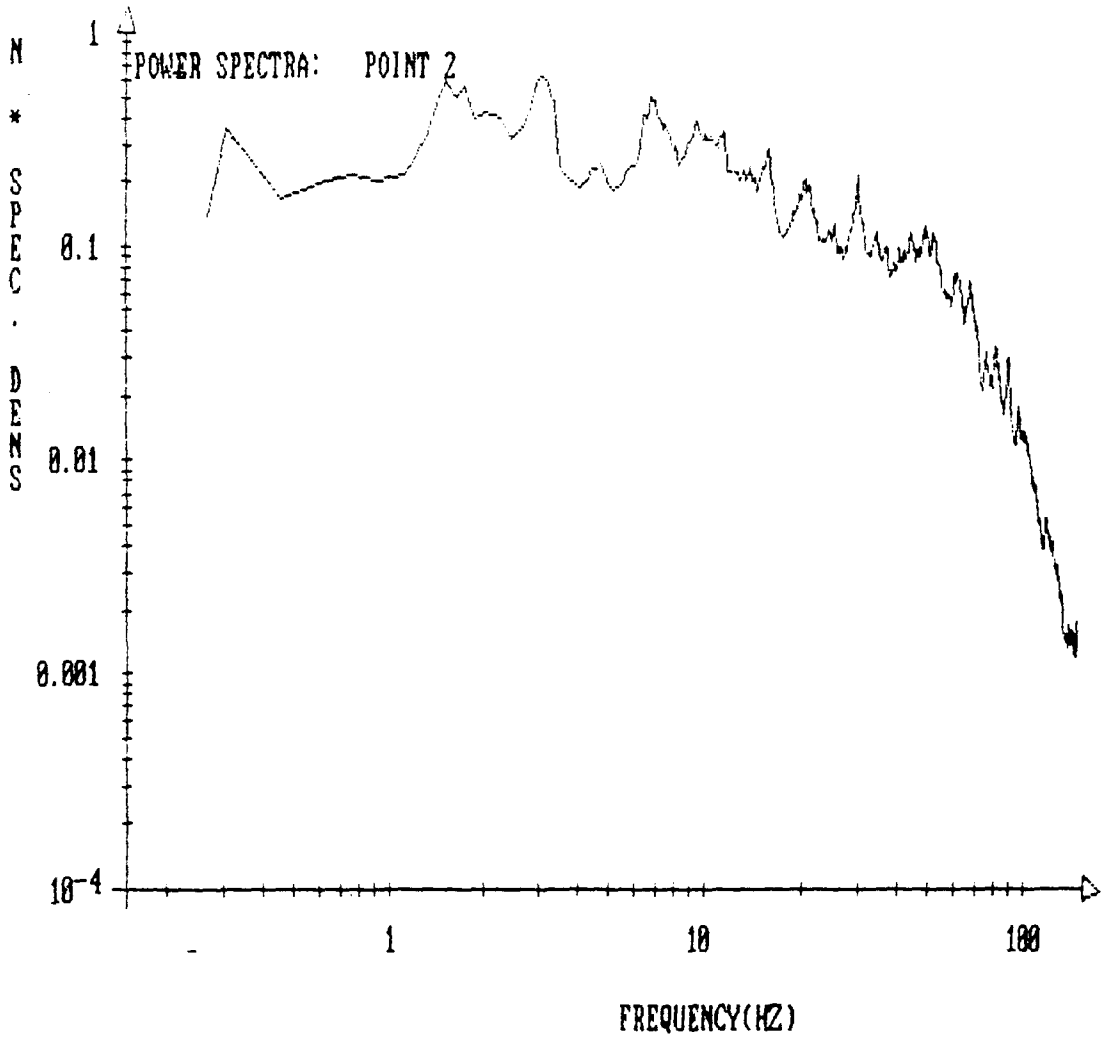

Figure 42. Spectral energy density of hot wire speeds at location 2.

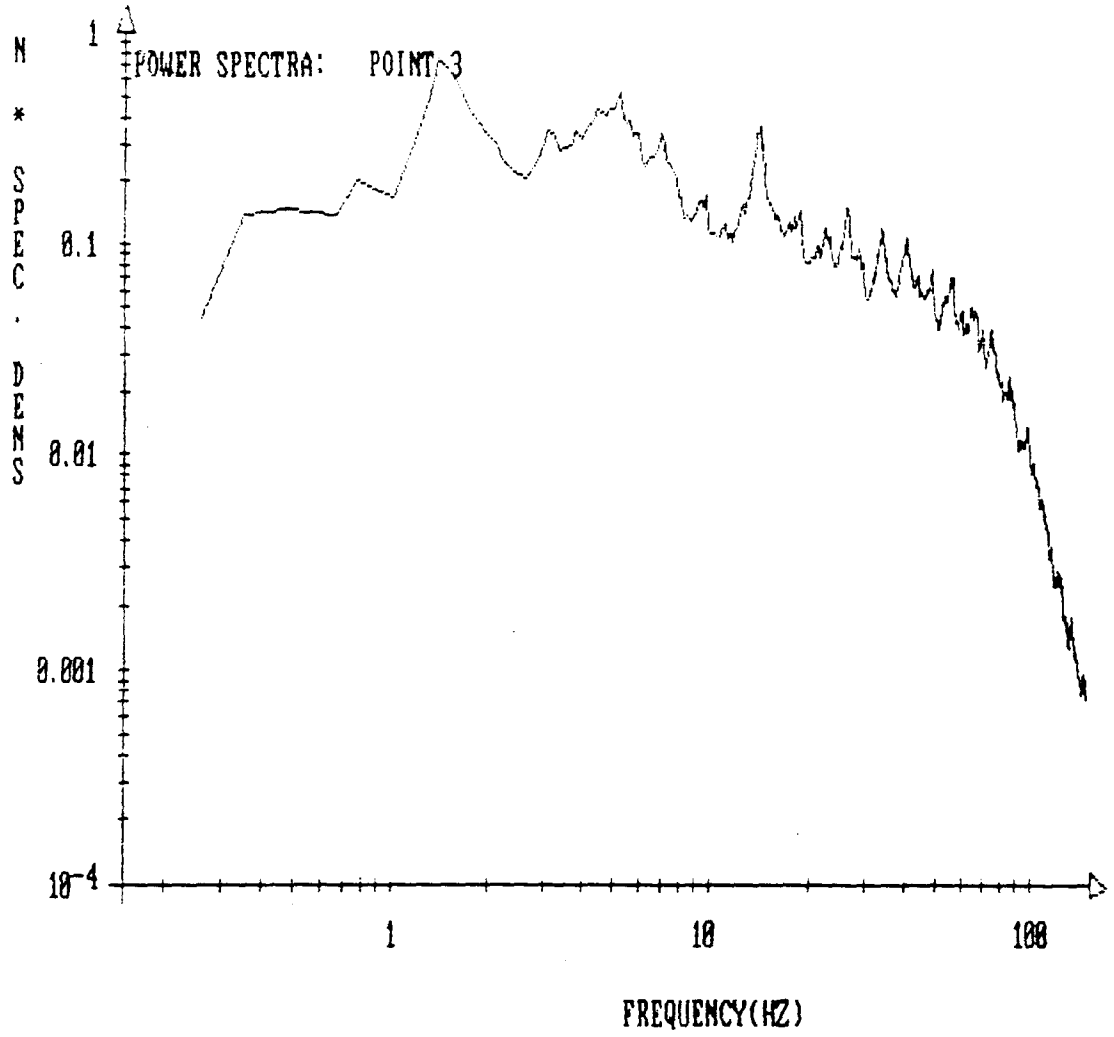

Figure 43. Spectral energy density of hot wire speeds at location 3.

falloff at the highest frequencies seen in each plot is a strong function of the initial time series smoothing window and, thus, should not be overinterpreted. However, the gentler sloped falloff at moderate frequenies and most prominent at points B, 2 and 3, is consistent in slope with the inertial subrange behavior of $nS(n) \propto n^{-2/3}$. The fact that only about one decade of this regime is seen is partly due to the rather low, 308 Hz, sampling frequency, but is also a characteristic limitation of the wind tunnel's ability to simulate the atmospheric boundary layer.

Further examination of these power spectra indicates:

- Strong suppression of the low frequencies (i.e., below 20 Hz) at points A and c. This was suspected from the 19W values of T_e and the knowledge that one effect of a geometrical boundary is to act as a high-pass filter. Thus, both σ_u and σ_w are likely to be suppressed so close (i.e., 1/4 in or 6.35×10^{-3}m) to a corner.

- Remarkable similarity in the shape of spectra at points B, 2, and 3 at all but the lowest frequencies (i.e., below 1 Hz). This low frequency suppression is likely due to the role of a street canyon as a geometrical high-pass filter. If one scales the suppression of corner eddies larger than ¼ in (0.35×10^{-3}m) at 20 Hz to the larger canyon width of 3.5 in (0.0889m), then one might anticipate frequencies below about 1.4 Hz to be suppressed.

- Unique appearance of the point 1 spectra with a broad mid-frequency maxima peaking at about 25 Hz. It is interesting that the advection speed at this point of u = 2.357 m/s (5.2 mi/h) divided by the canyon width of W = 0.0889m

(3.5 in) leads to a characteristic frequency f = u/W = 26.5 Hz. Whatever the mechanism for the turbulence production near the canyon top and in this frequency range, the short T_e suggests that the eddies are short lived and incoherent: surviving in integrity only about one-third of a cycle.

Conclusions

Turbulence near the bottom center of a W/H = 1 canyon is similar in character to that observed in the relatively unperturbed flow above the canyon (i.e., at points 2 and 3). The reduced σ at point B of about 60 percent of that observed at point 3 arises from a reduction at all contributing frequencies rather than at or below characteristic frequencies that would signal high-pass filter like behavior.

Turbulence in the corners (i.e., points A and C) shows pronounced high-pass filtering effects due to the presence of the geometrical boundaries.

The region directly at the top of the canyon involves large velocity shear, surprisingly low T_e, and an anomalous power spectra peaked at mid-range frequencies. While a full description of this region would require more detailed study the evidence at hand evokes a picture of a turbulent, shear-generated "reef zone" separating a "lagoon" and "open sea" regions; both of which are able to support more coherent, larger T_e waves.

APPENDIX E

POLLUTANT DISPERSION FROM A FINITE-LENGTH LINE SOURCE

The original CPB model (Yamartino and Wiegand, 1986 and appendix H) employed separate plume models for non-vortex conditions, defined by a cross-canyon turbulent intensity, $i_u (= \sigma_{ub}/u_b)$, exceeding 2.0, and the vortex condition defined when $i_u \leq 2.0$. Such a distinction was reasonable because the few instances of non-vortex conditions required a relatively expensive numerical integration along the line source and the summation of canyon wall reflection terms. In the calculation which follows, the need for such a numerical integration is eliminated; thus, permitting a unified treatment of the direct source impact problem for all crosswind turbulent intensities. Some specialized model components such as material recirculation and fresh air injection are, of course, still conditioned on the viable existence of a vortex.

Consider a line source oriented at an angle θ (measured from the perpendicular orientation) from a flow of velocity u. Assume that plume dimensions increase linearly with downwind distance, x', so that

$$\sigma_z(x') = \sigma_z(0) + i_z x' \tag{71}$$

$$\text{and} \quad \sigma_y(x') = \sigma_y(0) + i_y x'$$

and where $\sigma_z(0)$ is the initial vertical spread due to vehicle induced mixing and $\sigma_y(0)$ will be constrained to be $\sigma_y(0) = (i_y/i_z)\sigma_z(0)$ so that the proportionality $\sigma_y(x')/\sigma_z(x') = i_y/i_z$ is always preserved.[10] This fixing of $\sigma_y(0)$ is not overly restrictive since σ_y effectively drops out of the line source problem except for the nearly parallel flow case at $\theta \sim 90^\circ$.

---

[10]This proportionality assumption permits the integration to be accomplished.

As shown in figure 44, the upwind distance to the line is just x'_r ($= x_r/\cos\theta$) at a crosswind distance of $y' = \ell\cos\theta$ of zero. From geometrical considerations the point ℓ_r is at $\ell = -x_r\tan\theta$ and the relations between the various coordinates can be summarized as

$$\begin{aligned} x' &= x'_r + \ell\sin\theta = x_r/\cos\theta + \ell\sin\theta, \\ y' &= \ell\cos\theta, \text{ and} \\ y &= y_r + \ell - \ell_r = y_r + \ell + x_r\tan\theta \\ \text{or} \quad \ell &= y - y_r - x_r\tan\theta \end{aligned} \tag{72}$$

The concentration at the receptor can then be expressed as

$$C = \frac{q}{2\pi u} \quad I \tag{73}$$

$$\text{with} \quad I = \int_{\ell_1}^{\ell_2} \frac{d\ell \, \exp\left\{-1/2 \left[\frac{\ell\cos\theta}{i_y(a' + \ell\sin\theta)}\right]^2\right\}}{i_y i_z (a' + \ell\sin\theta)^2} \tag{74}$$

where $a' = \sigma_z(0)/i_z + x'_r$ includes the initial dispersion pseudo-distance $a = \sigma_z(0)/i_z = \sigma_y(0)/i_y$, and the limits of integration are given as

$$\ell_1 = \text{MAX}(\ell_0, \ \ell_{Id})$$

$$\begin{aligned} \text{with} \quad \ell_0 &= - x'_r/\sin\theta \text{ and} \\ \ell_{Id} &= y_{Id} - y_r - x_r\tan\theta \end{aligned} \tag{75}$$

and $\ell_2 = \ell_{Iu} = y_{Iu} - y_r - x_r\tan\theta$.

Transformation to the variable

$p = (a' + \ell\sin\theta)^{-1}$ allows one to re-express equation (74) as

$$I = \frac{-1}{i_y i_z \sin\theta} \int_{p_1}^{p_2} dp \, \exp\left\{ - \left(1 - a'p\right)^2 / \left(\sqrt{2} i_y \tan\theta\right)^2 \right\}$$

with corresponding limits p_1 and p_2. A second transformation using the variable $s = [1 - a'p]/(\sqrt{2}\, i_y\tan\theta)$ then reduces the problem further to

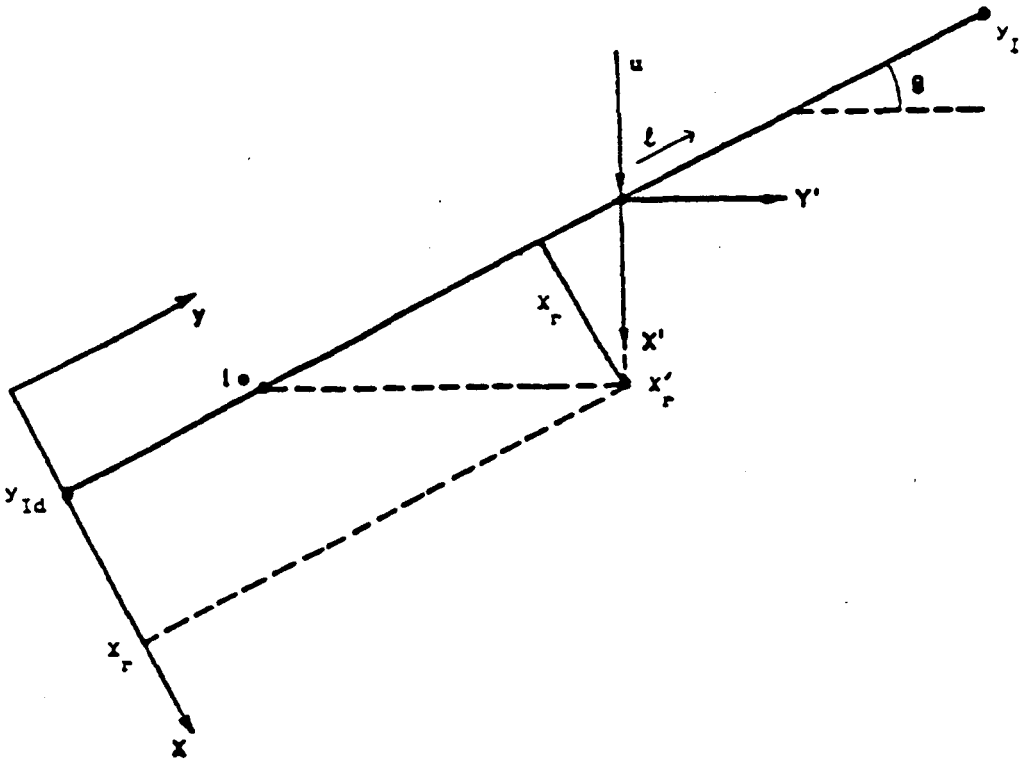

Figure 44. Coordinate systems for the line integral problem.

$$I = \frac{\sqrt{2} i_y \tan\theta}{a' i_y i_z \sin\theta} \int_{s_1}^{s_2} ds \exp\left\{-s^2\right\}$$

which involves the well-understood, probability integral or error function. As $a' i_z = \sigma_z(x'_r)$, the result may be written as

$$C = \frac{q}{\sqrt{2\pi}\, u\, \sigma_z(x'_r)\cos\theta} \cdot 1/2 \left\{\mathrm{erf}(s_2) - \mathrm{erf}(s_1)\right\} \qquad (76)$$

$$\text{where} \quad s = \frac{1}{\sqrt{2} i_y \tan\theta} \cdot \frac{(\ell/a')\sin\theta}{1 + (\ell/a')\sin\theta} \qquad (77)$$

and the appropriate values s_1, s_2 are obtained from the corresponding values of ℓ_1, ℓ_2 given in equation (75) and where $a' = \sigma_z(0)/i_z + x'_r$.

Now for the infinite line (i.e., no intersections) $y_{Id} = -\infty$ and $y_{Iu} = +\infty$, which by equation (75) then gives

$$\ell_1 = \ell_0 = -x'_r/\sin\theta \text{ and } \ell_2 = +\infty,$$

and subsequently

$$s_1 = \frac{-1}{\sqrt{2} i_y \tan\theta} \cdot \frac{x'_r i_z}{\sigma_z(0)} \qquad \text{and} \qquad (78)$$

$$s_2 = \frac{1}{\sqrt{2} i_y \tan\theta}$$

With the further simplification to the infinite perpendicular line source (i.e., $\theta \rightarrow 0$), the s limits blow-up and, as erf $(\pm \infty) = \pm 1$, one obtains the well-known result

$$C = q/[\sqrt{2\pi}\, u\, \sigma_z(x_r)] \qquad (79)$$

for the infinite crosswind line source (not including the factor-of-two coming from the ground reflection term).

The result given by equation (76) represents a new generalization of available analytic line source formulae. The additional generalization of arbitrary orientation angle was obtained by constraining both y and z plume growth rates to be linear in distance or travel time. Such an assumption would not be appropriate for σ_z at large distances from the line source, especially under z stable stratification. However, within the confines of an urban canyon, the relevant distances are appropriately small and the high degree of mechanical turbulence and local heat sources tend to inhibit the formation of a stable boundary layer.

A study of the angular dependence of equation (76) was carried out for the case of a receptor a fixed crosswind distance x_r from the infinite line source. Thus, θ variation corresponds to pure wind angle variation. Examination of the error function arguments, given by equation (78) shows that for $\theta < 45°$ and receptors well outside the initial mixing zone (i.e., $x_r >> (i_y/i_z)\sigma_z(0) = \sigma_y(0)$), the error function "saturates" to unity and the latter piece of equation (76) (i.e., $1/2\{\mathrm{erf}(s_2) - \mathrm{erf}(s_1)\}$) is about one. Figure 45 shows just how rapidly the error function "saturates" in terms of its argument x. All the remaining θ dependences are contained in the term

$$\sigma_z(x'_r)\cos\theta = [\sigma_z(0) + i_z x_r/\cos\theta]\cos\theta$$
$$= \sigma_z(0)\cos\theta + i_z x_r. \qquad (80)$$

Hence, for $\sigma_z(0) = 0$ this term will show no θ dependence, and only a weak θ dependence for finite initial mixing and receptors well outside the initial mixing zone, such that $i_z x_r >> \sigma_z(0)$. Figure 46 shows the weak variation of $C(\theta)/C(0)$ for moderate θ and a typical source-receptor configuration that one would expect based on the discussion above. In addition, this behavior is in agreement with the numerical integration studies of Calder (1973). Behavior at large θ is more dramatic, with $C(\theta)/C(0)$ falling to 1/2 (or less) as θ approaches 90°.

As a final "correction" to equation (76) let us consider the case of a line source having a finite breadth, B_L, due to the initial mixing induced by the

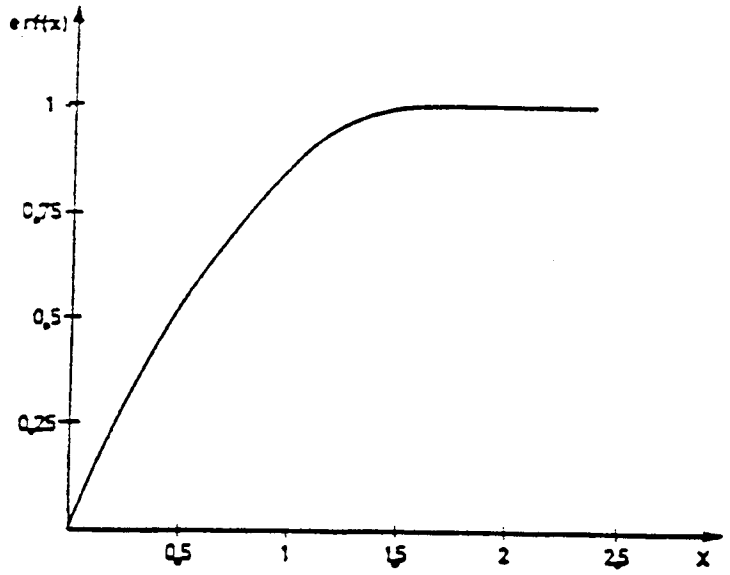

Figure 45. Error Function $\operatorname{erf}(x) = \frac{2}{\sqrt{\pi}} \int_0^x \exp(-t^2)dt$.

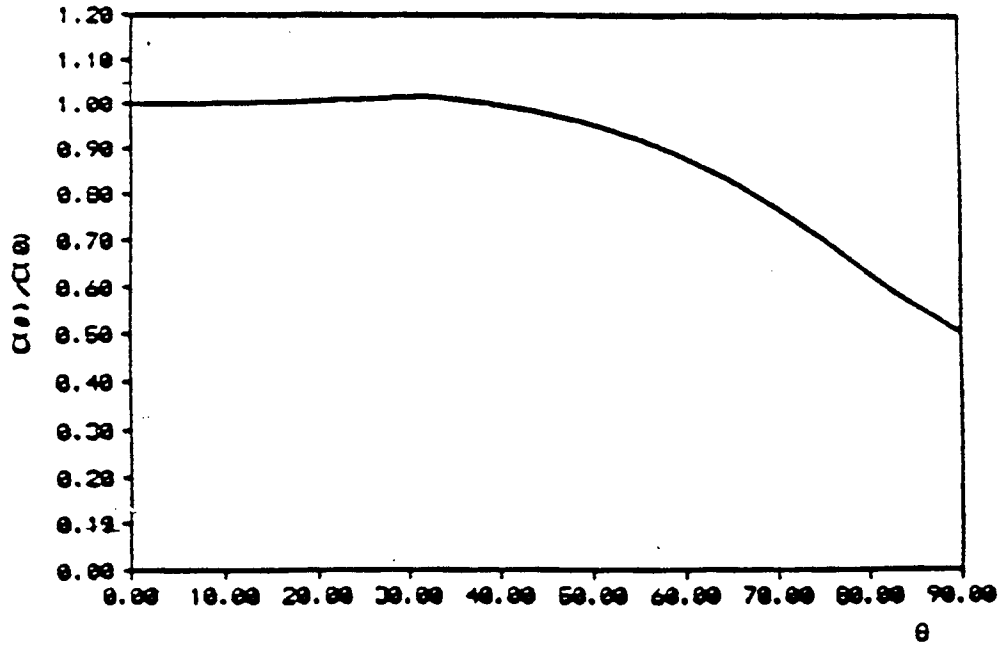

Figure 46. Typical wind angle dependence of equation (76) normalized by C(0).

moving automobiles. A complete solution of this problem for arbitrary orientation θ appears to require a numerical integration as the x_r', which is now varying, appears in many awkward places. Instead, let us consider computation of a multiplicative correction factor, F, at $\theta = 0$ and yet suitable for inclusion in equation (76). This factor is then just

$$F = \frac{\sigma_z(x)_r}{B_L} \int_{x_r - B_L/2}^{x_r - B_L/2} dx/\sigma_z(x) \tag{81}$$

which has the simple solution

$$F = \frac{\sigma_z(x_r)}{i_z B_L} \ell n \left[\frac{\sigma_z(x_r + B_L/2)}{\sigma_z(x_r - B_L/2)}\right] \tag{82}$$

or equivalently

$$F = \frac{\sigma_z(x_r)}{i_z B_L} \cdot \left\{\ell n\left[1 + \frac{\sigma_z(x_r + B_L/2) - \sigma_z(x_r)}{\sigma_z(x_r)}\right] - \ell n\left[1 + \frac{\sigma_z(x_r - B_L/2) - \sigma_z(x_r)}{\sigma_z(x_r)}\right]\right\}$$

This latter form, the knowledge that

$$\frac{\sigma_z(x_r \pm B_L/2) - \sigma_z(x_r)}{\sigma_z(x_r)} = \pm 1/2\ i_z B_L/\sigma_z(x_r) \equiv \pm \epsilon,$$

and the Taylor expansion

$$\ell n\ (1 + \epsilon) \cong \epsilon - \frac{\epsilon^2}{2} + \frac{\epsilon^3}{3} \ldots ,$$

then permits one to write

$$F \simeq 1 + 1/12 \left[\frac{i_z B_L}{\sigma_z(x_r)}\right]^2 . \tag{83}$$

Approximate generalization to arbitrary angle θ is then given as

$$F \simeq 1 + 1/12 \left[\frac{i_z B_L/\cos\theta}{\sigma_z(x_r')}\right]^2 \tag{84}$$

Sensitivity studies, carried out using equation (84), show that the role of such a term is quite small unless the receptor is very close to a broad source having a small $\sigma_z(0)$. For very broad lanes or where one considers B_L to span the width of an entire highway, equation (82), generalized to

$$F = \frac{\sigma_z(x'_r)}{i_z(B_L/\cos\theta)} \ell n \left[\frac{\sigma_z[x'_r + B_L/(2\cos\theta)]}{\sigma_z[x'_r - B_L/(2\cos\theta)]} \right] , \qquad (85)$$

should be used.

APPENDIX F

PARAMETERIZATION OF VEHICLE-WAKE INDUCED INITIAL MIXING

The CPB model accommodates vehicle-induced mechanical mixing through the inclusion of initial plume sigmas $\sigma_z(0)$ and $\sigma_x(0)$ for the vertical and cross-canyon dimensions respectively. However, the sophisticated vehicle wake theory of Eskridge and Hunt (1979) predicts the velocity and turbulence perturbation fields behind moving vehicles, and the relationship of these perturbation fields to initial plume spreads is not immediately obvious. Nevertheless, it is important to establish such a connection, as some full-scale roadway tracer studies (e.g., Eskridge et al., 1979; Eskridge and Rao, 1983) as well as numerous wind tunnel investigations (e.g., Eskridge and Thompson, 1982; Thompson and Eskridge, 1987) of block-shaped and realistic vehicle movement influences have shown that the Eskridge-Hunt theory leads to realistic predictions of the concentration fields in the near vicinity of moving vehicles.

The nature of this theory is such that it can only be incorporated into a numerical grid model and is a major component of the ROADWAY (Eskridge and Catalano, 1987) numerical pollution model. Rather than attempt to build a theoretical bridge between the flow/turbulence perturbation model and the initial spatial dispersion model, a number of ROADWAY model runs were carried out at varying vehicle speeds, and the concentrations at the vehicle cell were noted. Under perpendicular flow conditions, a simple box model would yield initial concentrations of

$$C = q/uH\ell \qquad (86)$$

where q (gm/m/sec) is the line source emission density
u is the wind speed, and
$H\ell$ is height of the mixing zone.

This initial mixing zone can then be related to plume sigmas via the relation

$$H\ell = \sqrt{2\pi}\ \sigma_z(0) \tag{87}$$

which has been rigorously shown (TA-Luft, 1987) to be the correct conversion from uniform box mixing to Gaussian plume sigma mixing.

Critics of using equation (86) to bridge the two approaches could correctly argue that one is able to achieve a "match" between the two approaches only at a single spatial point because the true vehicle wake survives over finite space-time and thus enhances plume dispersion further downwind as well as initially. The numerical model can incorporate such inhomogeneous, decaying turbulence, whereas the Gaussian model cannot (easily). However, the primary objective of this study is to extract the vehicle velocity, V, dependence of the phenomena and not necessarily its absolute normalization. Thus, one can be somewhat less sensitive to the criticism.

The ROADWAY model was run at a wind speed of u = 0.5 m/s, (1.1 mi/h) a q and mass-to-ppm conversion factor such that $H\ell = 2/C$, and for blocklike vehicles 1.5m (4.9 ft) high and 2.0m (6.6 ft) wide and operating at speeds ranging from 10 km/h (6.2 mi/h) to 100 km/h (62 mi/h). The resulting values of $H\ell$ are displayed in figure 47 along with the optimal power law fit

$$H_\ell = a(V/100)^b \qquad (88)$$

where V is vehicle speed in km/hr
a = 3.33m,
b = 0.586, and
H_ℓ is in meters.[11]

Runs were also performed at slower vehicle speeds and suggested that H_ℓ might take on the minimal value of about 0.77m (2.5 ft) as V goes to zero; however, one condition demanded by ROADWAY is that V>>u. Thus, these results are not used.

Also displayed in figure 47 is the empirical function,

$$H_\ell = H_V(0) + H_V(\infty)[1.0 - \exp(-V/V_C)] \qquad (89)$$

developed for the CPB-1 model by Yamartino and Wiegand (1986), but with the optimal values of $H_V(0)$ = 0.26m (0.85 ft), $H_V(\infty)$ = 3.40m (11.2 ft), and V_C = 55 km/h (34 mi/h) for these ROADWAY data. These parameter values lead to smaller values of H_ℓ than when using the CPB-1 parameter values of $H_V(0)$ = 2.0m (6.6 ft), $H_V(\infty)$ = 2.5m (8.2 ft), and V_C = 30 km/h (18.6 mi/h); however, a sensitivity study of these CPB-1 model parameters (Garben et al., 1987) showed no deterioration of model performance for smaller H_ℓ; thus indicating that the original CPB-1 parameters

[11] The residuals of $\ln H_\ell$ were minimized. Additional optimization studies showed that the addition of a constant term to equation (88) did not lead to any improvement.

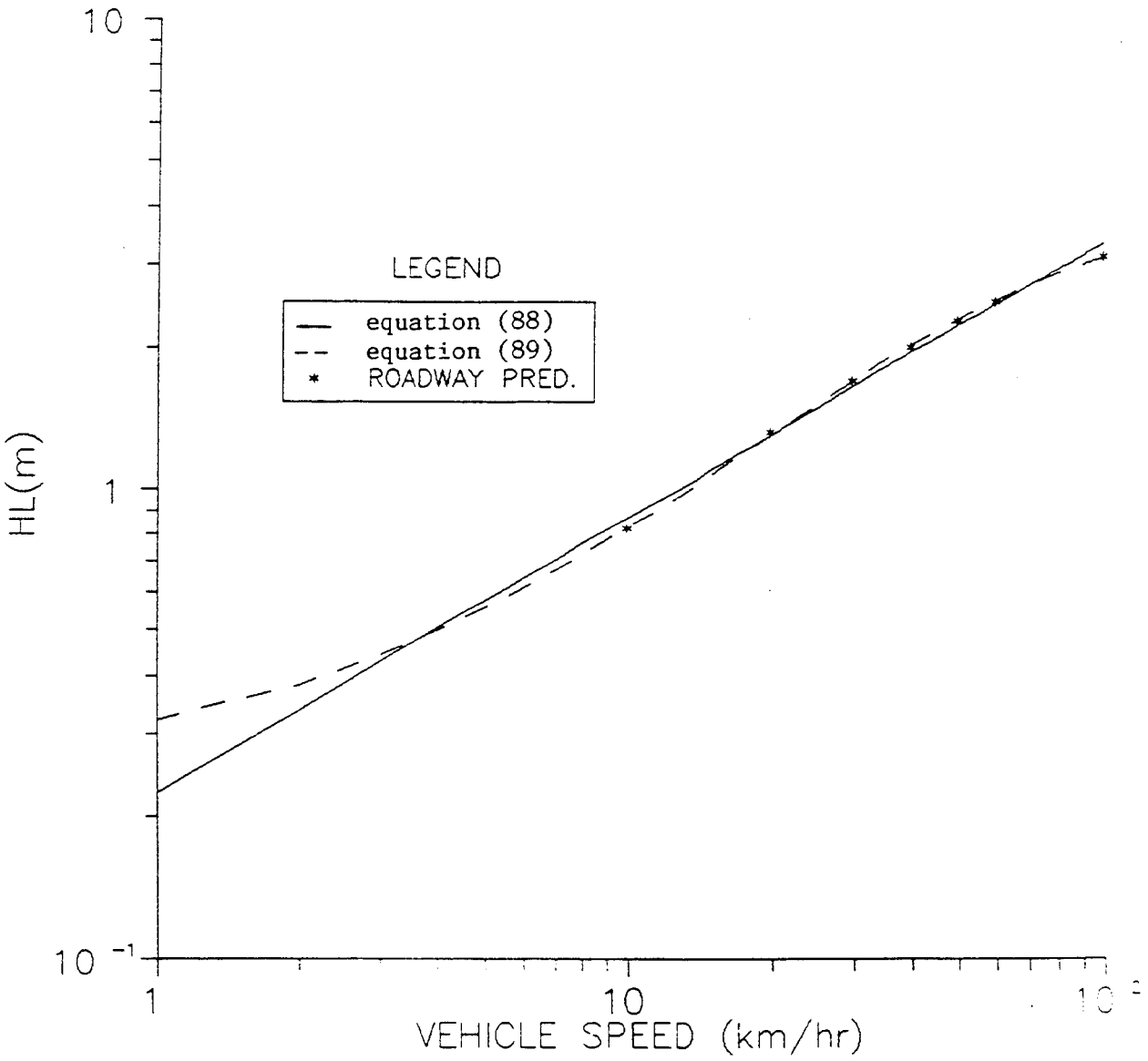

Figure 47. Comparison of the size of the vehicle-wake induced initial mixing zone inferred from the Eskridge-Rao-Thompson numerical model ROADWAY with predictions of empirical models given by equations (88-89).

represent upper limits on H_ℓ rather than true optimal parameter values.

Despite the superiority of equation (89) over equation (88) in fitting these ROADWAY-generated data, it should be emphasized that neither equation has a theoretical basis. Equation (88) is simply a power law conjecture, whereas equation (89) is based on the intuitive notions:

- That a motionless vehicle would generate some minimal (i.e., $H_v(0)$) mixing of pollutants due to its presence as a flow, obstacle or roughness element.

- That progressively faster vehicle speeds would eventually (i.e., $V>>V_c$) become less efficient at increasing H_ℓ such that an asymptotic value of H_ℓ would be reached (for example, consider a bullet).

The current data do not indicate any inconsistency with this intuitive picture of vehicle wake influence.

In addition, evaluation of equation (89) at the V = 80 km/h (50 mi/h) of the GM experiment (Chock, 1977) gives H_ℓ = 2.87m (9.4 ft), whereas analyses by Sedefian et al. (1981) for the nearest GM tower, transformed to H_ℓ and corrected for linear rather than quadrature σ_z additivity, gives H_ℓ = 3.35m (11.0 ft). Thus, the absolute normalization of equation (89) may not be far from reality; however, additional studies should be performed.

Finally, it should be noted that some windspeed and angle dependence may need to be considered to make equation (89) more general. For example, the scalar V should be redefined as

$$\vec{V}' = [\vec{V} - \vec{u}] \qquad (90)$$

where $\vec{u}$ is the vector wind at vehicle height, in order to ensure the proper invariance of the equations under translation. Additional wind speed or residence time dependence, as discussed by Benson (1982), may also be warranted.

APPENDIX G

THE SEATAC INTERNATIONAL AIRPORT STUDY

Introduction

A modern commercial airport has one of the prime ingredients for a carbon monoxide (CO) hotspot: a large number of slowly moving or stopped vehicles on the access roadway directly in front of the terminal building. Further complications at this location can include:

- Building wake effects due to the terminal and/or street canyon vortex effects created by the terminal and a parking garage, typically located just across the access roadway from the terminal.

- Additional ventilation (or added garage emissions) due to the open style construction of many of these garages.

- Curvature of the entire terminal/roadway/garage complex for airport design optimization purposes.

- "Covered over" roadways created by multi-level terminals or canopies over the sidewalk area; and (v) aircraft emissions impacts for the case of flow from the gate areas, over the terminal building, and into the access roadway street canyon.

While many of the BU wind tunnel measurements were oriented toward understanding the perturbative effects of unequal height buildings, building porosity (e.g., semi-open garages), roadway curvature, and a realistic airport-like, combination of all

three effects, our understanding and mathematical modeling of these perturbative effects on the within-canyon flow (appendix B, this volume) and turbulence (appendix C, this volume) fields is clearly less than perfect. Thus, measurement studies undertaken at an actual airport provide a necessary and valuable reference point to the real world.

The Seattle/Tacoma International Airport (SEATAC) was selected as the site of a 3-day pilot study because it contained many of the above-mentioned perturbations to the 2-D street canyon problem without excessive 3-D complications (e.g., isolated tall buildings, intersections) that are considerably more difficult to include in the modeling, and because the airport management was very supportive of our efforts.

Figure 48 shows a plan view of the curved terminal/roadway/ garage region whereas figure 49 shows a cross section of the double street canyon. The upper street canyon, from the garage to the canopy over the enplane drive, is about 33.4 m (110 ft) wide (W_u) and 16.2 m (53 ft) deep (H_u), whereas the lower canyon, from the garage to the edge of the enplane drive, is about 23.1 m (76 ft) wide (W_ℓ), extends 8.35 m (27.4 ft) below (H_ℓ), enplane drive on the terminal side with the 16.2 m (53 ft) (H_G) high garage on the other side. The radius of curvature to the edge of enplane drive is estimated at 59.9 m (196 ft) leading to estimated diameters of curvature (as measured to the middle of the canyon) of 107 m (351 ft) (D_u) for the upper canyon and 96.7 m (317 ft) (D_ℓ) for the lower canyon with subsequent dimensionless curvatures ($d = W/D$) of $d_i = 0.312$ and $d_\ell) = 0.239$, respectively. The curvature of this upper canyon corresponds very closely to the $d = 0.308$ airport complex measured in the wind tunnel, and the full-scale W_u/H_u ratio of 2.06 is only about 13 percent below the wind tunnel measured

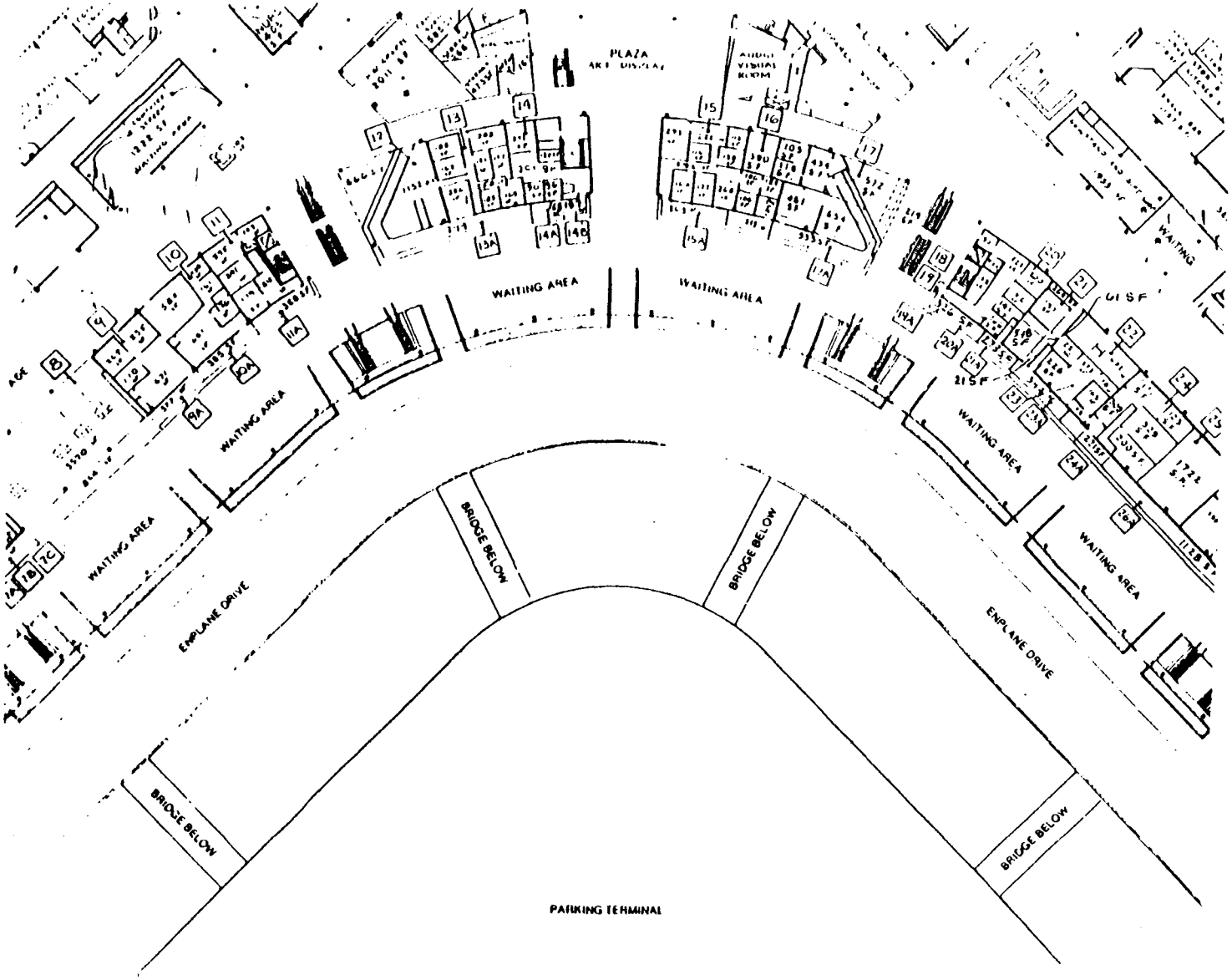

Figure 48. Plan view of the curved terminal/access roadway/garage complex at SEATAC.

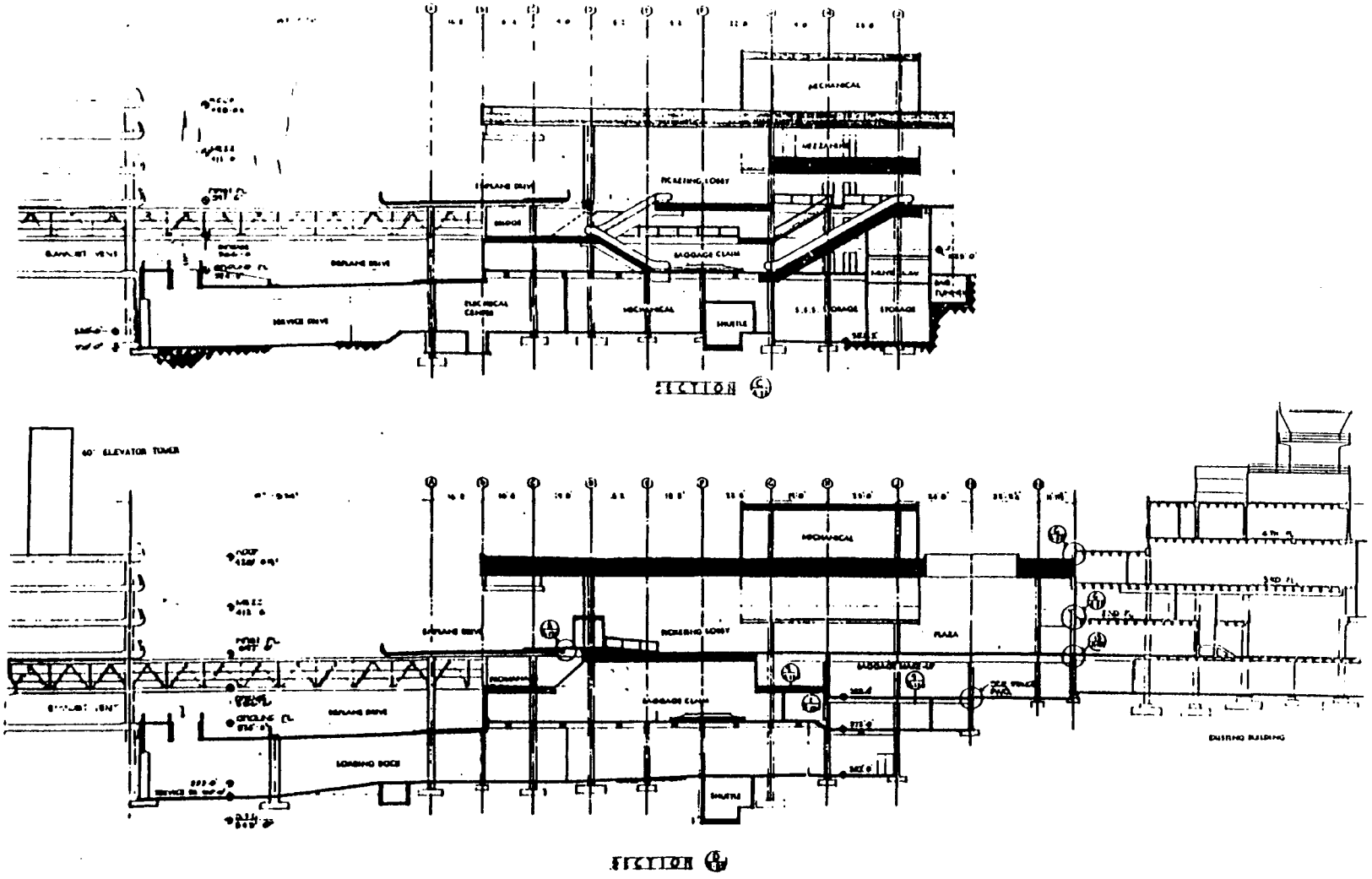

Figure 49. Cross-section of the "double" street canyon existing between the terminal and garage. The service drive is below ground and does not influence atmospheric flow.

ratio of 2.37. Unfortunately, it is difficult to estimate from the wind tunnel data what the effects on the flow, turbulence and pollutant fields from:

- The canyon within a canyon nature of SEATAC.
- The overhanging canopies.
- The straight segments of roadway and bounding structures that precede and follow the curved portion.

The porosity, p, of the garage, defined as the amount of open space at the edge divided by the total garage height, was computed from plans and photos to be 0.33 to 0.35, somewhat smaller than the p = 0.43 considered in the wind tunnel.

In the sections which follow we will describe the data collected during the 3-day study and undertake analyses of the meteorological data for the final day, June 26, 1987, including the period from about 1000 to 1800 PDT (i.e., often referred to as the "intensive" period) when U-V-W and CO data were collected as well as traffic and other meteorological data.

Data Collected

Traffic Data

The State of Washington Department of Transportation (WDOT) collected axle count data with 15-minute resolution at five critical locations including the upper and lower roadways and garage entrance and exit ramps for the entire 3-day period. In addition, fleet mix was evaluated for noon and 6 PM periods and is shown in table 15. Differences between the various levels and times are not very striking given the overall count statistics and can be aggregated in order of frequency to yield

Table 15. SEATAC access road fleet mix.

Vehicle Type	Percent Mix Upper Level Enplane	Percent Mix Lower Level Deplane
1300 - 1330 PDT		
Large Bus	3.2	4.7
Shuttle Van	15.3	20.3
Pickup/Carryall	17.7	18.0
Passenger Cars	55.7	46.5
Taxis	8.1	10.5
Sample Count[1]	24	172
1800 - 1830 PDT		
Large Bus	3.4	0.7
Shuttle Van	22.4	14.0
Pickup/Carryall	10.3	15.4
Passenger Cars	48.3	59.6
Taxis	15.6	10.3
Sample Count[2]	58	136

[1] Sample counts reflect 15-minute counting period on 6/24/87 (Weds).
[2] Sample counts reflect 10-minute counting period on 6/26/87 (Fri).

passenger cars (52.7 percent), shuttle vans (17.5 percent), pickup/carryall (16.3 percent), taxis (10.4 percent), and large buses (3.1 percent). These data may subsequently be used in a MOBILE 3 estimation of emissions.

MRI Mechanical Weather Stations

Two Meteorological Research Inc. (MRI) mechanical weather stations were sited on rooftops to record reference level, above-roof wind speed and direction. One unit (MRI-5) was placed on the roof of the terminal's "mechanical penthouse" with a sensor height of about $z = 23.8$ m (78 ft) or $z/H_G = 1.47$, whereas a second unit (MRI-9) was placed on top of the garage's 12.2 m (40 ft) high North elevator tower to give an overall sensor height of $z = 30.6$ m (100 ft) or $z/H_G = 1.89$. These sensor locations compare well with the reference level wind locations of $z/H = 1.41$ from the Bonner Strasse study and an approximate wind tunnel reference level of $z/H \simeq 2$ that corresponded to wind speeds of about 65 percent of geostrophic speeds.

A third station (MRI-4) was located for part of the study on garage level 3 to record the flow through the garage and later moved to the middle of the roof of the southernmost garage/terminal pedestrian bridge, which placed the sensor at about 10.0 m above the lower (deplane) roadway. This height of $z/H_G \simeq 0.62$ may be in the near vicinity of the vortex center (i.e., should it exist and fill the lower roadway canyon) and thus can render the cross-canyon component of this measurement difficult to interpret. The along-canyon wind component should, however, be well sampled by this sensor.

These three, battery-powered units employ cup anemometers, directional-vanes, and pressure-sensitive, clock-driven strip chart media for recording signals.

NOAA Meteorological Data

The SEATAC based NOAA station reports hourly measures of wind speed, direction, temperature, and cloud cover. These data are actually spot measures taken about 10 minutes before the hour (PST). Supplemental triple register data were also obtained, again reflecting wind speed and direction conditions in the open airfield, low roughness environment (z_0 = = few cm or in) at a sensor height of about 10 m (33 ft).

R.M. Young U-V-W Anemometer

A three axis (orthogonal), R.M. Young, Inc., U-V-W anemometer was co-located with MRI-4 on the pedestrian walkway roof (n.b., the U-V-W was actually displaced about 3 m (10 ft) cross-canyon and + 1 m (3.3 ft) vertically from the MRI unit to avoid interference) giving it a normalized height of $z/H_G \approx 0.68$. Average values and standard deviations were computed over 10-minute intervals using a sampling rate of 2 Hz. Signals were converted using a Remote Measurement Systems Inc. A/D converter and a NEC-PC8201A laptop computer.

Later, this instrumentation was moved down to the lower (deplane) roadway about 15 m (49 ft) upwind (NW) of the pedestrian walkway and nearly directly underneath the edge of the enplane drive (located about 8.0 m (26 ft) above the lower roadway level). The sensor height of about z = 3 m (10 ft) was reasonable for sensing any vortex penetration into this lower street canyon and was as far from obstacles and slowly moving

vehicles (i.e., about 4-5 m (13-16 ft) laterally) as could be managed.

Ecolyzer CO Measurements

Three battery-operated Ecolyzers were used in several modes to monitor CO levels within the access roadway street canyon. Basically, the most stable of these instruments remained approximately co-located (i.e., 2 m (6.6 ft) lower) with the U-V-W anemometer and output directly to the data logger. This instrument typically recorded 10-minute average values of 2-4 ppm with no value in excess of 5.1 ppm.

Two other Ecolyzers output to small battery driven strip chart recorders. These instruments were (i) located on the pedestrian walkway bridge roof and sampled at heights of about z = 8 m (26 ft) and z = 6.0 m (20 ft) or (ii) walked along the upper and lower level sidewalks to sample CO concentrations as experienced by pedestrians. Instantaneous values were observed to reach about 20 ppm but seldom stayed at these values for more than one minute. The values observed should usefully span the range of values one should expect from a reasonable model.

Supplemental Data

In addition to numerous photographs and videotape recordings, soap bubbles were released from several locations (i.e., street level and garage roof). On most occasions these bubble trajectories indicated significant vertical velocities (often in excess of cross canyon velocities) and a few cases indicated the presence of a street canyon vortex; however, bubble lifetimes were generally too short to confirm more than 1/4 to 1/2 of a revolution in this vortex.

Lightweight mylar streamers were also hung from the garage and garage/terminal walkway roof. These indicated that the flow is primarily along the canyon axis but also showed some evidence of a vortex-like, cross-canyon counterflow from the terminal toward the garage.

Processing of Meteorological Data

As previously mentioned, three types of meteorological data were obtained during the SEATAC field study: hourly NOAA observations at the airport; 10-minute average speeds and standard deviations from a U-V-W anemometer (the data collector sampled at 2 Hz); and speed and direction recorded on "strip-charts" from three MRI cup-and-vane anemometers. The data provided by the MRI windsets required the greatest amount of processing.

Airport data required two alterations. The times reported by the NOAA office are given in Pacific Standard Time. These times were converted to Pacific Daylight Time by adding 1-hour to that indicated. In addition, wind speeds are reported as knots and were converted to m/s via the factor 0.5144.

Raw wind data from the U-V-W windset were given in mV units. These were converted to m/s as follows. For the horizontal components (U, V), 300 rpm corresponds to 1.5 m/s (3.35 mi/h)and the output from the sensor is calibrated to 500 mV for 1800 rpm, so that 1 mV = 0.018 m/s (= 0.040 mi/h). For the vertical component (W), 300 rpm corresponds to 1.8 m/s (4.0 mi/h) and the output is calibrated to 500 mV for 1800 rpm so that 1 mV = 0.0216 m/s (= 0.0483 mi/h).

The first step in preparing the data from the MRI windsets was performed by the FHWA. Strip charts were magnified and digitized at 2-minute intervals yielding the following information:

Wind Direction:

- lower and upper values during the interval and
- flag indicating if the range passed through zero.

Wind Speed:

- chart width in inches and
- current "run" distance (integrated speed) in inches.

Note that with the MRI mechanical station, wind speed is given by the slope of the wind "run" trace versus time; hence, the trace was broken up into segments of nearly constant slope, and only the endpoints of these segments were reported.

The following procedures were then used to process these data into a time-series of speeds and directions:

Wind Direction:

- the 360/0° crossover flag was reset so that 0 represents no crossover, and 1 represents a crossover;
- a mean direction was estimated from the lower and upper values of the range by means of the formula;

$$D_m = 0.5(D_l + D_u) + \text{flag} * 180$$

- an adjustment was made to reference true North:

  MRI-4 19° added (6/24 to 1500 on 6/25)
  44° added (1500 on 6/25 to 6/26)

  MRI-5 19° added

  MRI-9 19° added.

Wind Speed:

- values of wind "run" were interpolated to each two-minute interval between the digitized endpoints;

- additional entries were included whenever the chart width was adjusted and whenever the trace passed through full scale. This allows the proper specification of differences in wind "run" when calculating speeds; and

- the mean wind speed in each interval was calculated by means of the formula

$$S = (R - R_o)\, L / (F\, \tau)$$

where R and R_o are the "run" at the end of the interval and the beginning of the interval, respectively; L is the physical distance represented by the full-scale range of the chart (10 mi = 16085 m); F is the full-scale dimension of the chart (same units as R); and τ is the length

of the interval in seconds. The resulting speed has units of m/s when L is given in meters.

All of these operations were carried out in LOTUS format. Once the speeds and directions were computed, extraneous entries were removed and the data were transferred to an ASCII file for further averaging.

Processing data from the MRI-5 windset involved an adjustment to the indicated times. The clock (i.e., the rate of advance of the strip chart) was observed to run slowly based on three time-checks noted in the log. Because wind data were only digitized for day 6/26, the last two points were used to obtain the following relation between the indicated time on the chart (t_c) and the true time (t_t):

$$t_t = 1.072\ t_c + 5.747$$

where the times are assumed to be given in hours, and the zero of the regression is assigned to the start of 6/26. Inspection of the trace of wind "run" showed a sequence of periodic jumps in the wind speed that occurred at intervals of approximately 30 minutes. These jumps have the appearance of being the result of periodic "slippage" of the chart drive. This suggests that the slow clock may have resulted from intermittent transport problems, rather than an overall slowness in the transport speed. Nonetheless, correction to the times indicated on the chart were made on the basis of the above formula.

These data were averaged to periods of 1 hour for comparisons among the three MRI windsets and the hourly observations from the airport. They were also averaged to periods of 10 minutes for comparisons with data obtained from the U-V-W windset. Wind

speed averages were computed as scaler averages. Mean directions were computed from estimates of the 2-minute wind direction as vector averages by assuming that the speed during each observation is constant.

Estimates of the standard deviation in wind direction (σ_θ) were made by means of the relations developed by Yamartino (1984), using the estimate of the mean direction for each 2-minute period as well as the lower and upper bounds to the range in wind directions. If D_{li} ,D_{ui} and D_{mi} denote the lower, upper, and mean directions for the ith interval, one may then assign a weight to each of these directions, with the mean direction assigned a weight of 1, and the two extreme values assigned a weight of wt = 0.5. Then,

$$s_a = \Sigma\ [\sin D_{mi} + wt(\sin D_{li} + \sin D_{ui}] \ /\ N(1 + 2wt)$$

$$c_a = \Sigma\ [\cos D_{mi} + wt(\cos D_{li} + \cos D_{ui}] \ /\ N(1 + 2wt)$$

$$\epsilon^2 \equiv 1 - (s^2{}_a + c^2{}_a), \text{ and finally}$$

$$\sigma_\theta = \sin^{-1}(\epsilon)\ [1.0 + 0.1547\ \epsilon^3].$$

This use of the lower and upper bounds to the range in wind direction during each of the periods allows the variability seen in wind directions on the 2-minute time-scale to enter the estimate of the total variability.

Analysis of Meteorological Data

Given the higher sampling location of the MRI-9 unit atop the garage's North elevator tower and the greater reliability of its strip chart clock drive (i.e., as compared with MRI-5 atop the terminal's mechanical penthouse roof), MRI-9 was considered the reference measure for wind speed and direction. Figure 50 compares hourly-average wind directions measured at this reference location with those measured on the roof of the pedestrian bridge, on the roof on the terminal's mechanical penthouse, and by NOAA. The fact that the walkway bridge wind directions do not restrict themselves to narrow zones around -45° (i.e., 315°), and 135°, corresponding to the direction of the roadway, indicates that there is substantial cross-canyon flow at this point. Whether this flow is due to flow through the garage or to street canyon vortices will be considered later using the u-v-w data.

These wind direction data are then replotted in figure 51 as differences from the reference wind versus reference wind angle. Given the location of the pedestrian bridge within the street canyon, it is not surprising that the deviations here are systematically large. Deviations between the two rooftop locations is somewhat larger than expected especially given the generally superior correspondence with NOAA spot measurements.

A portion of this condition may be due to MRI-5 clock drive problems. The fact that over 50 percent of the NOAA observations are within 20° of the reference height wind directions is encouraging given the relatively light-moderate wind, unstable

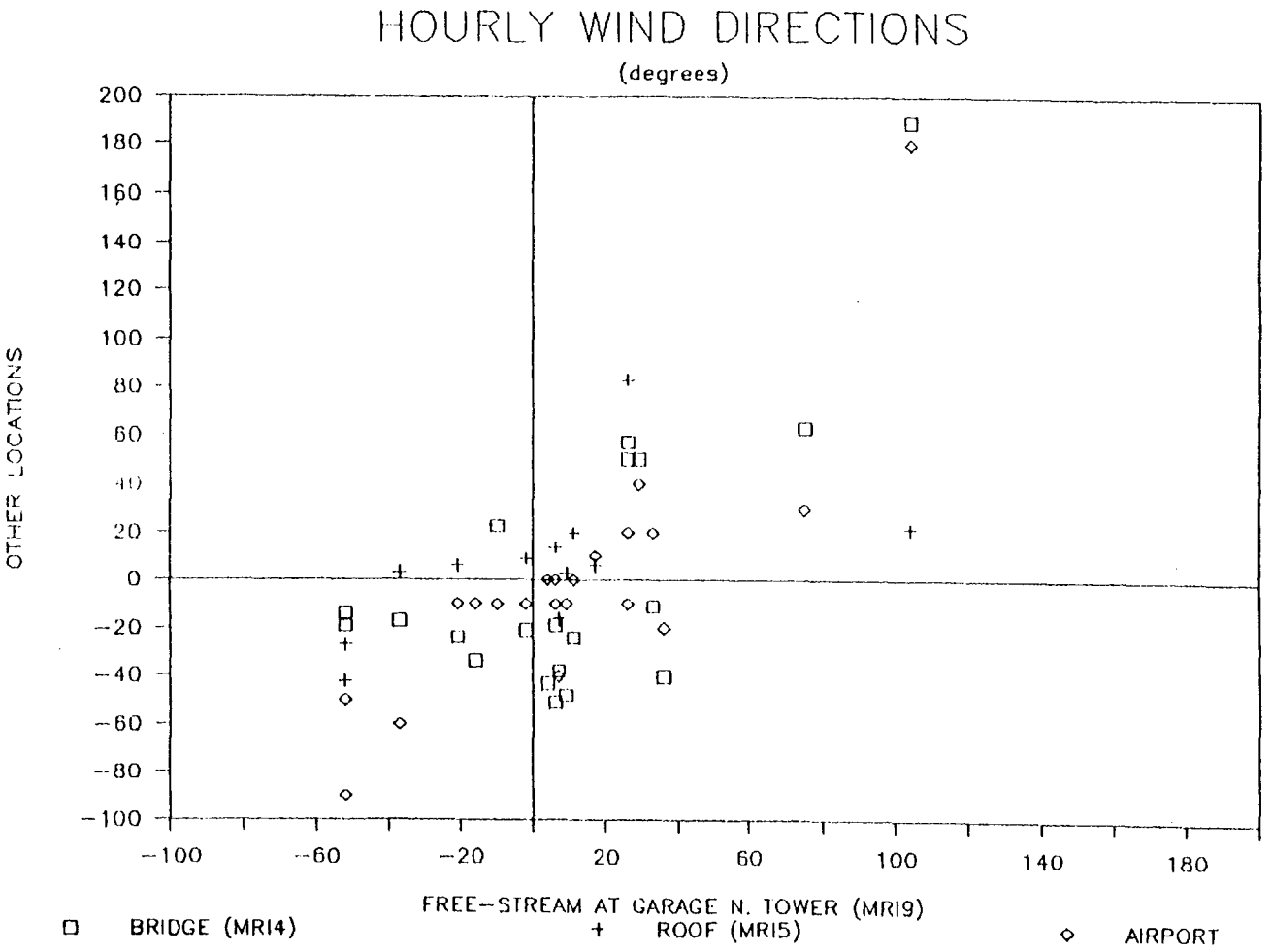

Figure 50. Comparison of hourly average wind directions observed from the pedestrian bridge, the terminal roof, and by the airport (NOAA) with the reference wind direction.

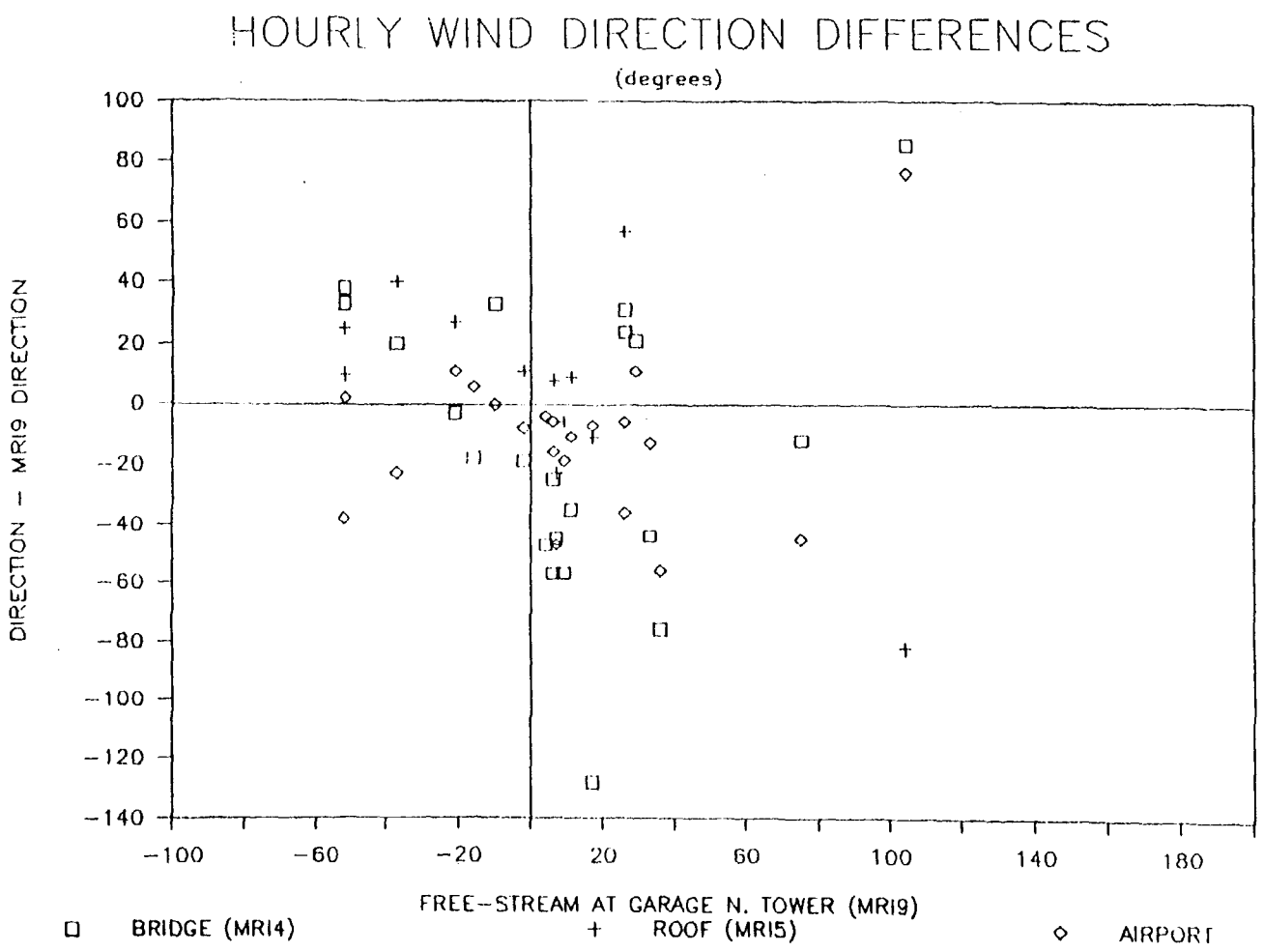

Figure 51. Hourly average wind direction differences from the reference wind direction for observations from the pedestrian bridge, the terminal roof, and by the airport (NOAA) versus reference wind direction.

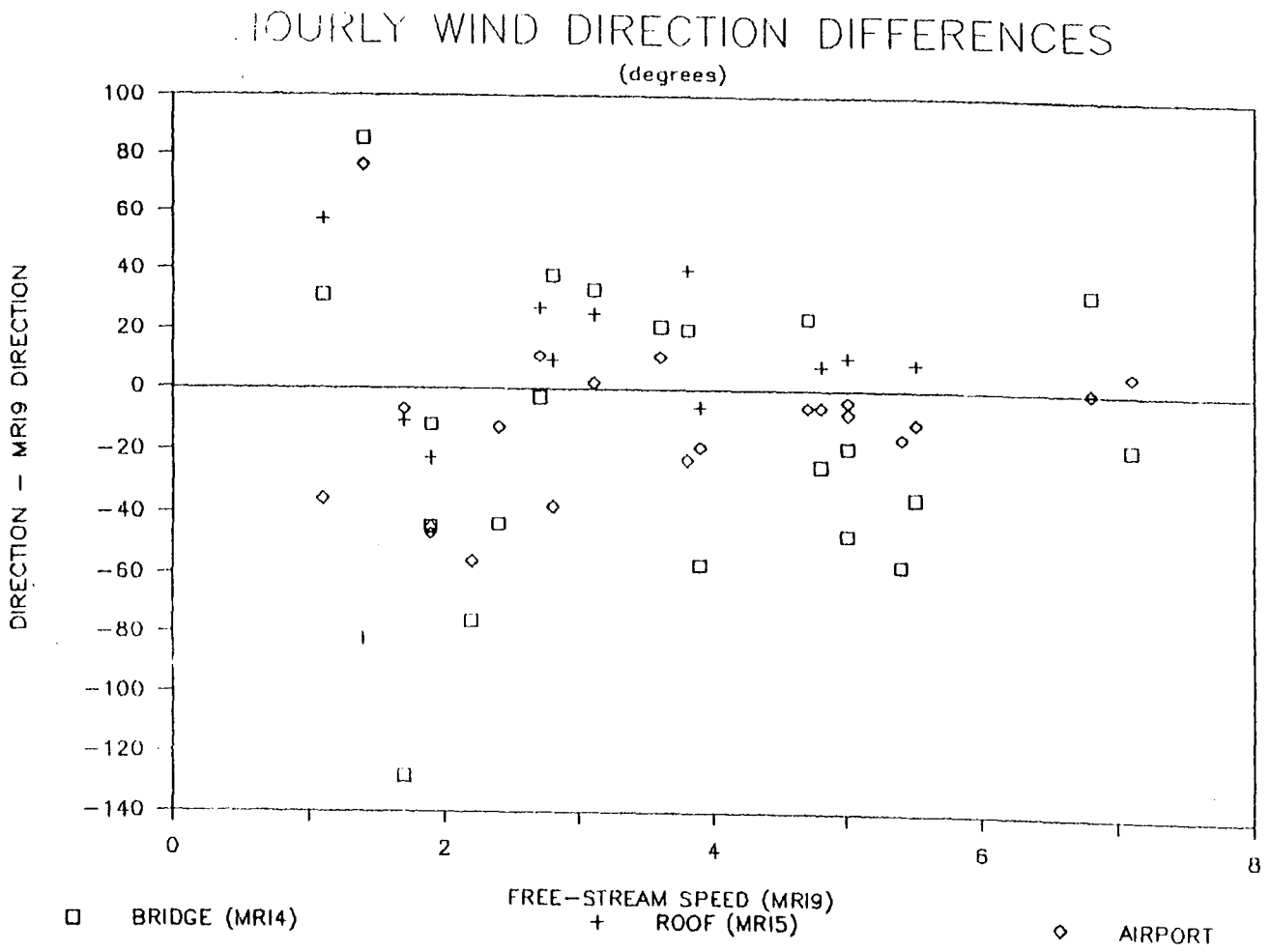

Figure 52. Hourly average wind direction differences from the reference wind direction for observations from the pedestrian bridge, the terminal roof, and by the airport (NOAA) versus reference wind speed.

meteorological conditions prevailing.[12] Reasonable agreement here is important as NOAA airport winds are usually all that one has available for air pollution modeling studies and because pollutant concentrations are often very sensitive to wind direction. Figure 52 shows these same wind direction differences as a function of reference height wind speed. As anticipated, deviations decrease with increasing wind speed where the wind direction becomes more persistent (i.e., smaller standard deviations of wind direction). Deviations at the walkway bridge site also show this decreasing trend with increasing wind speed but it is less pronounced than at the other two sites.

Figure 53 shows the intercomparison of hourly-average wind speeds at the three other locations with the reference level speed. Speeds on the terminal roof compare quite well, whereas speeds within the street canyon are suppressed by factors ranging from two to six. Surprisingly, NOAA reported speeds are typically about one-third to 50 percent higher than reference level winds. The only reason for this is that the long, low roughness fetch over the unobstructed airfield allows higher speeds than in the large roughness, terminal area zone.

Figure 54 presents an intercomparison of standard deviations of wind direction, σ_θ' observed at the three MRI sites (n.b., σ_θ is not reported for NOAA airport winds). One notices immediately the very large values of σ_θ, in the range of 30° to 70°, seen at the reference level. Agreement with terminal roof measured values is generally within 20 percent, whereas there is little or no correspondence with the highly scattered values seen on the walkway bridge.

---

[12]Skies were cloudless during the 3-day study and on 26 June, the day of these data, temperatures reached record levels of 88°F (31°C).

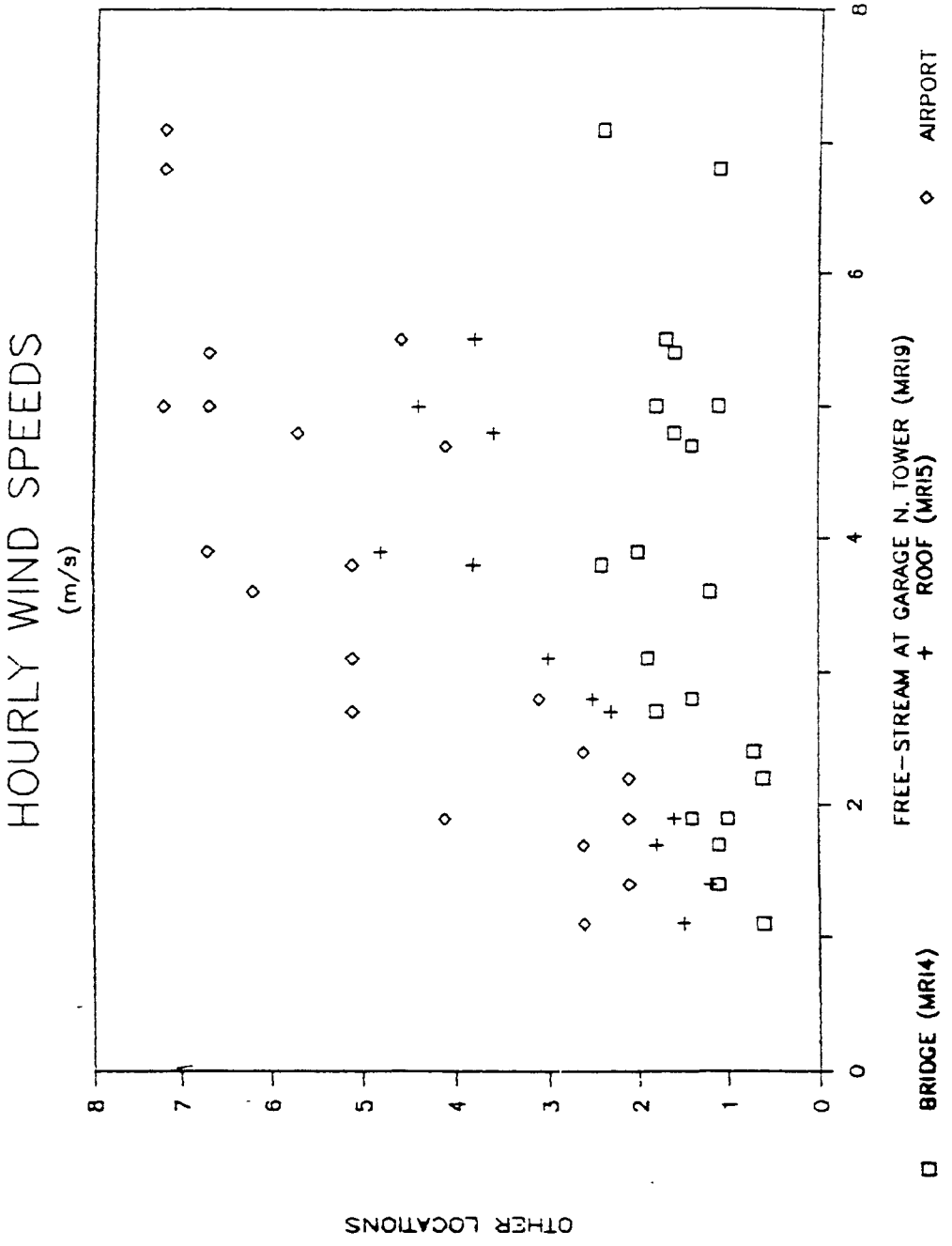

Figure 53. Comparison of hourly average wind speeds observed from the pedestrian bridge, the terminal roof, and by the airport (NOAA) with the reference wind speed.

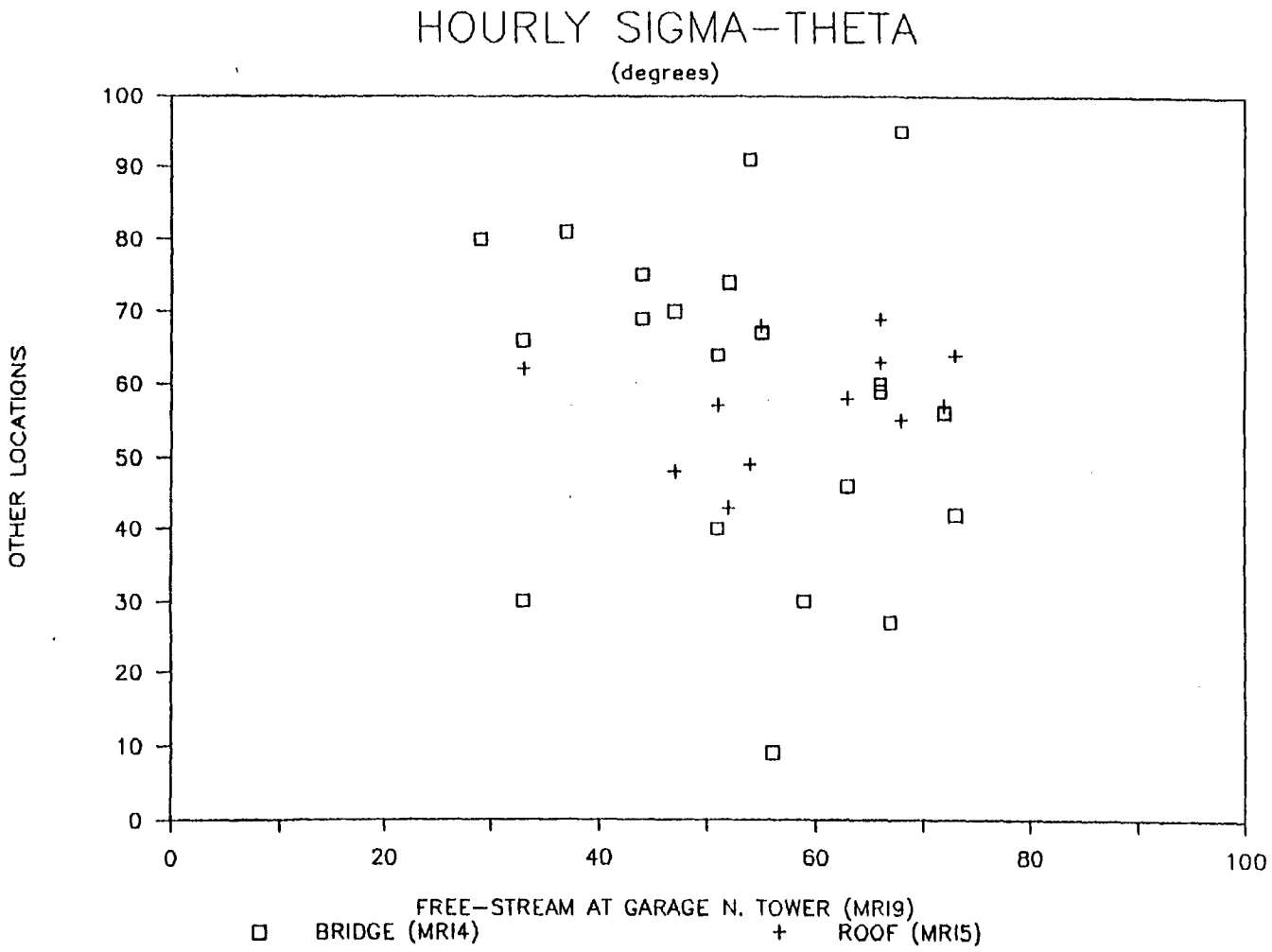

Figure 54. Comparison of hourly sigma theta observed from the pedestrian bridge and the terminal roof with the reference level sigma theta.

We now consider the 10-minute average U-V-W data taken at the bridge roof site near the middle of the deeper street canyon and, subsequently, at a height of 3 m (10 ft) above the lower level (deplane) roadway. Corresponding 10-minute average values of reference level (i.e., garage elevator rooftop) wind speed and direction were computed for intercomparison. The U-V-W coordinate system should also be clarified: + u corresponds to cross canyon flow from the garage toward the terminal, + v corresponds to canyon-parallel flow out of the NW and incidentally coincides with the direction of traffic flow, and + w corresponds to upward vertical flow. Corresponding reference level, free-stream, cross-canyon, u, and along-canyon, v, components are also computed to facilitate comparison with the CPB flow model assumptions of separable cross-and along-canyon components.

Figure 55 compares with U-V-W measured u component with that of the reference wind. All cases observed at street level have the same sign which means there is no counterflow vortex penetrating to this depth and that flow is primarily through the semi-open garage structure. However, on the walkway bridge, one observes several examples of this vortex-like counterflow, particularly for the negative reference U which corresponds to above-roof flow over the terminal building toward the garage.

Figure 56 indicates the U-V-W vertical component versus the reference level u component. The very small mean w values seen near street level confirms that previous observation of little, if any, vortex penetration into the deepest region of the street canyon whereas bridge level values suggest vortical flow for

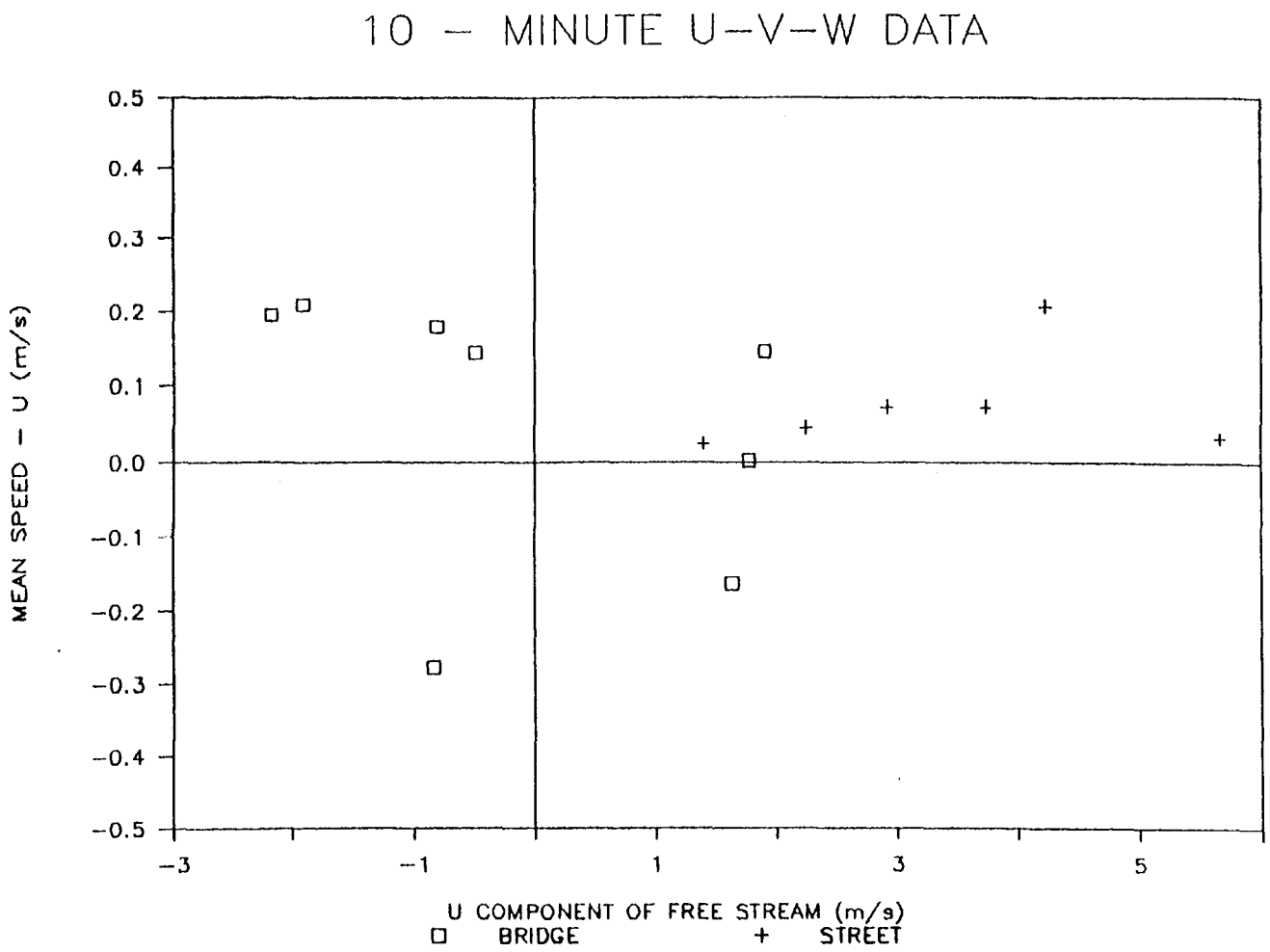

Figure 55. Ten-minute average cross-canyon wind velocities for U-V-W measurements from the pedestrian bridge and lower level roadway versus the same reference wind component.

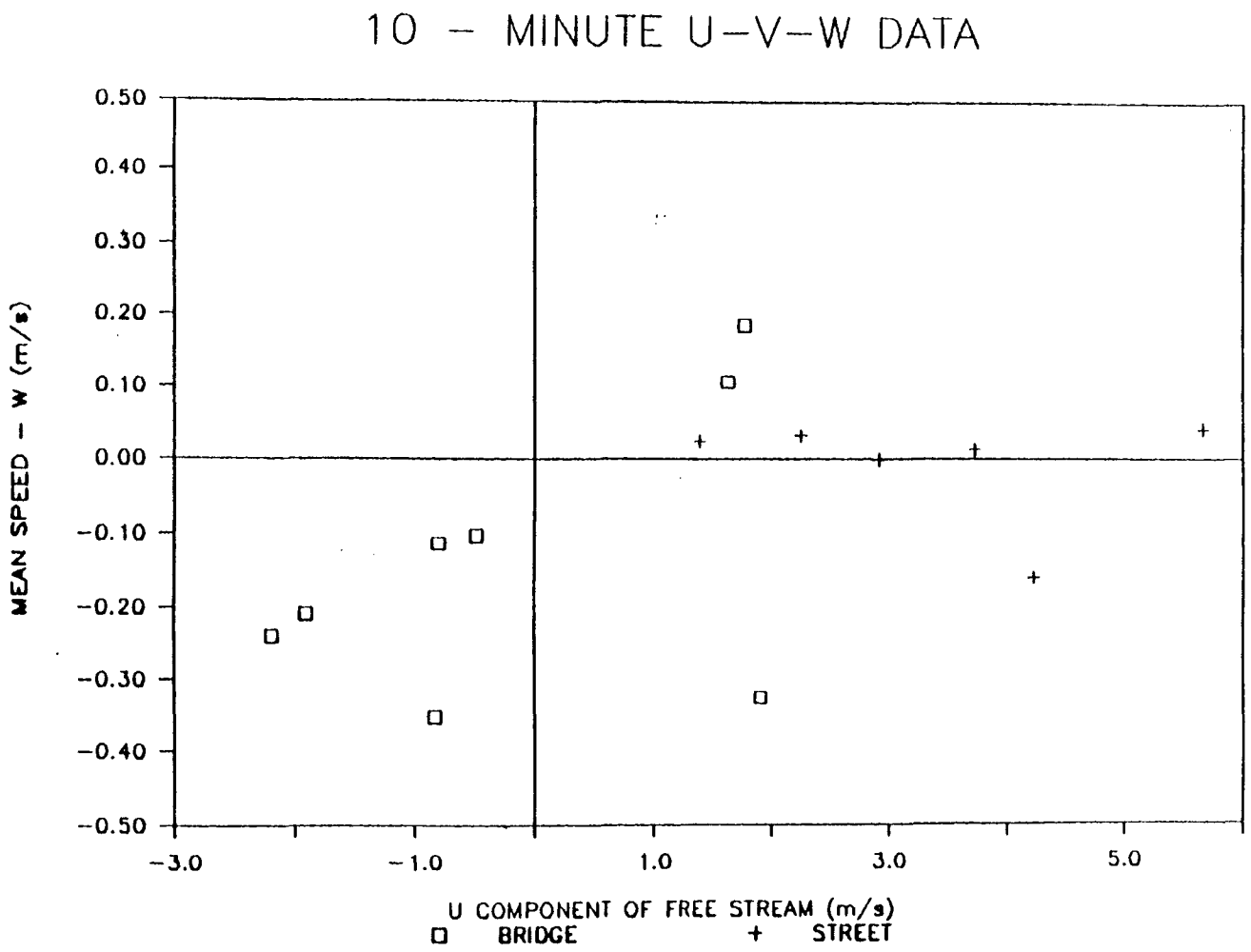

Figure 56. Ten-minute average vertical wind velocities for U-V-W measurements from the pedestrian and lower level roadway versus the cross-canyon component of the reference wind.

both positive and negative values of above roof, reference level u. Evaluation of the rotor case u and w velocities normalized by the reference velocity, u_o, above the garage gives values of $u/u_o \simeq 0.13$ and $w/u_o \simeq -0.17$. These values are not inconsistent with those expected from the Hotchkiss-Harlow flow model. In addition, one can compute the normalized rotor speed of $[u^2 + w^2]^{1/2}/u_o \simeq 0.21$, which is in excellent correspondence with the wind-tunnel-scale measured value of 0.21 for negative curvature but not with the value of 0.47 reported for positive curvature (i.e., reference $u < 0$ at SEATAC) conditions. Given the more complex canyon at SEATAC, even this partial agreement is encouraging.

Figure 57 shows the corresponding data for along-canyon flow. As expected, both above-canyon and within canyon axial flows have the same sign and thus are in the same direction. Mean v values observed near street level are rather low and insensitive to the reference wind v component, whereas higher, bridge values show larger scatter for a small range of reference component values.

Within-canyon turbulence levels are now considered. Figures 58 and 59 display σ_w versus σ_u for bridge and near-street level measurements. It appears that with or without vortical flow (i.e., at both levels), σ_w is highly correlated with, and about 20 percent larger than, σ_u. Analysis of the full-scale, Bonner Strasse study (Yamartino and Wiegand, 1986) also showed a close correspondence between σ_w and σ_u, and σ_w levels about 10 percent larger than σ_u.

Figure 60 compares the composite, transverse turbulence, $\sigma_T = [\sigma^2_u + \sigma^2_w]^{1/2}$, with the reference level wind speed. While there is some trend toward larger σ_T with increasing reference level

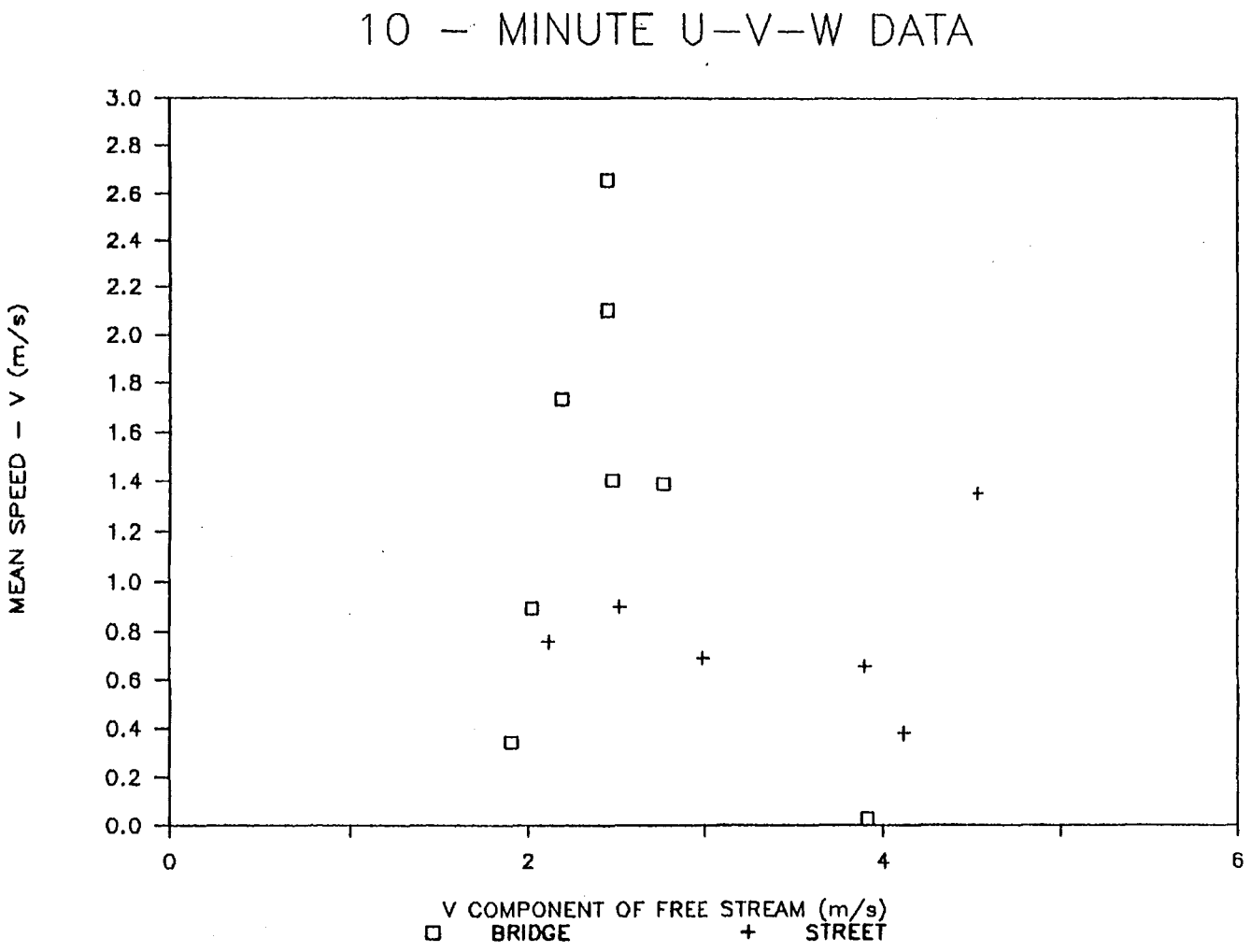

Figure 57. Ten-minute average along-canyon wind velocities for U-V-W measurements from the pedestrian bridge and lower level roadway versus the same reference wind component.

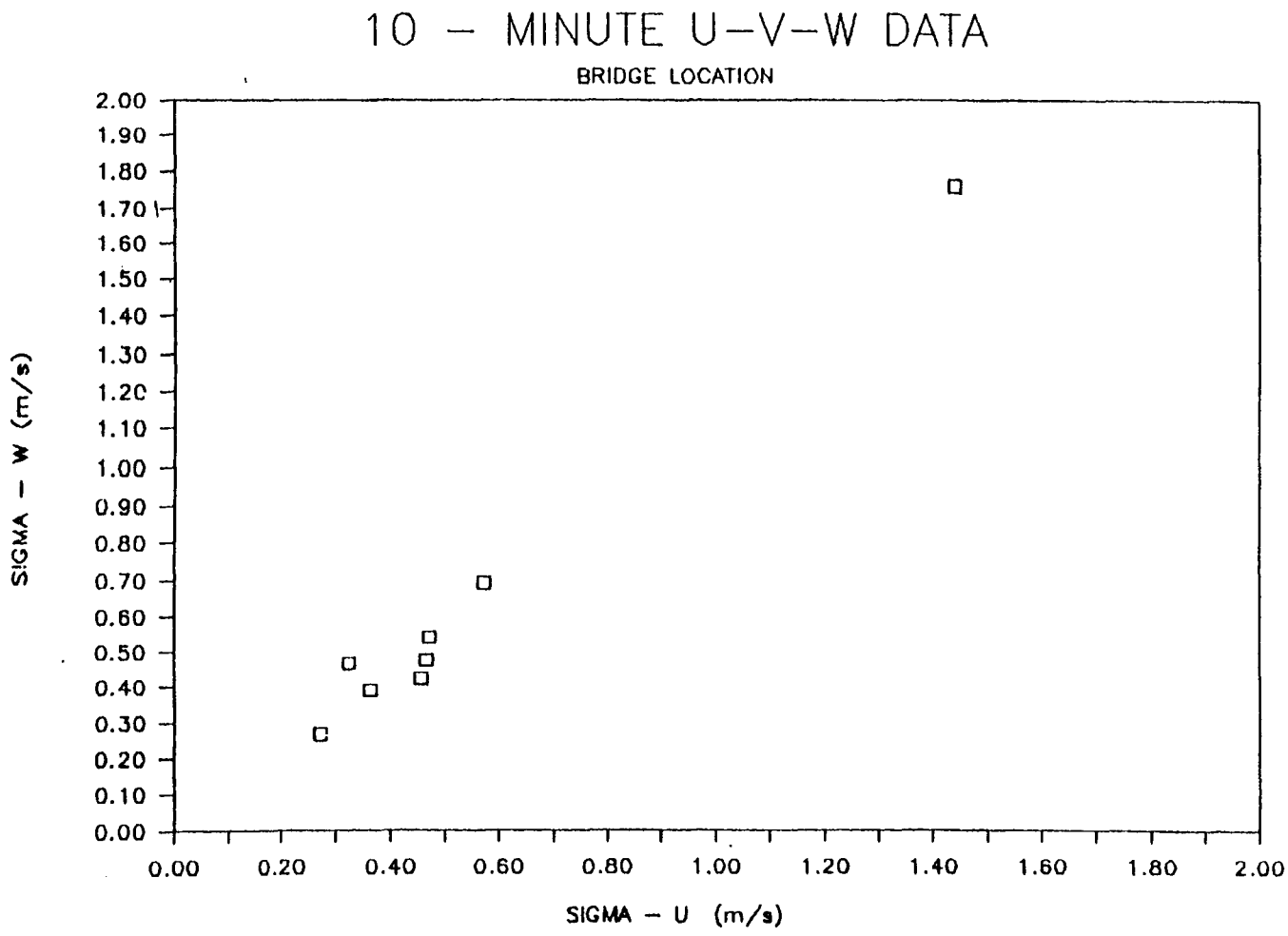

Figure 58. Ten-minute sigma-W versus sigma-U for U-V-W measurements from the pedestrian bridge.

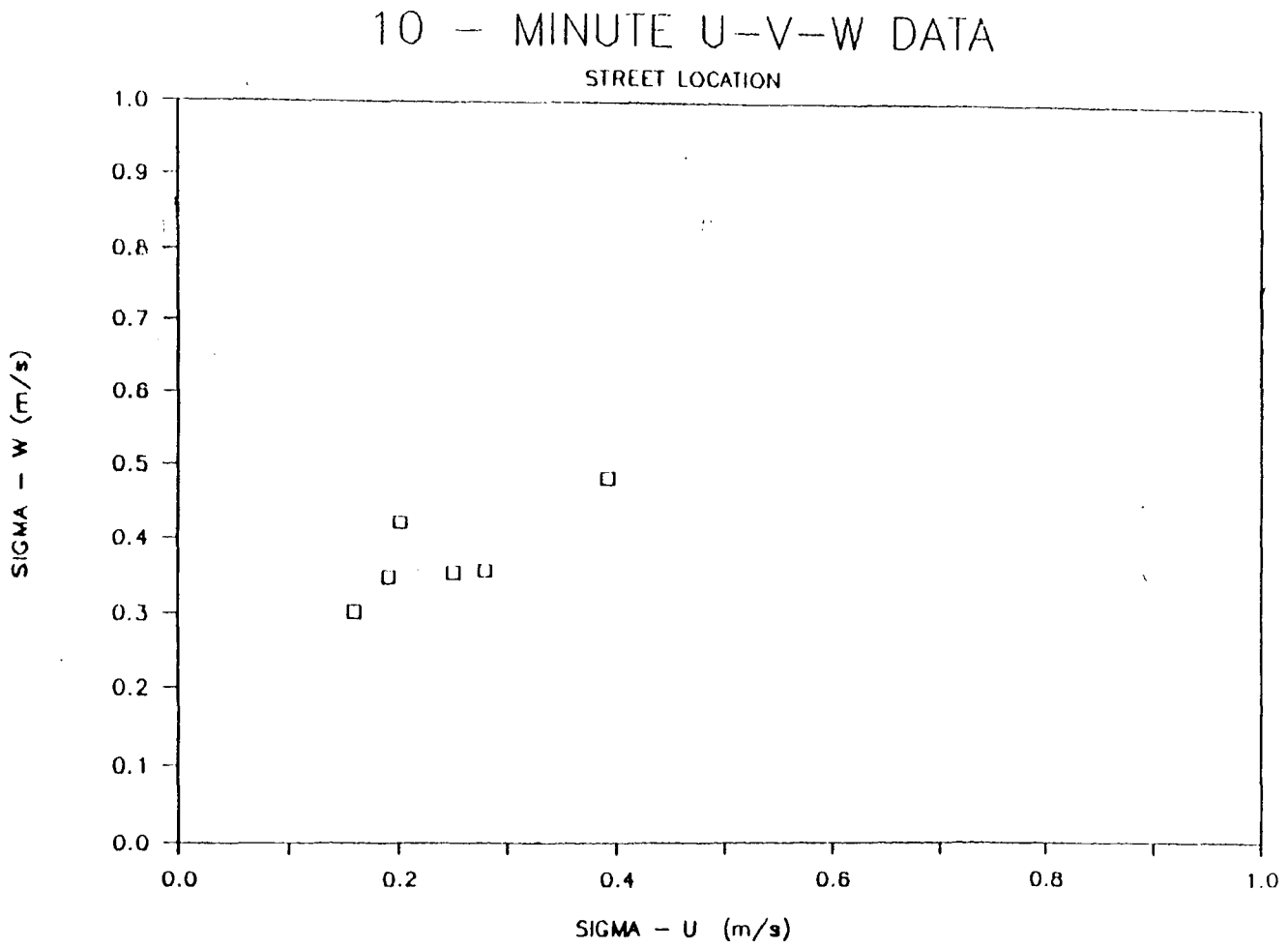

Figure 59. Ten-minute sigma-W versus sigma-U for U-V-W measurements from the lower level roadway.

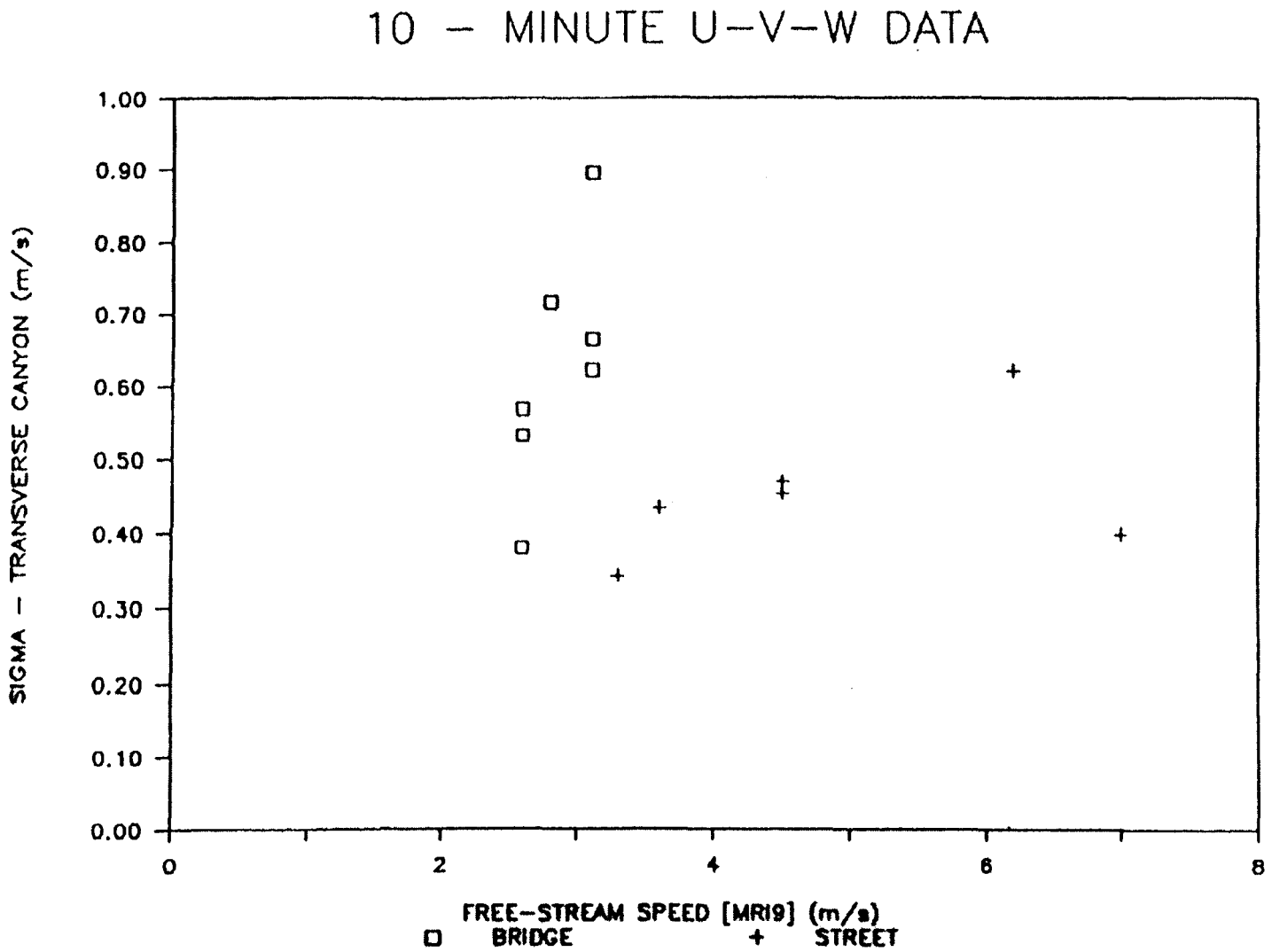

Figure 60. Ten-minute sigma-trasnverse ($\sigma_T = [\sigma^2_u + \sigma^2_w]^{1/2}$) for U-V-W measurements from the pedestrian bridge and lower level roadway versus the reference level wind speed.

wind speed, a stronger dependence is not necessarily expected as the large solar heating is expected, from the CPB-1 turbulence model, to contribute about 0.3 m/s (0.67 mi/h> to ^{o}T within-canyon values.

Canyon parallel turbulence levels, σ_v, versus reference level wind speed are displayed in figure 61. These turbulence values are nearly twice as large as the cross-canyon and vertical components which is also in agreement with the approximate 50 percent ^{o}v excess seen in Bonner Strasse. In addition the estimated ^{o}v = 0.4 m/s (0.89 mi/h> contributed by heat flux terms and computed from the CPB-1 turbulence model corresponds well with the minimal values seen in the canyon and with the near-street level values.

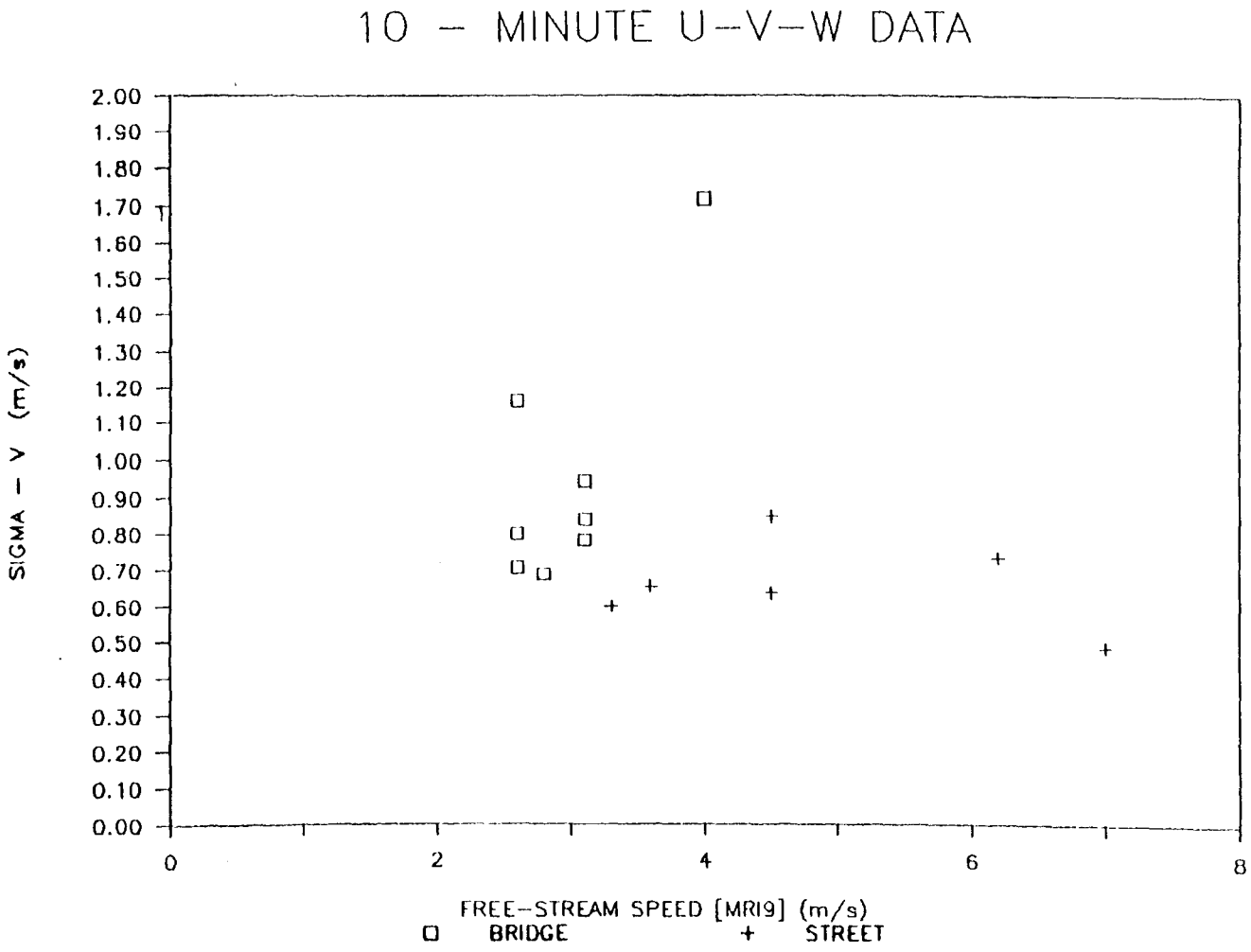

Figure 61. Ten-minute sigma-V for U-V-W measurements from the pedestrian bridge and lower level roadway versus the reference level wind speed.

Conclusions

Analyses of 1 day of wind and turbulence data collected at SEATAC suggest that:

- NOAA reported, airport wind directions correspond quite well with wind directions observed above the terminal area structures.

- NOAA reported, airport wind speeds correlate well with the above roof reference wind but are about 30-50 percent larger in magnitude.

- Flow within the canyon involves both flow through the garage at all levels and vortical flow generated by the building complex. The vortex flow shows up at the level of the pedestrian bridge roof but does not penetrate down to the lower level roadway.

- For the five, 10-minute average periods (i.e., about 60 percent of the cases) where vortical flow was measured on the bridge roof, the normalized flow velocities of $u/u_o \simeq 0.13$ and $w/u_o \simeq -0.17$ are not inconsistent with the range of values expected from the Hotchkiss-Harlow flow model.

- These normalized rotor speeds, $[u^2 + w^2]^{1/2} /u_o$, of 0.21 observed for both signs of above roof flow, u, correspond well with the wind-tunnel-scale measured value of 0.21 for negative curvature flows (i.e., reference $u > 0$ in this case) but not to the value of 0.47 reported for positive curvature flow (i.e., reference $u < 0$ at SEATAC).

- Turbulence values within the canyon are not inconsistent with those predicted by the empirical turbulence model in CPB-1, particularly when solar heat flux contributions are taken into account.

Despite the short duration of this study, a valuable full-scale, airport reference point has been obtained. It is hoped that further analyses involving concentrations and vehicle emissions can provide further insights into this interesting problem.

APPENDIX H

DEVELOPMENT AND EVALUATION OF SIMPLE MODELS FOR THE FLOW, TURBULENCE AND POLLUTANT CONCENTRATION FIELDS WITHIN AN URBAN STREET CANYON

Reprinted from *Atmospheric Environment* with permission of Pergamon Journals, Ltd.

Atmospheric Environment Vol. 20, No. 11, pp. 2137–2156, 1986.
Printed in Great Britain

0004-6981/86 $3.00 + 0.00
Pergamon Journals Ltd.

DEVELOPMENT AND EVALUATION OF SIMPLE MODELS FOR THE FLOW, TURBULENCE AND POLLUTANT CONCENTRATION FIELDS WITHIN AN URBAN STREET CANYON

ROBERT J. YAMARTINO
Sigma Research Corporation, 394 Lowell Street, Suite 11, Lexington, MA 02173, U.S.A.

and

GÖTZ WIEGAND
Geomet G.m.b.H., Bundesallee 129, 1000 West Berlin 41, Germany

(*First received* 28 *October* 1985 *and in final form* 28 *March* 1986)

Abstract—Simple models for the flow and turbulence fields within an urban street canyon are discussed and compared with data from an extensive monitoring program. These models for flow and turbulence then serve as input to a comprehensive urban canyon pollutant dispersion model, named the Canyon Plume-Box Model (CPBM), that is described and evaluated using traffic and pollutant data from the monitoring program. The CPBM model is found to perform significantly better than predecessor models and contains no canyon specific tuning parameters that would inhibit applying it to a variety of street canyon geometries.

Key word index: Street canyon, urban dispersion, air pollution.

1. INTRODUCTION

In 1981 the Federal Republic of Germany's (F.R.G.) Environmental Protection Agency (Umweltbundesamt) initiated a systematic, multi-disciplinary effort to develop a comprehensive tool for understanding and managing the impacts of urban automotive emissions. The project has drawn from subject areas including:

(i) traffic flow modeling,
(ii) vehicle emissions modeling,
(iii) wind tunnel simulation and numerical modeling of urban canyon flow and turbulence,
(iv) urban canyon flow, turbulence, and pollution monitoring programs, and
(v) air quality dispersion modeling (including photochemistry),

in order to improve understanding and predictability of the automobile's impact on air quality, both within the urban canyon as well as on larger scales, as a consequence of emitting pollutants within the confines of urban street canyons.

This paper will focus on the development and testing of simple models for the flow, turbulence and non-reactive pollutant concentration fields within the street canyon. The testing of these models relies heavily on data obtained by TÜV Rheinland (Leisen and Sobottka, 1980; Sobottka and Leisen, 1980a, b; Waldeyer *et al.*, 1981) during its street canyon monitoring in Bonner Strasse, Cologne, and on wind tunnel modeling studies of an idealized, two-dimensional model of Bonner Strasse and other idealized street canyons conducted by Builtjes (1983, 1984) in TNO's PIA atmospheric boundary layer wind tunnel (Builtjes and Vermeulen, 1980). Related, and yet more complex, modeling efforts involving a numerical flow model coupled to a Monte-Carlo Lagrangian trajectory model are described in Geomet (1985).

Section 2 of this paper begins with a brief description of the Bonner Strasse geometry and the experimental data base to be used in the evaluation of the models. Section 3 traces the development and evaluation of the simplified flow and turbulence models and their relationship to existing models. Section 4 describes the need for and development of a simple urban canyon pollutant dispersion model, named the Canyon Plume-Box Model (CPBM), that utilizes the flow and turbulence models and avoids parameters that would prevent applying the model to other street canyon geometries. The CPBM's performance for NO_x, NO_2 and CO is then considered in section 5 under the full range of meteorological conditions and is compared for CO with the SRI street canyon APRAC submodel (STREET) of Johnson *et al.* (1973) and the MAPS model of Sobottka and Leisen (1980a, b) under the full range of meteorological conditions, and also with STREET under the more restrictive meteorological conditions for which the STREET model was specifically designed.

The CPBM reduced the predicted/observed variance obtained with STREET by 40% for the full data sample. CPBM's superiority was most pronounced for

those meteorological conditions, occurring about one-third of the time, for which STREET was not specifically designed; nevertheless, a 20% reduction in variance was obtained for the well defined rotor conditions for which STREET was designed. Section 6 summarizes the results of the study and identifies issues not fully resolved. Areas for continued research and model development are also indicated.

2. BONNER STRASSE AND THE MEASUREMENT DATA BASES

A cross section of Bonner Strasse, Cologne, where the TÜV Rheinland study was performed is shown in Fig. 1. This street, of the type L2 categorized by Glück (1972), is characterized by a street width to building height ratio, B/H, of order unity, relatively uniform building heights (i.e. ± 2 m variation), nearly complete absence of interbuilding spaces, and a relatively large distance between intersections (i.e. $L \gg B, H$). Such a geometry is quite common for busy, four-lane streets in West German cities and, at the same time, is conducive to two-dimensional modeling with the third dimension (i.e. along the canyon) factorized out of the problem but added in afterwards as a correction term. Such a modeling assumption must, of course, be demonstrated.

The idea that this urban canyon (i.e. Bonner Strasse) situation might be best understood in terms of factorized cross-canyon and along-canyon pictures was, in fact, suggested by TNO videotapes of flow visualization experiments with their 250 to 1 model of Bonner Strasse, including its peaked building roofs. The videotape and associated triple-wire measurement data bases indicated that:

(i) a vortex is created in the street canyon for mean flows ranging from $\theta = 90°$ (i.e. perpendicular to the canyon) to 10–20°, where $\theta = 0$ defines flow parallel to the canyon axis;

(ii) the along-canyon flow component, v, exhibited a simple $v = U \cos\theta$ behavior, at least to first order;

(iii) the vortex was rarely static in time; instead, there was a cyclical pattern of rotor formation, slow acceleration, and sudden collapse with an associated brief, reverse sloshing of the smoke tracer in the bottom half of the canyon (i.e. the tracer went in the direction of the primary, above-canyon flow rather than in the usual, primary counterflow direction dictated by the secondary canyon vortex flow; and

(iv) the more sporadic existence or non-existence of vortex flows for $\theta < 20°$ 'appeared' to follow from (a)

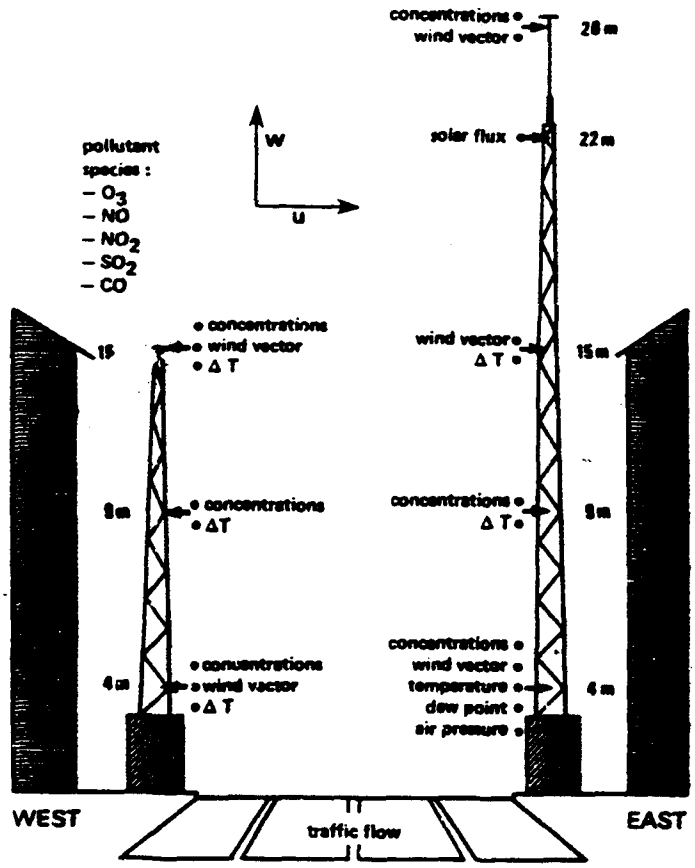

Fig. 1. View of the TÜV Rheinland street canyon monitoring experiment in Bonner Strasse, Cologne showing experimental configuration.

insufficient cross-canyon flow, $U \sin\theta$, to drive the vortex and/or (b) the end effects or finite length canyon effects, with $L/B \simeq 20$, began to dominate over the vortex, rather than from some distinctly new and different physical mechanism.

A portion of the year-long, full-scale, Bonner Strasse data base, kindly sent to us for study by P. Leisen of TÜV Rheinland, consisted of two, 11-day periods (28 March–4 April 1980 and 3–13 May 1981) of very high data capture. Allowing for calibrations and system down-time, this translates into just over 1000, 30-min duration events where the means and standard deviations of each quantity depicted in Fig. 1 were recorded. Of principal interest in this paper are the $u\ v\ w$ measurements of flow and turbulence (i.e. in the coordinate system where u = cross canyon, v = along canyon, and w = vertical) at 4 m and 15 m and 26.5 m (on East tower), the total radiation (0.3–3.0 μ) measured at 22 m, concentrations at 4 m and 9 m (on both towers), 15 m (on West tower), and traffic counts in each of the four lanes. While this data base undoubtedly represents the most extensive urban canyon study to date, potential limitations arise simply from the multiplexing and data acquisition methods, as documented in Hauschulz *et al.* (1980). Specifically, measurements are not simple half-hour measures of mean and standard deviation. Instead, there was an underlying 6-min cycle during which each instrument was interrogated for 1 min at an instrument dependent sampling frequency (e.g. 2 s for $u\ v\ w$ sensors and 5 s for CO values). Thus, each instrument is monitored for five, 1-min periods within the half-hour. One can then easily imagine short-term episodes (i.e. of a few minutes duration) of turbulence or pollution that are seen by some but not all instruments, thus creating some error in interpretation. Other limitations include:

the NEZ II* $u\ v\ w$ distance constant of 2.0 m, combined with a 1-s pulse counting time (i.e. averaging time) and a 2-s sampling interval, suggests that the high frequency turbulence generated by moving automobiles and local obstacles is not sensed;

traffic speed and vehicle mix were only spot measured, thus making determination of emission factors and rates more uncertain; and

the 26.5 m wind sensor was not high enough above the rooftop peaks at 18.4 m to be completely free of local, rooftop-induced flow. Whether the 26.5 m (or 1.4 H) sensor for pollutants truly represents background levels may thus also be questioned in light of the '2.5 H rule' (see Hosker, 1983) and the observed flow deflection mentioned above and discussed in the next section.

3. FLOW AND TURBULENCE FIELDS WITHIN THE URBAN CANYON

3.1. *Observed flow field behavior*

The existence of the secondary, vortex flow within the urban canyon was measured by Albrecht (1933); however, Georgii *et al.* (1967) conducted the first major field experiment involving both flow field and pollution measurements. The more recent and more extensive TÜV Rheinland field studies in Venloer and Bonner Strasse have already undergone (Sobottka and Leisen, 1980a, b; Leisen and Sobottka, 1980) substantial analysis and comparison with wind tunnel flow and tracer studies. In this section the previously mentioned 22-day subset of the Bonner Strasse data will be examined to:

(i) justify decomposition of the flow into canyon perpendicular and parallel components,

(ii) establish the relationship between the flows within the canyon and above the rooftops,

(iii) relate the turbulence levels measured within the canyon to above canyon winds and other readily available meteorological variables, and

(iv) assist in providing reasonable flow and turbulence fields for input to an urban canyon dispersion model.

Analysis and modeling of the flow fields within the canyon generally assumes that the incident or reference flow field is well measured and undisturbed by the canyon. A scatter plot analysis (Geomet, 1985) of elevation angle vs azimuthal angle for the reference sensor at $z = 26.5$ m above street level clearly indicated that this wind sensor is sensitive to the presence of the canyon. However, the rather small values of the elevation angles, as well as subsequent analyses where little difference was found between use of u or $(u^2 + w^2)^{1/2}$ at this reference height as the independent variable, suggest that the interference is not serious. A subsequent wind tunnel study (Builtjes, 1984) showed that a reference height of 40–50 m is required to eliminate any effect of the canyon on the reference wind sensor and that the presence of the perpendicularly oriented canyon reduces speeds at 26.5 m, about 10% below simple logarithmic profile estimates (i.e. with $z_o = 0.75$ m and a zero plane displacement of 4.25 m).

Comparison (Geomet, 1985) of the wind components measured in the canyon with above-roof winds has indicated that:

a vortex appears to exist at all finite values of cross canyon flow (as measured at the reference height);

the transverse vortex speed $(u^2 + w^2)^{1/2}$ in the canyon is proportional to the above-roof transverse component and independent of the above-roof, longitudinal (or along-canyon) component v;

the along-canyon wind component, v, in the canyon is directly proportional to the above-roof v component, though the constant of proportionality is a function of approach flow azimuth.

3.2. *Canyon-transverse flow model*

The issue of whether the observed speeds in the canyon correspond to any reasonable theoretical model has been addressed with a complex two-

* Manufactured by Alcyon Equipment of Switzerland.

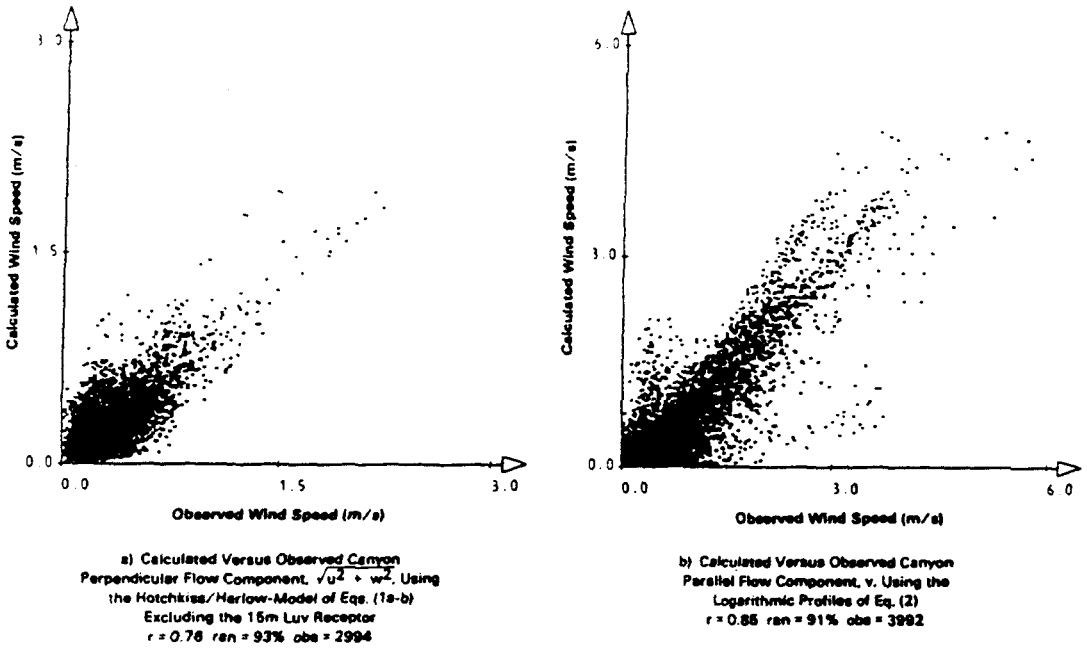

Fig. 2. Flow model results for Bonner Strasse.

dimensional flow model (Geomet, 1985) based on the approach of Pankrath (1975), as well as the simple model of Hotchkiss and Harlow (1973). The flow model of Hotchkiss and Harlow (1973), subsequently referred to as H–H, is based on the assumptions of incompressible flow, absence of sources or sinks of vorticity within the canyon, and appropriate boundary conditions for the simple 2-d rectangular notch of depth H and width B. Their solution for the mean velocity components within the canyon is

$$u = u_o(1-\beta)^{-1}[\gamma(1+ky) - \beta(1-ky)/\gamma]\sin(kx) \quad (1a)$$

and

$$w = -u_o ky(1-\beta)^{-1}[\gamma - \beta/\gamma]\cos(kx) \quad (1b)$$

where $k = \pi/B$, $\beta = \exp(-2kH)$,

$$\gamma = \exp(ky),\ y = z - H,$$

and u_o is the wind speed above the canyon (and at the point $x = B/2$, $z = H$).

Despite the fact that the H–H model does not explicitly deal with non-flat roofs, unequal lee/luv* canyon heights, or other 'real world' complications, numerical intercomparisons between it and the more complex numerical flow model indicated that:

(i) except for some improvements in explaining flow behavior near the stagnation streamline, the numerical model was not superior to the H–H model for simulating Bonner Strasse mean flow data, and

(ii) neither model was completely adequate or demonstrably superior in describing H/B ratio trends seen in the wind tunnel.

Thus, the H–H model was selected as the primary module for defining the canyon transverse flow components. Figure 2(a) shows a comparison of H–H predicted vs observed rotor speeds for all meteorological conditions and three (i.e. the 15-m luv sensor is excluded due to its proximity to the stagnation streamline) of the Bonner Strasse wind sensors. The results shown were obtained using the actual canyon width ($B = 20$ m), actual rooftop peak height ($H = 18.4$ m), and a u_o value equal to the 26.5 m reference height value of transverse speed, $s_r = (u_r^2 + w_r^2)^{1/2}$, as input to the H–H model. Somewhat lower mean square residuals were obtained via an optimization that allowed H and u_o/s_r to drift from these values but the marginal improvement did not justify the attendant loss of confidence associated with using 'non-physical' parameter values. Nevertheless, the fact that $u_o/s_r = 1.0$ gives reasonable results must be regarded as fortuitous, as any reasonable above-roof profile would suggest a value less than unity, so that some degree of canyon geometry specific 'tuning' of u_o/s_r cannot be precluded at this point.

3.3. *Along-canyon flow model*

Having found a model for the transverse flow (i.e. u and w components) that is independent of the along-canyon v component, we attempted a quantitative description of the v component in terms of a simple logarithmic profile,

$$v(z) = v_r \log[(z+z_o)/z_o]/\log[(z_r+z_o)/z_o], \quad (2)$$

* The German nautical word luv is chosen for simplicity to designate the downwind, or windward facing side of the canyon.

where v_r is the value at reference height z_r and z_o is surface roughness. It was soon discovered that reasonable results require a surface roughness that is a function of the approach flow direction θ. Such a $z_o(\theta)$ functional dependence represents a partial, but not surprising, breakdown of the transverse/parallel wind component factorization hypothesis that could be attributed to a variety of approach flow differences including fetch. The predicted vs observed results presented in Fig. 2(b) offer a reasonable, though clearly not perfect, description of the phenomenon and were obtained by dividing the wind compass into eight, 45° sectors and choosing an optimal z_o value for each sector. The actual z_o values effectively clustered above three values:

(i) $z_o = 0.4$ m corresponding to the mostly non-vortex flows along the street canyon and in a range typical for boundary layer flows in the urban environment.

(ii) $z_o \simeq 0$ (0.04 m actually used) corresponding to a nearly constant value of v with height and wind directions for which vortex flow predominates. The rapidly rotating vortex apparently forgets which way is up $(+z)$ since vortex top and bottom are quickly interchanged. If any meaning is to be attached to the value of 0.04 m it may be related to roughness elements (e.g. building facades, balconies, vehicles) in the canyon itself.

(iii) $z_o \simeq \infty$ (400 m actually used) corresponding to the linear profile, $v(z) = v_r(z/z_r)$, that results when unphysically large z_o are used in Equation (2). The 90° quadrant favoring this linear profile contains a building, significantly higher than its neighbors, that is apparently disturbing the flow.

The three resulting profiles are not as radically different as one might expect from the large range in z_o. In addition, the fact that the turbulence model is formulated in terms of the reference height value v_r and the dispersion model in terms of $v(z)$ averaged from $z = 0$ to $z = H$, further mitigates the significance of this 'factorization breaking' $z_o(\theta)$ dependence.

3.4. *Canyon turbulence model*

The more complex issue of expected turbulence levels within the urban canyon is one for which simple theoretical models are lacking. Thus, we attempt to develop a simple empirical relationship between each of the measured turbulence components, σ_i (where $i = u, v$ or w) and variables known to influence ambient turbulence. Suppressing i subscripts on all the model parameters, the model developed after numerous optimization attempts is

$$\sigma_i = f(x,z)\,[A_m(s_r^2 + \alpha^2 v_r^2)^{1/2} + (A_c + A_h h)] \quad (3a)$$

where
$$h = S + N_a e_a / B \quad (3b)$$

and
$$s_r^2 = u_r^2 + w_r^2 .$$

A_m and α are dimensionless parameters characterizing the mechanical turbulence induced by canyon transverse and parallel, vector mean winds s_r and v_r, respectively, measured at reference height z_r. A_c is a constant with units of m s^{-1} designed to characterize the turbulence under night-time, zero vector mean wind and zero traffic conditions, whereas A_h, with units such that its product with the total heat flux h (in kW m^{-2}) gives m s^{-1}, is needed to describe the increased turbulence driven by the total solar radiation S (in kW m^{-2} as measured in the Bonner Strasse experiment or estimated from solar angle and cloud cover) and the equivalent vehicle generated heat flux, computed as the product of the vehicle flow rate (s^{-1}), N_a, times the heat loss per vehicle per m of travel, e_a, divided by the effective transverse dimension this heat is dissipated over; assumed to be the full canyon width, B, in this problem. This addition of automotive and solar induced heat fluxes was also used successfully by Benson (1984) to compute Pasquill stability class using Smith's (1972) monogram. The function $f(x, z)$ is designed to describe the spatial variability of the turbulence field σ_i over the canyon and is known from the preliminary TNO wind tunnel measurements of total turbulence to vary slowly over the canyon; peaking near the luv side roofline, dropping to $\sim 70\%$ of this value at the equivalent of 4 m full scale, and then dropping further to a rather uniform level of $\sim 50\%$ of peak intensity in the lee side of the canyon.

Values of the parameters which gave best agreement between the logarithms of observed and modeled turbulence levels are presented in Table 1 and resulting theory vs observed scatterplots are presented in Figs 3(a)–(c) for σ_u, σ_v and σ_w, respectively. With correlation coefficients $r \sim 0.88$ and 0.91 for σ_u and σ_w, respectively, vs $r = 0.77$ for σ_v, Equation (3a) is clearly more adequate for the transverse components of turbulence. If one further theorizes that the turbulence field should rotate with the mean vortex flow field, then a superior theory could be built using flow-parallel and flow-transverse components. As the instantaneous velocity components u', w' were unavailable to compute the turbulent σs in this rotated coordinate frame, it was decided to test Equation (3a) on the rotationally-invariant (i.e. about the y-axis) quantity $\sigma_T = (\sigma_u^2 + \sigma_w^2)^{1/2}$. The residuals for this fit, presented in Table 1, are smaller than those obtained for σ_u or σ_w separately and thus lend some credence to this rotating coordinate system hypothesis. The computation of turbulence parameters in both the fixed and flow defined coordinate systems should definitely be considered for future experiments. Equation (3a) predicted vs measured values of σ_T are presented in Fig. 4.

The results given in Table 1 also suggest some additional conclusions including:

(i) lee side turbulence, relative to the $z = 15$ m luv side reference level of $f = 1.0$, is greater than that observed in the TNO wind tunnel and is found to increase with height in the canyon,

(ii) σ_v is extremely uniform throughout the canyon, and

(iii) purely mechanical turbulence levels (i.e. A_m) are in the range of those observed in the neutral, ambient

Table 1. Optimal parameters and fitting results for the turbulence model given by Equation (3) for different values of the vehicle heat output, e_s

Turbulence component:	σ_w			σ_v			σ_w			σ_T		
e_s(kJ m^{-1})	1.813	0.0*	7.5*	1.735	0.0*	7.5*	0.501	0.0*	7.5*	0.648	0.0*	7.5*
A_m	0.125	0.127	0.124	0.185	0.188	0.180	0.135	0.136	0.133	0.131	0.131	0.129
α	0.643	0.636	0.641	0.766	0.770	0.784	0.796	0.793	0.805	0.715	0.714	0.721
A_c(m s^{-1})	0.168	0.171	0.161	0.230	0.234	0.212	0.174	0.176	0.163	0.173	0.174	0.161
A_h(m^3 kW^{-1} s^{-1})	0.338	0.360	0.287	0.847	0.880	0.707	0.438	0.444	0.345	0.395	0.399	0.320
f(15 m luv)†		1.0			1.0			1.0			1.0	
f(4 m luv)	0.649	0.648	0.647	0.881	0.880	0.880	0.709	0.708	0.709	0.678	0.677	0.690
f(15 m lee)	0.779	0.774	0.773	0.877	0.881	0.879	0.810	0.810	0.810	0.792	0.792	0.806
f(4 m lee)	0.620	0.619	0.618	0.864	0.866	0.865	0.576	0.576	0.576	0.597	0.597	0.605
Correlation coefficient, r	0.881	0.880	0.879	0.772	0.772	0.769	0.905	0.905	0.901	0.910	0.910	0.908
Average percent deviation	16.2	16.2	16.2	24.6	24.6	24.8	14.9	14.9	15.3	13.9	13.9	14.3
r.m.s. percent deviation	21.0	21.0	21.1	32.4	32.4	32.6	19.2	19.2	19.6	17.9	17.9	18.3

* The parameter e_s is fixed at 0.0 or 7.5 kJ m^{-1} as discussed in the text. The number of half-hour events is 998 for each of the four components.
† f (15 m luv) is defined to be 1.0.

atmosphere (Pasquill, 1974), suggesting that a large portion of the turbulence in the canyon could result from the advection of 'frozen', above-roof turbulence into the canyon.

Equation (3a) could be criticized since the way it additively combines mechanically and thermally generated turbulence components ignores convective scaling considerations; however, formulations assuming quadratic or cubic additivity of u_* and w_* (i.e. friction and convective velocities) terms did not work as well. A comparison of the beta coefficients† shows that the significance of the mechanical turbulence term dominates the solar flux term by a factor of three and the automotive heat flux term by a factor of seven; thus, the present turbulence data cannot be expected to discriminate between slightly different reformulations of Equation (3a). In fact, a version of Equation (3a) that ignored the heat flux terms entirely caused the correlation coefficient for the σ_w model to drop only 0.05 (from 0.88 to 0.83); hence, the heat flux terms can be viewed as significant, though not critical, corrections to the turbulence model.

Perhaps the least statistically significant parameter in the model is the e_s value (in kJ m^{-1}) because;

(i) the traffic rate, N_s, is nearly in phase with the solar flux S, creating a co-linear parameter situation difficult to resolve, and

(ii) the maximum automotive heat flux is only about 10% of the peak solar flux of ~ 0.6 kW m^{-2}.

As a result, the e_s parameter was 'manually fixed' at values 0.0 and 7.5 kJ m^{-1} and the optimizations rerun. If the e_s value of 7.5 is divided by ~ 3, to compensate‡ for the fact that total solar radiation is about three times the daytime upward sensible heat flux, and corrected upward by (25 mpg/20 mpg) to reflect the European/American fuel use ratio, one obtains 3.1 kJ m^{-1}. This value lies about midway between the values of 3.46 kJ m^{-1} (i.e. 1.33×10^6 cal mile^{-1}), computed by Dabberdt *et al.* (1981) on the basis of time extrapolated U.S. Dept. of Transportation fuel consumption curves (Cope, 1973) and an 85% conversion efficiency of thermal energy to sensible heat, and 2.46 kJ m^{-1} (i.e. 6.82 mW h cm^{-1}), computed by Benson (1984) assuming a fleet average consumption of 20 mpg and a 60% conversion efficiency. Both the results obtained with e_s fixed at 0.0 and 7.5 are presented in Table 1. As can be seen from the small variations in r and error measures, turbulence levels are only marginally sensitive to the inclusion of e_s in Equation (3b), and the optimal e_s values shown are always well below the limiting case of interest. It is quite possible that much of the automotive heat

† Beta coefficients are defined as $\beta_i = A_i\,\sigma(x_i)/\sigma(y)$ for a multi-linear regression model $y = \Sigma_i A_i x_i$. The standard deviations of the dependent and ith independent variables are denoted $\sigma(y)$ and $\sigma(x_i)$, respectively.

‡ This would cause $A_h \cdot h$ to become $(3A_h)\,(h_s + N_s\,(e_s/3)/B)$ where $h_s \simeq S/3$ is the upward sensible heat flux.

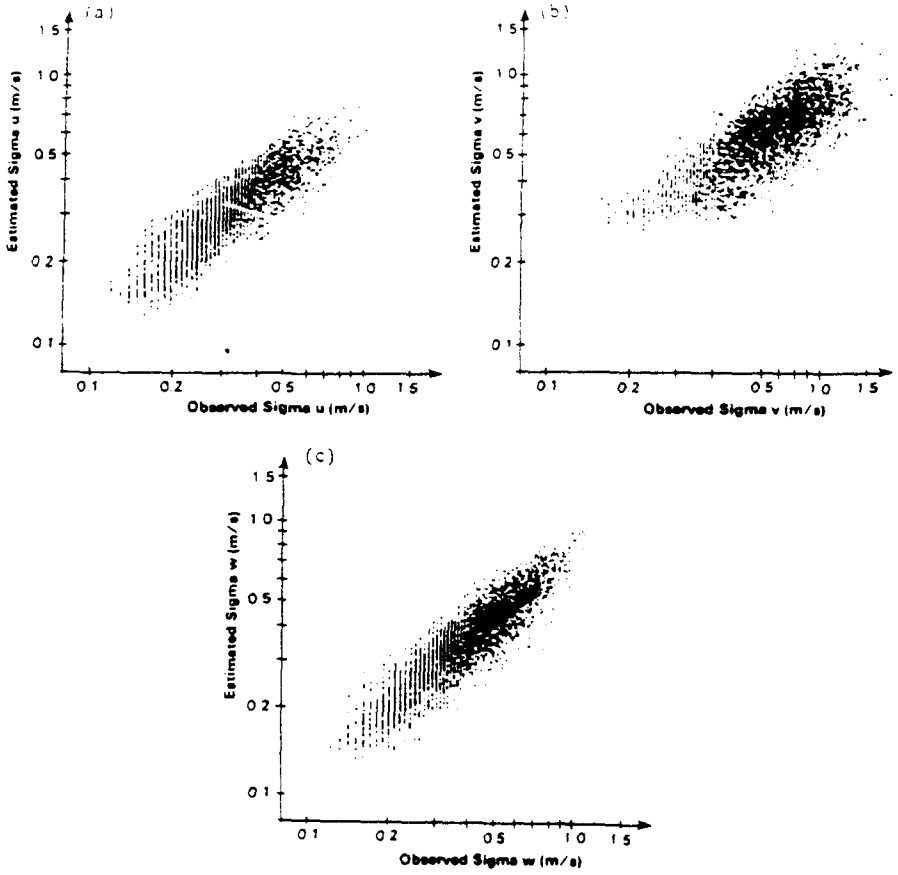

Fig. 3. Predicted turbulent velocity standard deviations ($m\,s^{-1}$) vs measured levels at the four anemometers in the canyon.

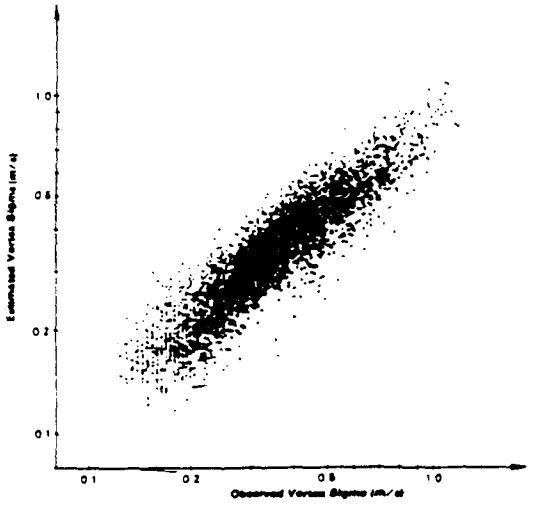

Fig. 4. Predicted transverse turbulent velocity standard deviations, $\sigma_T (m\,s^{-1})$, vs measured levels at the four anemometers in the canyon. $\sigma_T = (\sigma_v^2 + \sigma_w^2)^{1/2}$.

emissions are in the infrared and are not converted to turbulence within the canyon.

It should also be noted that no effect related to vehicle induced mechanical turbulence could be detected at any of the u, v, w anemometers; however, it should be pointed out that this component could be easily lost since

(a) vehicle velocities and thus vehicle induced turbulence levels are probably considerably smaller in the city than under the high speed conditions of the GM Sulfate Experiment (Chock, 1980),

(b) vehicle speeds were not routinely measured, thus eliminating this potentially useful regression variable and

(c) u v w response and sampling methods would have most likely missed this high-frequency turbulence component (Eskridge and Rao, 1983).

Modeled vehicle speeds did, however, influence concentrations in a way that will be subsequently modeled as a component of the initial pollutant mixing in the vehicle wake. Finally, it should be pointed out that potentially useful variables such as temperature differences within the canyon were not considered as it was desired to base the turbulence model on variables either routinely measured or easily estimable from routine data (e.g. solar flux is easily computed knowing solar angle and cloud cover).

In order to generalize Equation (3a) to a range of B/H values, TNO triple-wire measurements of turbulence were examined. While there was some dis-

crepancy between measured turbulent intensities within the recirculation zone for the full scale and wind tunnel studies, the TNO data suggest that for B/H in the range of 0.5–2, a multiplicative factor for the canyon transverse turbulent sigmas of the form

$$T_M = 0.12\,(B/H) + 0.8696, \tag{3c}$$

designed to yield $T_M = 1.0$ for the Bonner Strasse B/H of 1.087, is appropriate for renormalizing the wind tunnel measurements for $z \leq H$ and is assumed appropriate for the full-scale estimates. Turbulence observed in the one-sided canyon (i.e. $B/H \to \infty$) was not significantly greater than that measured at $B/H = 2.0$; thus, for lack of additional data, the B/H value used in Equation (3c) is constrained to be the smaller of B/H or 2.0.

4. URBAN CANYON MODEL DEVELOPMENT

4.1. *Historical perspective*

The complexity of the flow within the urban canyon and the paucity of full-scale experimental data has perhaps hindered the development and proliferation of models applicable to the urban canyon environment. The two basic two-dimensional urban canyon models in existence today, the empirically derived STREET submodel within APRAC (Johnson *et al.*, 1973; Ludwig and Dabberdt, 1972) and the box model of Nicholson (1975) are a decade old and have serious limitations.

The STREET canyon model is given as

$$C_{lee} = C_b + \frac{Kq}{(u + u_o)[(x^2 + z^2)^{1/2} + L_o]} \tag{4a}$$

$$C_{luv} = C_b + \frac{Kq(H - z)}{(u + u_o)HB} \tag{4b}$$

where C_b is the above-canyon background concentration, u is the wind speed at rooftop, u_o is a minimal dilution parameter set to 0.5 (m s^{-1}), q is the emission strength (g m^{-1} s^{-1}) of the lane of traffic a distance x (horizontally) and z (vertically) from the receptor, and $L_o \simeq 2$ m specifies an initial pollutant mixing length scale. The empirically determined constant, $K \simeq 7$, is presumably valid for canyons having a height to width ratio comparable to the ratio, $H/B \simeq 1$, of the San Jose study, although a subsequent evaluation by Dabberdt *et al.* (1973) did not suggest dramatic variation in K for two narrower canyons in St. Louis with H/B of 1.5 and 2.0. However, the lack of a sound theoretical basis for the value of K (and to a lesser extent, u_o) has inhibited the model's acceptance and transportability to other canyon geometries. The model is recommended for all wind directions, except for those within 30° of the canyon axis direction the concentration should be computed as the average of Equations (4a) and (4b). The same algorithm appears in the Intersection Midblock Model (Benesh, 1978) with the subsidiary condition

$$H > 7(DB/u)^{1/2},$$

where D is a stability class dependent diffusivity, but this criteria greatly limits the meteorological conditions for which (4a) and (4b) are applicable. Sobottka and Leisen (1980a, b) have made further modifications to the STREET model in order to reproduce the Venloer Strasse data showing the increase of concentrations as the leeside wall is approached; however, their 'MAPS' model is otherwise quite similar in form and performance to STREET.

The Nicholson (1975) model is a rather simple box model which yields street-canyon-average concentrations. Whereas the crude spatial resolution of this model has probably inhibited its use in regulatory settings, Nicholson's discussion of the basic physics underlying canyon ventilation is significant and fundamental. The extent to which ventilation is dominated by advective or turbulent transfer processes has yet to be decided for full-size canyons, despite recent data of DePaul (1984) (and DePaul and Sheih, 1985), suggesting dominance of turbulent transfer at the top of the canyon. The same controversy, of course, exists with wind tunnel data, yet neither the wake dominated, turbulent transfer dominance advocated by Hoydysh and Chiu (1971) and Hoydysh *et al.* (1974) or the advection dominance mechanism reported by Wedding *et al.* (1977) have been adequately evaluated.

4.2. *Model design criteria*

Given that 'hot spots' or highly localized high concentration zones are the key problem to be adequately modeled, it was decided that the resultant model must yield receptor specific values of concentration rather than canyon-average values. In addition, our modeling efforts should include reasonable and physically based consideration of

(i) atmospheric stability including calm conditions,

(ii) non-uniformity of emissions in the along-canyon direction,

(iii) non-vortex and canyon-parallel wind conditions,

(iv) varying canyon geometry (in the form of varying canyon height to width ratios),

(v) finite canyon lengths and receptor distance from the nearest upwind intersection,

(vi) concentrations at the nearest upwind intersection, and

(vii) vehicle induced turbulence caused by vehicle presence and speed (thermal emissions included in turbulent sigmas).

On top of this seemingly impossible list of requirements, UBA requested that the model be simple and inexpensive to run, thus ruling out sophisticated numerical grid models.

Two models were then constructed: a complex research model and a simple applications model. The research model is a Monte Carlo Lagrangian trajectory model, patterned after that of Lamb *et al.* (1979) but with capabilities to deal with generalized geometries and with the Legg and Raupach (1982) ap-

proach to avoid the unphysical buildup of particles in low turbulence zones. This model, its first-order closure wind field generator, and its performance are documented in Geomet (1985). It is perhaps sufficient to say that this research model has provided valuable conceptual input to the simple applications model design.

4.3. *The Canyon Plume-Box Model*

The simple applications model, referred to as the Canyon Plume-Box Model (CPBM), actually involves a series of assumptions and submodels that are now considered in detail.

Canyon flow and turbulence averaging. As discussed in the previous section, factorization of the flow into cross-canyon and along-canyon components is first assumed. The H–H wind field Equations (1a) and (1b) are then used as interpolators to define integrally averaged transport velocities u_b, u_t, w_{lee} and w_{luv} along the bottom, top and lee and luv sides, respectively of the canyon. The along-canyon velocity function, given by Equation (2), is similarly averaged over the canyon depth to yield a mean along-canyon transport speed v. Equation (3) is then used to estimate average turbulent velocities σ_u and σ_w along the top, bottom, and sides of the canyon. If the cross-canyon turbulence σ_{ub} divided by the cross-canyon advection speed u_b, both defined at a height $H_v(0)/2$ corresponding to the effective source height above the street, exceeds 2.0* then turbulence is assumed to dominate over advection and a major algorithmic split occurs.

Non-vortex dispersion model. For $\sigma_{ub}/u_b > 2.0$ cross-canyon turbulence dominates advective transport and no vortex flow is assumed. Concentrations are then computed by assuming a plume diluted with velocity v and travelling parallel to the canyon axis. Plume dispersion parameters are then defined as

$$\sigma_x(t) = B_l/\sqrt{2\pi} + \sigma_u \cdot t \qquad (5a)$$

$$\sigma_z(t) = H_l/\sqrt{2\pi} + \sigma_w \cdot t, \qquad (5b)$$

where B_l is a constant lane width of 3.0 m, σ_u and σ_w are arithmetic averages of the four path averaged values previously discussed, and t is travel time along the canyon. The lane height H_l is given as a function of vehicle speed, V, as

$$H_l = H_v(0) + H_v(\infty)\,[1.0 - \exp(-V/V_C)] \qquad (6)$$

where $H_v(0)$ and $H_v(\infty)$ are length scales designed to describe the height of the well mixed zone behind the vehicle for a range of vehicle speeds and V_C is a vehicle speed representing the transition speed from low speed to high speed induced wake regions. The Gaussian plume equation is then numerically integrated along the canyon for each lane of traffic until the upwind intersection is reached or until the advection/diffusion travel time exceeds five lifetimes τ, defined in terms of the e-folding time

$$\tau = (e - 1.0)\,H/\sigma_w. \qquad (7)$$

Pollutant reflections from the ground and building walls are included via the method of images, and the efficient summation method of Yamartino (1977) is used to reduce computational effort. Use of the image method to account for the confining effects of the buildings was also employed by Potenta *et al.* (1982) in their HWY2CAN model and found to yield reasonable results for a deep urban street canyon in New York city.

Vortex dispersion model. For $\sigma_{ub}/u_b \leqslant 2.0$ the somewhat more complex, vortex model depicted in Fig. 5 is used, and it is this model which combines the concept of plume modeling with box modeling of pollution that is recirculated repeatedly by the vortex. In addition, this model considers concentration inhomogeneities on the luv side created by the intrusion and entrainment of clean air, incorporates variations in the along-canyon emission rate, and allows for the presence of intersections. Each of these model features will now be considered in detail.

(a) Plume model. The largest impacts occur on the lee side where the direct impact of plume P_1 is combined with the recirculated concentration component C_R. As in the case of the non-vortex plume model, the vertical dispersion is given by Equations (5b) and (6), except that the turbulence, σ_{wb}, near the bottom of the canyon is used in place of the canyon average value σ_w. Along-plume, x, and along-canyon, y, dispersions are ignored as the steady-state, infinite length and perpendicular line source form of the Gaussian plume equation with dilution velocity u_b is assumed.

Rather than deal with a single plume that follows the curved path specified by the wind field module, we

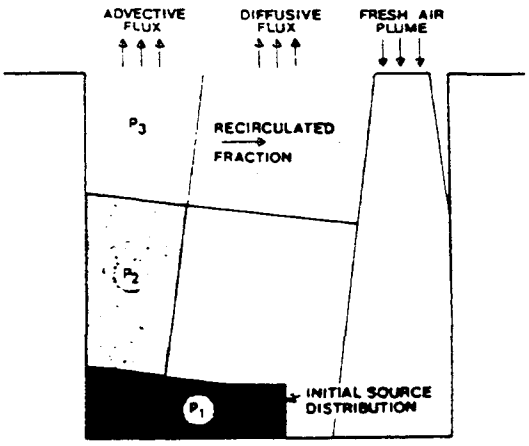

Fig. 5. Schematic diagram of the principal mechanisms of the vortex sub-model in the Canyon Plume-Box Model (CPBM). Components are described in the text.

* A value of 1.95 was determined from optimization studies; however, the broad structure of the chisquare minimum permitted judicious 'rounding' of this and other parameter values with negligible impact on the chisquare.

assume that the three straight line plumes, P_1–P_3, provide an adequate approximation. Initial plume spreads for plumes P_2 and P_3 are computed by taking the sigmas computed using P_1 and P_2 at the canyon lee wall and canyon top, respectively, and pivoting this length clockwise 90° about the lower left and upper left corners of the canyon, respectively. Transport time, t, to a receptor is computed based on the local wind speeds u_b, w_{lee}, and u_i for plumes 1, 2 and 3, respectively, and pseudo-transport times are used to ensure that initial sigmas correspond to the simple geometrical picture described above. Along-plume dilution is nevertheless based on the initial dilution, $1/u_b$, for all three plumes. Since it is not known in advance, for many receptors, which of the three plumes will generate the largest coupling coefficient, all three are computed and the largest taken as the most direct and hence the most physically reasonable. Plume reflections from the neighboring material surface are also considered. Finally, these direct impact concentrations are added to estimates of the vortex recirculated pollutant concentrations to yield a total (less ambient background) concentration.

(b) Pollutant recirculation model. Estimation of the recirculated concentration, C_R, or the fraction of material, F, that is recirculated requires consideration of the mass budget within the canyon. There are several ways to consider the mass budget within the street canyon. The simplest is to consider the canyon as a first-order linear system of volume (per unit length of canyon) BH, being supplied emissions (per unit length of canyon) at a rate q, and being depleted at a characteristic time scale or lifetime τ. This leads to a uniform canyon concentration of

$$C_R = q\tau/(BH) \tag{8}$$

that is reasonable only if all time scales associated with pollutant mixing within the canyon are short compared to τ. Given the dramatic anisotropy of within canyon concentrations and that SF_6 tracer determined lifetimes of 0.5–4 min (Drivas and Shair, 1974; Lamb, 1978; DePaul and Sheih, 1983) in street canyons are of the same order as transport times, Equation (8) is useful only as a large τ consistency check for a more detailed model.

Considering only the well mixed component, C_R, and postulating that material depletion occurs by a combination of turbulent transfer at an effective 'velocity' $\sigma_w/\sqrt{2\pi}$ at the top of the canyon and advective flushing by a 'jet' of clean air of size σ_j and speed w_j, the mass balance equation in the absence of emissions is just

$$(HB)\frac{dC_R}{dt} = -C_R\{B'\sigma_w/\sqrt{2\pi} + \sqrt{2\pi}\sigma_j w_j\}, \tag{9a}$$

where
$$B' = B - 2\sqrt{2\pi}\sigma_j \tag{9b}$$

is the width of the canyon where turbulent exchange processes are not overpowered by advective inflow and the corresponding outflow. Equation (9) has the solution $C_R(t) = C_R(0)\exp\{-t/\tau\}$ with the lifetime τ expressible in terms of advective and diffusive components τ_A and τ_D, respectively as

$$\tau^{-1} = \tau_A^{-1} + \tau_D^{-1} \tag{10a}$$

where
$$\tau_A^{-1} = \sqrt{2\pi}\sigma_j w_j/(H\cdot B) \tag{10b}$$

and
$$\tau_D^{-1} = B'\sigma_w/(\sqrt{2\pi}H\cdot B). \tag{10c}$$

An alternate, but quite general, way to envision recirculation is to consider the emissions q diluted by the velocity u_b, travelling up the lee half of the canyon, attenuated by the factor F, and travelling down the luv side. This cycling of material repeats itself indefinitely and yields the concentration

$$C_R = \frac{q}{u_b(B/2)}\cdot[F + F^2 + F^3 + \ldots]$$

$$= \frac{q}{u_b(B/2)}\frac{F}{(1-F)} \tag{11a}$$

where F, bounded by 0 and 1, must be expressible in the form

$$F = \exp\{-t_s/\tau\} \tag{11b}$$

with t_s as a yet undetermined time scale. In the very long lifetime limit, $F \simeq 1 - t_s/\tau$, and matching between Equations (11a) and (8) constrains t_s

to be
$$t_s \simeq 2H/u_b. \tag{11c}$$

Equations (10) and (11) now provide a complete model for the recirculated concentration C_R that is intuitively appealing and can be more rigorously justified by including emissions and direct plume losses into Equation (9).

(c) Clean air jet. The recirculation model just described leads to a uniform concentration C_R predicted for the luv side of the canyon; however, Johnson *et al.* (1973) observed a strong luv side vertical dependence that they parameterized as $(H-z)/H$. While the Bonner Strasse data do not show such a pronounced luv side z dependence, the intrusion and entrainment of the hypothesized clean air jet should give rise to concentration gradients, at least on the luv side.

There are several ways to model a clean air jet but simplicity and consistency with the other plume elements suggest a form

$$C(x,z) = A_j C_R[1 - (\sigma_j/\sigma_x(z))$$

$$\times \exp\{-\tfrac{1}{2}(x-x_j)^2/\sigma_x^2(z)\}] \tag{12a}$$

where A_j is determined from the normalization condition

$$C_R \equiv (2/B)\int_{B/2}^{B} dx\, C(x,z)$$

to be

$$A_j = \left\{ 1 - \sqrt{2\pi}\,\sigma_j, B \left[\operatorname{erf}\left(\frac{B - x_j}{\sqrt{2}\,\sigma_x(z)} \right) - \operatorname{erf}\left(\frac{B/2 - x_j}{\sqrt{2}\,\sigma_x(z)} \right) \right] \right\}^{-1}, \tag{12b}$$

$$\sigma_x(z) = \sigma_j + \sigma_{u,\mathrm{luv}} \cdot (H - z)/w_j, \tag{12c}$$

and x_j, σ_j (and w_j) are yet to be determined parameters of the clean air jet describing its position, size and initial strength, respectively. As the presence of three parameters is rather excessive for a 'correction term' it was decided to fix w_j as the vertically averaged value of the flow model w value [i.e. Equation (1b)] at the optimal position of the jet $x = x_j$. With the flow jet speed fixed, σ_j now becomes the controlling parameter for the jet's advective flushing strength in Equation (10b) and its inhomogeneity strength in Equation (12a).

(d) Variable along-canyon emissions. Unlike the non-vortex model which includes varying along-canyon emission density as part of the numerical integration along the canyon axis, the vortex model implicitly assumes a uniform emission line source extending over an infinite length canyon. The usual Gaussian type of crosswind integration procedures were rejected because they fail to recognize the recirculating nature of the vortex. This recirculation creates the problem that material from some upwind point, y, could impact the receptor directly with a characteristic σ_y but then impact after one vortex rotation at a later time and with a larger value of σ_y. While a self-consistent formulation can be generated along these traditional lines, the recirculation series, $F + F^2 + F^3 + \ldots$, of Equation (11a) becomes more complex and cannot be rewritten as $F/(1 - F)$, and the number of error function terms in the solution becomes unwieldy. A much simpler along-canyon averaging process was instead adopted.

The geometrical travel time between the source and receptor is first computed based on relative x, z positions, canyon transverse flow speeds, and knowledge of the specific plume (i.e. $P_1 - P_3$ or C_R only) generating the principal source–receptor coupling. The along-canyon upwind source location, $y_o = v\tau$, is then computed from this transit time and the along-canyon flow speed. An effective emission rate, q_e, is then computed as

$$q_e = \int_{y_o}^{y_I} q(y) \exp[-(y - y_o)/\ell]\, dy/\ell \tag{13}$$

where $\ell = v\tau$, τ is given by Equation (10) and y_I is the distance to the upwind intersection. Such an exponential weighting is consistent with the time constant formulation of concentration decay within a canyon, leads to a simple sum of exponential weights for a $q(y)$ defined 'piecewise' along the canyon by an emissions module, and enables incorporation of results from submodels for concentrations at intersections.

Intersection modeling. Although realistic modeling of concentrations and their gradients within an intersection must involve 3-d aspects of the flow (e.g. building edge vortices with vertically aligned axes), the net effect of intersections on receptors located some distance down one of the intersecting street canyons can probably be handled adequately in a simpler fashion. One approach would be to consider the intersection as a well mixed reactor of volume V_I being fed polluted air by one or more streets and being drained of pollution by the neighboring street canyons. Concentrations, $C_i(x, z)$, in the canyons providing air flow to the intersection are then computed, using the previously defined components of the CPB model, and averaged over the area, $H_i B_i$, of the 'feeder' canyons to yield C_i. The along-canyon flow rates v_i into the intersection then permit the computation of the air and pollutant fluxes, and mass conservation permits one to write the intersection concentration C_I as

$$C_I = \left[E_I + \sum_i C_i v_i H_i B_i \right] \Big/ \sum_i v_i H_i B_i, \tag{14}$$

where the sums are over only those street canyons feeding material into the intersection, and E_I are the emissions ($\mathrm{g\,s^{-1}}$) within the intersection volume V_I itself. The along-canyon averaging philosophy of Equation (13) is then invoked to yield the added contribution, C_A, at the in-canyon receptor as

$$C_A = (C_I - C_B) \exp\{-(y_I - y_o)/\ell\} \tag{15}$$

where C_B is the ambient, above-canyon, background, $\ell = v\tau$, and τ is given by Equation (7) for the non-vortex case and by Equation (10) for the vortex case. Further implicit in Equation (15) is the assumption that the receptor cannot 'see' past the intersection to sample structure in the upwind feeder canyons, but that assumption has already been invoked by Equation (14) for C_I. Unfortunately, the present data do not permit evaluation of the adequacy of Equations (14)–(15), though the size of the exponential term in Equation (15) suggests that contributions may be as large as 20% for the Bonner Strasse sampler locations. Thus, in the analyses that follow, C_A has effectively been set to zero by choosing a large positive value for the intersection distance y_I.

NO_2 *modeling.* The CPBM was specifically designed to predict nonreactive pollutant concentrations; however, F.R.G. regulatory agency interest in NO_2 'hot spots' has led to the addition of a 'postprocessor' that combines modeled NO_x concentrations, considered as the sum of NO and NO_2, with measured, above-canyon background levels of NO, NO_2 and O_3 to yield estimates of NO_2 within the canyon.

The basic approach is nearly identical to the photostationary state model (see Cole and Summerhays, 1979) except that, since the photostationary state assumption holds only for instantaneous concentrations and not their time averaged values, an empi-

rical quantity,

$$R \equiv [NO]^B[O_3]^B/[NO_2]^B, \quad (16a)$$

is defined in terms of above-canyon background concentrations in ppmV, denoted by the $[\ ]^B$ notation. Vehicle NO_x emissions are then considered to consist of the fraction f as NO_2 and $(1-f)$ as NO, so that

$$[NO_2]^V = f[NO_x]^V$$

and

$$[NO]^V = (1-f)[NO_x]^V, \quad (16b)$$

in the absence of chemical conversion. The fraction f is known to be in the range 0.05–0.10 at the tailpipe and $[NO_x]^V$ concentrations are estimated directly by the inert pollutant, CPB model. Switching on the NO, NO_2, O_3 chemistry and assuming that enough time has passed to achieve equilibrium then the total $[NO_2]^T$ level is just

$$[NO_2]^T = [NO_2]^B + [NO_2]^V + [X], \quad (16c)$$

where the unknown $[X]$ is obtained by solving* the quadratic relation

$$\frac{([NO]^B + [NO]^V - [X])([O_3]^B - [X])}{([NO_2]^B + [NO_2]^V + [X])} = R \quad (16d)$$

which assumes that production of an NO_2 molecule is accompanied by the elimination of an NO and an O_3 (actually singlet O).

Equation (16c) implies that equilibrium is achieved rapidly in comparison with the transport time scales. This is not true in the urban canyon and suggests that in Equation (16c) $[X]$ be replaced by a time dependent form, such as $[X](1-\exp(-pt))$, where p is the initial NO_2 production rate and t the transport time; however, our sensitivity studies do not presently show the need for this, or even more exact†, time dependent expressions.

Algorithm characteristics. While seemingly complex, the complete algorithm requires only about 400 FORTRAN statements and executes rapidly enough that analysis of a year of hourly cases (half-hourly in the F.R.G.) requires less than 1 h on an IBM PC-AT.

While more comprehensive than any previous canyon model, this Canyon Plume-Box Model (CPBM) may still require a module to treat fully calm conditions. An algorithm evaluated by Yamartino *et al.* (1979) is available if needed, but current data do not suggest the need for such an algorithm.

* The solution is simply

$$2[X] = b - (b^2 - 4c)^{1/2}$$

where $b = [NO]^B + [03]^B + R + [NO]^V$ and $c = [O_3]^B[NO]^V - R[NO_2]^V$. Note that $c > 0$ (< 0) implies the mixture is [NO]-rich (poor) so that $[X]$ is positive (negative).

† Benson, 1984 uses a more complete time dependent expression in the CALINE4 model.

5. MODEL EVALUATION

5.1. *CPBM parameter selection and* NO_x *performance*

The description of the CPB model in the previous section may, at first, give the impression of having enough free parameters to accommodate any data idiosyncrasies; however, a quick review of these parameters shows that their ability to alter fundamental algorithm behavior is quite limited.

The vehicle-induced, initial mixing zone, H_ℓ [Equation (6)], contains three parameters; however, if the automobile velocities are poorly known or cluster in a narrow range about a mean speed, the three parameters collapse into a single parameter describing the mean value of H_ℓ. In fact, after the model optimization it was found that the standard deviation of 0.15 m in H_ℓ about its mean value of 3.66 m indicated that the present value of the term containing $H_V(\infty)$ and V_C is rather marginal. Yet, the presence of these parameters gives the model a potential that is desirable on both theoretical and experimental grounds. Similarly, the optimal parameter values for the clean air jet showed that it accounts for only about 10% of the canyon ventilation in Bonner Strasse and that switching it off entirely (i.e. $\sigma_j \to 0$) provides only slightly worse model performance. However, ignoring the possibility of advective flushing *a priori* could lead to disastrous performance in another canyon (e.g. a canyon with a higher buildings on the luv side than on the lee side as studied by DePaul and Sheih, 1983) and would have prejudged an existing controversy.

As a result, the CPBM turned out to be critically dependent in Bonner Strasse on only two 'parameters':

(1) an average value of H_ℓ describing initial mixing and thus controlling maximum lee side concentrations, and

(2) the value of σ_{wb}/u_b where the algorithm switches from vortex to non-vortex formulations.

In order to optimize these CPBM parameters it was decided to 'tune' the model using NO_x data and conduct a model intercomparison using the independent CO data. The principal reasons for 'tuning' the model on NO_x were:

(1) canyon signal-to-background ratios were higher and percentage measurement errors* lower for the NO_x data, and

(2) the NO_x emission line density, $e(=Q/V)$, is nearly independent of vehicle velocity whereas CO varies dramatically. Thus the infinite uniform line source approximation is likely to be much better satisfied for NO_x.

The data sample consisted of all half-hour periods for which good traffic count and wind field data were available. These cuts resulted in a sample of 673 half-hour periods containing 3279 positive (i.e. > 2 ppb),

* NO_x overall measurement errors were generally less than 10% whereas CO uncertainties were in the 20–30% range (Leisen, private communication, TÜV).

Table 2.
a. Optimal CPBM parameters for NO_x

Parameter	Value	Equation
$H_V(0)$	2.0 m	6
$H_V(\infty)$	2.5 m	6
V_C	30 km h^{-1}	6
σ_v	0.25 m	10
x_j	0.85 B	12
Switch	2.0	Values of σ_{ub}/u_b where CPBM switches from non-vortex to vortex models
e	2.444 mg m^{-1}	NO_x emissions per vehicle per meter of travel

b. Optimized CPBM NO_x performance measures

r.m.s. error = 35 ppb
mean square error/C^2_{OBS} = 0.23
correlation coefficient (r) = 0.814 (0.80, 0.83 are 95% confidence level bounds)

Variance decomposition:
mean bias = 0.1%
dynamic bias = 5.3%
stochastic = 94.6%

slope (obs. = slope * pred.) = 0.99

Percent of predictions within factor of x for the upper 90% of observations

X	Cumulative percent
1.1	18
1.3	52
1.5	73
2.0	93

Above performance measures based on 673 half-hour measurement periods in Bonner Strasse and involve 3279 NO_x samples

background-subtracted NO_x concentrations. Thus, fewer than 100 concentration measurements were rejected as 'bad data' because above roof concentrations exceeded within canyon values. An additional requirement that the wind speed at 26.5 m exceed 0.1 m s^{-1} did not eliminate any events as the lowest speed in the sample was 0.18 m s^{-1}. All variables required by the flow, turbulence, and CPB models were available as half-hourly measured quantities, except for vehicle velocities. Spot measurements of vehicle mid-block speeds suggested that an equation of the form

$$V(\text{km h}^{-1}) = 44.6/(1 + 1.5\,N_s), \qquad (17)$$

where the factor 1.5 reduces speeds by 50% at a four-lane vehicle flow-rate of $N_s = 0.67$ s^{-1} (i.e. 1200 vehicles per half-hour), captures the leading N_s dependence in the vehicle speed data.

Optimal values of the CPB model parameters, presented in Table 2a, were then obtained with the aid of several, non-linear optimization packages by searching for those 'rounded-off' parameter values that gave the minimum variance between predicted and observed NO_x concentrations. Because there was substantial uncertainty in the vehicle speeds and some question about the effective emission rate for the mix of cars and trucks in Bonner Strasse, the emission density, e (mg m^{-1}), per vehicle was left as a free parameter. This in turn creates a tremendous amount of freedom which was eliminated by first fitting the CPBM parameters on normalized concentrations, so that the emission rate $q(= e\,N_s)$ cancelled out, and then fixing the CPBM parameters and allowing e to take on the single optimal value needed to fit all the measured concentrations. Such a two-step procedure guarantees that the CPBM parameters are accounting for spatial variations within the canyon and e is merely establishing an overall scaling factor.

As mentioned earlier, the highly interdependent triplet of variables, $H_V(0)$, $H_V(\infty)$ and V_C, are rather poorly resolved. However, the mean H_v of 3.66 m is equivalent to an initial dispersion standard deviation of $\sigma_z(0) = 1.46$ m. This value of initial dispersion is consistent with the highest instantaneous SF_6 concentrations measured by Lamb (1978) in a Norwegian street canyon.† Other model parameters are presently

† The gas chromatograph calibration curve in the Lamb (1978) experiment suggests it is difficult to resolve concentrations above 20,000 ppt SF_6, and this concentration corresponds to $\sigma_z(0) = 1.855$ m. They report one value above 20,000 ppt and estimate it at 10^5 ppt, which corresponds to $\sigma_z(0) = 0.8$ m. Our value of 1.46 m is equivalent to a measurement of 32,000 ppt, and thus is considered here to imply consistency.

more difficult to confirm; however, the small value of σ_j suggests dominance of turbulent transfer in determining the pollutant lifetime τ of Equation (10). This in turn suggests a simple dimensionless lifetime of

$$\hat{\tau} = \tau_D u_t / H \simeq \sqrt{2\pi}/i_{zt}, \tag{17}$$

where i_{zt} is the z turbulent intensity at the top of the canyon. Table 4 values of A_m then yield a $\hat{\tau}$ of 20 that should compare with wind tunnel results at large Reynolds numbers. Builtjes's (1984) measurements of $\tau = 2.4$ s at H/u_t of about 0.1 s in a 1:250 scale wind tunnel study of Bonner Strasse yields a $\hat{\tau}$ of 24, in reasonable agreement with Equation (17) and supportive of the recirculation model of section 4.3.

The resulting scatterplot of CPBM predicted vs observed NO_x concentrations is shown in Fig. 6 with accompanying statistical measures presented in Table 2b. Beyond the low r.m.s. error of 35 ppb and a correlation coefficient exceeding 0.8, perhaps the most significant statistical statements are that

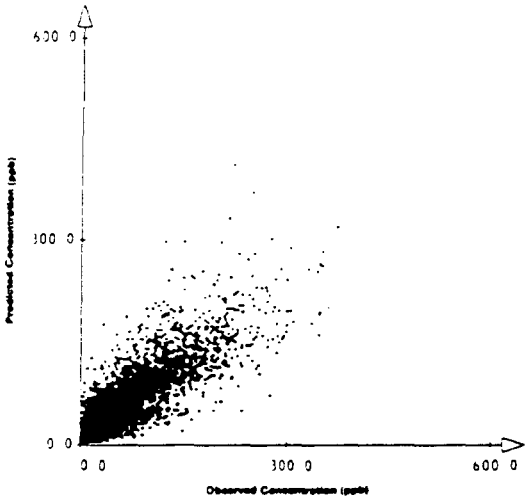

Fig. 6. CPBM predicted vs observed, background-subtracted NO_x concentrations (ppb). Performance measures are presented in Table 2b.

(i) for the upper 90% of observed concentrations, over 50% are modeled to within ±30% and a full 93% are modeled to within a factor of two, and

(ii) 95% of the remaining variance is stochastic in nature. That is, it cannot be attributed to a mean bias between predictions and observations or a failure of the model to reproduce the dynamic variability of observations about the observed mean.

5.2. *CPBM* NO_2 *performance*

Using the CPBM parameters established from the NO_x optimization, the NO_2 predictions using Equation (16) were compared with observations, as were versions of CPBM assuming

full 'ozone limiting' conversion of NO into NO_2, or
no atmospheric chemistry production of NO_2.

Results presented in Table 3 indicate that Equation (16) yields a significantly lower mean square error than either the 'ozone limiting' or 'without chemistry' assumptions. In addition, the fraction, f, of NO_x directly emitted as NO_2 that was required to obtain a minimum variance fit in each case was outside the measured 5–10% range for the 'ozone limiting' and 'without chemistry' cases (although one reviewer has suggested that direct NO_2 emissions may be of the order 20% for ambient temperatures below 5°C). The modified photostationary state approximation [i.e. Equation (16)] also led to the highest correlation coefficient and the largest variance fraction attributable to stochastic variability.

Scatter plots of predicted vs observed total NO_2 concentrations are presented in Fig. 7 for the modified photostationary state assumption. Total concentration distributions are displayed due to the coupled nature of the background and vehicle attributable NO_2 levels.

5.3. *CPBM* CO *performance and model intercomparison*

Two data samples were considered in the CO evaluation. Both samples required the presence of good traffic count and wind field data plus the requirement that the wind speed at 26.5 m exceed 0.1 m s^{-1}.

Table 3. NO_2 model evaluation (includes background)

Optimal NO_2/NO_x emitted (%)	Slope	m.s.e./$\bar{C}^2_{OBS}$	Percent stochastic	Corr. coeff.
(a) Photostationary state				
8.66	0.96	0.044	99	0.83
(b) Ozone limiting				
1.27	0.91	0.075	92	0.72
(c) Without chemistry				
13.8	1.00	0.059	91	0.81

Above performance measures based on 673 half-hour measurement periods in Bonner Strasse and involves 3109 NO_2 samples.
m.s.e. is mean square error.
Slope defined as obs. = slope • pred.

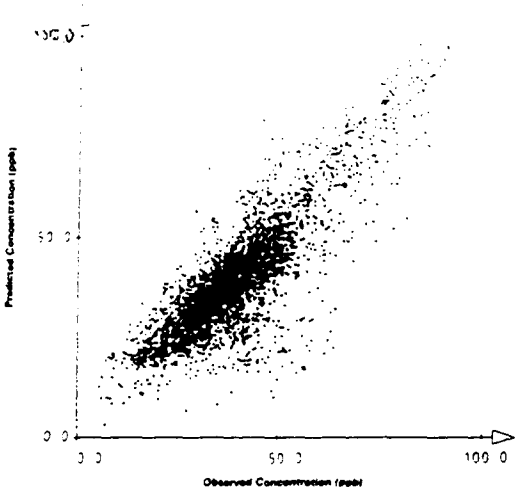

Fig. 7. CPBM predicted vs observed total NO_2 concentrations (ppb). Performance measures are presented in Table 3.

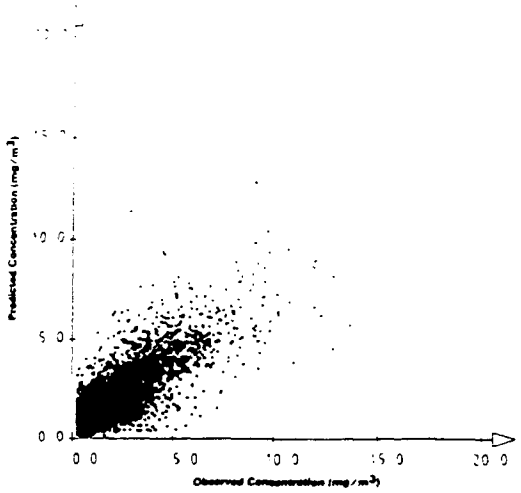

Fig. 8. CPB model predicted vs observed, background-subtracted CO concentrations (mg m^{-3}) for the larger data sample (see text). Performance measures are presented in Table 4a.

As in the NO_x sample, the wind speed cutoff was so low that no events were eliminated and the other cuts resulted in a sample of 673 half-hour events containing 2943 accepted CO background subtracted concentrations.* A smaller sample had the added constraints that the average wind speed at 26.5 m had to exceed 1.0 m s^{-1}, that wind direction satisfy the STREET condition of being within 60° of perpendicular to the canyon, and that flow conditions (as defined by the difference between vector and scalar average wind azimuths at 26.5 m) be well defined and persistent. This smaller data base, well suited for STREET application, contained 440 events and 1930 concentration values.

The CPB model was first applied to the larger more complete CO data sample. Despite the fact that these data preferred somewhat different values of $H_v(0)$ and $H_v(\infty)$, all model parameters were held fixed at the optimal values obtained from the NO_x analysis and presented in Table 2. Only the emission density, e, was allowed to take on a new value of 39.5 mg m^{-1} for CO. It should be noted that use of a speed independent value of e is less justifiable for CO than for NO_x, and that the numerical value coincides with a surprisingly low mean vehicle-speed of about 9 km h^{-1} using TUEV emission rate vs speed curves; however, alternative approaches to the estimation of CO emissions did not yield improved CPBM performance. The scatterplot of CPBM predicted vs observed CO values is presented in Fig. 8, with some accompanying statistical measures of performance in Table 4a.

The CPB model was compared initially with the original APRAC street canyon submodel and the analytical, K-theory model suggested by Hotchkiss and Harlow (1973). Using the value of emission density described above, the STREET model showed a strong underpredictive bias but appeared promising, whereas the Hotchkiss and Harlow (1973) solution did not appear suitable without major modifications and was abandoned. Since the STREET model is admittedly empirical, we wanted to consider it at its best rather than penalize it for being tuned to data from another street canyon. Thus, the parameters K, u_o, and L_o in Equations (4a) and (4b) were allowed to be free so that a better agreement between predicted and observed CO concentrations might be achieved. These studies showed that while L_o was nearly optimal, there was a slight preference for values of u_o as high as 4 m s^{-1}, but with an accompanying value of K far above reasonable estimates. Therefore, u_o and L_o were held at their original values of 0.5 m s^{-1} and 2 m, respectively, but K was allowed to rise to an optimal value of 10.2, a value which eliminated the aforementioned underprediction bias. The resulting scatterplot of APRAC predicted vs observed CO values is shown in Fig. 9(a) and accompanying performance measures included in Table 4a.

Sobottka and Leisen (1980a, b) applied the STREET model to their Venloer Strasse measurements and obtained an optimal K of 8. Their finding that STREET was unable to explain the positive concentration gradients as one approached the lee building face led them to develop a modified version of STREET named MAPS. The major modification involved redefining the distance term in the denominator of Equation (4a) to force the pollutant to first reach the building face by lateral transport before advecting upward and outward to impact the receptor.

*All CO concentrations considered were 'background subtracted' by substracting off observed concentrations at the 26.5 m reference height. Occasional negative background subtracted concentrations and values less than 0.25 mg m^{-3} were rejected as 'bad data' or noise.

Table 4. CO model performance

Model	m.s.e./$\bar{C}^2_{OBS}$	Percent m.s.e. stochastic	Corr. coeff.	Slope
(a) Bonner Str.		Full data set	673	half- hours
			2943	measurements
CPB	0.25	94	0.76	1.00
STREET	0.41	99	0.66	0.99
MAPS	0.39	100	0.66	0.90
(b) Bonner Str.		'STREET' data set	441	half-hours
			1935	measurements
CPB	0.22	90	0.79	1.03
STREET	0.28	95	0.76	1.00
(c) Venloer Str.*		Full data set	505	half-hours
			2388	measurements
CPB	0.35	81	0.78	1.00

* Preliminary analysis. Details not described in the text.
m.s.e. is mean square error.
Slope defined as obs. = slope * pred.

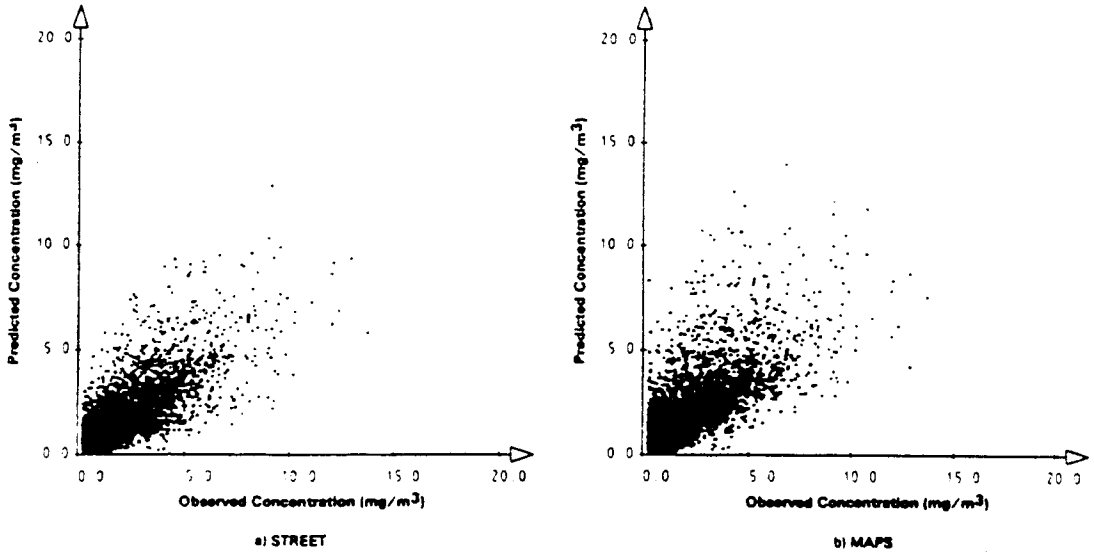

Fig. 9. APRAC (STREET) and MAPS predicted vs observed, background-subtracted concentrations (mg m^{-3}) for the larger data sample (see text). Performance measures are presented in Table 4a.

Results of applying the MAPS model to the Bonner Strasse CO data are presented in Fig. 9(b) and Table 4a. Aside from the fact that MAPS requires a larger K of 14.8, due primarily to the fact that MAPS assumes that all emissions are released at the center of the street, the improvement over STREET appears rather marginal, especially in comparison with the 40% reduction in mean square error provided by CPBM over STREET.

The CPB and STREET models were then applied to the smaller, STREET suited data base. Figures 10 and 11 show the scatterplots of predicted vs observed concentrations using the CPB and STREET models, respectively.

While the results are visually quite similar, the derived performance measures presented in Table 4b show that the CPBM provides a 20% lower mean square error than STREET. Nevertheless, the empirical STREET model performs quite well for the meteorological conditions for which it was designed. Intercomparison of Tables 4a and 4b shows that the main advantage of CPBM is that it retains its low mean square error characteristics under meteorological conditions that occur about one-third of the time and for which STREET performance degrades significantly.

5.4. *CPBM low-wind speed performance*

The current CPBM algorithm does not provide for cases where the above-roof wind speed falls below 0.1 m s^{-1}. Such cases, if important, would need to be described by a special calm wind, puff algorithm. Figures 12(a) and (b) show that the CPBM model performs quite well for CO and NO_x, respectively, for the six cases with above-roof speeds below 0.5 m s^{-1}

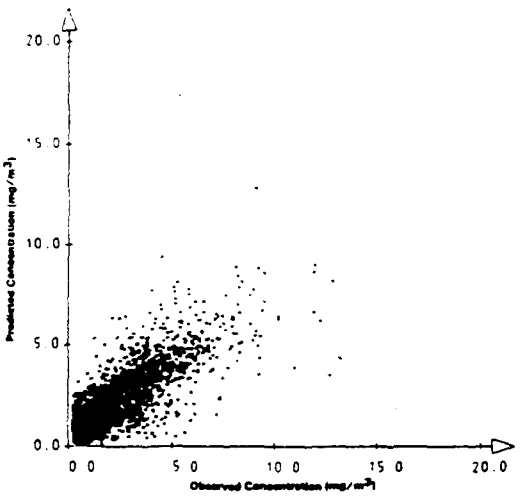

Fig. 10. CPB model predicted vs observed, background-subtracted CO concentrations (mg m^{-3}) for the smaller, STREET-suited data sample (see text). Performance measures are presented in Table 4b.

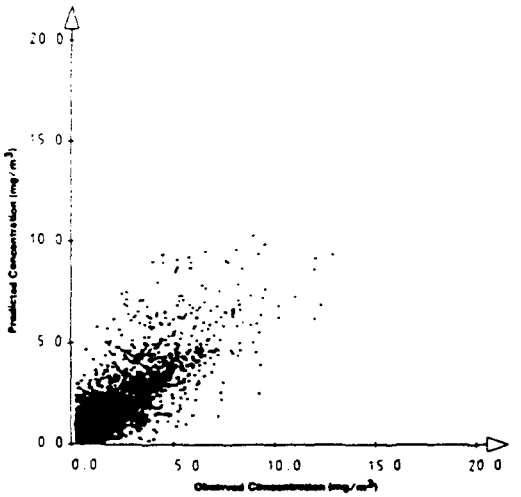

Fig. 11. APRAC (STREET) model predicted vs observed, background-subtracted CO concentrations (mg m^{-3}) for the smaller, STREET-suited data sample (see text). Performance measures are presented in Table 4b.

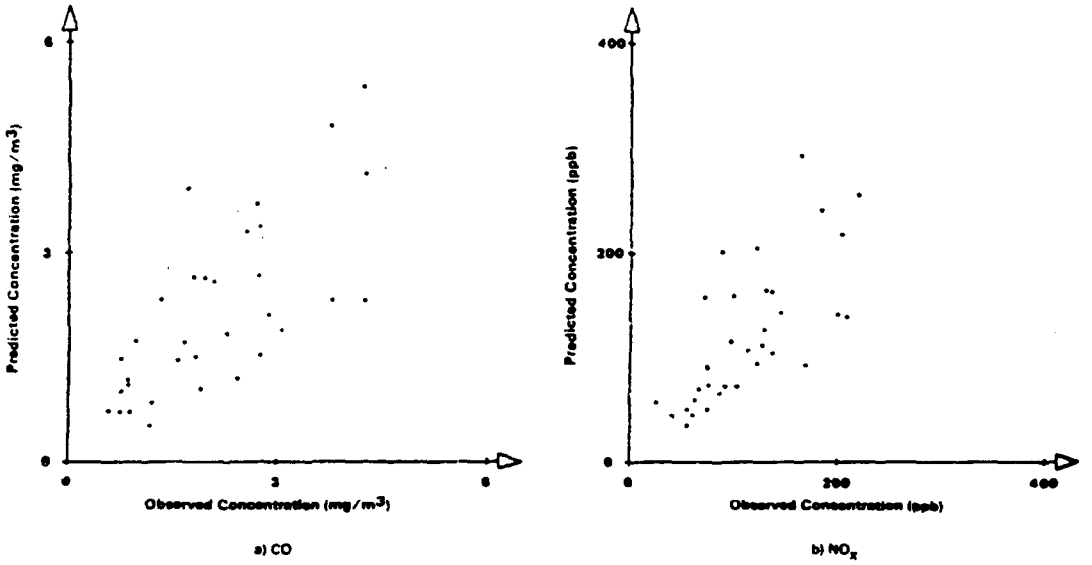

Fig. 12. CPBM predicted vs observed, background-subtracted CO and NO_x concentrations (mg m^{-3} and ppb, respectively) for above-roof wind speeds between 0.1 and 0.5 m s^{-1}. Performance measures are consistent with those of the corresponding larger samples.

What is also striking about these plots is that peak observed concentrations above background are well below the values observed at the higher wind speeds and included in Figs 6 and 8. In fact, whereas peak total CO levels (i.e. including background) reach 15 ppm in the canyon, all cases of total CO levels above 7 ppm are associated with above-roof wind speeds exceeding 0.5 m s^{-1}. Thus, low wind speed conditions do not appear to generate the more serious impact situations in the urban canyon, so that the need for the addition of a calm wind module for the CPBM is substantially less than estimated at the outset of this project.

6. CONCLUSIONS AND DISCUSSION

Simple models for the flow, turbulence and dispersion of pollutants within the urban street canyon have been developed and evaluated. Analyses performed on two, 11-day periods of the TÜV Rheinland Bonner Strasse data base indicate that:

(i) Canyon parallel and transverse flows are largely decoupled from one another; thus greatly simplifying the three-dimensional modeling process.

(ii) Canyon transverse flow quite consistently gives rise to a vortex flow that can be reasonably ap-

proximated in the mean with the Hotchkiss and Harlow (1973) flow model of Equations (1a) and (1b).

(iii) Canyon parallel flow shows vertical profiles that can be simulated with the logarithmic-type profiles of Equation (2); however, the specific z_0 values associated with these profiles depend upon the overall approach flow direction and on canyon specific characteristics such as the presence of isolated and substantially larger buildings.

(iv) Canyon turbulence components σ_u and σ_w appear to be well approximated by the simple model given by Equation (3). The fact that the combined transverse turbulence $(\sigma_u^2 + \sigma_w^2)^{1/2}$ yields an even better fit suggests that the turbulence field rotates with the mean flow. The model includes terms that account for mechanically and thermally induced turbulence in the mean vortex flow as well as that produced by the waste heat emitted by vehicles in the canyon. Wind tunnel measured height-to-width dependencies are superposed to generalize the model to other canyon geometries. The along-canyon turbulence σ_v may have additional dependences that have yet to be understood.

(v) A simple model (CPBM), developed from first principles, covers nearly the full range of meteorological conditions (i.e. totally calm conditions are presently not considered) and performs significantly better than the highly empirical APRAC street canyon submodel. The overall 40% mean square error performance superiority of the CPBM is most pronounced for those meteorological conditions, occurring about one-third of the time, for which STREET was not specifically designed; however, the smaller, 20% mean square error improvement over STREET under STREET-designed conditions is encouraging, since some of the observed dependencies in the data, such as decreasing concentrations with height on the luv side, are not easy to generate in a simple model.

The CPB model is actually a series of submodels for vehicle induced initial dispersion, plume transport and dispersion on the lee side of the canyon, advective and turbulent exchanges at the top of the canyon, pollutant recirculation, and the effects of clean air injection on the downwind (or luv) side. In addition, there are separate algorithms for non-vortex dispersion and inclusion of the impacts from upwind intersections. Despite the fact that the CPBM contains several parameters and depends on the output of flow and turbulence models which themselves contain parameters, the difference between these parameters and purely empirical parameters, such as the K in STREET [Equation (4)], is the possibility of understanding or modeling them in terms of distinct physical phenomena. Whereas the K in STREET arises from a combination of

— reduced velocities in the canyon,
— pollutant recirculation, and
— the turbulence to mean flow ratio,

CPBM parameters can be assigned values by well defined studies. Unfortunately, the data from the San Jose study did not permit resolving these individual effects so that an overall factor of K was probably the best choice under such circumstances.

Interestingly (but not described in this report), the CPB model performs significantly better than STREET on the high concentration lee side but often not as well on the luv side. The current CPB model considers the luv side profile to result from a combination of pollutant plume recirculation and clean air injection at the top of the canyon, but it is also possible that such a dependence could arise from the vortex intermittency, collapse, and subsequent short-lived flow reversal seen in some of TNO's flow visualization videotapes. Future modeling efforts will include testing of a model for vortex intermittency as an alternative (or supplement) to the current model features that control luv side concentrations. Also anticipated is the testing of the CPB model on the TNO wind tunnel flow, turbulence and concentration data at varying H/B ratios. Though the number of data points for which simultaneous flow, turbulence and concentration data are available number less than 100, the dramatic variation in C/q that they measure (plus the fact that q is well known) should provide a severe test of the CPB Model and its constituent submodels.

A number of other model features were evaluated during the course of this study but are not discussed in this paper because they failed to improve the model performance at all, or to a degree insufficient to warrant the added complexity; yet, these failings are interesting and in some cases puzzling. Each is discussed briefly below.

(i) Finite Lagrangian time scale. Studies with the Monte Carlo research model suggested optimal Lagrangian time scales of tens of seconds, but dropping rapidly with increasing flow speeds and turbulence levels to as low as a few seconds. The corresponding Eulerian time scale in CPBM tended toward large values, such that the infinite value, model version finally adopted proved to be as good as the more computationally burdensome, finite time scale version.

(ii) Turbulent exchange 'efficiency'. Similar to the time scale issue, the current CPBM uses the mean, upward turbulent velocity, $\sigma_w/\sqrt{2\pi}$, as the simplified mechanism for removing pollutants from the top of the canyon. Such a model implicitly assumes an infinitesimally thick transfer layer or pollutant transit times across the canyon top that are long compared with vertical diffusion time scales for a finite depth transfer layer and yet short compared to Lagrangian time scales. A simple model for transfer efficiency, displaying falling transfer efficiency with increasing vortex speed, lowered mean square errors an additional one percent, but such a small improvement did not appear to justify the added complexity and parameters.

(iii) Detailed along-canyon emissions profiles. The CPBM performance discussed in section 5 assumes that emissions, $q(y)$, are independent of along-canyon distance y. Attempts using Equation (13) to fold in the

detailed $q(t)$ profiles, produced by an emissions model that considers all vehicle modes (i.e. acceleration, deceleration, constant speed and idling modes), have so far yielded poorer CPBM performance than the constant emission density assumption. If emissions are variable in y then Equation (13) must capture the spirit, if not the precise detail, of such a dependence. Hence, the failing suggests along-canyon 'smearing' or averaging mechanisms that might include

— 'dragging' of emissions by vehicles in their wakes,
— large, low-frequency oscillation components dominating the relatively high values of along-canyon turbulence, σ_v, or
— engine, thermal memory times smearing the detailed modal emissions (as modal emission factors are apparently measured after steady state conditions are reached).

(iv) Plume-building face standoff distance. The present CPBM assumes that material emitted at the bottom of the street canyon actually impinges onto the lee wall rather than 'standing off' some centerline distance, x_c, as suggested by potential flow solutions. Optimization studies suggest $x_c \simeq 0$ in agreement with TÜV's Venloer Strasse measurements of peak CO at the building face. Yet other experiments (Jaeschke *et al.*, private communication) suggest peak CO levels at some distance from the building face. Perhaps a detailed model of the building face boundary layer is necessary to address this issue properly.

Additional areas for improving, or increasing the generality of, the CPB Model include

— replacement of the constant lane width B_f with a vehicle velocity dependent function,
— consideration of the effect of gaps or alleyways between buildings on within-canyon concentrations,
— inclusion of canyon asymmetry (i.e. different lee vs luv building heights) into the modeling,
— investigation of the significance of secondary vortices (i.e. building/sidewalk corner or behind parked vehicles) on concentrations at pedestrian breathing levels, and
— inclusion of distinctly three-dimensional effects (i.e. isolated buildings and vertical axis vortices present near intersections).

Further research on dispersion in the microcosm of the urban street canyon is currently being pursued in full scale and wind tunnel scale studies in Europe, Japan and the United States.

Acknowledgements—Funding for the development and evaluation of this model was provided to Geomet Gmb H by the Umweltbundesamt of the Federal Republic of Germany.

The authors wish to thank Dipl. Met. C. Ludwig, the Project Officer, for constructive guidance throughout the project and Dr P. Builtjes of TNO for his interpretations of the wind tunnel results and a careful review of the manuscript. We are also grateful to Dr P. Leisen of TUV for his assistance in using the Bonner Strasse data and Dipl. Met. B. Strobel for his contributions to the data processing.

Continued funding is being provided for model applications by the Umweltbundesamt and for advanced model development by the U.S. Federal Highway Administration (U.S. DOT FHWA).

REFERENCES

Albrecht F. (1933) Untersuchungen der vertikalen Luftzirkulation in der Grossstadt. *Meteorol. Z.* **50**, 93–98.
Benesh F. (1978) Carbon monoxide hot spot guidelines, Vol. V. User's manual for intersection-midblock model. EPA-450/3-78-037.
Benson P. E. (1984) CALINE4—a dispersion model for predicting air pollution concentrations near roadways. FHWA/CA TL-85 15
Builtjes P. J. H. (1983) Determination of the flow field in a street canyon by means of wind tunnel experiments. TNO Progress Report 83-09553.
Builtjes P. J. H. (1984) Determination of the flow and concentration fields in a street canyon by means of wind tunnel experiments. Draft TNO Final Report.
Builtjes P. J. H. and Vermeulen P. (1980) Atmospheric boundary layer simulation in the PIA and MIA wind tunnels of TNO-Apeldoorn. TNO Report 80-0290.
Chock D. P. (1980) General Motors sulfate dispersion experiment—an analysis of the wind field near a road. *Boundary-Layer Met.* **18**, 431–451.
Cole H. S. and Summerhays J. E. (1979) A review of techniques available for estimating short-term NO_2 concentrations. *J. Air Pollut. Control Ass.* **29**, 812–817.
Cope E. M. (1973) The effect of speed on automobile gasoline consumption rates. U.S. DOT., Washington, DC.
Dabberdt W. F., Ludwig F. L. and Johnson W. B. (1973) Validation and applications of an urban diffusion model for vehicular pollutants. *Atmospheric Environment* **7**, 603–618.
Dabberdt W. F., Shelar E., Marimont D. and Skinner G. (1981) Analyses, experimental studies, and evaluations of control measures for air flow and air quality on and near highways, Vol. 1. FHWA/RD-81/051.
De Paul F. T. (1984) A study of pollutant dispersion in an urban street canyon. PhD dissertation, Illinois Institute of Technology.
De Paul F. T. and Sheih C. M. (1983) Measurements of wind velocities in a street canyon. Argonne National Laboratory draft report ERC-83-10. Subsequently released in final form as ANL.ER-84-1.
DePaul F. T. and Sheih C. M. (1985) A tracer study of dispersion in an urban street canyon. *Atmospheric Environment* **19**, 555–559.
Drivas P. J. and Shair F. H. (1974) Probing the air flow within the wake downwind of a building by means of a tracer technique. *Atmospheric Environment* **8**, 1165–1175.
Eskridge R. E. and Rao S. T. (1983) Measurement and prediction of traffic-induced turbulence and velocity fields near roadways. *J. Climate appl. Met.* **22**, 1431–1443.
Geomet (1985) Kfz-Schadstoffbelastungen in Strassenschluchten. Final Report. Geomet G.m.b.H., Bundesallee 129, 1000 West Berlin 41 (in German).
Georgii H. W., Busch H. W. and Weber E. (1967) Untersuchung uber die zeitliche und raumliche Verteilung der Immissions-Konzentration des Kohlenmonoxid in Frankfurt am Main. Berichte des Institutes für Meteorol. und Geophys. der Universitat Frankfurt/Main No. 11 (available as NAPCA translation 0477).
Gluck K. (1972) Untersuchung der Umweltbelästigung und Umweltschadigung durch den Strassenverkehr in Stadtgebieten-Larm und Abgase. EG-Enquete, Herausg. VDI.
Hauschulz G., Heich H. J., Leisen P., Raschke J., Waldeyer H. and Winckler J. (1980) Emissions—und Immissionsmesstechnik im Verkehrswesen. TÜV, Rheinland.

Hosker R. P. (1983) The effects of buildings on local dispersion. AMS Specialty Conf. on Air Quality Modeling of the Urban Boundary Layer, Baltimore, MD, 4 Nov.–31 Oct.

Hotchkiss R. S. and Harlow F. H. (1973) Air pollution transport in street canyons. EPA-R4-73-029.

Hoydysh W. G. and Chiu H. H. (1971) An experimental and theoretical investigation of the dispersion of carbon monoxide in the urban complex. American Institute of Aeronautics and Astronautics Paper No. 71-523, Urban Technology Conference, 24–26 May, New York.

Hoydysh W. G., Griffiths R. A. and Ogawa Y. (1974) A scale model study of the dispersion of pollution in street canyons. APCA Paper No. 74-15.7, Presented at the 67th Annual Meeting, 9–13 June, Denver, CO.

Johnson W. B., Ludwig F. L., Dabberdt W. F. and Allen R. J. (1973) An urban diffusion simulation model for carbon monoxide. *J. Air Pollut. Control Ass.* **23**, 490–498.

Lamb B. (1978) A tracer investigation of pollutant dispersion in an urban street canyon. Norwegian Institute of Air Research Report 2577.

Lamb R. G., Hogo H. and Reid L. E. (1979) A Lagrangian approach to modeling air pollutant dispersion: development and testing in the vicinity of a roadway. EPA-600/4-79-023.

Legg B. J. and Raupach M. R. (1982) Markov-chain simulation of particle dispersion in inhomogeneous flows: the mean drift velocity induced by a gradient in Eulerian velocity variance. *Boundary-Layer Met.* **24**, 3–13.

Leisen P. and Sobottka H. (1980) Simulation of the dispersion of vehicle exhaust gases in street canyons: comparison of wind tunnel investigations and full scale measurements. IMA Conference on Modeling of Dispersion in Transport Pollution, Southend-on-Sea, England, 17–18 March.

Ludwig F. L. and Dabberdt W. F. (1972) Evaluation of the APRAC-1A urban diffusion model for carbon monoxide. Final Report, Coordinating Research Council contract CAPA-3-68 (1-69). NTIS No. PD 210819.

Nicholson S. E. (1975) A pollution model for street-level air. *Atmospheric Environment* **9**, 19–31.

Pankrath J. (1975) Numerische Modellierung der Substanz- und Wärmeausbreitung in der Wirbelstromung einer Geländevertiefung. *Beiträge zur Physik der Atmosphäre*, **48**, 327–348.

Pasquill F. (1974) *Atmospheric Diffusion*. 2nd Edn. John Wiley, New York.

Potenta E. J., Fahrer V. S. and Tai R. C. (1982) State-of-the-art approach to predicting pollutant concentrations in urban street canyons. APCA Paper No. 82-50.6, presented at the 75th Annual Meeting, 20–25 June, New Orleans, LA.

Sobottka H. and Leisen P. (1980a) Vehicle exhaust gas emissions in city streets and their distribution; comparison of measurements and model aspects. IMA Conference on Modeling of Dispersion in Transport Pollution, Southend-on-Sea, England, 17–18 March.

Sobottka H. and Leisen P. (1980b) Pollutant dispersion of vehicle exhaust gases in street canyons. *Proc. of the 5th International Clean Air Congress*, Buenos Aires.

Smith F. B. (1972) A scheme for estimating the vertical dispersion of a plume from a source near ground level. NATO/CCMS Proceedings No. 14.

Waldeyer H., Leisen P., and Müller W. R. (1981) Die Abhängigkeit der Immissionsbelastung in Strassenschluchten von meteorologischen und verkehrsbedingten Einflussgrössen. *Proc. Conf on Vehicle Exhaust Impacts in the Vicinity of Major Streets*, 20–21 October, 1981, TÜV Rheinland, Cologne, West Germany.

Wedding J. B., Lombardi D. and Cermak J. (1977) A wind tunnel study of gaseous pollutants in city street canyons. *J. Air Pollut. Control Ass.* **27**, 557–566.

Yamartino R. (1977) A new method for computing pollutant concentrations in the presence of limited vertical mixing. *J. Air Pollut. Control Ass.* **27**, 467–468.

Yamartino R. J., Lühring P. G. and Stern R. M. (1979) Analysis of several low wind speed tracer experiments. *Proc. Tenth NATO/CCMS International Technical Meeting on Air Pollution Modeling and its Application*, Rome, 23–26 Oct. Umweltbundesamt, West Berlin.

REFERENCES

Albrecht, R , 1933. Untersuchungen der vertikalen Luftzirkulation in der Grosstadt. Meteorol. Z. 50, 93-98.

Bemis, G.R., P.E. Benson, A.J. Ranzieri and K.O. Pinkerman, 1977. Air Pollution and Roadway Location, Design, and Operation - Project Overview. FHWA-CA-TL-7080-77-25.

Benesh, F., 1978. Carbon monoxide hot spot guidelines, Volume. V: User's Manual for Intersection-Midblock Model. EPA-450/3-78-037.

Benson, P.E., 1979. CALINE-3, A versatile dispersion model for predicting air pollutant levels near highways and arterial streets FHWA/CA/TL-79/23, NTIS-PB-220842.

Benson, P.E., 1982. Modifications to the Gaussian vertical dispersion parameter, σ_z, near roadways. Atmos. Environ., 16, 1399-1405.

Benson, P.E., 1984. CALINE4 - A dispersion model for predicting air pollution concentrations near roadways. FHWA/CA/TL-85/15.

Bernier, J., 1985. Laboratoire National D'Hydraulique: Rapport D'Activite 1985. Annual Report of the National Hydraulics Laboratory, Electricite de France, 78400 Chatou, France (in French).

Briggs, G.A., 1973. ATDL file contribution summarized in: Gifford, F.A., 1976. Turbulent Diffusion - Typing Schemes: A Review. Nuclear Safety, 17, 68-86.

Britter, R.E. and J.C.R. Hunt, 1979. Velocity measurements and order of magnitude estimates of the flow between two buildings in an atmospheric boundary layer. J. Industrial Aerodynamics, 4, 165-182.

Builtjes, P.J.H. and P. Vermeulen, 1980. Atmospheric boundary layer simulation in the PIA and MIA wind tunnels of TNO-Apeldorn. TNO Report 80-0290.

Builtjes, P.J.H., 1983. Determination of the flow field in a street canyon by means of wind tunnel experiments. TNO Progress Report 83-09553.

Builtjes, P.J.H., 1984. Determination of the flow and concentration fields in a street canyon by means of wind tunnel experiments. Draft TNO Final Report.

Bullin, J.A., J.C. Polasek and N.J. Green, 1980a. Analytical and experimental assessment of highway impact on air quality: Data analysis and model evaluation. FHWA/TX-79/218-5F.

Bullin, J.A., J.C. Polasek, and N.J. Green, 1980b. Analytical and experimental assessment of highway impact on air quality. Texas Transportation Institute Report TTI-2-8-75-218-4.

Cadle, S.H., D.P. Chock, J.M. Heuss and P.G. Monson, 1976. Results of the General Motors sulfate dispersion experiment, GMR-2107, General Motors Research Laboratories, Warren, Michigan.

Calder, K.L., 1973. On Estimating Air Pollution Concentrations from a Highway in an Oblique Wind. Atmospheric Environment, 7, 863-868.

Cermak, J.E., D.J. Lombardi and R.S. Thomson, 1974. Applications of physical modeling to the investigation of air pollution problem in urban areas. Presented at the 67th Annual Meeting of the Air Pollution Control Association, Denver, Colorado, June 9-13.

Champagne, F.H. and C.A. Sleicher, 1967. Turbulence measurements with inclined hot-wires: Part 2 Hot-wire response equations. J. Fluid Mechanics, 28, 177-182.

Champagne, F.H., C.A.. Sleicher, and O.H. Wehrman, 1967. Turbulence measurements with inclined hot-wires: Part 1. Heat transfer experiments with inclined hot-wire. J. Fluid Mechanics, 28, 153-175.

Checkel, M.D., 1985. Measurements of turbulence generated by 60 percent solid perforated plates. Am. Soc. Mech. Engineers Paper 85-WA/FE-2, presented at Winter Annual Meeting, Miami Beach, FL, November 17-21, 1985.

Chock, D.P., 1977. General Motors sulfate dispersion experiment - An overview of the wind, temperature and concentration fields. Atmos. Environ., 11, 553-59.

Chock, D.P., 1978a. A simple line-source model for pollutant dispersion near roadways. Atmos. Environ., 12, 823-29. A separate user's guide is also available.

Chock, D.P., 1978b. An advection-diffusion model for pollutant dispersion-near roadways, J. Appl. Meteorol., 17, 976-989.

Chock, D.P., 1980. General Motors sulfate dispersion experiment - An analysis of the wind field near a road. Boundary Layer Meteorol., 18, 431-451.

Chock, D.P., 1982. Pollutant dispersion near roadways - experiments and modelling. The Science of the Total Environment, 25, 111-132.

Csanady, G.T., 1973. Turbulent Diffusion in the Environment. D. Reidel Publishing Company, Boston, Massachusetts.

Dabberdt, W.F., F.L. Ludwig and W.B. Johnson, 1973. Validation and applications of an urban diffusion model for vehicular pollutants. Atmos. Environ, 7, 603-18.

Dabberdt, W.F., E. Shelar, D. Marimont, and G. Skinner, 1981. Analyses, experimental studies, and evaluations of control measures for airflow and air quality on and near highways; Volume 1. FHWA/RD-81/051, Federal Highway Administration, Washington, D.C.

Dabberdt, W.F., 1977. Air quality on and near roadways: Experimental studies and model development, SRI Project 2761.

Danard, M.B., 1972. Numerical modeling of carbon monoxide concentrations near highways. J. Appl. Meteor., 11, 947-957.

De Paul, F.T., 1984. A study of pollutant dispersion in an urban street canyon. Ph.D. dissertation, Illinois Institute of Technology.

De Paul, F.T. and C.M. Sheih, 1983. Measurements of wind velocities in a street canyon. Argonne National Laboratory draft report ERC-83-10. Subsequently released in final form as ANL/ER-84-1.

De Paul, F.T. and C.M. Sheih, 1985. A tracer study of dispersion in an urban street canyon. Atmos. Environ., 19, 555-559.

Drivas, P.J. and F.H. Shair, 1974. Probing the airflow within the wake downwind of a building by means of a tracer technique. Atmospheric Environment, 8, 1165-75.

Egan, B.A., A. Epstein, and M. Keefe, 1973. Development of procedures to simulate motor vehicle pollution levels. Dept. of Highways and Traffic Report, NTIS-PB-233-938.

Eskridge, R.E., F.S. Binowski, J.C.R. Hunt, T.L. Clark and K.L. Demerjian, 1979. Highway modeling. Part II: Advection and diffusion of SF_6 tracer gas, J. Appl. Meteorol., 18, 401-12.

Eskridge, R.E. and J. Catalano, 1987. ROADWAY - a numerical model for predicting air pollutants near highways: User's Guide. U.S. EPA Report EPA/600/8-87/010.

Eskridge, R.E. and K.L. Demerjian, 1977. A highway model for the advection, diffusion, and chemical reaction of pollutants released by automobiles. Proc. Joint Conf. on Applications of Air Poll. Meteorology, Salt Lake city, Utah.

Eskridge, R.E. and J.C.R. Hunt, 1979. Highway modeling-I. Prediction of velocity and turbulence fields in the wakes of vehicles. J. Appl. Met., 18, 387-400.

Eskridge, R.E. and S.T. Rao, 1983. Measurement and prediction of traffic-induced turbulence and velocity fields near roadways. J. Climate and Appl. Meteor., 22, 1431-43.

Eskridge, R.E. and S.T. Rao, 1986. Turbulent diffusion behind vehicles: Experimentally determined turbulence mixing parameters. Atmos. Environ., 20, 851-860.

Eskridge, R.E. and R.S. Thompson, 1982. Experimental and theoretical study of the wake of a block-shaped vehicle in a shear-free boundary flow. Atmos. Environ., 16, 2821-36.

Garben, M., G. Wiegand, P. Builtjes, R. Yamartino, R. Stern, and K. Glueck, 1987. Ermittlung der durch Kfz-Emissionen verursachten Immisionsfelder verschiedener Strassentypen. Band 2 - Schadstoffausbreitung in Strassenschluchten (Vol. 2 - Pollutant Dispersion in Street Canyons) Umweltbundesamt Research Report 10402432/01, West Berlin.

Georgii, H.W., E. Busch, and E. Weber, 1967. Untersuchung ueber die zeitliche und raumliche Verteilung der Immissions-Konzentration des Kohlenmonoxid in Frankfurt am Main. Berichte des Institutes fuer Meteorol. und Geophys. der Universitaet Frankfurt/Main #11, 60 pp. (avail. as NAPCA translation 0477).

Groenskei, K.E., 1988. The influence of car speed on dispersion of exhaust gases. Atmos. Environ., 22, 273-281.

Hauschulz, G., H.J. Heich, P. Leisen, J. Raschke, H. Waldeyer, and J. Winckler, 1980. Emissions - und Immissionsmesstechnik im Verkehrswesen. TUV Rheinland.

Hicks, B.B., 1985. Behavior of turbulence statistics in the convective boundary layer. J. Climate and Appl. Met., 24, 607-614.

Hosker, R.P., Jr., 1981. Methods for estimating wake flow and effluent dispersion near simple block-like buildings. U.S. Nucl. Reg. Comm. report NUREG/CR-2521 and NOAA Tech Memo. ERL-ARL-108. NOAA/ERL/Atmospheric Turbulence and Diffusion Laboratory, Oak Ridge, TN, 138 pp.

Hosker, R.P., 1983. The effects of buildings on local dispersion. AMS Specialty Conf. on Air Quality Modeling of the Urban Boundary Layer, Baltimore, MD, Oct. 31 - Nov. 4.

Hosker, R.P., 1987. The effects of buildings on local dispersion. In Modeling the Urban Boundary Layer. American Meteorological Society, Boston, MA.

Hotchkiss, R.S. and F.H. Harlow, 1973. Air pollution transport in street canyons. EPA-R4-73-029.

Hoydysh, W.G. and H.H. Chiu, 1971. An experimental and theoretical investigation of the dispersion of carbon monoxide in the urban complex. American Institute of Aeronautics and Astronautics Paper No. 71-523, Urban Technology Conference, May 24-26, New York, N.Y.

Hoydysh, W.G. and Y. Ogawa, 1972. Characteristics of wind, turbulence, and pollutant concentration in and above a model city. Report ERL TR 110 prepared under NASA Grant; No. NGR 33-016-149.

Hoydysh, W.G., Griffiths, R.A. and Y. Ogawa, 1974. A scale model study of the dispersion of pollution in street canyons. APCA Paper No. 74-157, presented at the 67th Annual Meeting, June 9-13, Denver, CO.

Hoydysh, W.G. and R. Piva, 1975. A combined experimental and numerical study of flow in street canyons. Proc. Second U.S. National Conf. on Wind Engineering Research, Fort Collins, CO, June 22-25.

Hoydysh, W.G. and W.F. Dabberdt, 1986. Kinematics and dispersion characteristics of flows in asymmetric street canyons. Presented at the Third International Workshop on Wind and Water Tunnel MOdeling of Atmopspheric Flow and Dispersion, Lausanne, Switzerland, September 15-19.

Hunt, J.C.R., 1981. Mechanisms for dispersion of pollutants around buildings and vehicles. Proc. Conf. on Vehicle Exhaust Impacts in the vicinity of Major Streets, Oct. 20-21, TUEV Rheinland, Cologne, West Germany, pp. 235-268.

Janicke, L., 1981. Particle simulation of inhomogeneous turbulent diffusion. Proc. 12th Intl. Tech. Meeting on Air Pollut. Modeling and its Application. Menlo Park, CA, August 25-28 (Published as Air Pollution Modeling and its Application, Plenum Press, New York, 1983), pp. 527-35.

Johnson, W.B., W.F. Dabberdt, F.L. Ludwig and R.J. Allen, 1971. Field study for initial evaluation of an urban diffusion model for carbon monoxide. Comprehensive Report, Coordinating Research Council Contract CAPA-3-68(1-69) Stanford Research Institute, Menlo Park, California, 144 pp. (NTIS-PB-203469)

Johnson, W.B., F.L. Ludwig, W.F. Dabberdt and R.J. Allen, 1973. An urban diffusion simulation model for carbon monoxide. J. Air Pollut. Control Assoc., 23, 490-498.

Joumard,, R. and R. Vidon, 1980. Dispersion de pollutants dans une rue en U. Pollution Atmospherique, 88, 405-411 (in French).

Kirsch, J.W. and B.F. Mason, 1975. Mathematical models for air pollution studies involving the Oregon I-205 highway project. Systems, Science, and Software, Inc. Report SSS-R-76-2774.

Kitabayashi, K., K. Sugawara and S. Isomura, 1976. A wind tunnel study of automobile exhaust gas diffusion in an urban district. Proceedings of the Fourth International Clean Air Congress, Tokyo, April.

Kotake, S. and T. Sano, 1981. Simulation model of air pollution in complex terrains including streets and buildings. Atmos. Environ., 15, 1001-9.

Lamb, B., 1978. A tracer investigation of pollutant dispersion in an urban street canyon. Norwegian Institute of Air Research Report 2577.

Lamb, R.G., H. Hogo, and L.E. Reid, 1979. A Lagrangian approach to modeling air pollutant dispersion: development and testing in the vicinity of a roadway. EPA-600/4-79-023.

Legg, B.J. and M.R. Raupach, 1982. Markov-chain simulation of particle dispersion in inhomogeneous flows: the mean drift velocity induced by a gradient in Eulerian velocity variance. Boundary Layer Meteorol., 24, 3-13.

Leisen, P. and H. Sobottka, 1980. Simulation of the dispersion of vehicle exhaust gases in street canyons: Comparison of wind tunnel investigations and full scale measurements. IMA Conference on Modeling of Dispersion in Transport Pollution, Southend-on-Sea, England, March 17-18.

Lombardi, D.J., 1978. Steady state pollutant concentrations in an urban area. Master's Thesis, Colorado State University, Fort Collins, CO.

Maldonado, C., 1976. Computer simulation of the dispersion of carbon monoxide from roadways. M.S. Thesis, Chemical Engineering Department, Texas A&M University, College Station, Texas.

Martinez, J.R., H.S. Javitz, R.E. Ruff, A. Valdes, K.C. Nitz and W.F. Dabberdt, 1981. Methodology for evaluating highway air pollution dispersion models. National Cooperative Highway Research Program Report 245 (available from Transportation Research Board, National Academy of Sciences).

McElroy, J.L. and F. Pooler, 1968. The St. Louis Dispersion Study, U.S. Public Health Service, NAPCA Report AP-53.

Mellem, N.E. and J.P. Halvorson, 1985. Calibration of a Microscale model for carbon monoxide estimates. Paper 85-39.4, presented at the 78th Annual Meeting of the Air Pollution Control Asosociation, Detroit, MI, June 16-21, 1985.

Messina, A.D., J.A. Bullin, J.P. Nelli, and R.D. Moe, 1983. Estimates of air pollution near signalized intersections, FHWA/RD-83/009, Federal Highway Administration, Washington, D.C..

Midurski, T.P., 1978. Carbon Monoxide hot spot guidelines. Vol. 1: Techniques, EPA-450/3-78-033.

Nelli, J.P., A.D. Messina, and J.A. Bullin, 1983. Analysis and modeling of air quality and street intersections. J. Air Poll. Control Assoc., 33, 760-764.

Nicholson, S.E., 1975. A pollution model for street-level air. Atmospheric Environment, 9(1), 19-31.

Noll, K.E., T.L. Miller, and M. Clagget, 1978. A comparison of three highway line source dispersion models. Atmos. Environ., 12, 1323-1329.

Pasquill, F., 1974. Atmospheric Diffusion, 2nd edition, John Wiley and Sons, New York, 429 pp.

Petersen, W.B., 1978. User's Guide for PAL: A Gaussian-plume algorithm for point, area, and line sources. EPA-600/4-78-013.

Petersen, W.B., 1980. User's Guide for HIWAY-2, A highway air pollution model, EPA-600/8-80-018, May.

Petersen, W.B., R.E. Eskridge, S.T. Rao and V. Pagnotti, 1984. Effects of traffic speed on the ambient pollution concentration near roadways. Proc. 77th Annual Meeting of the Air Poll. Control Assoc., San Francisco, CA, June 224-299. Paper 84-118.6.

Plate, E., 1982. Engineering Meteorology. Elsevier Press, Amsterdam, 740 pp.

Potenta, E.J., V.S. Fahrer, and R.C. Tai, 1982. State-of-the-art approach to predicting pollutant concentrations in urban street canyons. APCA Paper No. 82-50.6, presented at the 75th Annual Meeting, June 20-25, New Orleans, LA.

Ragland, K.W. and J.J. Pierce, 1975. Boundary layer model for air pollutant concentrations due to highway traffic. J. Air Poll. Control Assoc., 25, 48-51.

Raithby, G.D., W.L. Hallett, T.L. Crawford, and P.R. Slawson, 1978. Measurements and predictions of turbulent recirculating flow over a rectangular depression. Boundary-Layer Meteorol., 15, 181-194.

Rao, S.T., M. Chen, M.T. Keenan, G. Sistla, P.J. Samson and D. Romano, 1979a. Overview of the NYS-Long Island expressway dispersion experiment. Transportation Research Record 670, Transportation Research Board, National Academy of Sciences, December.

Rao, S.T., L. Sedefian and U.H. Czapski, 1979b. Characteristics of turbulence and dispersion of pollutants near major highways, J. Appl. Meteorol., 18, 283-293.

Rao, S.T. and M.T. Keenan, 1980. Suggestions for improvement of the EPA-HIWAY model. J. Air Poll. Control Assoc., 30, 247-256.

Roshko, A., 1955. Some measurements of flow in a rectangular cutout. NACA Tech. Note 3488. National Advisory Committee for Aeronautics (now NASA), Washington, D.C.; avail. NTIS, Springfield, VA, 21 pp.

Ross, S.M., 1972. Introduction to Probability Models. Academic Press, New York, 272 pp.

Samson, P.J., 1988. Atmospheric transport and dispersion of air pollutants associated with vehicular emissions. In Air Pollution, the Automobile, and Public Health, National Academy Press, Washington, D.C.

Sedefian, L., S.T. Rao, and U. Czapski, 1981. Effects of traffic generated turbulence on near-field dispersion. Atmos. Environ., 15, 527-536.

Shen, C. and J.M. Floryan, 1985. Low Reynolds number flow over cavities. Phys. Fluids, 28, 3191-3202.

Sistla, G., P. Samson, M. Keenan and S.T. Rao, 1979. A study of pollutant dispersion near highways, Atmos. Environ., 13, 669-685.

Skinner, G.T. and G.R. Ludwig, 1976. Experimental studies of CO dispersion from a highway model in the atmospheric simulation facility. CALSPAN Report No. NA-5411-A-1, Buffalo, NY, under Contract DOT-FH-11-8125 and SRI Subcontract 13855.

Smith, F.B., 1972. A scheme for estimating the vertical dispersion of a plume from a source near ground level. NATO/CCMS Proceedings No. 14.

Snyder, W.H., 1981. Guidelines for fluid modeling of atmospheric diffusion, EPA-600/8-81-009. U.S. Environmental Protection Agency, Environmental Sciences Research Laboratory, Research Triangle Park, NC, xiv and 185 pp.

Sobottka, H. and P. Leisen, 1980a. Vehicle exhaust gas emissions in city streets and their distribution; comparison of measurements and model aspects. IMA Conference on Modeling of Dispersion in Transport Pollution, Southend-on-Sea, England, March 17-18.

Sobottka, H. and P. Leisen, 1980b. Pollutant dispersion of vehicle exhaust gases in street canyons. Proc. of the 5th International Clean Air Congress, Buenos Aires.

Sontowski, J., 1978. A dispersion model for deep street canyons. Internal memo to Bureau of Science and Technology, New York City.

Spielberg, D., 1984. Users' Guide for Program CANNY (Deep-Canyon Diffusion Model). Internal memo to Bureau of Science and Technology, New York City.

TA-Luft, 1987. Erste Allgemeine Verwaltungs-vorschrift zum Bundes-Immissions-Gesetz (Technische Anleitung zur Reinhaltung der Luft) vom 27 Februar 1986 GMBL, S.95.

Thompson, R.S. and R.E. Eskridge, 1987. Turbulent diffusion behind vehicles: Experimentally determined influence of vortex pair in vehicle wake. Atmos. Environ., 21, 2091-2097.

Turner, D.B., 1970. Workbook of Atmospheric Dispersion Estimates. Air Resources Research Office, Environmental Science Services Administration, Public Health Service Publication No. 999-AP-26, Cincinnati, Ohio.

Tutu, N.K. and R. Chevray, 1975. Cross-wire anemometry in high-intensity turbulence, J. Fluid Mechanics, 71, 785-800.

Wackter, D. and P. Bodner, 1986. Evaluation of Mobile Source Air Quality Simulation Models. EPA-450/4-86-002.

Wang, I.T. and D.M. Rote, 1975. A finite line source dispersion model for mobile source air pollution. J. Air Poll. Control Assoc., 25, 730-733.

Wang, P.N., P.M. Chang, and A. Lin, 1972. Circulation and diffusion of the separated flow in a rectangular trough. University of Utah Scientific Report for the Period 1 May 1970 to 30 April 1972, prepared for the U.S. Environmental Protection Agency under Grant AP 01126.

Weaving, J.H. and S.F. Benjamin, 1980. A strategy for pollution control in European cities. VDI-Berichte, 370, pp. 375-381.

Wedding, J.B., D. Lombardi and J. Cermak, 1977. A wind tunnel study of gaseous pollutants in city street canyons. J. Air Pollut. Control Assoc., 27, 557-566.

Wise, A.F.E., 1971a. Architectural aerodynamics. 1: Effects due to groups of buildings. The Canadian Architect, 27, 467-468.

Wise, A.F.E., 1971b. Effects due to groups of buildings. Phil. Trans. Roy. Soc. Lond. A., 269, 469-485.

Yamartino, R., 1977. A new method for computing pollutant concentrations in the presence of limited vertical mixing. J. Air Pollut. Control Assoc., 27, 467-468.

Yamartino, R.J., 1984. A comparison of several "single-pass" estimators of the standard deviation of wind direction. J. Climate Appl. Meteor., 23, 1362-1366.

Yamartino, R.J. and G. Wiegand, 1986. Development and evaluation of simple models for the flow, turbulence, and pollutant concentration fields within an urban street canyon. Atmos. Environ., 20, 2137-2156. (Reprinted as appendix H of this report).

Zamurs, J., 1984. Assessing the effect of transportation control strategies on urban carbon monoxide concentrations. J. Air Poll. Control Asosoc., 34 637-642.

Zimmerman, J.R. and R.S. Thomson, 1975. User's Guide for HIWAY: A highway air pollution model. EPA 650/4-74-008.